

NUREG/CR-3646  
LA-10548-MS

Los Alamos National Laboratory is operated by the University of California for the United States Department of Energy under contract W-7405-ENG-36

***TRAC-PF1***  
***Independent Assessment***

**Los Alamos** Los Alamos National Laboratory  
Los Alamos, New Mexico 87545

9512050451 9511307-210-175  
PDR NUREG  
CR-3646-R PDR

An Affirmative Action/Equal Opportunity Employer

Prepared by Vera Metzger, Group Q-9

NOTICE

This report was prepared as an account of work sponsored by an agency of the United States Government. Neither the United States Government nor any agency thereof, or any of their employees, makes any warranty, expressed or implied, or assumes any legal liability or responsibility for any third party's use, or the results of such use, of any information, apparatus, product or process disclosed in this report, or represents that its use by such third party would not infringe privately owned rights.



## **TRAC-PF1 Independent Assessment**

Compiled by  
Thad D. Knight and Vera B. Metzger

Contributors  
C. P. Booker  
B. E. Boyack  
P. Coddington\*  
T. D. Knight  
J. K. Meier  
J. R. White\*\*

Manuscript submitted: September 1985  
Date Published: October 1985

Prepared for Division of Accident Evaluation  
Office of Nuclear Regulatory Research  
US Nuclear Regulatory Commission  
Washington, DC 20555

NRC FIN No. A7053

\*Atomic Energy Establishment, Winfrith, Dorchester, Dorset, ENGLAND.

\*\*Consultant in Nuclear Reactor Safety Analysis, 2100 Belmont Ave., Idaho Falls, ID 83401.

# TRAC-PF1 INDEPENDENT ASSESSMENT

ABSTRACT . . . . .	1
EXECUTIVE SUMMARY . . . . .	2
I. INTRODUCTION . . . . .	6
II. COMPARISON OF TRAC-CALCULATED RESULTS WITH SEMISCALE . . . . .	9
NATURAL-CIRCULATION S-NC-2B, S-NC-5, S-NC-6, AND S-NC-7C	
TEST DATA	
A. Facility and Experiment Description . . . . .	9
B. TRAC Model . . . . .	10
C. Results . . . . .	14
1. Test S-NC-2B . . . . .	14
2. Test S-NC-5 . . . . .	19
3. Test S-NC-6 . . . . .	21
4. Test S-NC-7C . . . . .	24
D. Conclusions . . . . .	28
III. TRAC-PF1 POSTTEST ANALYSIS OF SEMISCALE TEST S-UT-2 . . . . .	29
A. Semiscale Mod-2A System Description . . . . .	29
B. Test Description . . . . .	32
C. TRAC Version . . . . .	32
D. TRAC Model . . . . .	32
E. Results . . . . .	37
1. General System Behavior . . . . .	37
2. Break Flows . . . . .	38
3. System Pressure . . . . .	39
4. Loop Hydraulic Response . . . . .	39
5. Upper-Head Fluid Behavior . . . . .	42
6. Core Behavior . . . . .	46
7. Timing Data . . . . .	48
F. Conclusions . . . . .	51
IV. TRAC-PF1 POSTTEST ANALYSIS OF SEMISCALE TESTS S-UT-6 AND S-UT-7 . . . . .	52
A. Semiscale Mod-2A System Description . . . . .	52
B. Test Description . . . . .	55
C. TRAC Version . . . . .	55
D. TRAC Model . . . . .	55
E. Results . . . . .	60
1. General System Behavior . . . . .	60
2. Break Flows . . . . .	62
3. System Pressure . . . . .	62
4. Loop Hydraulic Response . . . . .	64
5. Core Behavior . . . . .	68
6. Upper-Head Fluid Behavior . . . . .	76
7. Timing Data . . . . .	76
F. Conclusions . . . . .	76

# CONTENTS (cont.)

V.	TRAC-PF1 POSTTEST ANALYSIS OF LOFT INTERMEDIATE-BREAK . . . . .	78
	EXPERIMENTS L5-1 AND L8-2	
A.	LOFT System Description . . . . .	78
B.	Test Description . . . . .	80
C.	TRAC Model . . . . .	80
D.	Results . . . . .	81
	1. Base-Case Results . . . . .	81
	2. L5-1 Posttest Analysis Results . . . . .	88
	3. L8-2 Posttest Analysis Results . . . . .	112
E.	Conclusions . . . . .	122
VI.	TRAC-PF1 ANALYSIS OF LOFT STEAM-GENERATOR . . . . .	131
	FEEDWATER TRANSIENT L9-1/L3-3	
A.	Test Description . . . . .	131
B.	TRAC-PF1 Input Model Description . . . . .	131
C.	Data Comparisons . . . . .	134
D.	Conclusions . . . . .	138
VII.	TRAC-PF1 ANALYSIS OF LOFT L6-7/L9-2 . . . . .	139
A.	Test Apparatus . . . . .	140
B.	Experimental Phenomena . . . . .	141
C.	Description of TRAC Input . . . . .	145
D.	Presentation and Discussion of Data Comparisons . . . . .	147
E.	Computer Use . . . . .	153
VIII.	TRAC-PF1 ONE-DIMENSIONAL ANALYSIS OF THE CRYSTAL RIVER . . . . .	154
	UNIT-3 PLANT TRANSIENT OF FEBRUARY 26, 1980	
A.	Summary Description of Transient . . . . .	155
B.	Model and Code Description . . . . .	156
	1. TRAC Noding . . . . .	156
	2. TRAC Description . . . . .	160
C.	Reactor Initial Conditions and Transient Boundary . . . . .	160
	Assumptions	
D.	Calculational Results . . . . .	162
	1. Steady-State Calculation . . . . .	162
	2. Transient Calculations . . . . .	166
E.	User Experience and Calculation Timing Statistics . . . . .	187
F.	Summary and Conclusions . . . . .	190
IX.	TIMING STATISTICS . . . . .	193
X.	CONCLUSIONS . . . . .	200
	REFERENCES . . . . .	202

## FIGURES

1.	TRAC noding for Semiscale Test S-NC-2B . . . . .	11
2.	TRAC noding for Semiscale Tests S-NC-2B and S-SN-6 . . . . .	12
3.	TRAC noding for Semiscale Test S-NC-7C . . . . .	14
4.	Comparison of TRAC-calculated and measured . . . . . pressure histories for Test S-NC-2B	15
5.	Comparison of TRAC-calculated and measured . . . . . hot-leg mass flows as a function of system inventory with a nominal 30-kW core power for Test S-NC-2	16
6.	Comparison of TRAC-calculated and measured . . . . . hot-leg mass flows as a function of system inventory with a nominal 60-kW core power for Test S-NC-2	16
7.	Comparison of TRAC-calculated and measured . . . . . hot-leg mass flows as a function of system inventory with a nominal 100-kW core power for Test S-NC-2	17
8.	Comparison of TRAC-calculated and measured . . . . . primary pressures as a function of system inventory with a nominal 30-kW core power for Test S-NC-2	17
9.	Comparison of TRAC-calculated and measured . . . . . primary pressures as a function of system inventory with a nominal 60-kW core power for Test S-NC-2	18
10.	The TRAC-calculated and measured primary pressures . . . . . as a function of system inventory with a nominal 100-kW core power for Test S-NC-2	18
11.	Comparison of TRAC-calculated and measured . . . . . pressure histories for Test S-NC-5	19
12.	Comparison of TRAC-calculated and measured . . . . . hot-leg mass flows for Test S-NC-5	20
13.	Comparison of TRAC-calculated and measured . . . . . pressures for Test S-NC-5 with the TRAC interfacial drag increased by a factor of 100	20
14.	Comparison of TRAC-calculated and measured . . . . . mass flows for Test S-NC-5 with the TRAC interfacial drag increased by a factor of 100	21
15.	Comparison of TRAC-calculated and measured . . . . . pressure histories for Test S-NC-6	22

# FIGURES (cont.)

16.	Comparison of TRAC-calculated and measured . . . . .	23
	reflux rates as a function of the injected nitrogen for the upside of the steam generator for Test S-NC-6	
17.	The TRAC-calculated reflux rate as a function . . . . .	23
	of the injected nitrogen for the downside of the steam generator for Test S-NC-6. The dashed line represents the maximum reflux rate and the circular symbols, the individual reflux rate	
18.	Comparison of TRAC-calculated and measured . . . . .	24
	primary pressure histories for Test S-NC-7C	
19.	Comparison of TRAC-calculated and measured . . . . .	25
	broken-loop steam-generator secondary-side pressure histories for Test S-NC-7C	
20.	Comparison of TRAC-calculated and measured . . . . .	25
	intact-loop cold-leg mass flows for Test S-NC-7C	
21.	Comparison of TRAC-calculated and measured . . . . .	26
	broken-loop cold-leg mass flows for Test S-NC-7C	
22.	Comparison of TRAC-calculated and measured . . . . .	27
	intact-loop mass flows for system inventories above 70% for Test S-NC-7C.	
23.	Comparison of TRAC-calculated and measured . . . . .	27
	broken-loop mass flows for system inventories above 70% for Test S-NC-7C.	
24.	Comparison of TRAC-calculated and measured . . . . .	28
	downcomer mass flows for system inventories above 70% for Test S-NC-7C.	
25.	Semiscale Mod-2A system isometric . . . . .	30
	(cold-leg-break configuration)	
26.	Semiscale Mod-2A system for cold-leg-break . . . . .	31
	configuration--schematic	
27.	TRAC input model for the Semiscale Mod-2A facility . . . . .	33
28.	TRAC downcomer and vessel noding for the Semiscale . . . . .	34
	Mod-2A facility	
29.	Calculated break flows for Test S-UT-2 . . . . .	39
30.	Calculated integrated break flows for Test S-UT-2 . . . . .	40



# FIGURES (cont.)

31.	System pressure response for Test S-UT-2 . . . . .	40
32.	Broken-loop hot-leg density for Test S-UT-2 . . . . .	41
33.	Broken-loop cold-leg density for Test S-UT-7 . . . . .	41
34.	Intact-loop cold-leg density for Test S-UT-2 . . . . .	42
35.	Collapsed liquid level in intact-loop . . . . . pump-suction downflow leg for Test S-UT-2	43
36.	Collapsed liquid level in intact-loop . . . . . pump-suction upflow leg for Test S-UT-2	43
37.	Collapsed liquid level in the broken-loop . . . . . pump-suction downflow leg for Test S-UT-2	44
38.	Collapsed liquid level in the broken-loop . . . . . pump-suction upflow leg for Test S-UT-2	44
39.	Broken-loop hot-leg mass flow for Test S-UT-2 . . . . .	45
40.	Broken-loop pump-suction mass flow for Test S-UT-2 . . . . .	45
41.	Collapsed liquid level in the upper head for Test S-UT-2 . . . . .	46
42.	Collapsed core liquid levels for Test S-UT-2 base case . . . . .	47
43.	Collapsed core liquid levels for Test S-UT-2 parametric case . . . . .	47
44.	Base-case cladding temperatures at the 1.37-m level . . . . . for Test S-UT-2	48
45.	Base-case cladding temperatures at the 2.27-m level . . . . . for Test S-UT-2	49
46.	Base-case cladding temperatures at the 3.21-m level . . . . . for Test S-UT-2	49
47.	Parametric-case cladding temperatures at the 1.37-m . . . . . level for Test S-UT-2	50
48.	Parametric-case cladding temperatures at the 2.27-m . . . . . level for Test S-UT-2	50
49.	Parametric-case cladding temperatures at the 3.21-m . . . . . level for Test S-UT-2	51
50.	Semiscale Mod-2A system isometric (cold-leg-break . . . . . configuration)	50

# FIGURES (cont.)

51.	Semiscale Mod-2A system for cold-leg-break . . . . .	54
	configuration--schematic	
52.	TRAC input model for the Semiscale Mod-2A facility . . . . .	56
53.	TRAC downcomer and vessel noding for the Semiscale . . . . .	57
	Mod-2A facility	
54.	Break flow for Test S-UT-7 . . . . .	62
55.	Integrated break flow for Test S-UT-7 . . . . .	63
56.	System pressure response for Test S-UT-7 . . . . .	63
57.	Broken-loop hot-leg density for Test S-UT-7 . . . . .	64
58.	Broken-loop cold-leg density for Test S-UT-7 . . . . .	65
59.	Intact-loop hot-leg density for Test S-UT-7 . . . . .	65
60.	Collapsed liquid level in intact-loop pump-suction . . . . .	66
	downflow leg for Test S-UT-7	
61.	Collapsed liquid level in intact-loop pump-suction . . . . .	66
	upflow leg for Test S-UT-7	
62.	Intact-loop hot-leg mass flow for Test S-UT-7 . . . . .	67
63.	Intact-loop cold-leg mass flow for Test S-UT-7 . . . . .	67
64.	Collapsed liquid level in the broken-loop pump-suction . . . . .	68
	downflow leg for Test S-UT-7	
65.	Collapsed liquid level in the broken-loop pump-suction . . . . .	69
	upflow leg for Test S-UT-7	
66.	Broken-loop hot-leg mass flow for Test S-UT-7 . . . . .	69
67.	Broken-loop pump-suction mass flow for Test S-UT-7 . . . . .	70
68.	Collapsed core liquid levels for Test S-UT-7 . . . . .	70
69.	Collapsed core liquid levels for Test S-UT-6 . . . . .	71
70.	Core density at the 2.53-m level for Test S-UT-7 . . . . .	72
71.	Core density at the 2.53-m level for Test S-UT-6 . . . . .	72
72.	Cladding temperatures at the 2.27-m level for Test S-UT-7 . . . . .	73

# FIGURES (cont.)

73.	Cladding temperatures at the 2.53-m level for Test S-UT-7 . . . .	73
74.	Cladding temperatures at the 3.21-m level for Test S-UT-7 . . . .	74
75.	Cladding temperatures at the 2.27-m level for Test S-UT-6 . . . .	74
76.	Cladding temperatures at the 2.53-m level for Test S-UT-6 . . . .	75
77.	Cladding temperatures at the 3.21-m level for Test S-UT-6 . . . .	75
78.	Collapsed liquid level in the upper head for Test S-UT-7 . . . .	76
79.	Collapsed liquid level in the upper head for Test S-UT-6 . . . .	77
80.	LOFT major components (Ref. 24) . . . . .	79
81.	TRAC noding for LOFT Experiment L8-2 . . . . .	82
82.	TRAC noding for LOFT Experiment L8-2 . . . . .	83
83.	TRAC reactor-vessel noding for LOFT Experiment L8-2 . . . . .	83
84.	LOFT broken-loop cold-leg spool piece (Ref. 24) . . . . .	84
85.	LOFT break spool piece noding . . . . .	85
86.	Comparison of TRAC-calculated and measured . . . . . primary-system pressures	86
87.	Comparison of TRAC-calculated and measured break flows . . . . .	86
88.	Comparison of TRAC-calculated and measured break fluid . . . . . densities upstream of the break	87
89.	Comparison of TRAC-calculated and measured vapor . . . . . fractions upstream of the break	87
90.	TRAC-calculated break flow vs break vapor fraction . . . . .	88
91.	Comparison of TRAC-calculated and measured break flows . . . . .	89
92.	Valve area at the break . . . . .	89
93.	Comparison of TRAC-calculated and measured . . . . . primary-system pressures	90
94.	Comparison of TRAC-calculated and measured . . . . . pressurizer pressures	91

# FIGURES (cont.)

95.	Comparison of TRAC-calculated and measured . . . . .	91
	steam-generator secondary-side steam-dome pressures	
96.	Comparison of TRAC-calculated and measured . . . . .	92
	primary-system pressures during the early portion of the transient	
97.	Comparison of TRAC-calculated and measured . . . . .	93
	fluid densities upstream of the break	
98.	Comparison of TRAC-calculated and measured . . . . .	93
	intact-loop cold-leg fluid densities	
99.	Comparison of TRAC-calculated and measured . . . . .	94
	intact-loop hot-leg fluid densities	
100.	Comparison of TRAC-calculated and measured . . . . .	94
	intact-loop cold-leg fluid velocities	
101.	Comparison of TRAC-calculated and measured . . . . .	95
	fluid temperatures upstream of the break	
102.	TRAC-calculated cladding temperatures for . . . . .	96
	average-power rod at different axial elevations	
103.	TRAC-calculated cladding temperatures for . . . . .	96
	high-power rod at different axial elevations	
104.	TRAC-calculated cladding temperatures for . . . . .	97
	low-power rod at different axial elevations	
105.	Axial temperature profiles of high-power rod . . . . .	97
	at different times during the blowdown portion of the experiment	
106.	Axial temperature profiles of high-power rod . . . . .	98
	at different times during the reflood portion of the experiment	
107.	Comparison of TRAC-calculated and measured . . . . .	98
	cladding temperatures at the 5-in. elevation for the high-power rod	
108.	Comparison of TRAC-calculated and measured . . . . .	99
	cladding temperatures at the 8-in. elevation for the high-power rod	
109.	Comparison of TRAC-calculated and measured . . . . .	99
	cladding temperatures at the 11-in. elevation for the high-power rod	



# FIGURES (cont.)

110.	Comparison of TRAC-calculated and measured . . . . .	100
	cladding temperatures at the 15-in. elevation for the high-power rod	
111.	Comparison of TRAC-calculated and measured . . . . .	100
	cladding temperatures at the 24-in. elevation for the high-power rod	
112.	Comparison of TRAC-calculated and measured . . . . .	112
	cladding temperatures at the 28-in. elevation for the high-power rod	
113.	Comparison of TRAC-calculated and measured . . . . .	113
	cladding temperatures at the 30-in. elevation for the high-power rod	
114.	Comparison of TRAC-calculated and measured . . . . .	102
	cladding temperatures at the 32-in. elevation for the high-power rod	
115.	Comparison of TRAC-calculated and measured . . . . .	103
	cladding temperatures at the 34.5-in. elevation for the high-power rod	
116.	Comparison of TRAC-calculated and measured . . . . .	103
	cladding temperatures at the 37-in. elevation for the high-power rod	
117.	Comparison of TRAC-calculated and measured . . . . .	104
	cladding temperatures at the 39-in. elevation for the high-power rod	
118.	Comparison of TRAC-calculated and measured . . . . .	104
	cladding temperatures at the 41-in. elevation for the high-power rod	
119.	Comparison of TRAC-calculated and measured . . . . .	105
	cladding temperatures at the 45-in. elevation for the high-power rod	
120.	Comparison of TRAC-calculated and measured . . . . .	105
	cladding temperatures at the 49-in. elevation for the high-power rod	
121.	Comparison of TRAC-calculated and measured . . . . .	106
	cladding temperatures at the 58-in. elevation for the high-power rod	
122.	Comparison of TRAC-calculated and measured . . . . .	106
	cladding temperatures at the 15-in. elevation for the low-power rod	



# FIGURES (cont.)

123.	Comparison of TRAC-calculated and measured . . . . .	107
	cladding temperatures at the 21-in. elevation for the low-power rod	
124.	Comparison of TRAC-calculated and measured . . . . .	107
	cladding temperatures at the 26-in. elevation for the low-power rod	
125.	Comparison of TRAC-calculated and measured . . . . .	108
	cladding temperatures at the 30-in. elevation for the low-power rod	
126.	Comparison of TRAC-calculated and measured . . . . .	108
	cladding temperatures at the 38-in. elevation for the low-power rod	
127.	Comparison of TRAC-calculated and measured . . . . .	109
	cladding temperatures at the 15-in. elevation for the average-power rod	
128.	Comparison of TRAC-calculated and measured . . . . .	109
	cladding temperatures at the 30-in. elevation for the average-power rod	
129.	Comparison of TRAC-calculated and measured . . . . .	110
	cladding temperatures at the 37-in. elevation for the average-power rod	
130.	Comparison of TRAC-calculated and measured . . . . .	110
	cladding temperatures at the 41-in. elevation for the average-power rod	
131.	Comparison of TRAC-calculated and measured . . . . .	111
	cladding temperatures at the 45-in. elevation for the average-power rod	
132.	Time-step size for LOFT L5-1 posttest calculation . . . . .	111
133.	Comparison of TRAC-calculated and measured break flows . . . . .	113
134.	Valve area at the break . . . . .	113
135.	Comparison of TRAC-calculated and measured . . . . .	114
	primary-system pressures	
136.	Comparison of TRAC-calculated and measured . . . . .	114
	steam-generator secondary-side steam-dome pressures	
137.	Comparison of TRAC-calculated and measured . . . . .	115
	average fluid densities in broken-loop cold leg	

# FIGURES (cont.)

138.	Comparison of TRAC-calculated average density . . . . .	115
	and measured average fluid density	
	in the broken-loop cold leg	
139.	Comparison of TRAC-calculated and measured . . . . .	116
	average fluid densities in intact-loop hot leg	
	in the broken-loop cold leg	
140.	Comparison of TRAC-calculated average fluid density . . . . .	116
	and measured average fluid density	
	in the intact-loop hot leg	
141.	Comparison of TRAC-calculated and measured . . . . .	117
	fluid temperatures in broken-loop cold leg	
142.	Comparison of TRAC-calculated and measured . . . . .	118
	pump speeds for pump 1	
143.	Comparison of TRAC-calculated and measured . . . . .	118
	pump speeds for pump 2	
144.	TRAC-calculated fuel-rod-cladding temperatures . . . . .	119
	at different axial elevations for average-power rod	
145.	TRAC-calculated reactor-vessel vapor fractions . . . . .	119
	at different axial locations	
146.	Comparison of TRAC-calculated and measured . . . . .	120
	cladding temperatures at the 11-in. elevation	
	for the high-power rod	
147.	Comparison of TRAC-calculated and measured . . . . .	120
	cladding temperatures at the 24-in. elevation	
	for the high-power rod	
148.	Comparison of TRAC-calculated and measured . . . . .	121
	cladding temperatures at the 28-in. elevation	
	for the high-power rod	
149.	Comparison of TRAC-calculated and measured . . . . .	121
	cladding temperatures at the 31-in. elevation	
	for the high-power rod	
150.	Comparison of TRAC-calculated and measured . . . . .	122
	cladding temperatures at the 37-in. elevation	
	for the high-power rod	
151.	Comparison of TRAC-calculated and measured . . . . .	123
	cladding temperatures at the 45-in. elevation	
	for the high-power rod	

# FIGURES (cont.)

152.	Comparison of TRAC-calculated and measured . . . . .	123
	cladding temperatures at the 62-in. elevation for the high-power rod	
153.	Comparison of TRAC-calculated and measured . . . . .	124
	cladding temperatures at the 26-in. elevation for the low-power rod	
154.	Comparison of TRAC-calculated and measured . . . . .	124
	cladding temperatures at the 32-in. elevation for the low-power rod	
155.	Comparison of TRAC-calculated and measured . . . . .	125
	cladding temperatures at the 37-in. elevation for the low-power rod	
156.	Comparison of TRAC-calculated and measured . . . . .	125
	cladding temperatures at the 11-in. elevation for the average-power rod	
157.	Comparison of TRAC-calculated and measured . . . . .	126
	cladding temperatures at the 21-in. elevation for the average-power rod	
158.	Comparison of TRAC-calculated and measured . . . . .	126
	cladding temperatures at the 26-in. elevation for the average-power rod	
159.	Comparison of TRAC-calculated and measured . . . . .	127
	cladding temperatures at the 32-in. elevation for the average-power rod	
160.	Comparison of TRAC-calculated and measured . . . . .	127
	cladding temperatures at the 37-in. elevation for the average-power rod	
161.	Comparison of TRAC-calculated and measured . . . . .	128
	cladding temperatures at the 45-in. elevation for the average-power rod	
162.	Comparison of TRAC-calculated and measured . . . . .	128
	cladding temperatures at the 49-in. elevation for the average-power rod	
163.	TRAC-calculated time-step size . . . . .	129
164.	TRAC-PF1 input model of the intact loop for LOFT L9-1/L3-3 . . . .	133
165.	TRAC-PF1 input model of the broken loop for LOFT L9-1/L3-3 . . . .	133

# FIGURES (cont.)

166.	Comparison of TRAC-calculated and measured . . . . .	135
	primary-system cold-leg temperatures for LOFT L9-1/L3-3	
167.	Comparison of TRAC-calculated and measured . . . . .	136
	mass flows for LOFT L9-1/L3-3	
168.	Comparison of TRAC-calculated and measured . . . . .	136
	pressures on the steam-generator secondary side for LOFT L9-1/L3-3	
169.	Comparison of TRAC-calculated and measured . . . . .	137
	pressurizer for LOFT L9-1/L3-3	
170.	Comparison of TRAC-calculated and the measured . . . . .	137
	pressures controlled by the pressurizer spray for LOFT L9-1/L3-3	
171.	LOFT major components (Ref. 31) . . . . .	140
172.	Reflood-assist bypass lines (Ref. 25) . . . . .	141
173.	Reactor-vessel schematic with flow paths . . . . .	142
	(EGG, Idaho, Semiscale LOFT Modeling Workshop, August 19-20, 1981)	
174.	LOFT primary-system hot and cold legs . . . . .	143
	(EGG, Idaho, Semiscale LOFT Modeling Workshop, August 19-20, 1981)	
175.	Primary-system pressure . . . . .	144
176.	Vessel and broken-loop component diagram . . . . .	145
177.	Intact-loop component diagram . . . . .	146
178.	Steam-generator outlet temperature . . . . .	148
179.	Intact-loop hot-leg temperature . . . . .	148
180.	Broken-loop cold-leg temperature . . . . .	149
181.	Intact-loop mass flow rate . . . . .	149
182.	Intact-loop cold-leg temperature . . . . .	150
183.	Experiment downcomer temperatures (D. C. Stalk 1) . . . . .	150
184.	Experiment downcomer temperatures (D. C. Stalk 2) . . . . .	151
185.	Calculated downcomer temperatures . . . . .	151



# FIGURES (cont.)

186.	Loop component diagram . . . . .	157
187.	One-dimensional vessel component diagram . . . . .	158
188.	Comparison of TRAC-calculated and measured . . . . . system pressures	168
189.	Comparison of TRAC-calculated and measured . . . . . upper-plenum temperatures	169
190.	Comparison of TRAC-calculated and measured . . . . . plant Loop-A mass flows	169
191.	Comparison of TRAC-calculated and measured . . . . . plant Loop-B mass flows	170
192.	Comparison of TRAC-calculated and measured . . . . . plant Loop-B steam-generator secondary-side pressures	170
193.	Void fraction at the top of Loop-A candy cane . . . . .	172
194.	Void fraction at the top of Loop-B candy cane . . . . .	173
195.	Void fraction in vessel upper head . . . . .	173
196.	Loop-B Case 1 steam-generator primary . . . . . inlet and outlet temperatures	174
197.	Loop-B Case 2 steam-generator primary . . . . . inlet and outlet temperatures	175
198.	Loop-A steam-generator secondary-side pressures . . . . .	175
199.	Pressurizer collapsed liquid level . . . . .	176
200.	Pressurizer mass flow through PORV and SRV . . . . .	177
201.	Loop-A HPIS mass flows . . . . .	181
202.	Loop-B HPIS mass flows . . . . .	178
203.	Loop-B downcomer temperatures (cell below . . . . . cold-leg connection)	181
204.	Loop-B cold-leg temperatures (at HPIS connection) . . . . .	181
205.	Loop-A mass flows . . . . .	182
206.	Loop seal--steam-generator primary-side geometry . . . . .	182



# FIGURES (cont.)

207.	RHO-G-H pressure difference in Loop A between . . . . .	183
	bottom of the loop seal and (1) top of loop seal and	
	(2) equivalent height in steam-generator primary.	
208.	RHO-G-H pressure drop terms around Loop A . . . . .	183
209.	Downcomer temperature, immediately below Loop-A . . . . .	184
	cold-leg connection	
210.	Loop-A cold-leg temperature opposite HPIS . . . . .	185
	injection location	
211.	Water temperature in Loop-A seal . . . . .	185
212.	Water temperature at inlet to vent valves . . . . .	186
213.	Mass flow through Loop-A vent valve . . . . .	186
214.	Mass flow through Loop-B vent valve . . . . .	187
215.	CPU time for Crystal River transients, . . . . .	188
	run on a CDC 7600 computer	
216.	Total number of time steps for Crystal River transients . . . . .	189
217.	CPU-time utilization for the LOFT L2-2 calculation . . . . .	195
	with the three-dimensional VESSEL component	
218.	CPU-time utilization for the LOFT L2-2 calculation . . . . .	196
	with the one-dimensional vessel representation	
219.	CPU-time utilization for the LOFT L3-7 calculation . . . . .	196
220.	CPU-time utilization for the Semiscale . . . . .	197
	Test S-UT-2 calculation	
221.	CPU-time utilization for the Semiscale . . . . .	197
	Test S-UT-6 calculation	
222.	CPU-time utilization for the Semiscale . . . . .	198
	Test S-UT-7 calculation	
223.	CPU-time utilization for the LOFT L5-1 calculation . . . . .	198
224.	CPU-time utilization for the LOFT L8-2 calculation . . . . .	199

# TABLES

I.	TRAC MODEL COMPONENTS . . . . .	35
II.	TEST S-UT 2 INITIAL CONDITIONS . . . . .	37
III.	TEST S-UT-2 EVENTS . . . . .	38
IV.	TRAC MODEL COMPONENTS . . . . .	58
V.	TEST S-UT-7 INITIAL CONDITIONS . . . . .	60
VI.	TEST S-UT-7 EVENTS . . . . .	61
VII.	KEY INITIAL CONDITIONS FOR LOFT EXPERIMENT L5-1 . . . . .	85
VIII.	KEY INITIAL CONDITIONS FOR LOFT EXPERIMENT L8-2 . . . . .	85
IX.	KEY PARAMETERS FOR LOFT EXPERIMENT L5-1 . . . . .	112
X.	KEY PARAMETERS FOR LOFT EXPERIMENT L8-2 . . . . .	130
XI.	SEQUENCE OF EVENTS FOR LOFT L9-1/L3-3 . . . . .	132
XII.	SEQUENCE OF EVENTS FOR EXPERIMENT L6-7/L9-2 . . . . .	143
XIII.	TOTAL HPIS FLOW VS PRESSURE . . . . .	161
XIV.	SECONDARY PRESSURE RELIEF CAPACITY . . . . .	162
XV.	STEADY-STATE CONDITIONS FOR CRYSTAL RIVER UNIT-3 PLANT . . . . .	163
XVI.	ONCE-THROUGH STEAM-GENERATOR SECONDARY-SIDE STEADY-STATE CONDITIONS . . . . .	164
XVII.	TRANSIENT EVENT SEQUENCE TIME . . . . .	167
XVIII.	TIMING STATISTICS FOR CRYSTAL RIVER . . . . . TRAC-PF1 ONE-DIMENSIONAL CALCULATIONS	189
XIX.	CODE TIMING STATISTICS . . . . .	194

## TRAC-PF1 INDEPENDENT ASSESSMENT

Compiled by

Thad D. Knight and Vera B. Metzger

Contributors

C. P. Booker, B. E. Boyack, P. Coddington,

T. D. Knight, J. K. Meier, and J. R. White

### ABSTRACT

The Los Alamos National Laboratory is developing the Transient Reactor Analysis Code (TRAC) under the sponsorship of the Office of Nuclear Regulatory Research, US Nuclear Regulatory Commission (USNRC). The code provides an advanced, best-estimate analysis capability for pressurized water reactors and for many thermal-hydraulic test facilities. The most recent publicly released version of TRAC is TRAC-PF1. This code version includes a full two-fluid modeling capability in both the three-dimensional vessel component and the one-dimensional components. We have improved the numerical methods in the one-dimensional components to provide a more stable solution and to permit the code to run faster. The Los Alamos report, "TRAC-PF1: An Advanced Best-Estimate Computer Program for Pressurized Water Reactor Analysis," LA-9944-MS (NUREG/CR-3567), provides a detailed description of the code.

This report documents the Los Alamos results of the second assessment phase, independent assessment for TRAC-PF1. We documented the results of the developmental assessment for TRAC-PF1 in an earlier report. This report described calculations run with the released versions of TRAC-PF1. We analyzed separate-effects tests in the Semiscale facility to investigate natural-circulation and reflux cooling. We analyzed integral tests from the Semiscale and the Loss-of-Fluid Test facilities to explore the small- and intermediate-break loss-of-coolant-accident (LOCA) capability and the non-LOCA capability. We also analyzed the loss-of-feedwater transient in the Crystal River plant. The results show reasonably good agreement with the data, but indicate that improvements are required for the critical-flow model and the interphasic-condensation model.

## EXECUTIVE SUMMARY

This report documents the independent assessment of the TRAC-PF1 code at the Los Alamos National Laboratory. The Transient Reactor Analysis Code (TRAC) is an advanced best-estimate systems code for analyzing light-water reactor accidents. The Office of Nuclear Regulatory Research, USNRC, sponsors the development of the code at Los Alamos. We released TRAC-PF1 to the National Energy Software Center at the Argonne National Laboratory in the fall of 1981. This version of TRAC is the fourth in a series of publicly available codes intended primarily for the analysis of pressurized water reactors (PWRs). The code is capable of performing small-, intermediate-, and large-break loss-of-coolant-accident (LOCA) analyses and non-LOCA analyses. The generality of the code permits direct application to a large variety of analyses such as blowdowns in simple pipes, integral LOCA tests in multiloop test facilities, and separate-effects tests. Integral tests involve the simulation of multiple system components, and generally cover several phases of a LOCA transient.

The TRAC-PF1 code is based on a developmental derivative of TRAC-PD2 with a complete two-fluid hydrodynamic model in both the one- and three-dimensional components. In the TRAC-PF1 code we have provided the capability to track a noncondensable gas in the gas phase and a solute in the liquid phase. The code is completely modular by component and function. The one-dimensional components implement a new numerical technique [the stability-enhancing two-step (SETS) numerics] that permit the time step to exceed the material Courant limit; this numerical technique replaces both the semi-implicit and fully implicit numerics in the one-dimensional components that were available in the TRAC-PD2 code. The three-dimensional VESSEL component uses semi-implicit numerics and is therefore subject to the material Courant limit. Relative to its predecessors, this code also provides a generalized trip capability and a new critical-flow model. The critical-flow model eliminates the requirement for detailed noding of breaks and the accompanying problems associated with the interphase mass-transfer model (lack of a delayed-nucleation capability). The code continues to provide a consistent code input and thermal-hydraulic analysis capability for generating the steady-state conditions and calculating entire transient sequences. While the code permits renoding on restart, renoding is not required at any time during the complete analysis.

We have previously reported the final TRAC-PF1 developmental-assessment results. Because we performed these analyses with the released version of the code, the results constitute the initial set of independent-assessment results. The developmental-assessment analyses covered large- and small-break LOCA tests and natural-circulation and reflux cooling tests. This current report does not describe the developmental-assessment work but rather provides the necessary reference.

Following the release of TRAC-PF1, we provided updates in the form of two newsletters. These updates made error corrections and further generalized the input, based on early analyses performed after the code release. The input changes permit better representation of material properties in the heat



slabs and improve the representation of boundary conditions for several experiment facilities. The independent assessment uses these updates.

For independent assessment, we analyzed four tests from the Semiscale natural-circulation test series, three Semiscale small-break LOCA tests, two Loss-of-Fluid Test-Facility (LOFT) intermediate-break LOCA tests, two LOFT non-LOCA transients, and the loss-of-feedwater transient in the Crystal River plant. The four tests from the Semiscale natural-circulation test series investigated single- and two-phase natural-circulation and reflux cooling without a noncondensable gas, reflux cooling with noncondensable injection, two-phase natural circulation with noncondensable injection, and asymmetries in the coolant-loop behavior due to asymmetric control of the steam-generator secondaries. The three Semiscale small-break LOCA tests investigate the sensitivity of the break size and the effects of upper-head safety injection on the transient. The two LOFT intermediate-break LOCA tests investigate the effect of reduced emergency core-cooling system (ECCS) capacity and pump operation during the transient. The two LOFT non-LOCA transients simulate a loss-of-feedwater transient with delayed scram and a turbine-trip transient. The Crystal River transient tests the code at full scale during a transient induced by the loss of feedwater.

The report discusses the various analyses in detail and provides a description of the facility and test, the TRAC input, and comparisons to data. After each set of analyses, the report provides conclusions based on that particular set of analyses, with summary conclusions contained in the final section. Because of the diverse nature of the transients analyzed with TRAC-PF1 and because we have defined key parameters for only a subset of the transients, we have discussed the key parameters separately in each section. Tables III, VI, IX, and X together with the discussion in Sections III.E.6 and IV.E.5 highlight the key parameters. The key parameters for small-break LOCA are in Tables III and VI and in Sections III.E.6 and IV.E.5. Tables IX and X summarize the key parameters for intermediate-break LOCA.

Computer timing statistics for all analyses except the Crystal River transient are discussed in Section IX, with specific information given in Table XIX and Figs. 217-224. Although the timing comparisons are not rigorous among the facilities, Table XIX makes it evident that the code runs faster for larger-scale facilities for the same type of transient and similar noding. Table XVIII and Fig. 215 provide the timing statistics for the Crystal River calculation.

The calculation of the LOFT small-break-LOCA Test L3-7 (from the developmental assessment) required ~2 s of central-processor unit (CPU) time in the computer for every second of transient time, although the first 2500 s of the transient ran much faster than real time. An interesting comparison in Table XIX involves the three- and one-dimensional analyses of LOFT large-break-LOCA Test L2-2 (again from the developmental assessment). Relative to the three-dimensional modeling of the LOFT vessel, the results with the one-dimensional representation of the LOFT vessel lose the detailed flow patterns in the vessel and the multidimensionality in the core thermal response; however, the one-dimensional calculation is an order of magnitude faster than the three-dimensional calculation and is only ~30 times slower than real time.



The TRAC-PF1 code calculates many phenomena very well. The major discrepancies in the data comparisons generally can be traced to the critical-flow model and to the interphasic condensation model. The critical-flow model does not yield the correct dependence of critical flow on void fraction. The condensation model appears to underpredict the condensation rate under certain conditions and overpredict it in others.

The Semiscale natural-circulation comparisons show that the code calculates the magnitude of the natural-circulation flows as a function of system inventory reasonably well. The code also correctly makes the transition from natural-circulation cooling to reflux cooling. The comparisons indicate that the wall-condensation heat transfer in the released code is low. The reflux test with the noncondensable injection shows that the calculated behavior of the noncondensable gas is correct, although the natural-circulation test with the noncondensable-gas injection shows that the code does not predict the measured flow recovery well.

The Semiscale small-break LOCA comparisons confirm the problems with the critical-flow model. However, when the multipliers to the critical-flow model are adjusted to offset the errors in the model, the comparisons throughout the primary system are reasonably good. The code calculates the core dryouts to occur early and the peak cladding temperature to be high, by as much as 50 K. Because the core volume is very small, small changes in the primary-system liquid inventory have significant impact on the core inventory and consequently on the thermal response.

The comparisons for the LOFT intermediate-break LOCA tests show that the core should be noded more finely in the axial direction to track better the core liquid level and its effect on core dryout. Conversely, if an interpolative scheme were used to distribute the fluid along the fuel rod, then the coarser noding scheme in the core would be acceptable. If the interface-sharpener logic were incorporated in the one-dimensional CORE component, these types of tests could be successively run in a one-dimensional calculation. The comparisons offer further confirmation of the inadequacy of the critical-flow model. An underprediction of condensation at high-subcooling and low void fraction adversely affected the system pressure calculation, causing the calculated pressure not to drop as rapidly as the data when the cladding temperature exceeded the saturation temperature (subcooled nucleate boiling generated vapor, which later failed to condense in the upper plenum). This problem does not occur with the one-dimensional CORE component because the subcooled nucleate-boiling heat-transfer mode does not exist in the one-dimensional components. Sensitivity calculations conducted as a part of the L5-1 and L8-2 analyses show the calculated results to be remarkably insensitive to the time-step size, and the mass errors are negligible.

The code calculated well the behavior of the two non-LOCA transients in LOFT. The results indicate the importance to the overall system response of modeling all structural mass and heat-transfer area, together with the leakage paths in the vessel, because of the impact on the energy balance. The heat- and mass-transfer mechanisms in the steam-generator secondary and in the pressurizer are also important factors in these tests.

The Crystal River analysis is significant in showing the application of the code to a real reactor transient. The code calculated the sequence of events very well and the calculated pressures, flows, and temperatures compare well with the data. The refill of the hot legs shows an adverse effect of interphase condensation on filling individual cells. The code requires a combined wall- and interphasic-condensation model to smooth the condensation process as cells fill and the pressure increases.

The overall results of the independent assessment of TRAC-PF1 indicate that, while the code has some problems, the user can successfully apply the code to a variety of transients. The problem areas, primarily dealing with deficiencies in the critical-flow model and in the interphase-condensation model, can be overcome through judicious choice of multipliers for the critical-flow model and noding in areas where the condensation problems are likely to occur. The TRAC-PF1 code provides significant improvements over TRAC-PD2/MOD1 with regard to trip capability and user convenience in applications to small-break LOCAs and non-LOCA transients; however, until the problems with the critical-flow and condensation models are corrected, the TRAC-PD2/MOD1 code provides superior large-break LOCA capability.

## I. INTRODUCTION

The Transient Reactor Analysis Code (TRAC) is an advanced best-estimate systems code for analyzing light-water reactor (LWR) accidents. The Office of Nuclear Regulatory Research, USNRC, sponsors the development of the code at the Los Alamos National Laboratory. We released TRAC-PF1 (Ref. 1) to the National Energy Software Center at the Argonne National Laboratory in the fall of 1981. This version of TRAC is the fourth in a series of publicly available codes intended primarily for the analysis of pressurized water reactors (PWRs). The code is capable of performing small-, intermediate-, and large-break loss-of-coolant-accident (LOCA) analyses and non-LOCA analyses. The generality of the code also permits direct application to a large variety of analyses such as blowdowns in simple pipes, integral LOCA tests in multiloop test facilities, and separate-effects tests. Integral tests involve the simulation of multiple system components, and generally cover several phases of a LOCA transient. The Idaho National Engineering Laboratory (INEL) is developing a TRAC version for application to boiling-water reactors (BWRs); this BWR version of TRAC is based on a developmental derivative of TRAC-PD2 with a complete two-fluid hydrodynamic model in both the one- and three-dimensional components. The TRAC-PF1 code is based on the same derivative of TRAC-PD2 with substantial changes in the numerics and component modeling. We will make improvements to various models and the numerical techniques in future versions of TRAC to facilitate and enhance applications to various reactor transients.

Reference 1 describes the TRAC-PF1 code. The code is completely modular by component and function. Both the one- and three-dimensional components utilize a full two-fluid thermal-hydraulic model with the capability to track a noncondensable in the gas phase and a solute in the liquid phase. The one-dimensional components implement a new numerical technique [the stability-enhancing two-step (SETS) numerics] that permit the time step to exceed the material Courant limit. The three-dimensional VESSEL component uses semi-implicit numerics and therefore is subject to the material Courant limit. The code provides a consistent code input and thermal-hydraulic analysis capability for generating the steady-state conditions and calculating entire transient sequences. While the code permits renoding on restart, renoding is not required at any time during the complete analysis.

The assessment of TRAC is a two-stage process. The first stage is the developmental assessment and is coupled closely to the code development process. Developmental assessment principally involves posttest analyses of a variety of thermal-hydraulic experiments. The primary objectives of developmental assessment are to define the limits of validity of the methods, models, and correlations in the developmental version of the code and to establish values for various empirical parameters; these objectives are achieved by comparing the calculated results with experiment data. Other objectives include the determination of code sensitivity to input data, model assumptions, and solution techniques; recommendation of standard calculational procedures for various classes of problems; and identification of code and model improvements.



Independent assessment is the second stage of the assessment process. This second stage begins following the release of the code for external use. Independent assessment uses publicly available and documented versions of TRAC. The primary objective is to determine the predictive capability of the code when applied to new tests involving different scales and facility configurations or different initial and boundary conditions. All of the developmental assessment objectives also apply to independent assessment; however, in independent assessment, the results are factored into the future code development without updating the current, released code. Discrepancies between the calculations and data are resolved by performing additional posttest analyses as required. Code changes related to better representation of boundary conditions and improved editing of output information are allowed in the independent-assessment process if the basic modeling and calculational techniques are not changed.

We reported the final TRAC-PF1 developmental-assessment results in Ref. 2. We performed the analyses with the released version of TRAC-PF1; these analyses, therefore, constitute the initial set of independent-assessment results for TRAC-PF1. The developmental-assessment analyses covered large- and small-break LOCA tests and natural-circulation and reflux cooling tests.

Following the release of TRAC-PF1, two newsletters<sup>3,4</sup> provided a series of updates to the code to correct errors and to generalize the input. The input changes permit better representation of material properties in the heat slabs and improve the representation of boundary conditions for several experiment facilities. The independent assessment uses these updates.

For independent assessment, we analyzed four tests from the Semiscale natural-circulation test series, three Semiscale small-break LOCA tests, two Loss-of-Fluid Test Facility (LOFT) intermediate-break LOCA tests, two LOFT non-LOCA transients, and the loss-of-feedwater transient in the Crystal River plant. The four tests from the Semiscale natural-circulation test series investigated single- and two-phase natural-circulation and reflux cooling without a noncondensable gas, reflux cooling with noncondensable injection, and two-phase natural circulation with noncondensable injection. The three Semiscale small-break LOCA tests investigate the sensitivity of break size and the effects of upper-head injection on the transient. The two LOFT intermediate-break LOCA tests investigate the effect of reduced emergency core-cooling system (ECCS) capacity and pump operation during the transient. The two LOFT non-LOCA transients simulate a loss-of-feedwater transient with delayed scram and a turbine-trip transient. The analyses are discussed in the order just described, with the Crystal River transient described last.

The figures showing the comparisons between the TRAC calculations and the data follow the general rule that a solid line represents the calculation, and a dashed line represents the data unless otherwise stated in the text. Most of the comparison figures will contain a legend box on the right-hand side of the figure; this legend normally gives information such as the TRAC component number, cell (or interface) number, the component type, and an indication of the data symbols. For the figures relating to the TRAC VESSEL component, the cell designation is replaced by counts of rings (R), azimuthal segments (TH), and the axial levels (Z). Figures showing calculated



temperatures in the rods will show the axial elevation ( $Z = \text{XXX.}$ ), the calculational rod number (ROD), and the radial node location count (R). The data will be indicated by the word DATA or by an instrument designation that is facility defined.

## II. COMPARISON OF TRAC-CALCULATED RESULTS WITH SEMISCALE NATURAL-CIRCULATION S-NC-2B, S-NC-5, S-NC-6, AND S-NC-7C TEST DATA

We assessed the capability of TRAC-PF1 to make accurate posttest predictions for Semiscale Natural-Circulation Tests S-NC-2B, S-NC-5, S-NC-6, and S-NC-7C. These experiments involve single- and two-phase natural circulation and reflux, all of which are important heat-rejection mechanisms in PWR accidents. Test S-NC-2B is a base-case test that covers three core power levels and several system inventories; single- and two-phase natural circulation and reflux are observed. The TRAC-calculated results for mass flow compare well with the experiment results. Test S-NC-5 examines the effect of a noncondensable gas on two-phase natural circulation. The code could not predict the results for Test S-NC-5 because the nitrogen in the experiment dissolves in the water, a phenomenon that TRAC currently cannot calculate. Test S-NC-6 is a reflux test with various amounts of nitrogen injected into the hot leg of the system. The TRAC-predicted reflux rate is close to the test value when there is no nitrogen in the system. Ultimately, the maximum TRAC-predicted reflux rate is ~20% higher than the measured rate. Test S-NC-7C, a two-loop experiment, examines the imbalances between the intact and broken loops. The TRAC-calculated results are reasonable while the primary system drains, but they do not predict correctly the oscillations in the flow between the intact and broken loops as the broken-loop steam generator drains.

In the following sections, the TRAC input models are described briefly, comparisons are made between the TRAC predictions and the experiment data, and a concise analysis of the TRAC results is presented.

### A. Facility and Experiment Description

The Semiscale natural-circulation tests provide a natural-circulation and reflux data base to assess best-estimate codes. Tests S-NC-2B, S-NC-5, S-NC-6, and S-NC-7C were selected because they cover a broad spectrum of the natural-circulation and reflux tests. These tests use an abridged version of the Semiscale facility.

For Test S-NC-2B, only the vessel and the intact loop are used. The intact-loop pump is replaced by a spool piece with orifices to avoid uncontrolled primary-fluid loss through the leaky pump;<sup>5</sup> the orifice does not block the lower half of the pipe.\* The upper head of the vessel is removed to avoid a nonuniform heating of the entire system and to avoid condensation on the upper-head structures.<sup>5</sup> The core power is stabilized at ~30 kW. The data cover the 100% inventory condition. Some liquid is drained from the lower plenum. After the system stabilizes, measurements are made for various system inventories. The core power stabilizes at ~60 kW and the system is refilled to 100% inventory. Measurements are made again at various inventories. The process is repeated for a 100 kW core power.

---

\*This information was provided by David Shimeck, EG&G Idaho, Inc. on August 17, 1982.

In Test S-NC-5, the system configuration is the same as in Test S-NC-2B except that nitrogen is injected just below the steam-generator inlet plenum. In this test, an initial steady state is established with a full liquid inventory; the system is drained to 88.5% of full liquid inventory and a new steady state is established. Thereafter, various amounts of nitrogen are injected into the hot leg just below the steam-generator inlet plenum. Throughout the test, the core power is maintained at a nominal 33 kW.

In Test S-NC-6, the system configuration is the same as in Test S-NC-5. Because this is a reflux test, additional measurement techniques are used to measure the reflux rate; a reflux meter is attached to the steam-generator inlet piping. This meter consists of a tee in the primary piping with a weld bead around the inside circumference and a stand pipe that collects and measures the reflux fluid.<sup>6</sup> To offset this net loss of liquid from the system, water is injected into the lower plenum. The core power is maintained at a nominal 30 kW. Measurements are made when there is no nitrogen in the system and again as increased amounts of nitrogen are injected into the system.

Test S-NC-7C is the only one of the four tests that uses both the intact and the broken loops of the Semiscale facility.<sup>7</sup> The intact loop is the same as that described above for Test S-NC-2B. The broken loop is the same as that normally used in the Semiscale facility; the broken-loop pump is left in the loop but the rotor is locked during the test. The core power level is maintained at ~100 kW. The test consists of two main segments. In the first segment, the primary inventory is reduced discretely through a drain in the vessel lower plenum; measurements are made when each inventory reaches steady state. In the second segment, the primary inventory remains at 73.1%. The broken-loop steam generator is drained to discrete inventories; as before, measurements are made when each broken-loop secondary inventory achieves steady state.

During all the tests, the pressurizer establishes the initial steady state for each core power level. Then, valves are used to isolate the pressurizer from the system before measurements are made and before the system inventory is reduced. Further, no emergency core coolant (ECC) is required.

#### B. TRAC Model

The TRAC noding for Test S-NC-2B (Fig. 1) reflects the simplicity of the abridged Semiscale facility. The noding for Tests S-NC-5 and S-NC-6 (Fig. 2) is similar except that an extra hot-leg TEE component allows nitrogen injection just below the steam-generator inlet plenum.

The TRAC-PF1 one-dimensional CORE component is used as part of the overall one-dimensional vessel representation for simplification. Because the height of the Semiscale core is large compared to its horizontal width, the one-dimensional core model works well. Also, the one-dimensional CORE component uses the faster "two-step" numerics, whereas the three-dimensional vessel does not; thus, considerable central-processing-unit (CPU) time is saved. Although the upper head is not modeled in the TRAC model, the capped core support tube and guide tube are modeled explicitly with the TEE components above the CORE component. The draining of the primary system is

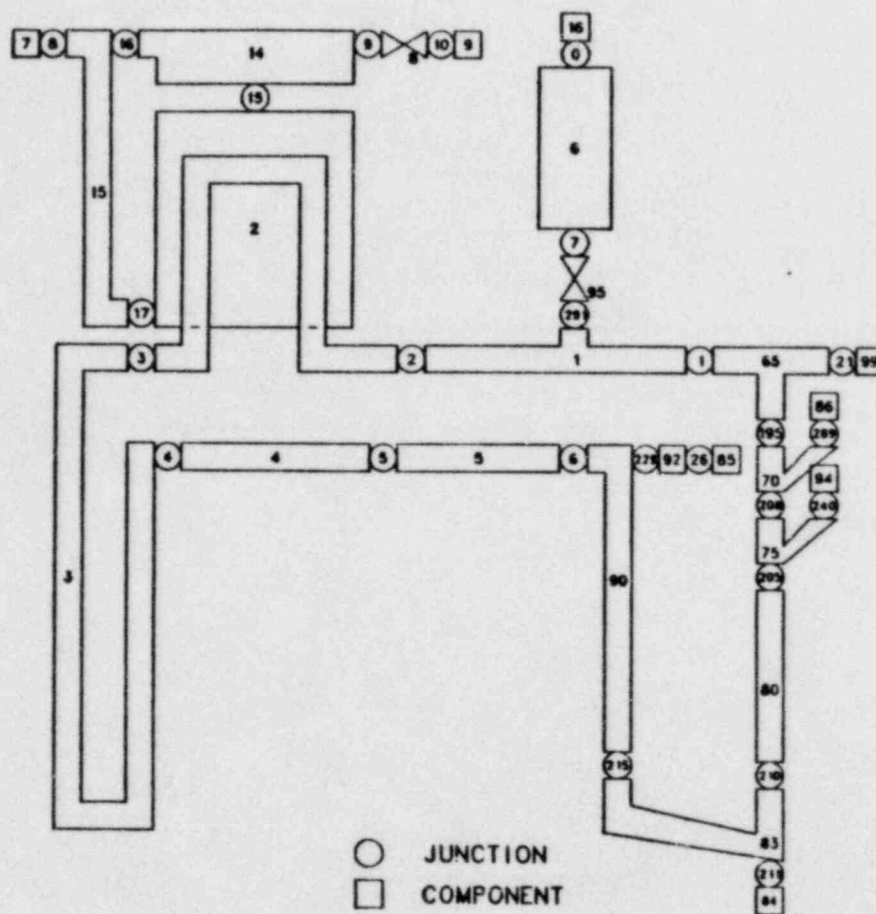
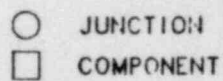


Fig. 1.  
TRAC noding for Semiscale Test S-NC-2B.





12

accomplished with a FILL component attached to the bottom of a TEE that represents the lower plenum.

The recirculation path, steam dome, and main steam-line valve are modeled specifically for the steam-generator secondary side. The steam-line valve, represented by a VALVE component controlled by a trip, maintains a secondary pressure that is within 0.005 MPa of the experiment value. The feedwater is supplied by a FILL component that is controlled by the collapsed level in the steam generator; the feedwater maintains a level of ~9.4 m.

Although the Semiscale external-loop piping heaters are designed to offset the system heat loss, the data indicate that this technique is insufficient for these tests. For example, in the intact-loop pump suction, the heaters generally increase the fluid temperature for these experiments; further, the S-NC-2B experiment data report states that the pump-suction and cold-leg heaters were deactivated when boiling was observed in the steam-generator primary-outlet piping. Accordingly, the TRAC model incorporates both the external heat losses and the external heaters to simulate more accurately the actual experiment. The heater power for each component is taken directly from the experiment data. The heat losses are not specified sufficiently to distribute accurately the heat losses for each component in the model. Yet the distribution and magnitudes of these losses are important for a natural-circulation test. To distribute these losses properly, several steady-state TRAC runs were made and the individual component heat losses were varied until the liquid temperatures throughout the model closely matched those in the data.

When the intact-loop pump is replaced by an spool piece with orifices, the TRAC model represents this section by a two-cell pipe with a large additive friction factor FRIC (on the order of 10) at the second face. Because this orifice does not block the lower half of the pipe, it is impractical to calculate FRIC; instead, FRIC was determined by adjusting its value in several TRAC runs to achieve the test mass flow for the full liquid system at steady state.

The TRAC input model for the Test S-NC-7C (Fig. 3) is similar to those for Tests S-NC-2B, S-NC-5, and S-NC-6. The main difference is that the S-NC-7C model includes the broken loop, which is similar to the intact loop except for two changes. The broken loop has a PUMP component with a locked rotor (that is, no angular velocity). On the secondary side, the steam-line valve is open fully so that the secondary pressure is controlled by a pressure vs time table incorporated into the BREAK component. The reason for using a BREAK rather than a steam-line valve is discussed in Sec. II.C.4. The steam-generator models for this test are changed slightly from the preceding ones to incorporate more recent geometry information in the riser and downcomer sections.

Because the natural-circulation flows, especially reflux, are of such a low magnitude, any spurious flows resulting from elevation errors could mask the true flows. A null transient, where all wall heat transfer is deactivated and any pump is disabled, was run before the TRAC prediction runs.



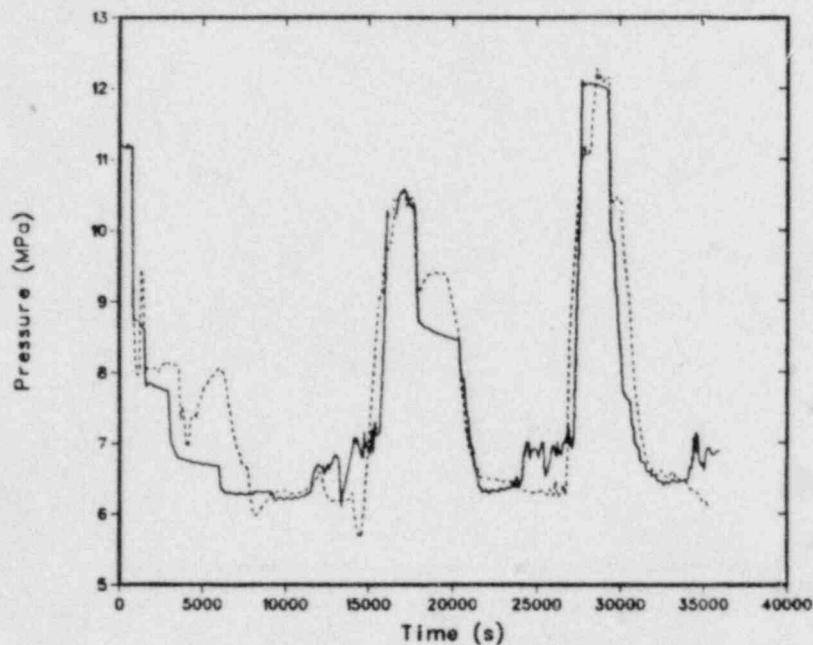


Fig. 4.  
Comparison of the TRAC-calculated and measured pressure histories for Test S-NC-2B.

Figures 5-7 show the hot-leg mass flows as a function of system inventory both for TRAC and for the experiment data. In general, the peak-in-mass flow occurs just before the voids are entrained beyond the tops of the tubes for the steam-generator primary side. For the 30-kW case (Fig. 5), the peak mass flow occurs for a higher system inventory than in the data. However, the magnitude and subsequent behavior are close to that of the data. The TRAC prediction of the mass-flow peak (Fig. 6) occurs at a slightly smaller inventory than in the data. Still, the general prediction compares very well with the data. In the high-power case, 100 kW (Fig. 7), TRAC tracks the data closely.

Figures 8-10 show the primary pressure as a function of system inventory for the three power levels. In all three cases, TRAC does a reasonable job of predicting the system pressure above a 77% inventory. Below that value, the TRAC pressure prediction in the reflux regime is always high because the TRAC-PF1 condensation heat-transfer model underpredicts the heat transfer. When the TRAC-PF1/MOD1 model is used, the system pressure behaves properly. The experiment does not measure the reflux rate.

Overall, the comparison of the S-NC-2B test data with the TRAC-calculated results shows that TRAC predicts well single- and two-phase natural-circulation behavior.



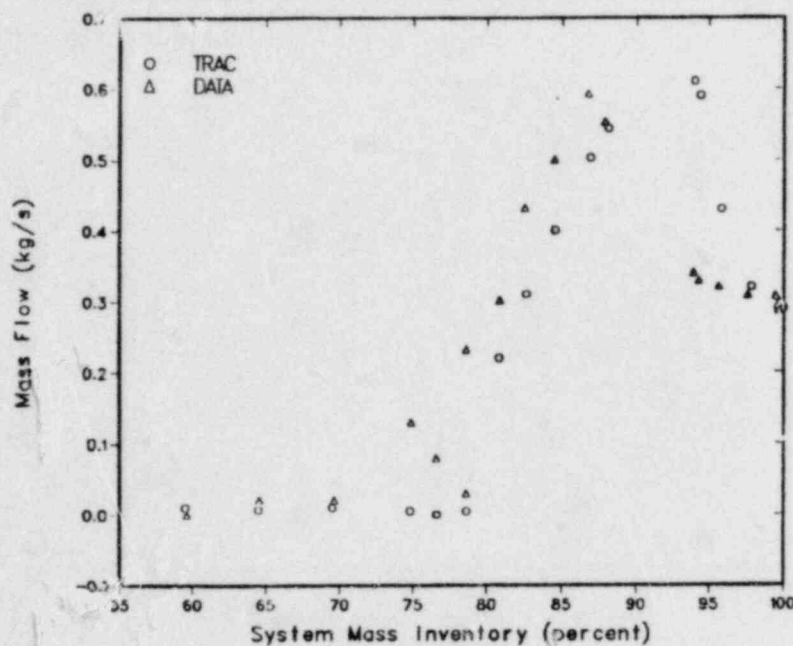


Fig. 5.

Comparison of the TRAC-calculated and measured hot-leg mass flows as a function of system inventory with a nominal 30-kW core power for Test S-NC-2.

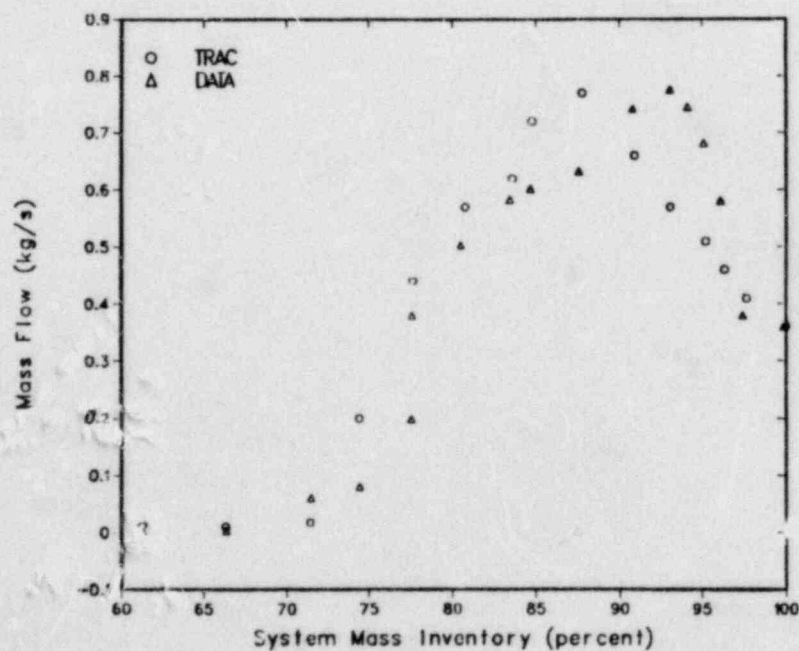


Fig. 6.

Comparison of the TRAC-calculated and measured hot-leg mass flows as a function of system inventory with a nominal 60-kW core power for Test S-NC-2.

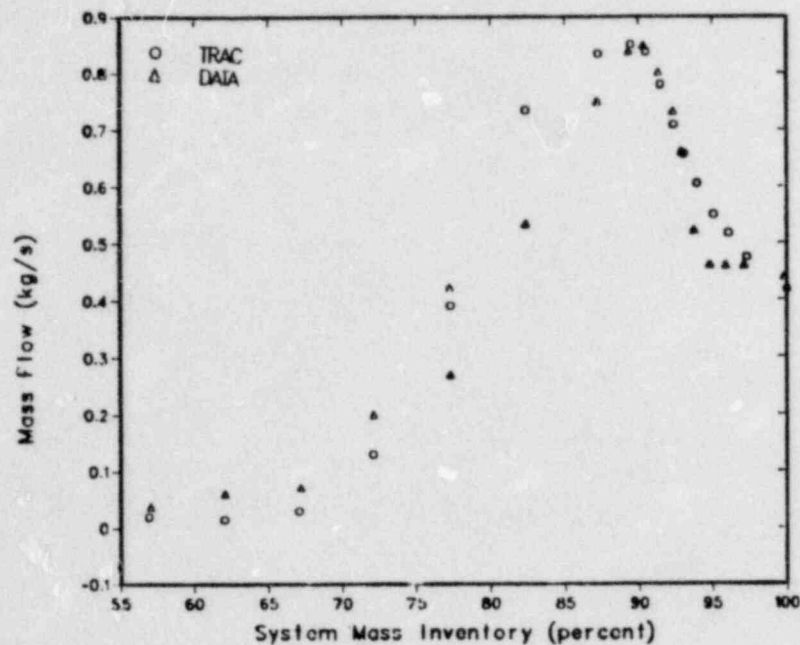


Fig. 7.  
Comparison of the TRAC-calculated and measured hot-leg mass flows as a function of system inventory with a nominal 100-kW core power for Test S-NC-2.

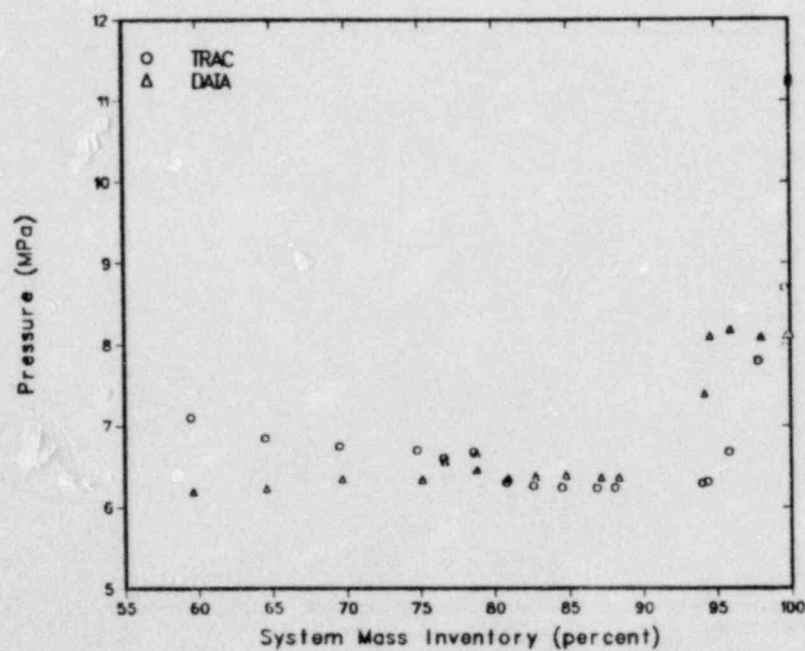


Fig. 8.  
Comparison of the TRAC-calculated and measured primary pressures as a function of system inventory with a nominal 30-kW core power for Test S-NC-2.

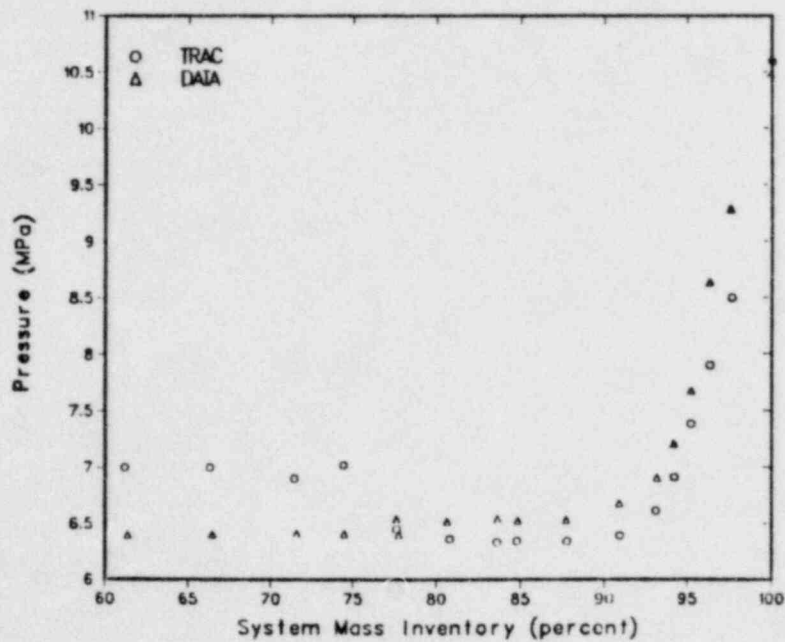


Fig. 9.

Comparison of the TRAC-calculated and measured primary pressures as a function of system inventory with a nominal 60-kW core power for Test S-NC-2.

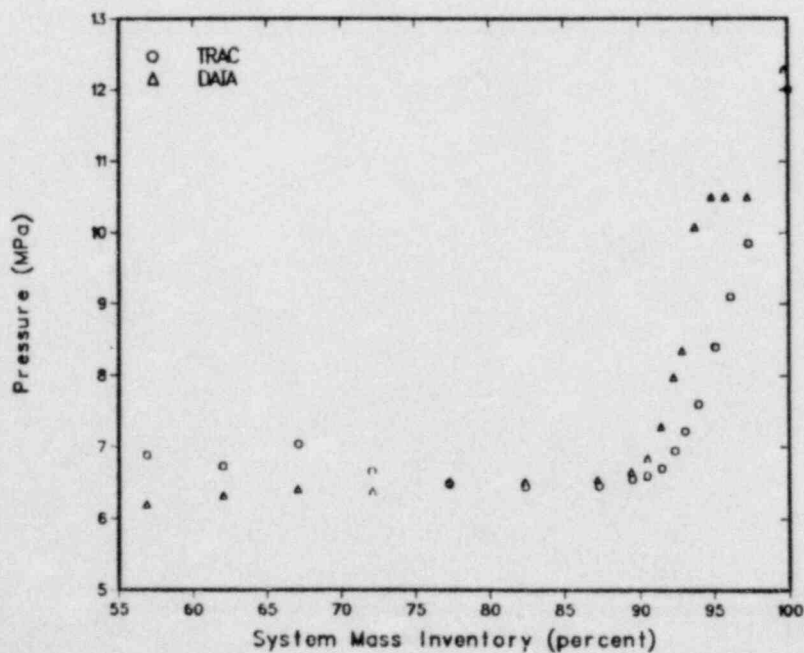


Fig. 10.

The TRAC-calculated and measured primary pressures as a function of system inventory with a nominal 100-kW core power for Test S-NC-2.

2. Test S-NC-5. In Test S-NC-5, nitrogen is injected into the hot leg just below the steam-generator inlet plenum during two-phase natural circulation. Figure 11 compares the measured and TRAC-calculated pressure histories. Figure 12 compares the hot-leg mass flows. Clearly, TRAC correctly predicts the steady-state mass flow, the rise in mass flow after 11.5% of the primary liquid is drained, and the stagnation in the flow when the nitrogen is first injected. However, TRAC cannot predict the mass-flow recovery ~5.5 min after the nitrogen is injected. Consequently, TRAC overpredicts the system pressure for each subsequent nitrogen injection. Loomis and Soda<sup>8</sup> claim that in the experiment the nitrogen bubble, which blocks the top of the steam-generator tubes, is compressed by the increasing system pressure until a bridging of the flow reestablishes natural circulation. Certainly, if this were the case, TRAC should be able to predict that phenomenon and duplicate the experiment. We believe that the nitrogen in the experiment was carried away from the top of the steam-generator tubes by other means, either entrainment or dissolution in the water. At first we thought that the TRAC interfacial drag was insufficient to entrain the nitrogen and to carry it away from the top of the steam-generator tubes. Therefore, the interfacial drag coefficients, bubble and droplet, were increased by a factor of 10 000, which effectively increased the drag by 100. Figures 13 and 14 show the results obtained from this change for only one nitrogen injection; the drag was increased where stagnation occurred in the flow. With the drag increased, the flow-recovery prediction is correct and the pressure prediction improves. However, running TRAC with such a high drag causes severe oscillations (Fig. 14). Therefore, the experiment was studied

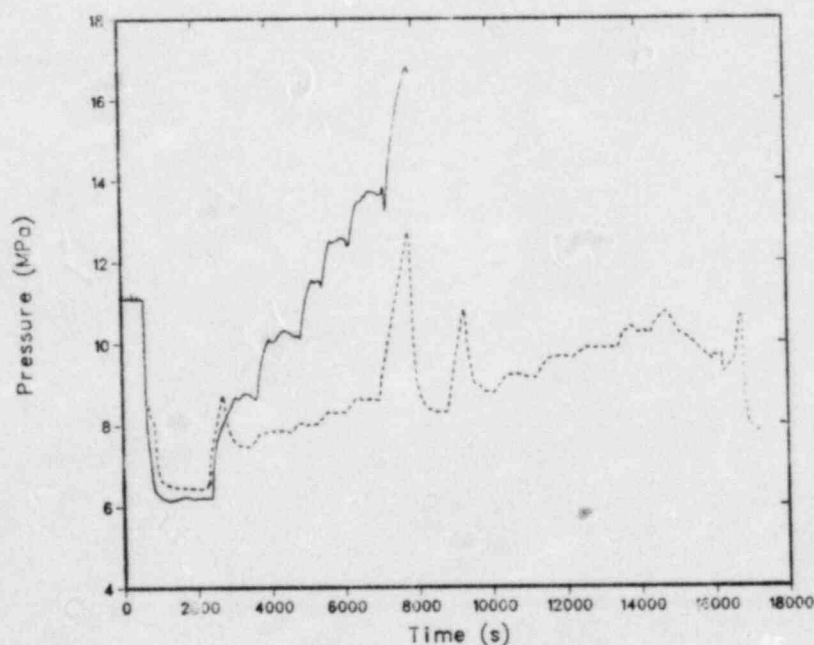


Fig. 11.  
Comparison of the TRAC-calculated and measured pressure histories for Test S-NC-5.



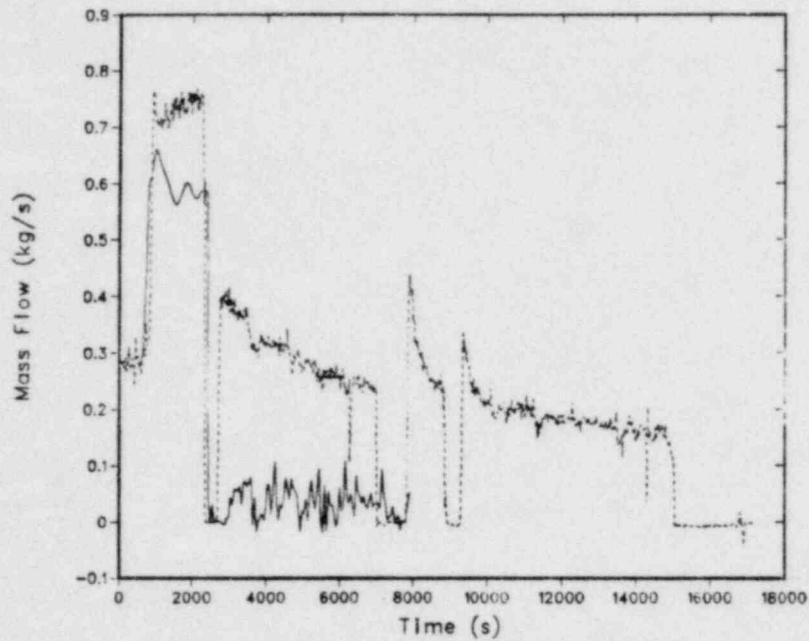


Fig. 12.

Comparison of the TRAC-calculated and measured hot-leg mass flows for Test S-NC-5.

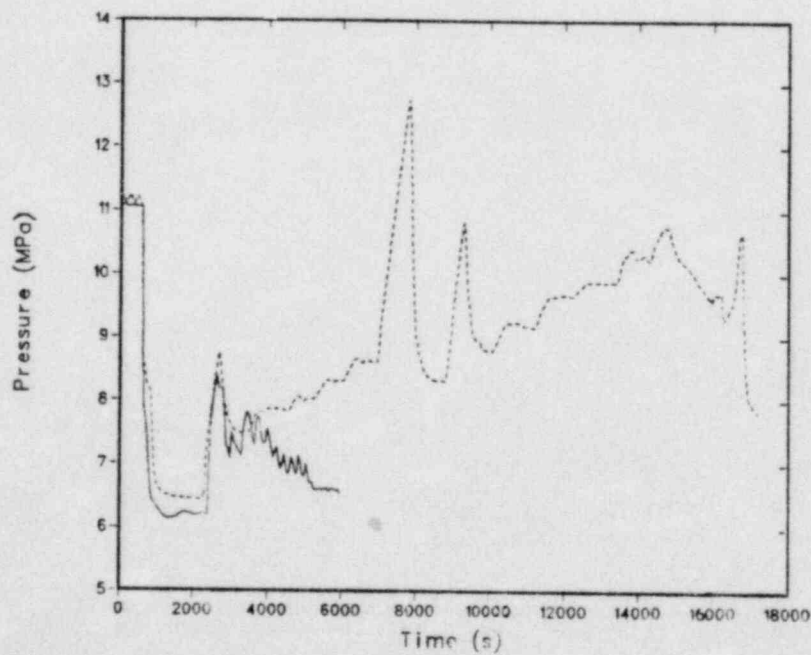


Fig. 13.

Comparison of the TRAC-calculated and measured pressures for Test S-NC-5 with the TRAC interfacial drag increased by a factor of 100.

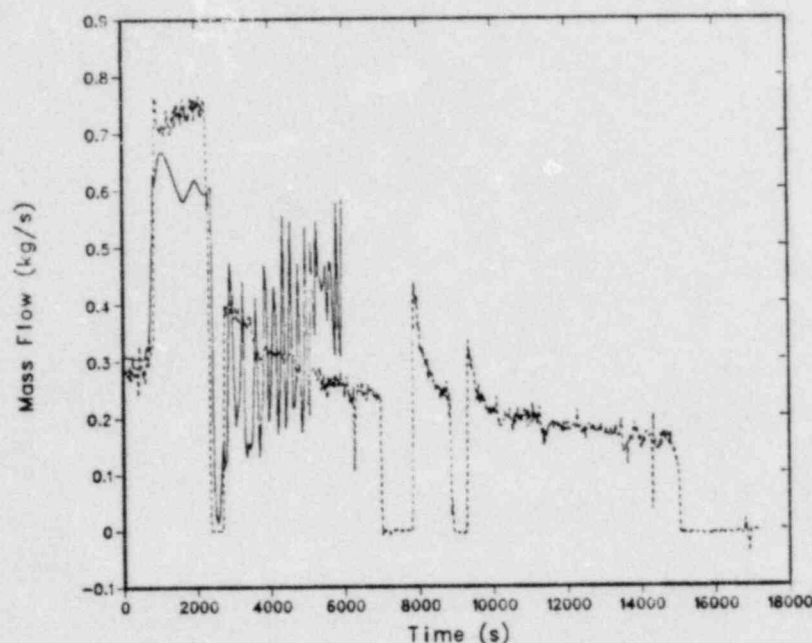


Fig. 14.

Comparison of the TRAC-calculated and measured mass flows for Test S-NC-5 with the TRAC interfacial drag increased by a factor of 100.

to find other ways to remove the nitrogen blockage in the steam-generator tubes. Currently, we think that a significant portion of the nitrogen may have dissolved into the water during the ~5.5 min of stagnation. The TRAC-predicted partial pressure is 264 psia with a 523F° temperature when the flow should be reestablished. In the TRAC predictions, which are not at equilibrium, Henry's law coefficient is ~0.3 psia/cc-solute/kg-water (obtained from Fig. 5 in Ref. 9). From Henry's law, the nitrogen concentration should be ~881.0 cm<sup>3</sup>-nitrogen/kg-water at equilibrium. The first nitrogen injection is 2020.1 cm<sup>3</sup>. Obviously, this rough analysis with nonequilibrium quantities implies that a significant portion of the nitrogen could have dissolved into the water in the experiment and could have reduced the blockage in the top of the steam-generator tubes. In fact, one TRAC run was made with only half of the prescribed nitrogen injection; the prediction went smoothly and the flow reestablished at the time shown in the data. In addition to the primary water available for nitrogen dissolution in the steam generator, the delta-P taps contain cold water at high pressure that should have a greater affinity for nitrogen. In any event, the current TRAC version cannot model the dissolution of a noncondensable gas into the liquid.

3. Test S-NC-6. The TRAC run for Test S-NC-6 tracks the experiment data as closely as possible. Figure 15 compares the measured and TRAC-calculated pressure histories. In addition to the TRAC and data curves, a third dotted curve plots the pressure history obtained from the TRAC-PF1 condensation heat-transfer model. Because this model underestimates the heat transfer, it maintains an excessive primary pressure during reflux. The TRAC

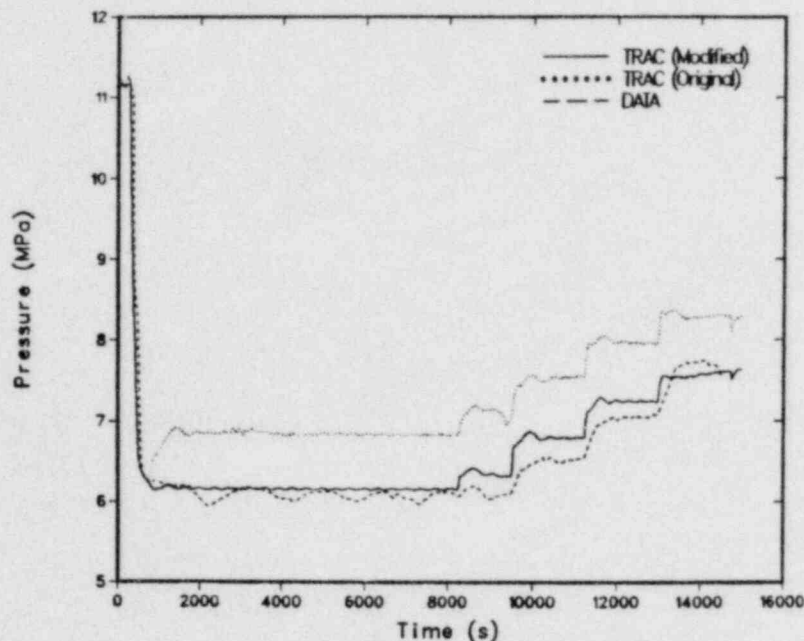


Fig. 15.

Comparison of the TRAC-calculated and measured pressure histories for Test S-NC-6.

predictions for this experiment are based on an update of the TRAC-PF1 code that uses the TRAC-PF1/MOD1 model. The solid curve in Fig. 15 shows that the updated condensation heat-transfer model substantially improves the TRAC pressure prediction.

Figure 16 shows the reflux rate as a function of the injected nitrogen (air in the case of TRAC) for the upside of the steam generator. The circular and triangular symbols represent the individual reflux rates for TRAC and for the data, respectively. The dashed line is the maximum vapor flow rate into the steam generator, and thus the maximum reflux rate for the TRAC prediction; the chain-dot line is the maximum reflux rate for the data. When there is no nitrogen in the system, the TRAC prediction and the data are quite close but the TRAC prediction is ~10% lower. When nitrogen constitutes 0.86% of the primary volume, the TRAC prediction and the data are even closer; the TRAC prediction is only 3% higher than the data. When the nitrogen volume is 2.98% or higher, both the TRAC prediction and the data have reached the maximum reflux rate, but the TRAC prediction is ~20% higher. No data for the downside of the steam generator exist, but Fig. 17 shows the TRAC prediction. The dashed line represents the maximum reflux rate, and the circular symbols represent the individual reflux rate. When there is no nitrogen in the system, slightly more than half of the reflux flow occurs in the downside of the steam generator. This value is the same as that observed in the experiment.<sup>9</sup> As the amount of nitrogen increases, more of the reflux occurs in the upside of the steam generator. When the nitrogen volume is 2.98% or above, all the reflux occurs in the upside of the steam generator.

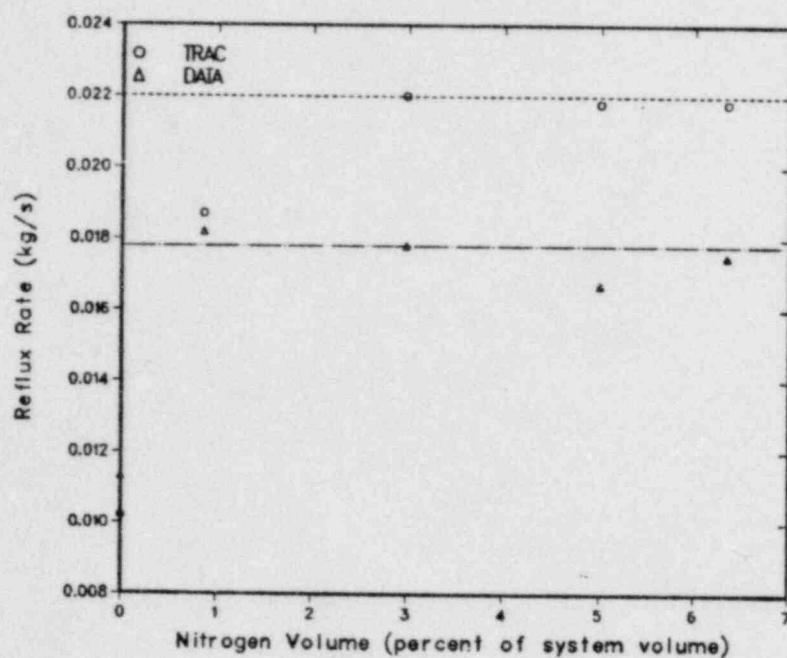


Fig. 16.  
Comparison of the TRAC-calculated and measured reflux rates as a function of the injected nitrogen for the upside of the steam generator for Test S-NC-6.

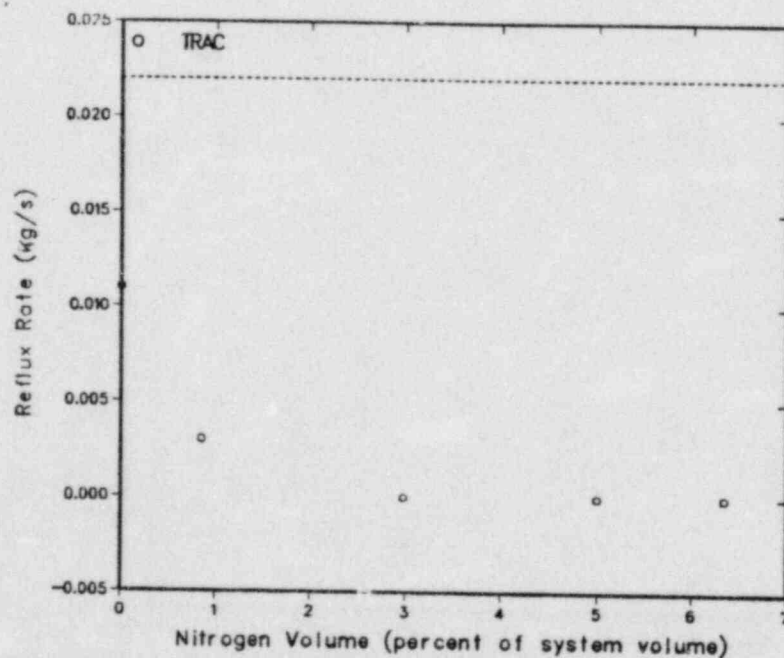


Fig. 17.  
The TRAC-calculated reflux rate as a function of the injected nitrogen for the downside of the steam generator for Test S-NC-6. The dashed line represents the maximum reflux rate, and the circular symbols represent the individual reflux rate.



Currently, we cannot explain the higher TRAC-predicted maximum reflux rate. One possible cause may be that the TRAC model does not model exactly the way in which the reflux liquid is removed from the system and then replaced. In the TRAC model, the reflux liquid simply is allowed to run unimpeded into the core. An alternative possibility is that a significant portion of the nitrogen is dissolved in the water, and is thus removed from the reflux region.

4. Test S-NC-7C. Figures 18 and 19 compare the TRAC-calculated and measured primary pressure histories and the broken-loop steam-generator secondary-side pressure histories, respectively, for Test S-NC-7C. The TRAC-predicted pressure (Fig. 18) drops rapidly when the system drains.

By the final system drain, the TRAC prediction is close to the experiment data. The TRAC broken-loop steam-generator secondary-side pressure (Fig. 19) tracks the data because of a controlling BREAK component. In the preliminary runs for this experiment, the secondary pressure was maintained at a constant pressure with a steam control valve; from these runs, it became obvious that the secondary pressure has a significant effect on the split of the mass flow between the intact and broken loops. Thus, for the runs presented here, the secondary pressure for the broken-loop steam generator only is controlled by a BREAK component. The intact-loop steam-generator secondary-side pressure is maintained by a steam control valve. Figures 20 and 21 compare the mass flows in the intact- and broken-loop cold legs, respectively. Obviously, the TRAC code fails to predict the proper

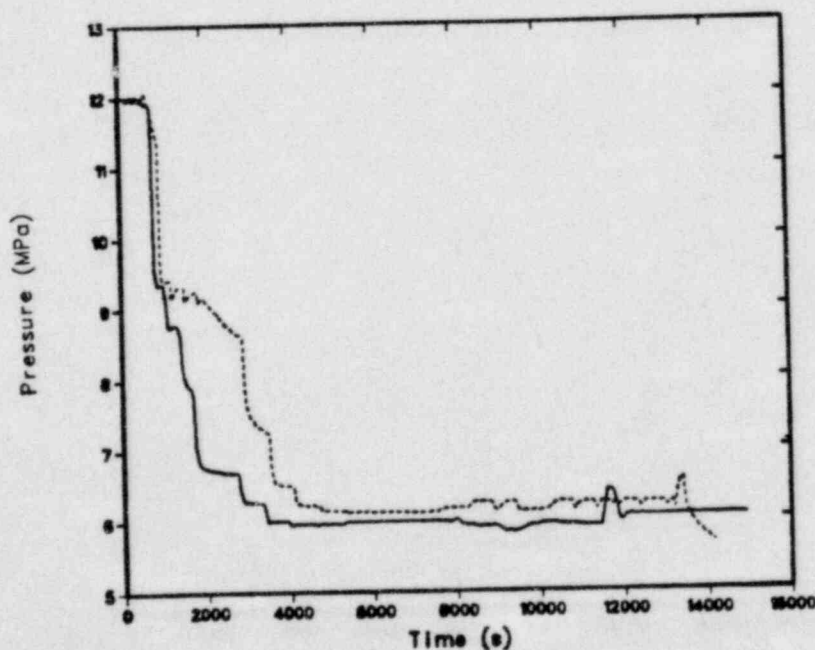


Fig. 18.

Comparison of the TRAC-calculated and measured primary pressure histories for Test S-NC-7C.

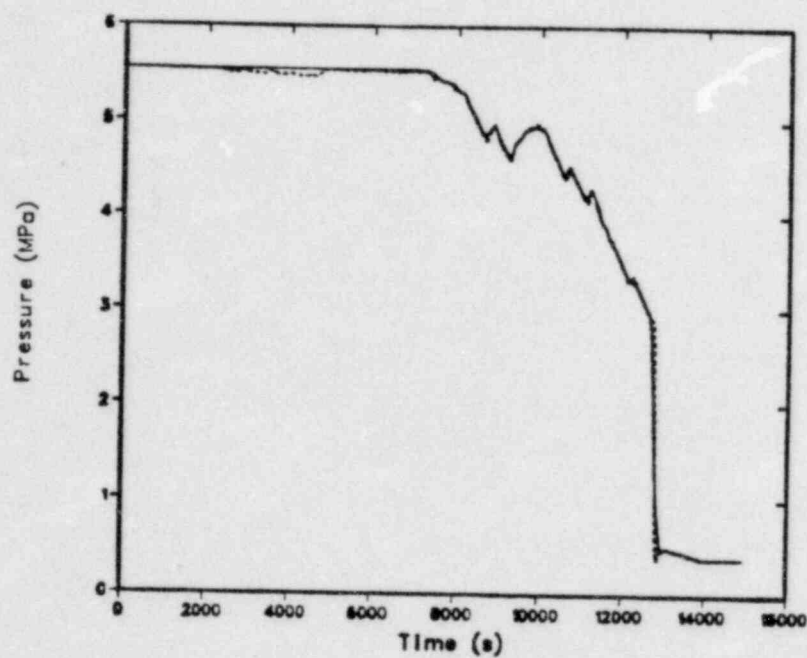


Fig. 19.  
Comparison of the TRAC-calculated and measured broken-loop steam-generator secondary-side pressure histories for Test S-NC-7C.

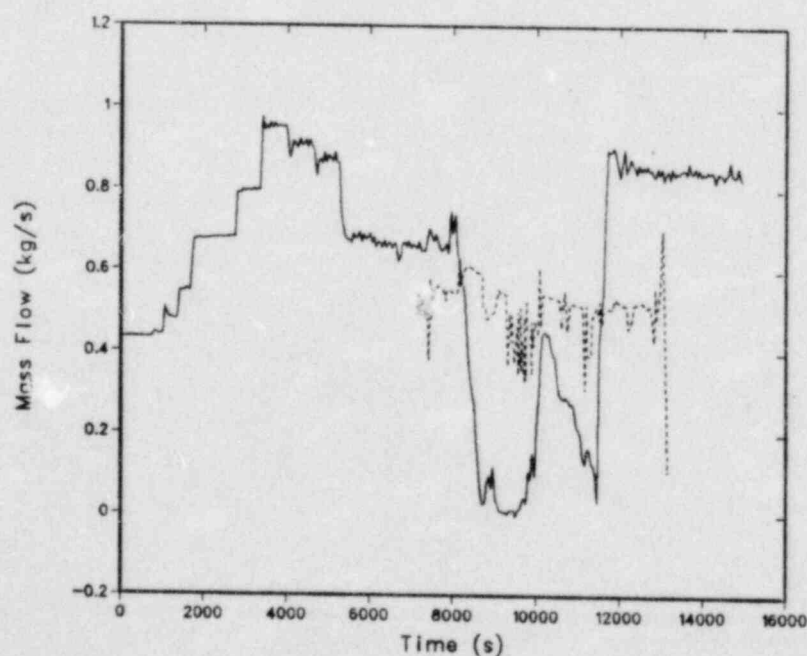


Fig. 20.  
Comparison of the TRAC-calculated and measured intact-loop cold-leg mass flows for Test S-NC-7C.

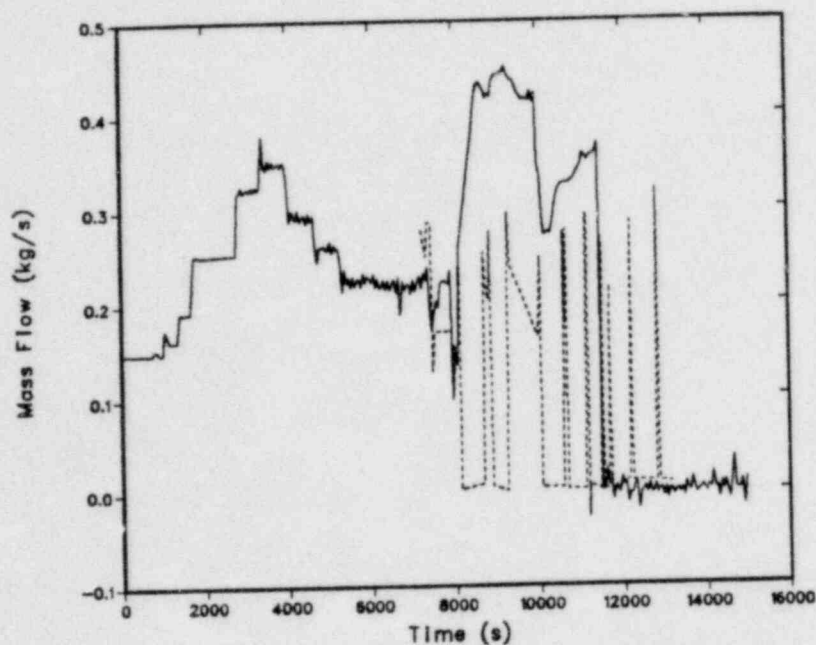


Fig. 21.

Comparison of the TRAC-calculated and measured broken-loop cold-leg mass flows for Test S-NC-7C.

oscillations in the flow split observed in the experiment for system inventories below 7% when the broken-loop steam-generator level is varied. This discrepancy was anticipated because some of the characteristics of these oscillations are attributed to the differences in height of the broken-loop steam-generator tubes.<sup>8</sup> The code models only a single average tube. This may also be the reason why no decoupling is calculated by TRAC between the intact and broken loops. Figures 22, 23, and 24 summarize the mass flows for the TRAC prediction and the experiment for system inventories above 70%; the circular symbols represent the TRAC prediction, whereas the triangular symbols represent the data. For the intact loop, the TRAC predictions for this experiment are good. For the broken loop, the peak in the TRAC prediction is higher and occurs at a larger inventory than in the data. Because the broken loop represents such a small amount of the mass flow compared to that in the intact loop, the TRAC-predicted downcomer mass flow compares favorably with the data; however, the peak in the TRAC prediction does occur at a higher inventory.

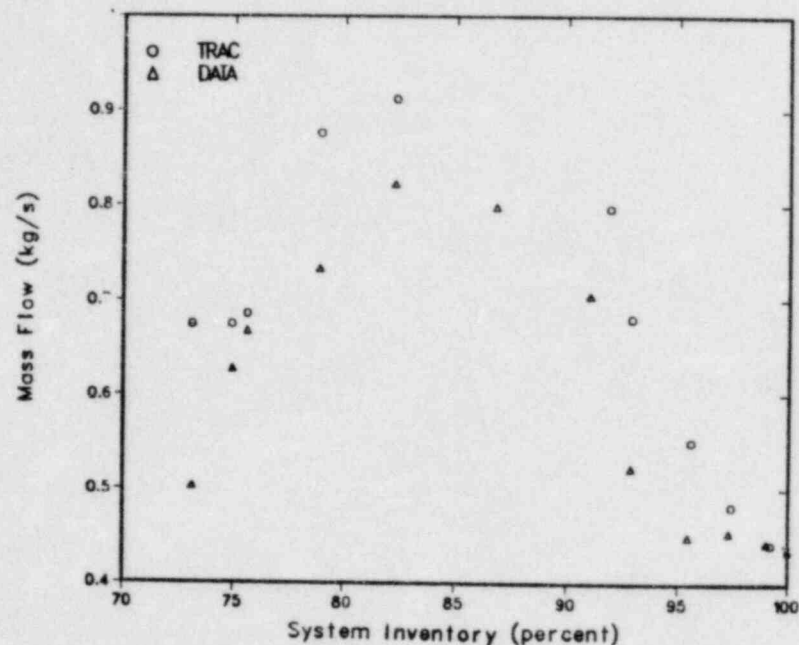


Fig. 22.  
Comparison of the TRAC-calculated and measured intact-loop mass flows for system inventories above 70% for Test S-NC-7C.

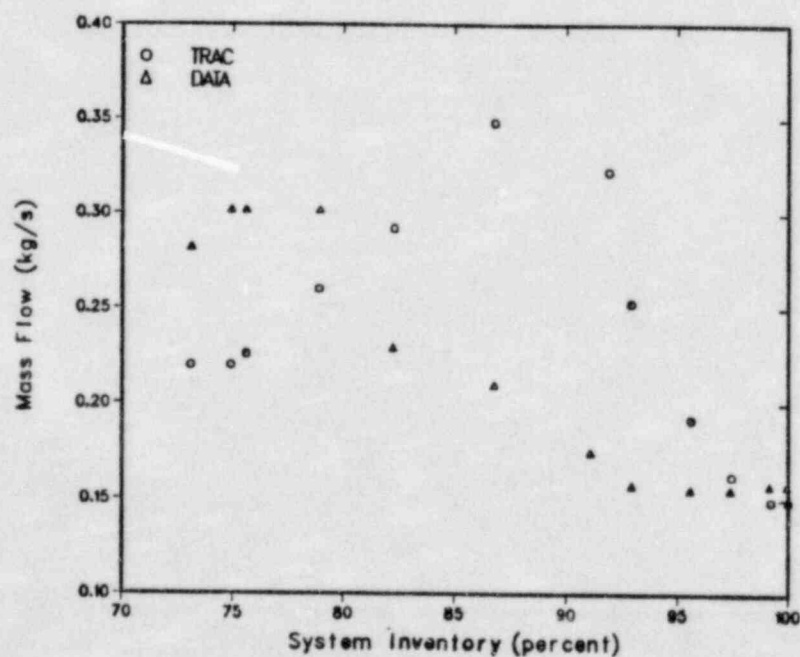


Fig. 23.  
Comparison of the TRAC-calculated and measured broken-loop mass flows for system inventories above 70% for Test S-NC-7C.



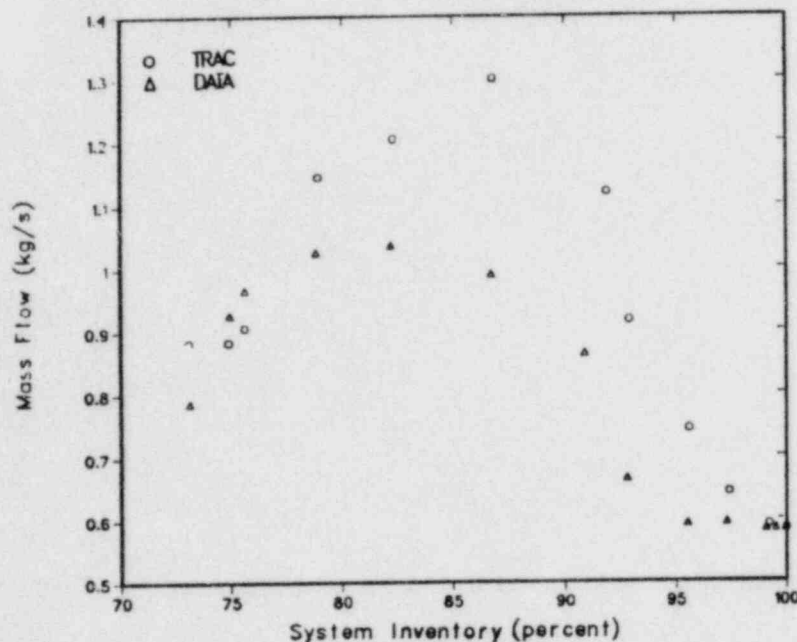


Fig. 24.

Comparison of the TRAC-calculated and measured downcomer mass flows for system inventories above 70% for Test S-NC-7C.

#### D. Conclusions

Overall, the TRAC predictions for the Semiscale natural-circulation tests in this report are good. The results for Test S-NC-2B show that TRAC can predict single- and two-phase natural circulation. From Test S-NC-6, it is obvious that TRAC can model reflux behavior adequately even though the input model may require refinement to simulate this particular experiment better. The S-NC-7C test results show that TRAC can predict adequately natural circulation in a two-loop system even though the model for this experiment may require some refinement. However, in experiments where a noncondensable gas may be dissolved in the liquid, as occurs in Test S-NC-5, TRAC may have difficulty because the code has no provision for the dissolution of gasses in the liquid.

### III. TRAC-PF1 POSTTEST ANALYSIS OF SEMISCALE TEST S-UT-2

An experiment conducted in the Semiscale Mod-2A facility at INEL has been selected as one element in the TRAC-PF1 assessment program. The test selected was S-UT-2, which simulated a small-break LOCA resulting from a 10% communicative break in the cold leg of a PWR. The test included upper-head injection (UHI). TRAC-PF1 (Ref. 10) is the latest version of the TRAC computer code developed for predicting LOCA events in a PWR. While retaining all the essential features of earlier code versions, TRAC-PF1 specifically was developed as a fast-running version for long transients such as small-break LOCAs.

Several Semiscale small-break LOCA experiments were used earlier in the developmental assessment of TRAC-PF1.\* However, these experiments were run with the Semiscale facility in the Mod-3 configuration. Test S-UT-2 was run after the Semiscale facility was modified to the Mod-2A configuration. Therefore, it was necessary to modify the existing TRAC-PF1 model before performing assessments. Detailed assessment results for UHI Test S-UT-2 are presented, as well as results of a parametric study.

#### A. Semiscale Mod-2A System Description

The Semiscale Mod-2A system<sup>11,12</sup> is a scaled integral test facility at INEL used to obtain thermal-hydraulic data for a variety of postulated transients and operating conditions. The Mod-2A system (Fig. 25) is a two-loop PWR primary-coolant-system simulator. The intact loop is scaled to simulate three loops of a large PWR, and the broken loop simulates a single loop in which a break is postulated to occur. Geometric similarity has been maintained between a PWR and Mod-2A, most notably in the design of a full-length (3.66-m) electrically heated core, full-length upper plenum and upper head, component layout, and relative elevations of various components. The instrument spool pieces for the cold-leg break tests are identified as circled numbers in Fig. 26. Major configuration changes between the Mod-2A configuration and the previous Mod-3 configuration resulted from:

1. installation of a new intact-loop steam generator,
2. modification of the broken-loop steam generator,
3. installation of insulation inside the downcomer and lower pressure vessel plenum, and
4. addition of external heaters on the outside surfaces of the coolant piping. These heaters were not operated for Test S-UT-2.

\*This information was provided by M. S. Sahota, Los Alamos National Laboratory, Energy Division, Safety Code Development Group (January 1982).

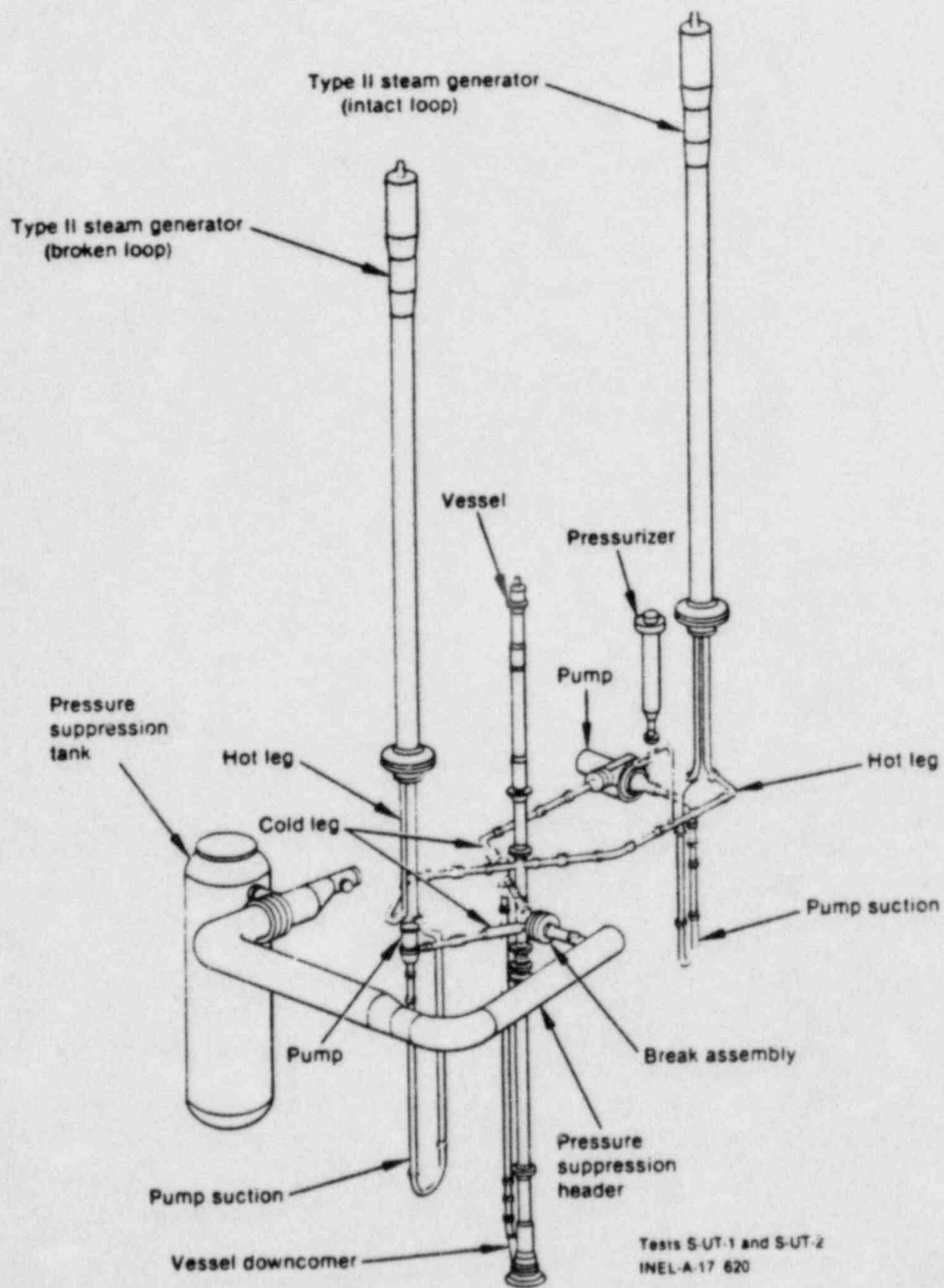


Fig. 25.  
Semiscale Mod-2A system isometric (cold-leg-break configuration).

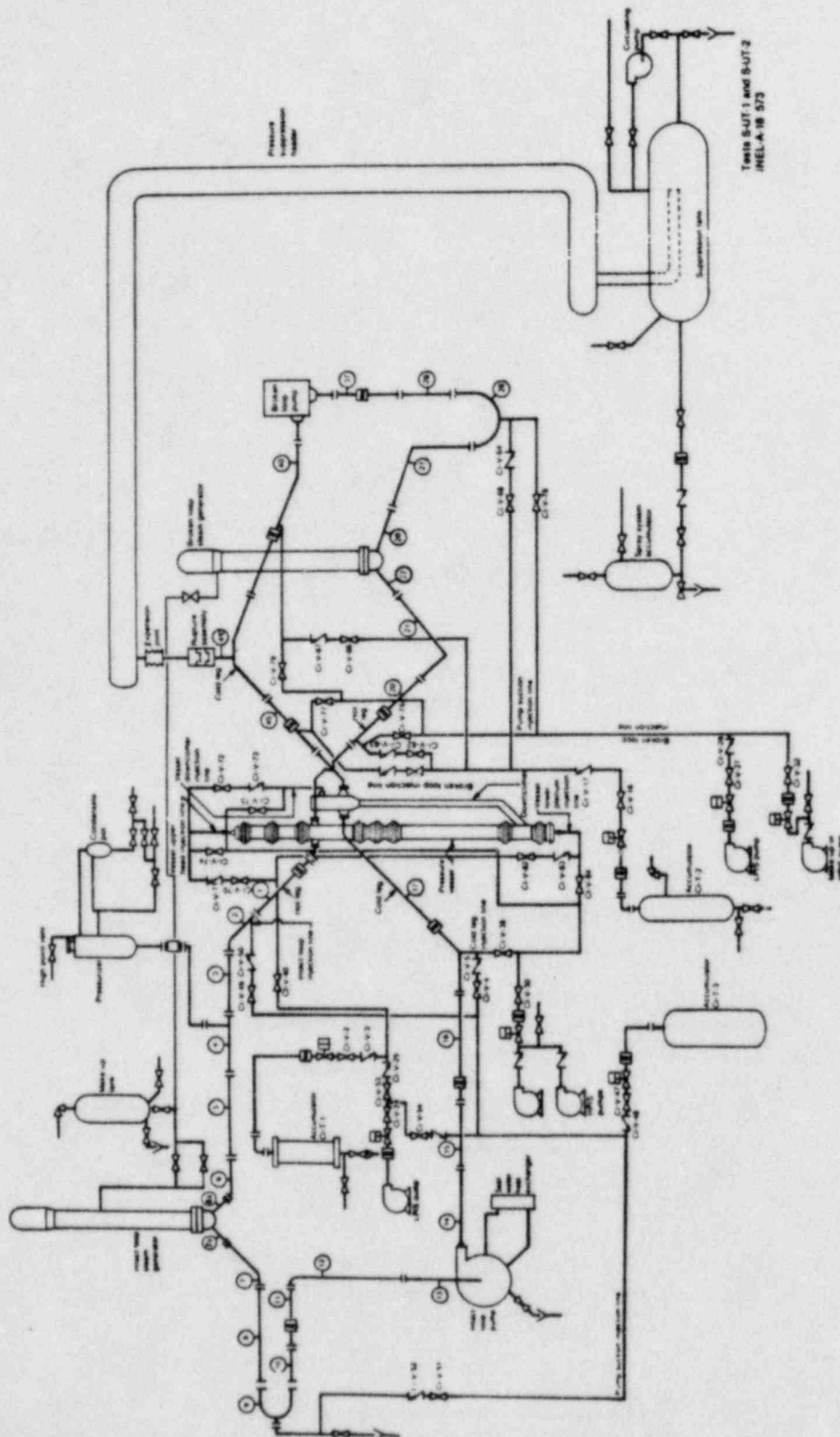


Fig. 26.  
Semiscale Mod-2A system for cold-leg-break configuration--schematic.



## B. Test Description

Semiscale small-break Test S-UT-2 (Ref. 13) simulated a LOCA resulting from a 10% communicative break in the cold leg of a PWR. The primary objective was to investigate the distribution of UHI water (and its influence on transient behavior) through comparisons between Semiscale Mod-2A Tests S-UT-1 and S-UT-2. The break size for each test was  $0.2278 \text{ cm}^2$ , which was volumetrically scaled to represent a 22.2-cm-diam pipe break in a PWR. The Mod-2A system for Test S-UT-2 was configured to simulate a PWR with ECC injection into the vessel upper head. The upper-head accumulator was pressurized to 8.5 MPa and the loop accumulator pressures were set at 2.98 MPa, as is nominally specified for UHI plants. The initial test conditions were equivalent to or scaled from typical PWR operating conditions. The tests were conducted as specified.<sup>14</sup>

## C. TRAC Version

All calculations were performed using TRAC-PF1 7.0/EXTUPD 7.6.\*

## D. TRAC Model

The TRAC input model for the Semiscale Mod-2A facility is shown in Figs. 27 and 28 in its cold-leg-break configuration. The input model consisted of 49 one-dimensional components containing a total of 198 computational cells. Table I lists the components. The input model corresponded to the Semiscale Mod-2A hardware configuration with the following exceptions.

1. The pressure-suppression system was modeled indirectly. A BREAK component was introduced, and the pressure and temperature at the break were specified as boundary conditions.
2. The secondary feedwater systems, both main and auxiliary, were represented by FILL components 7 and 26 for the intact and broken loops, respectively.
3. The high-pressure injection system (HPIS) was represented by FILL components 13 and 43 for the intact and broken loops, respectively.
4. The UHI coolant was delivered at a discrete elevation in the upper head, but the physical system was designed to distribute the coolant uniformly over the full height of the upper head.

---

\*This information was provided by Thad D. Knight, Los Alamos National Laboratory, Energy Division, Safety Code Development Group (June 1982).

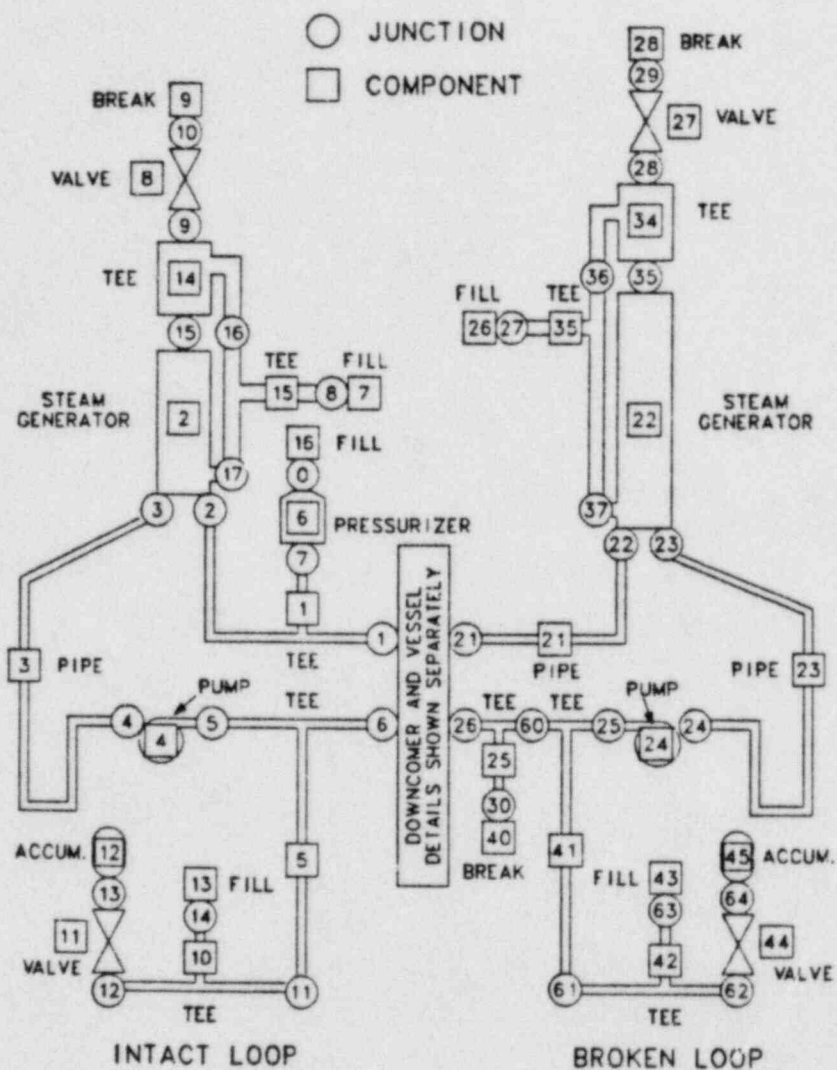


Fig. 27.  
TRAC input model for the Semiscale Mod-2A facility.

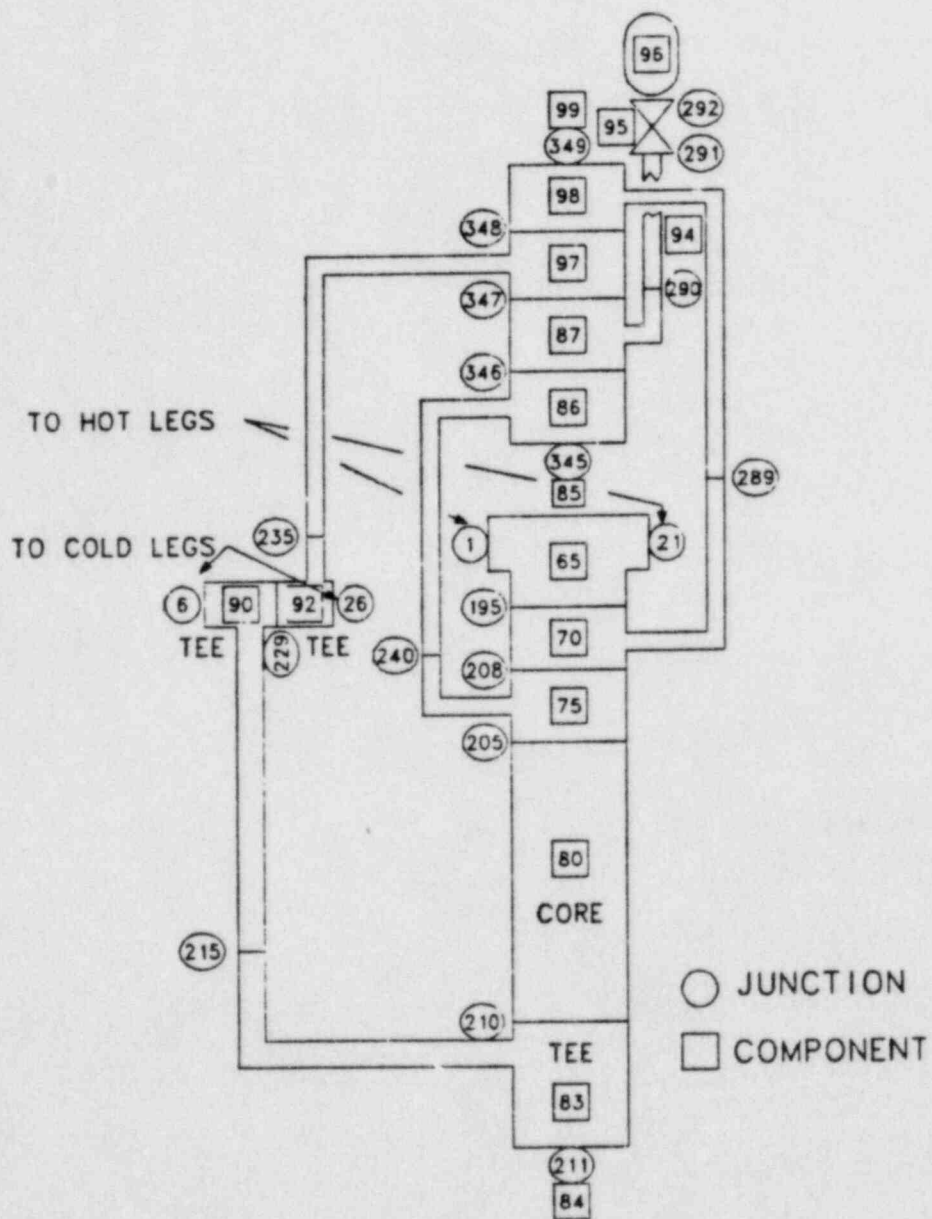


Fig. 28.  
TRAC downcomer and vessel noding for the Semiscale Mod-2A facility.

TABLE I  
TRAC MODEL COMPONENTS

Component Number <sup>a</sup>	Component Type	Description	Number of Fluid Cells (Primary Side Secondary Side) <sup>b</sup>
1	TEE	Intact-loop hot leg	6, 3
2	STGEN	Intact-loop steam generator	12, 6
3	PIPE	Intact-loop pump suction	8
4	PUMP	Intact-loop pump	2
5	TEE	Intact-loop cold leg	5, 1
6	PRIZER	Intact-loop pressurizer	5
7	FILL	Intact-loop steam-generator feedwater	1
8	VALVE	Intact-loop steam line	2
9	BREAK	Intact-loop steam-generator-secondary pressure set point	1
10	TEE	Intact-loop ECC line	2, 1
11	VALVE	Intact-loop accumulator valve	2
12	ACCUM	Intact-loop accumulator	4
13	FILL	Intact-loop high-pressure injection system	1
14	TEE	Intact-loop steam-generator-secondary steam dome	2, 1
15	TEE	Intact-loop steam-generator-secondary downcomer	6, 1
16	FILL	Pressurizer inlet	1
21	PIPE	Broken-loop hot leg	5
22	STGEN	Broken-loop steam generator	12, 6
23	PIPE	Broken-loop pump suction	7
24	PUMP	Broken-loop pump	2
25	TEE	Broken-loop cold leg	3, 2
26	FILL	Broken-loop steam-generator feedwater	1
27	VALVE	Broken-loop steam line	2
28	BREAK	Broken-loop steam-generator-secondary pressure set point	1
34	TEE	Broken-loop steam-generator-secondary steam dome	2, 1
35	TEE	Broken-loop steam-generator-secondary downcomer	6, 1
40	FILL, BREAK	Fill for steady-state run, break for transient run	1
41	TEE	Broken-loop cold leg	2, 1
42	TEE	Broken-loop ECC line	2, 1
43	FILL	Broken-loop HPIS	1
44	VALVE	Broken-loop accumulator valve	2
45	ACCUM	Broken-loop accumulator	4



TABLE 1 (cont.)

Component Number <sup>a</sup>	Component Type	Description	Number of Fluid Cells (Primary Side Secondary Side) <sup>b</sup>
65	TEE	Upper section of upper plenum	1, 1
70	TEE	Middle section of upper plenum	1, 2
75	TEE	Lower section of upper plenum and guide and core support tubes	1, 1
80	CORE	Core	9
83	TEE	Lower plenum and lower downcomer	3, 2
84	FILL	Bottom lower plenum	1
85	FILL	Bottom upper head	1
86	TEE	Lower section of upper head	1, 2
87	TEE	Lower mid section of upper head	1, 2
90	TEE	Intact-loop side downcomer inlet and downcomer	2, 10
92	TEE	Broken-loop side downcomer inlet and upper-head bypass	2, 1
94	PIPE	Upper-head injection tube	2
95	VALVE	Upper-head injection valve	2
96	ACCUM	Upper-head injection accumulated	4
97	TEE	Middle upper section of upper head	1, 2
98	TEE	Upper section of upper head	2, 2
99	FILL	Top upper head	1

<sup>a</sup>The total number of components is 49.

<sup>b</sup>The total number of cells is 198.

The TRAC-PF1 choked-flow model was used to calculate the break flow. The break orifice had a sharp entrance with a length-to-diameter ratio of 0.27 (length, 1.45 mm; diameter, 5.38 mm). The secondary side of break TEE 25 for this test was modeled using two cells with the second cell representing the break orifice.

A new pipe material was defined for the downcomer tube (TEE 90 secondary) and the vessel lower plenum (TEE 83) to simulate the thermal conductivity of a composite steel wall clad with honeycomb insulation. Primary-system heat losses to the environment were set to the values reported in Ref. 15. The intact- and broken-loop steam generators were modified to reflect the geometry and heat-transfer characteristics of the Type-II steam generator installed in the Mod-2A facility.

The primary data base for the input model geometric specifications included the system design description,<sup>11,12</sup> the Semiscale Mod-3 drawings,<sup>16</sup> and the RELAP5 standard model description for the Semiscale Mod-2A system.<sup>17</sup>

The data base for the initial and boundary conditions incorporated in the TRAC input model included the experiment data report<sup>13</sup> and the quick-look report.<sup>18</sup>

#### E. Results

The following sections present and discuss results obtained during posttest calculations of Semiscale Mod-2A Test S-UT-2. The counterpart non-UHI test (S-UT-1) was not calculated as part of the assessment activity but will be included in the assessment set for TRAC-PF1/MOD1.

1. General System Behavior. The initial conditions and specified test parameters for Test S-UT-2 are presented in Table II. The intact- and broken-loop flows differ from those measured, and further loop flow balancing could be performed. The calculated and measured primary-loop temperatures compare well.

Table III presents the calculated event times for the base and parametric cases. The latter varies from the former in the use of two multipliers on the critical flow model. The first multiplier (value 3.5) increased the break flow during the subcooled and two-phase blowdown phases. The second multiplier (value 0.45) decreased the break flow for the remainder of the transient. The intent of the parametric study was to specify the measured break flow (or a

TABLE II  
TEST S-UT-2 INITIAL CONDITIONS

<u>Parameter</u>	<u>Actual</u>	<u>Calculated</u>
Core Power (MW) <sup>a</sup>	1.907	1.907 <sup>b</sup>
Pressurizer pressure (MPa)	15.55	15.55 <sup>b</sup>
Pressurizer liquid mass (kg)	10.4	10.2
Intact-loop flow (l/s)	10.6	9.6
Intact-loop cold-leg temperature (K)	557.	556.3
Intact-loop hot-leg temperature (K)	590.	589.6
Broken-loop flow (l/s)	3.6	4.3
Broken-loop cold-leg temperature (K)	558.	558.5
Broken-loop hot-leg temperature (K)	590.	589.6
Intact-loop pump speed (rad/s)	225.4	235. <sup>b</sup>
Broken-loop pump speed (rad/s)	1714.	1830. <sup>b</sup>
Intact-loop steam-generator-secondary pressure (MPa)	5.74	5.45 <sup>b</sup>
Intact-loop steam-generator-secondary feedwater temperature (K)	501.	501. <sup>b</sup>
Broken-loop steam-generator-secondary pressure (MPa)	5.78	4.71 <sup>b</sup>
Broken-loop steam-generator-secondary feedwater temperature (K)	501.	501. <sup>b</sup>

<sup>a</sup>Flat radial profile.

<sup>b</sup>Specified as input parameter.

TABLE 111  
TEST S-UT-2 EVENTS

Event	Time (s)		
	Actual	Base Case	Parametric Case
Pressure trip	5.6	4.4	4.0
Intact-loop main-feedwater valves begin to close	6.4	4.4	3.9
Broken-loop main-feedwater valves begin to close	6.2	5.0	4.5
Intact-loop main-steam valves begin to close	6.4	5.1	4.8
Broken-loop main-steam valves begin to close	6.4	4.9	4.5
Intact-loop pump coastdown initiated	7.3	6.6	5.8
Broken-loop pump coastdown initiated	7.6	6.4	6.0
Upper-head injection begins	17.	19.6	17.8
Intact-loop pump-suction downflow leg clears	73.	77.	56.
Upper-head accumulator injection ends	155.	140.	105.
Intact-loop accumulator injection begins	345.	301.	341.

intent of the parametric study was to specify the measured break flow (or a close approximation) as a boundary condition. However, because a reliable break flow measurement was not available, the multipliers were chosen to produce a calculated pressure history close to the measured pressure history. The multipliers are not interpreted to have a physical meaning (for example, discharge coefficients). Small variations from the measured timing were calculated during the first 10 s of the base-case transient, but the variations are not considered significant. The calculated time of intact-loop accumulator injection was early because the calculated system pressure was underpredicted, resulting in an early accumulator trip. A partial core dryout was both measured and calculated, but the calculated time of dryout was late, occurring after clearance of the intact- and broken-loop pump seals. In the test, the dryouts occurred early and were terminated by the influx of liquid into the core following clearance of the intact-loop pump-suction seal. For the parametric case, the system pressure history calculation was improved and the predicted time of accumulator injection was better. The calculation of core hydraulics also was improved.

2. Break Flows. The measured instantaneous break flow for Test S-UT-2 was not reliable.\* In a previous assessment of Tests S-UT-6 and 7

\*These data were provided by M. L. Leonard, EG&G Idaho, Inc.

(Ref. 19), both the instantaneous and integrated break flow measurements were available and proved to be valuable in the assessment study. In the absence of reliable break flow measurements, the multipliers in the parametric study were set to produce a close match to the total pressure transient. The approach used in Ref. 19 was followed; break flow was increased during the subcooled and two-phase blowdown phases (multiplier value 3.5) and decreased (value 0.45 thereafter). The calculated base-case and parametric-case instantaneous and integrated break flows are presented in Figs. 29 and 30, respectively.

3. System Pressure. The calculated base-case, parametric-case, and measured system pressure responses for Test S-UT-2 are compared in Fig. 31. The calculated base-case and measured pressures compare well for ~100 s, but by ~200 s the calculated pressure is underpredicted. The parametric calculation offers an improved overall comparison to the data. The dominant factor in underpredicting the base-case system pressure response appears to be the timing and rate of discharge through the break.

4. Loop Hydraulic Response. Predictions of loop hydraulic response generally displayed the correct qualitative behavior, but quantitative differences existed. The calculated base-case and measured mixture densities in the broken-loop hot leg, broken-loop cold leg, and intact-loop cold leg are shown in Figs. 32-34. The data show a rapid decay of density early in the transient; TRAC-PF1 calculates the density decrease to occur later in each case. The density oscillations after 400 s are due to accumulator injection of subcooled liquid into the intact-loop cold leg. Similar oscillations were

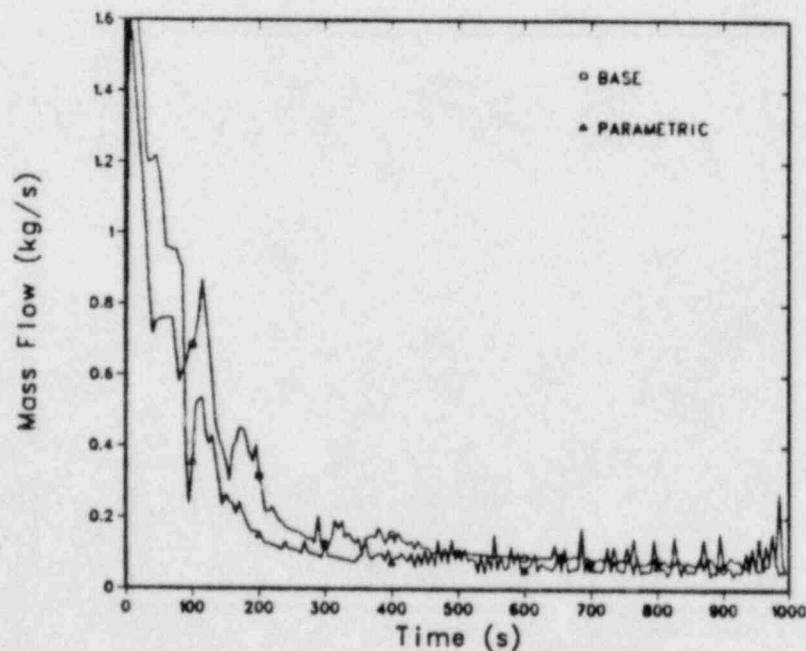


Fig. 29.  
Calculated break flows for Test S-UT-2.



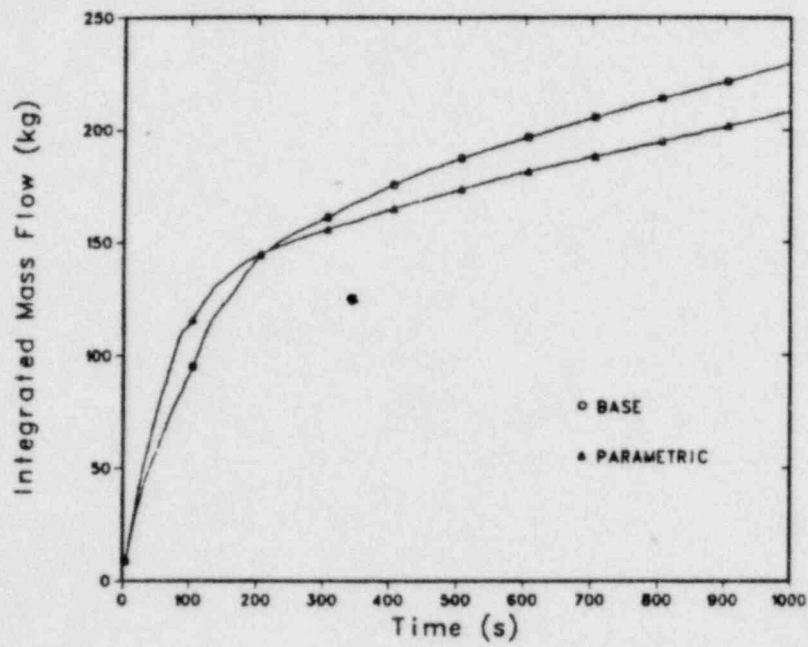


Fig. 30.  
Calculated integrated break flows for Test S-UT-2.

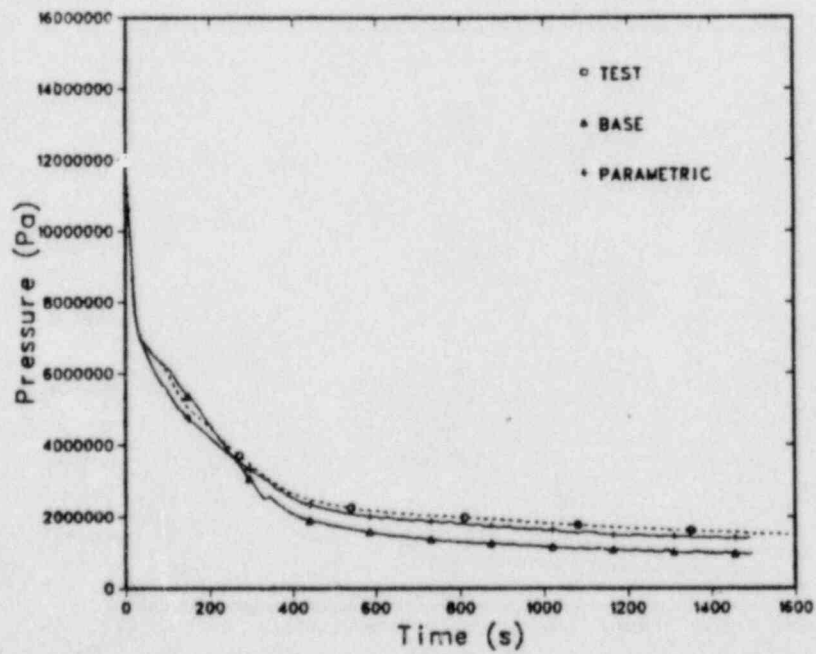


Fig. 31.  
System pressure response for Test S-UT-2.

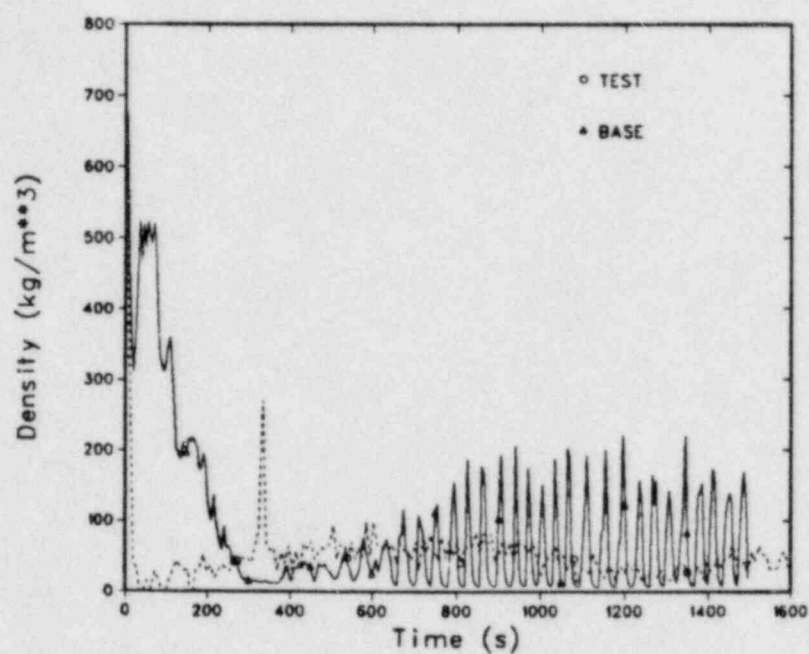


Fig. 32.  
Broken-loop hot-leg density for Test S-UT-2.

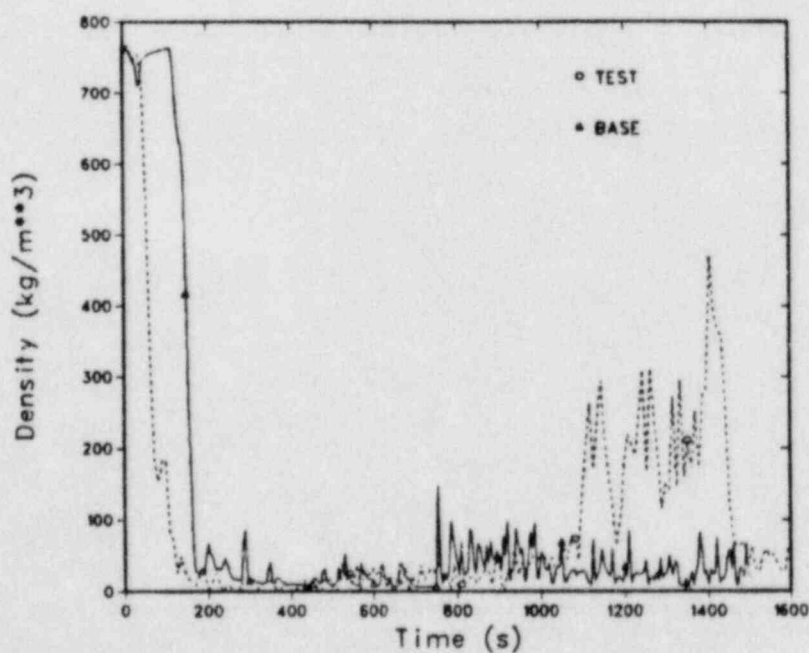


Fig. 33.  
Broken-loop cold-leg density for Test S-UT-7.

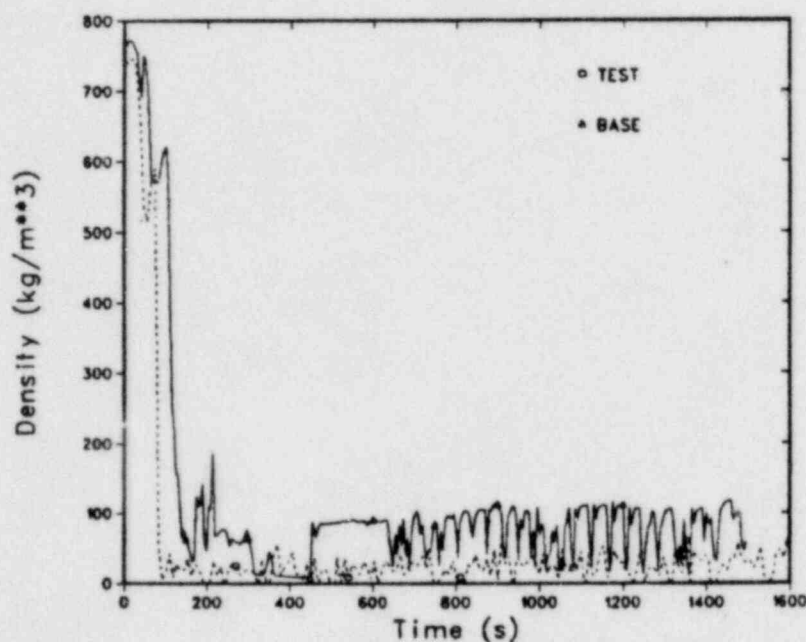


Fig. 34.  
Intact-loop cold-leg density for Test S-UT-2.

measured.<sup>18</sup> For the parametric case, the calculated density decay occurs earlier than in the base case but is still later than the data.

The collapsed liquid levels in the intact-loop pump-suction downflow and upflow legs are shown in Figs. 35 and 36. It can be seen that the initial clearance of the loop seal in both legs is delayed when compared to the test. It also can be observed that more liquid remained in each of the legs than was measured and that complete clearance of the intact-loop pump-suction seal was not calculated. The predicted initial clearance of the intact-loop pump-suction seal was improved in the parametric case but, again, the amounts of liquid remaining in each of the legs was similar to the base case. The collapsed liquid levels in the broken-loop pump-suction downflow and upflow legs are shown in Figs. 37 and 38. Both show the delayed clearance of the loop seal. Timing of the initial loop-seal clearance was improved for the parametric calculation of both the intact and broken loops. Measured and calculated base-case mass flows in the broken-loop hot and pump-suction legs are presented in Figs. 39 and 40.

5. Upper-Head Fluid Behavior. The behavior of the fluid in the upper head was not calculated well for Test S-UT-2. The initial flows for the bypass, guide, and core support tubes were 0.443 l/s, 0.334 l/s, and 0.108 l/s compared to the measured values of 0.43 l/s, 0.305 l/s, and 0.100 l/s, respectively. The summed result of the various upper-head inflows and outflows is shown in Fig. 41 for the base case. TRAC-PF1 calculates a rapid and early drain of the liquid in the upper head compared to the test. This liquid entered the top levels of the core as will be discussed in Sec. III.E.6. It

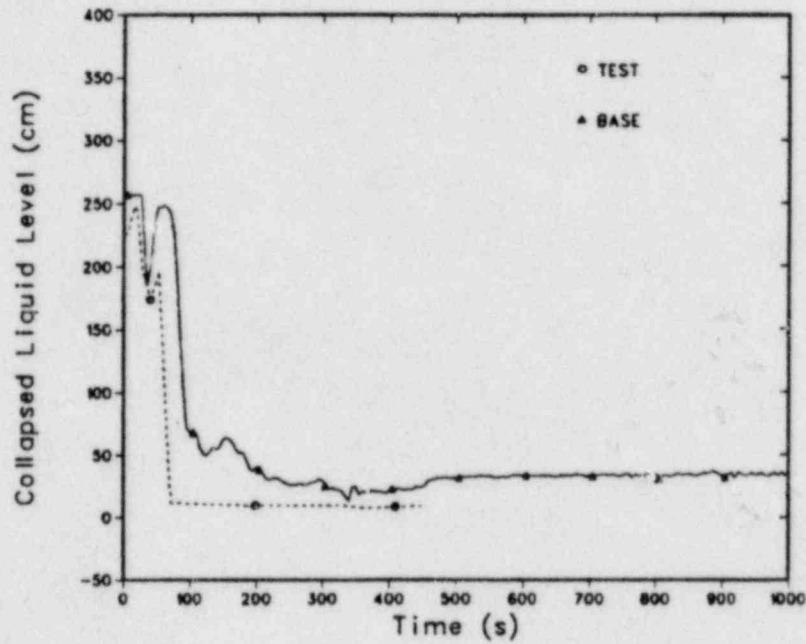


Fig. 35.

Collapsed liquid level in intact-loop pump-suction downflow leg for Test S-UT-2.

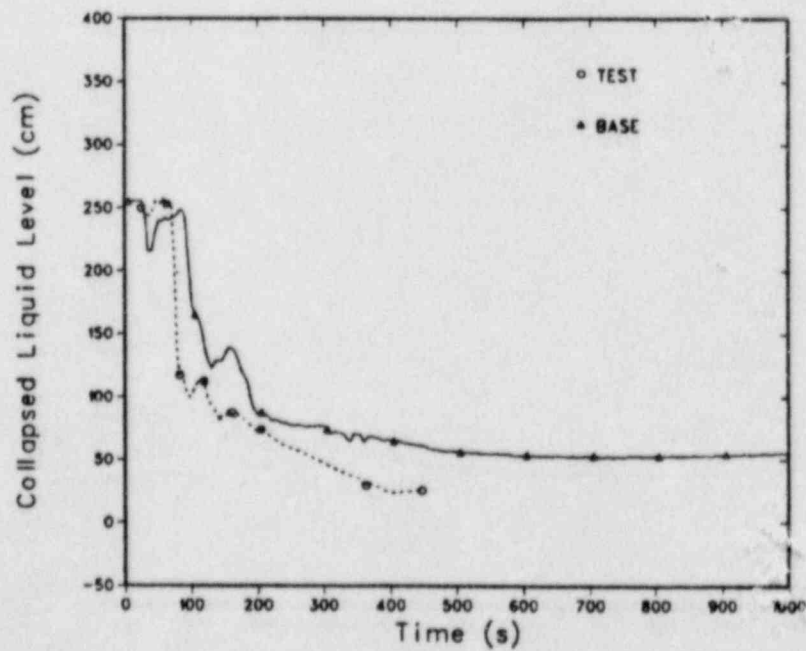


Fig. 36.

Collapsed liquid level in intact-loop pump-suction upflow leg for Test S-UT-2.



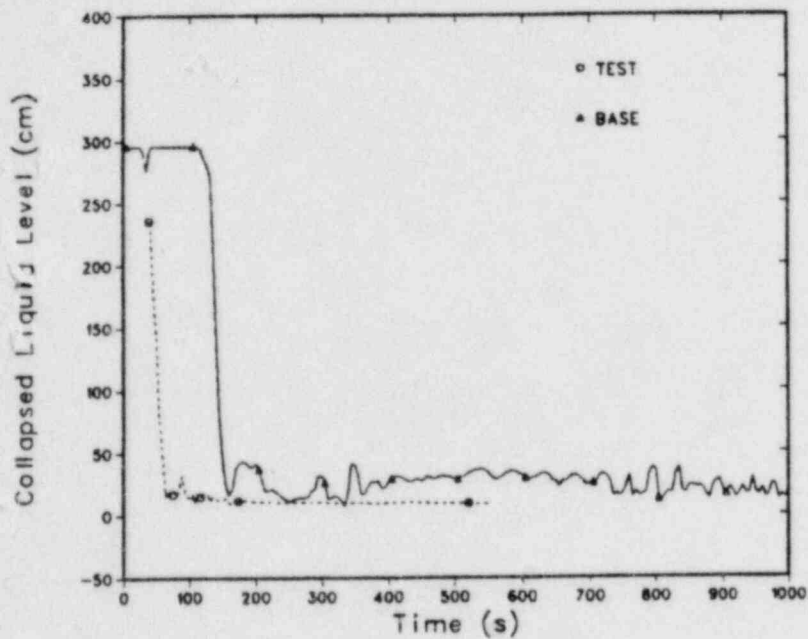


Fig. 37.

Collapsed liquid level in the broken-loop pump-suction downflow leg for Test S-UT-2.

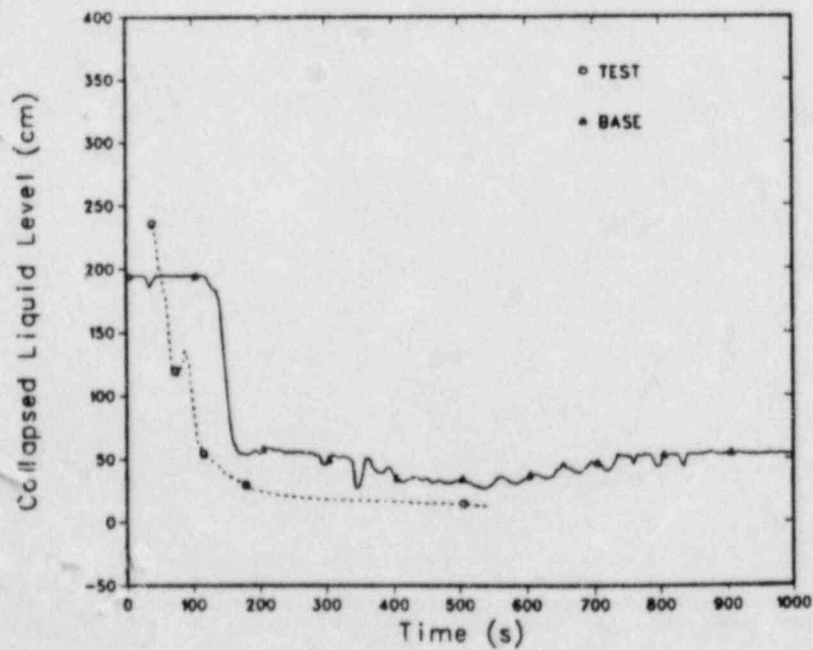


Fig. 38.

Collapsed liquid level in the broken-loop pump-suction upflow leg for Test S-UT-2.

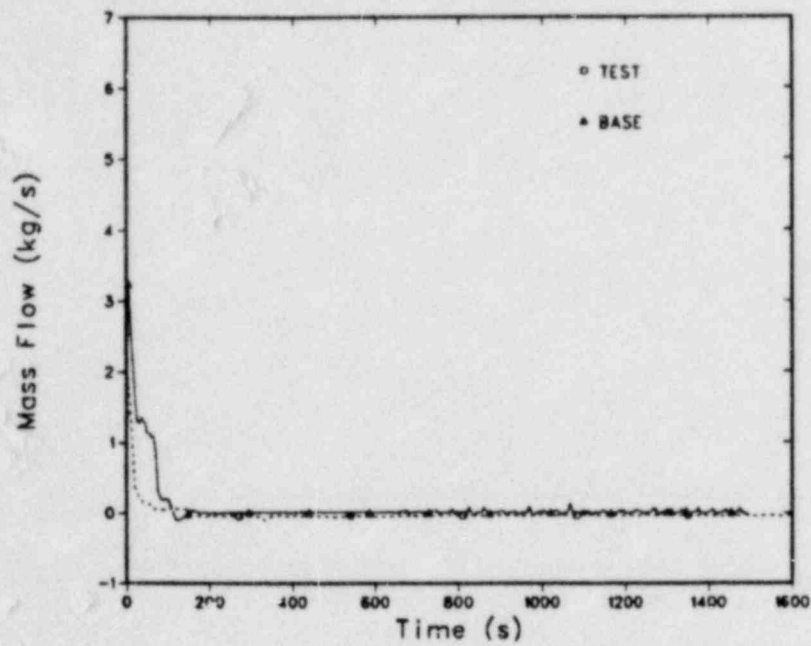


Fig. 39.  
Broken-loop hot-leg mass flow for Test S-UT-2.

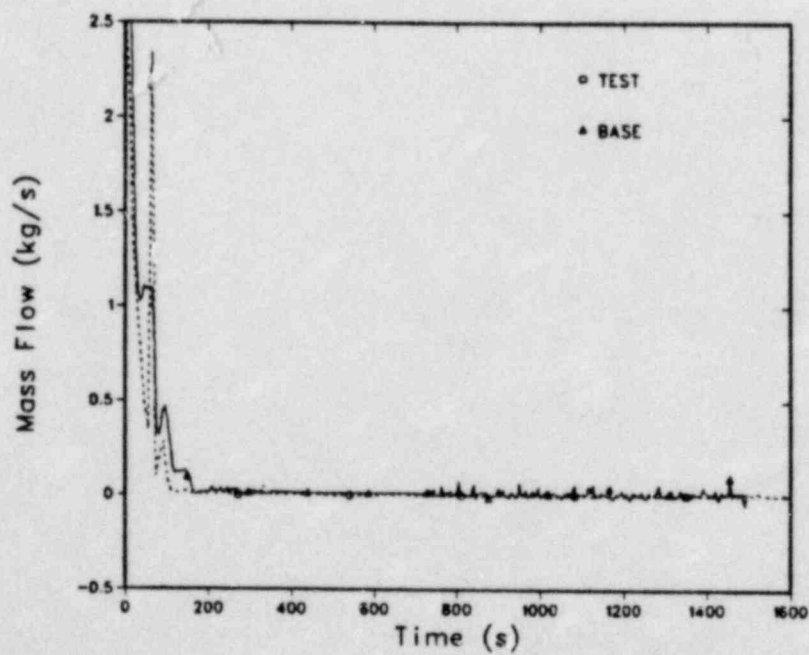


Fig. 40.  
Broken-loop pump-suction mass flow for Test S-UT-2.

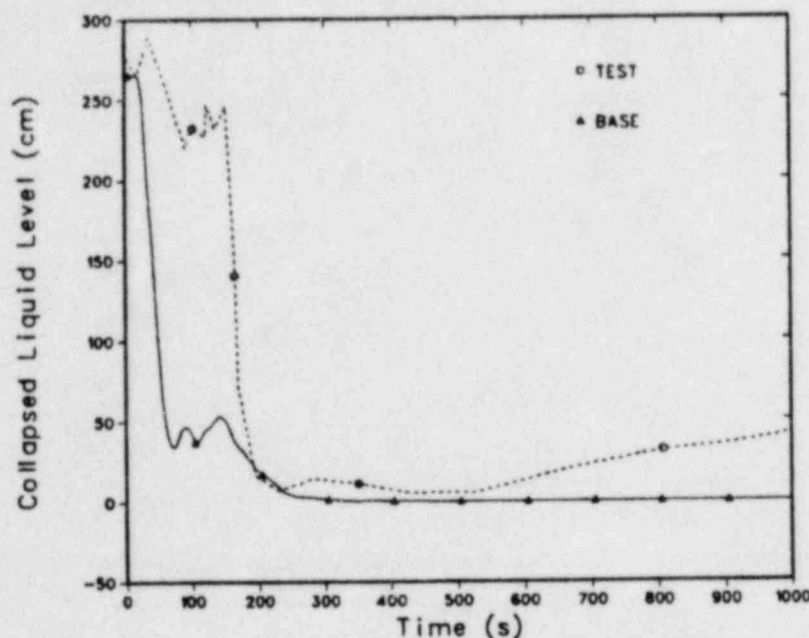


Fig. 41.  
Collapsed liquid level in the upper head for Test S-UT-2.

appears that the upper-head modeling is not correct. The same trends were reported in Ref. 19 for Test S-UT-7.

6. Core Behavior. Insight regarding core behavior can be obtained by reviewing the vessel collapsed liquid levels for the base and parametric cases shown in Figs. 42 and 43, respectively. For the base case, the measured and calculated minimum collapsed liquid levels are close but the history is quite different. The calculated minimum occurred late and persisted for over 100 s. The minimum occurred early in the test and was terminated by the clearance of the intact-loop pump-suction seal that injected fluid into the core. This phenomenon was not calculated in the base case. The calculated refill after accumulated injection (~300 s) was both measured and calculated.

An improved vessel liquid level history was calculated for the parametric case shown in Fig. 43. TRAC-PF1 still calculated the early depression of the vessel liquid level to occur slightly late, but the refill following the loop-seal clearance was shown. The calculation of refill following accumulator injection was improved. Low-frequency oscillations in the core were both measured and calculated following accumulator injection of subcooled liquid into the intact loop. The parametric calculation of vessel liquid level is another strong indication that the break flow predicted by the TRAC-PF1 critical-flow model needs additional review and revision. Clearly, the parametric case displays an improved calculation of vessel hydraulics.

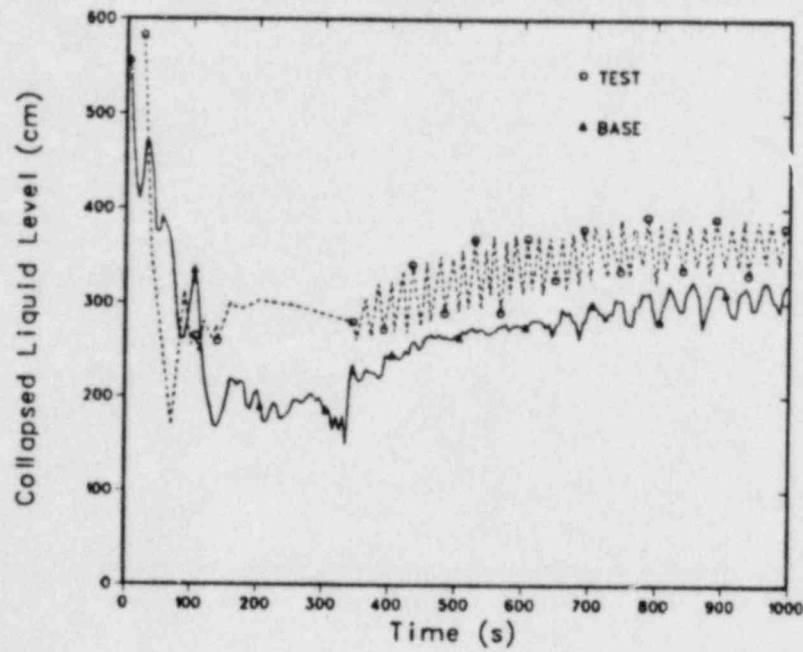


Fig. 42.  
Collapsed core liquid levels for Test S-UT-2 base case.

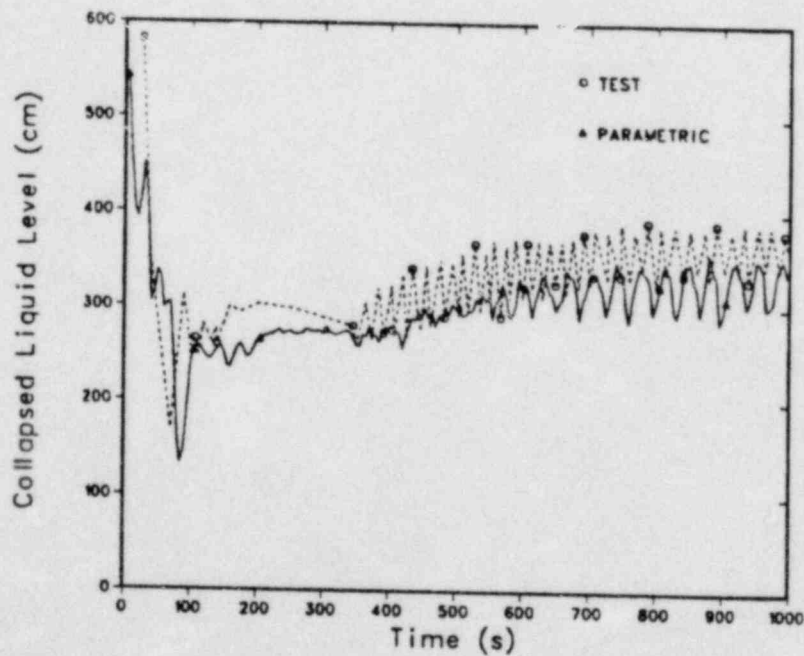


Fig. 43.  
Collapsed core liquid levels for Test S-UT-2 parametric case.



Calculated and measured cladding temperatures at the 1.37-m, 2.27-m, and 3.21-m levels in the core for the base case are presented in Figs. 44-46, respectively. A short dryout was both measured and calculated at the 2.27-m level. However, the calculated dryout was late. That the calculated dryout should persist to a later time can be understood from Fig. 42, which shows the near minimum vessel liquid level continued until fluid from the accumulator injection reached the core at ~350 s. However, the initiation of the dryout occurred well after the early minimum vessel liquid level was calculated (~150 s). This delay appears to be related to the presence of subcooled liquid from the UHI system at the top of the core. The presence of subcooled UHI fluid at the top of the core can be seen in Fig. 46 as a depression of the cladding temperature. At the 2.27-m level, the measured time of dryout and the peak cladding temperature were 53 s and 617 K; the corresponding calculated parameters were 128 s and 605 K, respectively. Calculated parametric-case and measured cladding temperatures at the same level are presented in Figs. 47-49. At the 1.37-m level an incipient dryout is calculated, but at the 2.27-m and 3.21-m levels the penetration of UHI liquid produced a depressed cladding temperature, and thus the early dryout was not predicted. The depressed cladding temperature for the parametric case is greater than in the base case because the UHI accumulator discharge was more rapid (Table III).

7. Timing Data. The CDC-7600 CPU time required for the 1500 s base-case transient was 5837 s. Thus, the ratio of CPU to real time for the transient was 3.9.

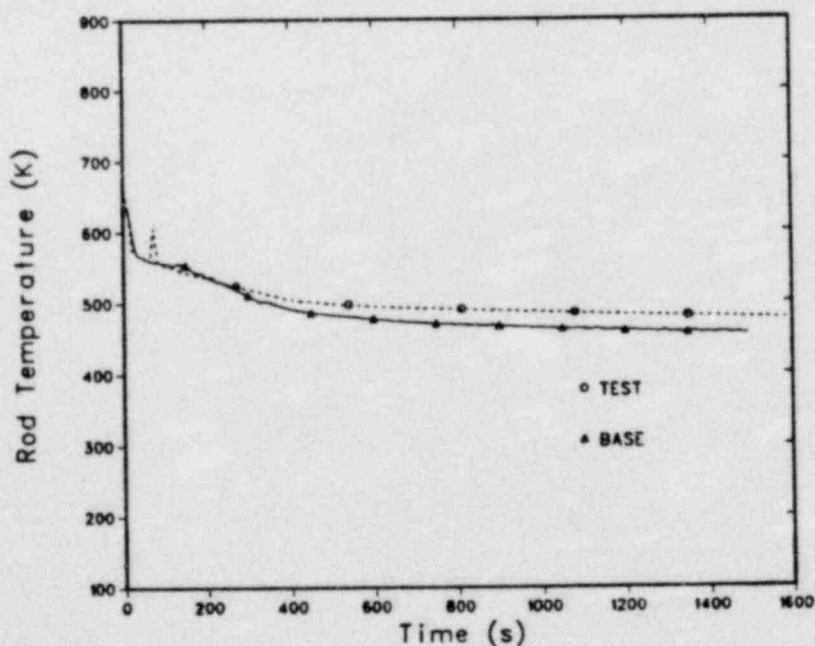


Fig. 44.  
Base-case cladding temperatures at the 1.37-m level for Test S-UT-2.

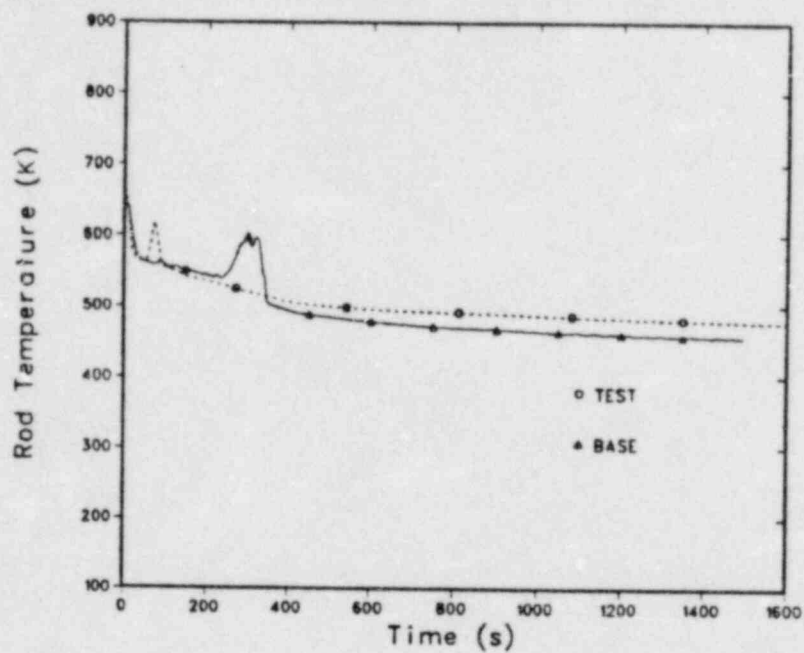


Fig. 45.  
Base-case cladding temperatures at the 2.27-m level for Test S-UT-2.

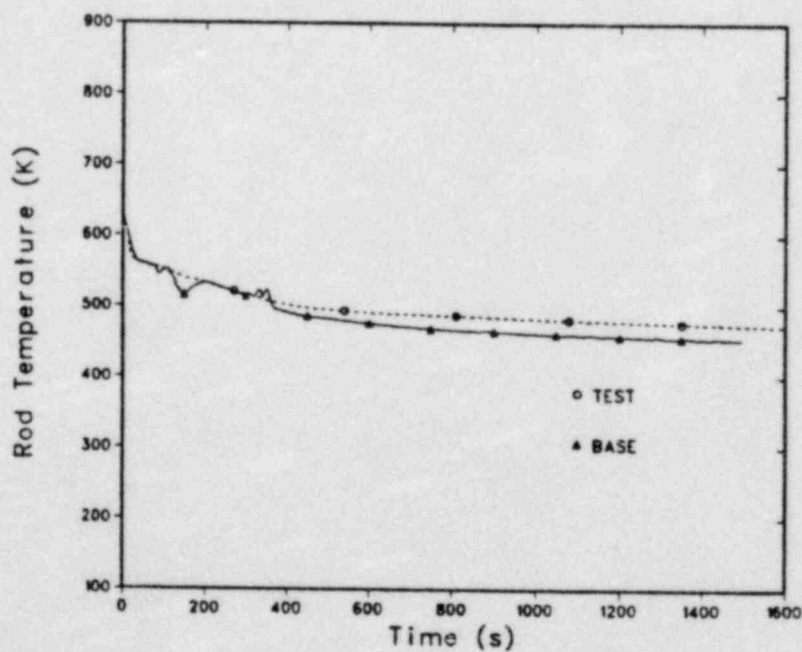


Fig. 46.  
Base-case cladding temperatures at the 3.21-m level for Test S-UT-2.

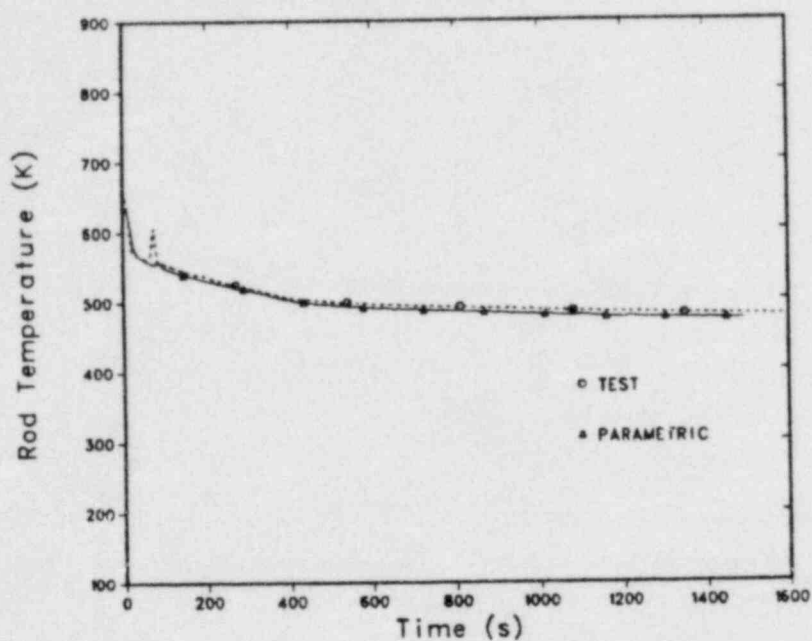


Fig. 47.  
Parametric-case cladding temperatures at the 1.37-m level for Test S-UT-2.

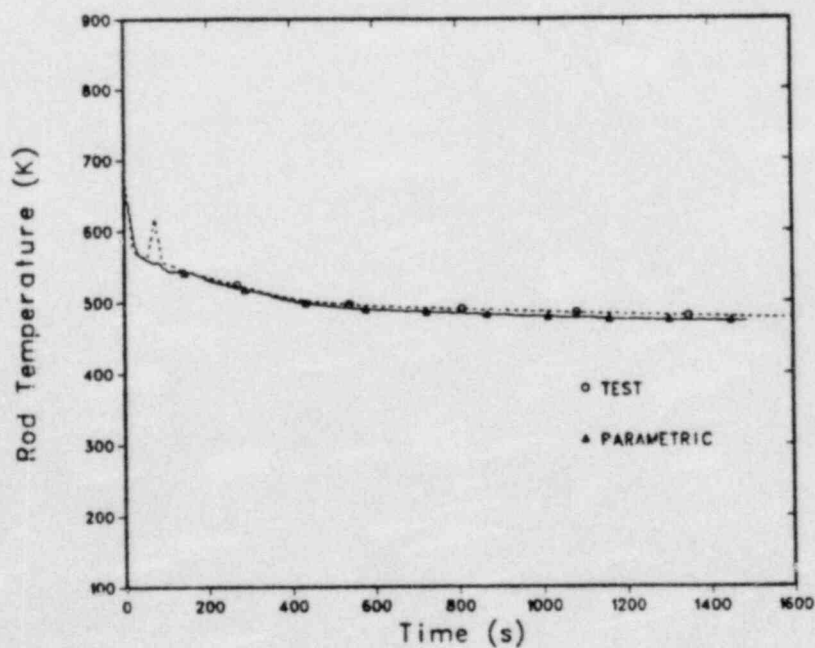


Fig. 48.  
Parametric-case cladding temperatures at the 2.27-m level for Test S-UT-2.

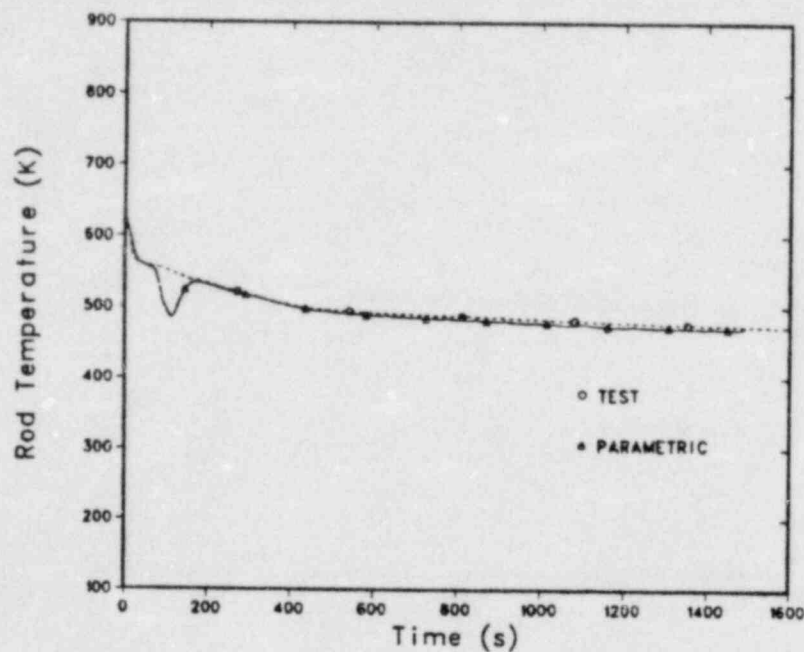


Fig. 49.

Parametric-case cladding temperatures at the 3.21-m level for Test S-UT-2.

TRAC-PF1 calculated the features of Semiscale UHI Test S-UT-2 well, but only after effectively decoupling the critical-flow model using multipliers to alter the calculated break flow. The calculated base case did not predict the system pressure response or vessel hydraulics well, but both were markedly improved in the parametric calculation. It is recommended that the TRAC-PF1 critical-flow model and its coupling to upstream nodes be reviewed.

Upper-head dynamics were poorly calculated. It appears that the TRAC-PF1 input model of the Semiscale Mod-2A upper-head region is not correct. As the model now exists, the upper head rapidly passes UHI fluid to the upper core through the core support tubes. A smaller flow through the support tubes is measured, resulting in a slower drain of UHI liquid into the upper core. The too-rapid introduction of subcooled UHI fluid into the upper core suppressed the early dryout observed in the test. The upper-head model is consistent with the system description in Ref. 17; in the future, noding-sensitivity studies for the upper-head modeling should be made to investigate the upper-head draining.



#### IV. TRAC-PF1 POSTTEST ANALYSIS OF SEMISCALE TESTS S-UT-6 AND S-UT-7

A paired experiment set conducted in the Semiscale Mod-2A facility at INEL has been selected as one element in the TRAC-PF1 assessment program. The tests selected were S-UT-6 and S-UT-7, which simulated a small-break LOCA resulting from a 5% communicative break in the cold leg of a PWR. The test specifications were identical except for UHI in Test S-UT-7. TRAC-PF1 (Ref. 10) is the latest version of the TRAC computer code developed for predicting LOCA events in a PWR. While retaining all the essential features of earlier code versions, TRAC-PF1 specifically was developed as a fast-running version for long transients such as small-break LOCAs.

Several Semiscale small-break LOCA experiments were used earlier in the developmental assessment of TRAC-PF1.\* However, these experiments were run with the Semiscale facility in the Mod-3 configuration. Tests S-UT-6 and S-UT-7 were run after the Semiscale facility was modified to the Mod-2A configuration. Therefore, it was necessary to modify the existing TRAC-PF1 model before performing assessments. Detailed assessment results for UHI Test S-UT-7 are presented, whereas results for non-UHI Test S-UT-6 are presented to highlight the primary differences.

##### A. Semiscale Mod-2A System Description

The Semiscale Mod-2A system<sup>11,12</sup> is a scaled integral test facility at INEL used to obtain thermal-hydraulic data for diverse postulated transients and operating conditions. The Mod-2A system (Fig. 50) is a two-loop PWR primary-coolant-system simulator; the intact loop is scaled to simulate three loops of a large PWR and the broken loop simulates a single loop in which a break is postulated to occur. Geometric similarity has been maintained between a PWR and Mod-2A, most notably in the design of a full-length (3.66-m) electrically heated core; full-length upper plenum and upper head; component layout; and relative elevations of various components. The instrument spool pieces for the cold-leg break tests are identified as circled numbers in Fig. 51. Major configuration changes between the Mod-2A configuration and the previous Mod-3 configuration resulted from:

1. installation of a new intact-loop steam generator,
2. modification of the broken-loop steam generator,
3. addition of external heaters on the outside surfaces of the coolant piping, and
4. installation of insulation inside the downcomer and lower pressure vessel plenum.

\*This information was provided by M. S. Sahota, Los Alamos National Laboratory, Energy Division, Safety Code Development Group (January 1982).

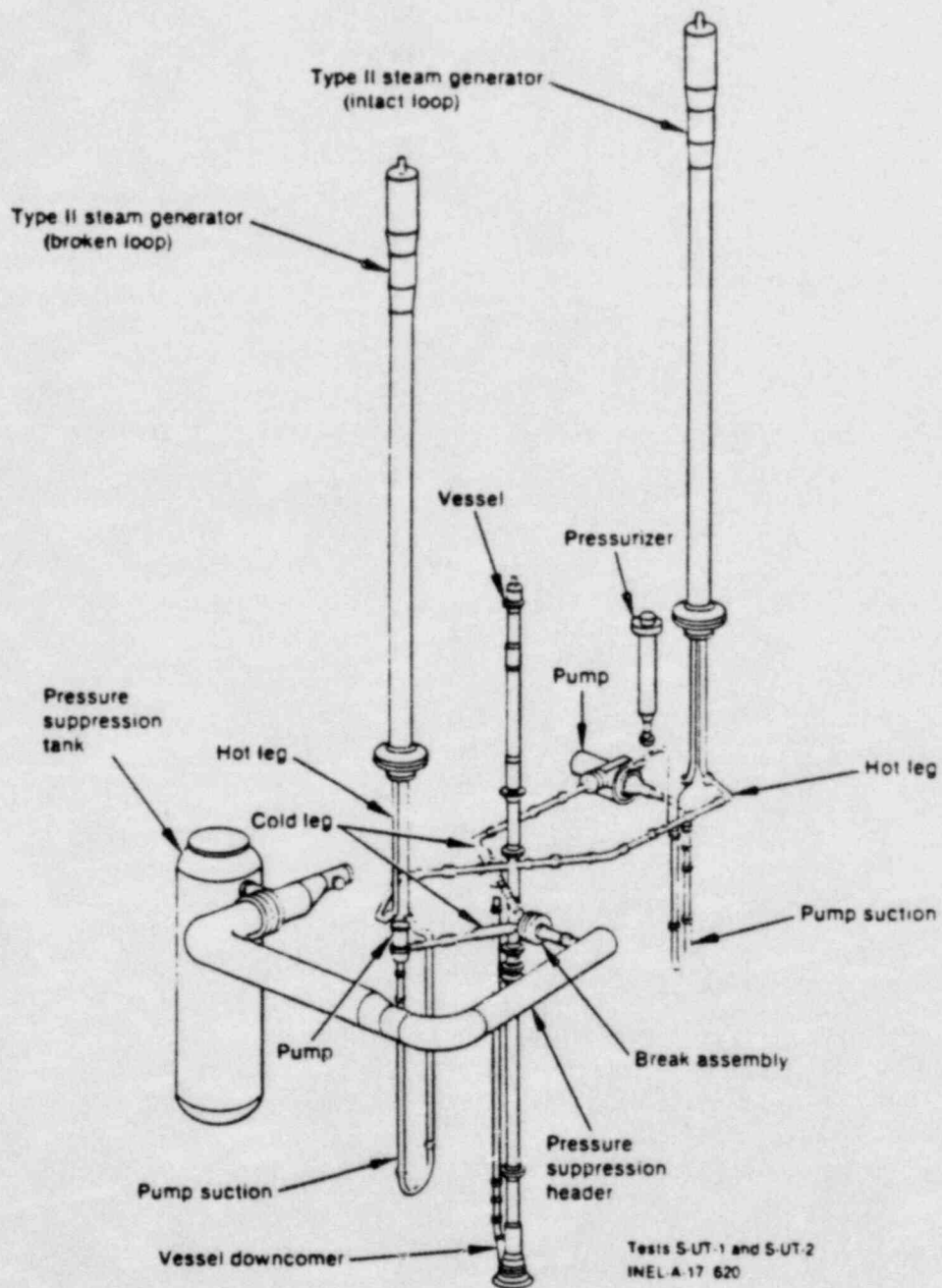


Fig. 50.  
Semiscale Mod-2A system isometric (cold-leg-break configuration).

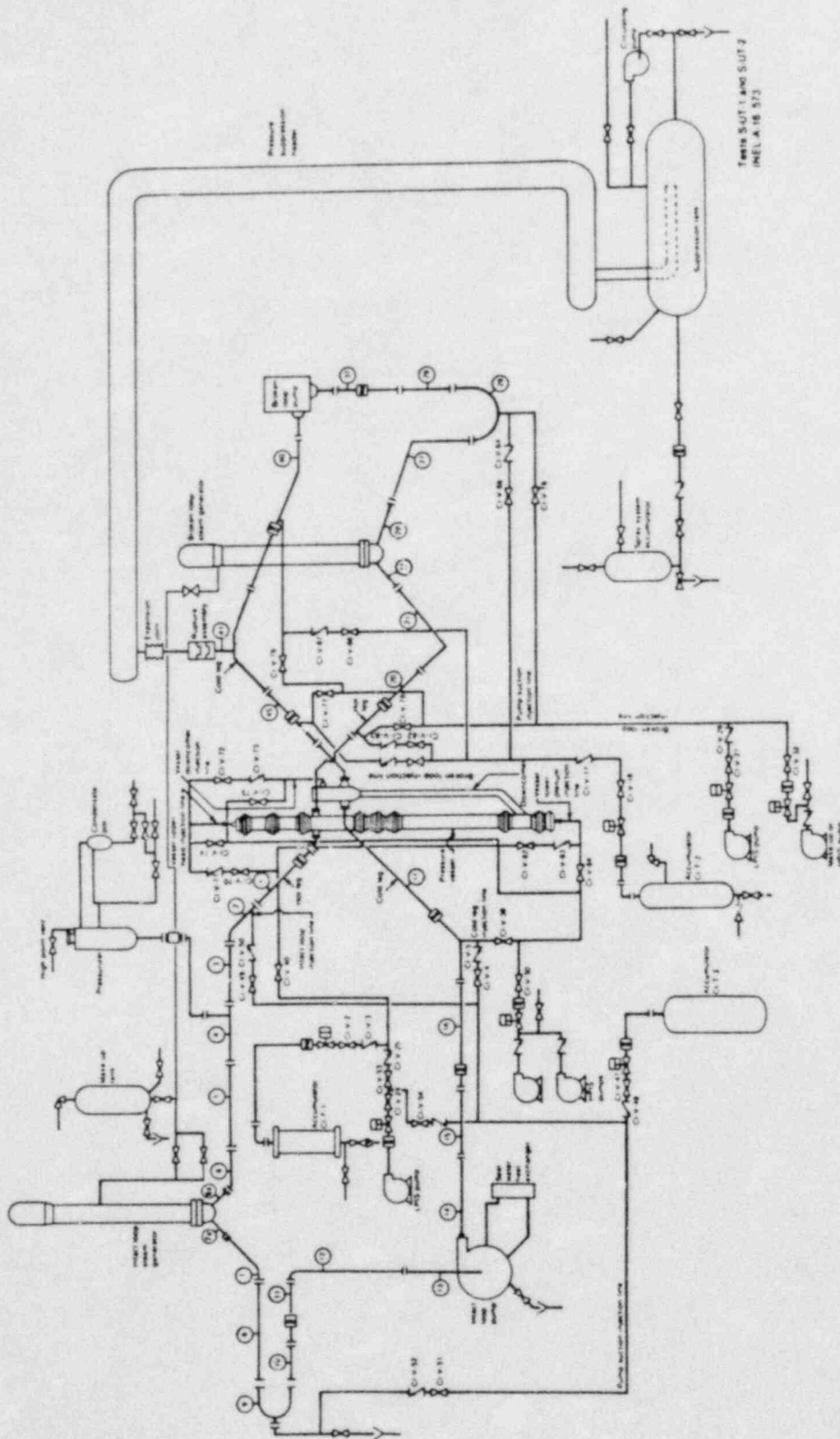


Fig. 51.  
Semiscale Mod-2A system for cold-leg-break configuration--schematic.

## B. Test Description

Semiscale small-break Tests S-UT-6 and S-UT-7 (Ref. 20) simulated a LOCA resulting from a 5% communicative break in the cold leg of a PWR. The primary objective was to investigate the distribution of UHI water (and its influence on transient behavior) through comparisons between Semiscale Mod-2A tests S-UT-6 and S-UT-7. The break size for each test was  $0.1123 \text{ cm}^2$ , which was volumetrically scaled to represent a 15.6-cm-diam pipe break in a PWR. The Mod-2A system for Test S-UT-7 was configured to simulate a PWR with ECC injection into the vessel upper head. The upper-head accumulator was pressurized to 8.6 MPa and the loop accumulator pressures were set at 2.86 MPa, as is nominally specified for UHI plants. Initial conditions for S-UT-6 were identical to S-UT-7, except UHI was not specified. The remaining initial test conditions were equivalent to or scaled from typical PWR operating conditions. The tests were conducted as specified<sup>21</sup> except that the broken-loop high- and low-pressure injection pump was mistakenly not operated during Test S-UT-7.

## C. TRAC Version

All calculations were performed using TRAC-PF1 7.0/EXTUPD 7.6.\*

## D. TRAC Model

The TRAC input model for the Semiscale Mod-2A facility is shown in Figs. 52 and 53 in its cold-leg-break configuration. The input model consisted of 49 one-dimensional components containing 187 computational cells. Table IV lists the components. The input model corresponded to the Semiscale Mod-2A hardware configuration with the following exceptions.

1. The pressure-suppression system was modeled indirectly. A BREAK component was introduced and the pressure and temperature downstream of the break were specified as boundary conditions.
2. The secondary feedwater systems, both main and auxiliary, were represented by FILL components 7 and 26 for the intact and broken loops, respectively.
3. The HPIS was represented by FILL components 13 and 43 for the intact and broken loops, respectively.
4. The UHI coolant was delivered at a discreet elevation in the upper head, but the physical system was designed to distribute the coolant uniformly over the full height of the upper head.

\*This information was provided by Thad D. Knight, Los Alamos National Laboratory, Energy Division, Safety Code Development Group (June 1982).



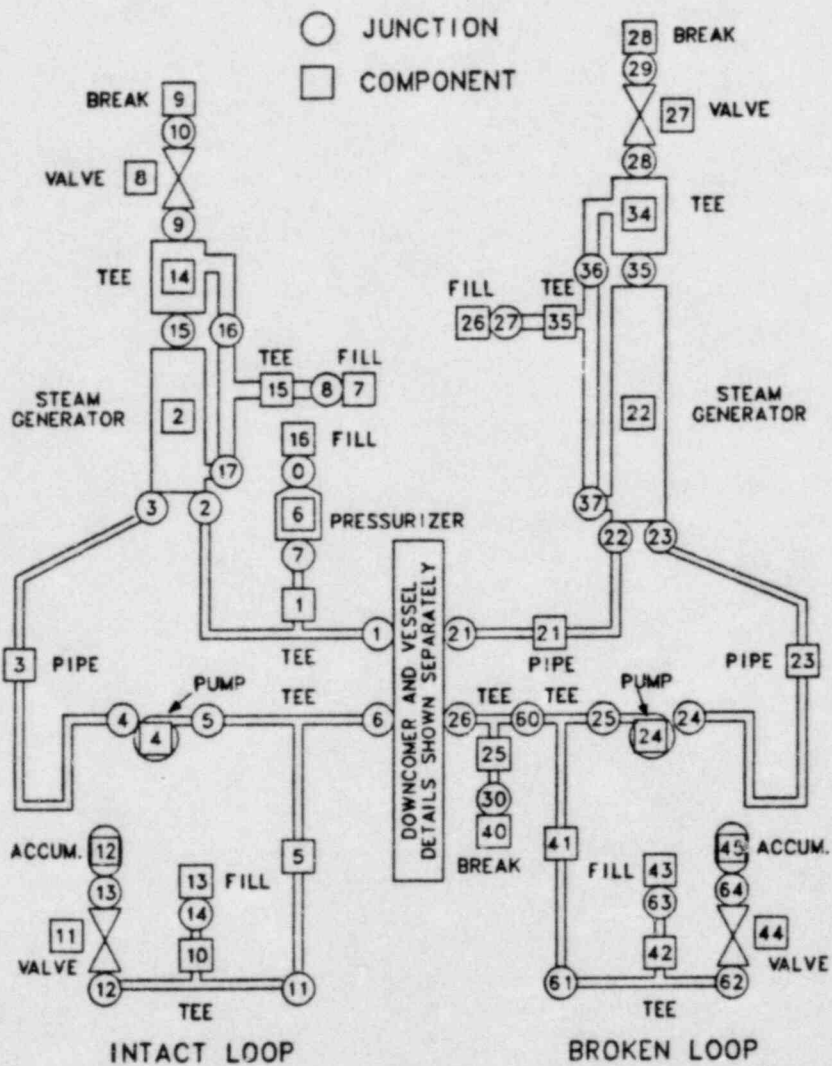


Fig. 52.  
TRAC input model for the Semiscale Mod-2A facility.



TABLE IV  
TRAC MODEL COMPONENTS

Component Number <sup>a</sup>	Component Type	Description	Number of Fluid Cells (Primary Side Secondary Side) <sup>b</sup>
1	TEE	Intact-loop hot leg	6, 3
2	STGEN	Intact-loop steam generator	12, 6
3	PIPE	Intact-loop pump suction	8
4	PUMP	Intact-loop pump	2
5	TEE	Intact-loop cold leg	5, 1
6	PRIZER	Intact-loop pressurizer	5
7	FILL	Intact-loop steam-generator feedwater	1
8	VALVE	Intact-loop steam line	2
9	BREAK	Intact-loop steam-generator-secondary pressure set point	1
10	TEE	Intact-loop ECC line	2, 1
11	VALVE	Intact-loop accumulator valve	2
12	ACCUM	Intact-loop accumulator	4
13	FILL	Intact-loop HPIS	1
14	TEE	Intact-loop steam-generator-secondary steam dome	2, 1
15	TEE	Intact-loop steam-generator-secondary downcomer	6, 1
16	FILL	Pressurizer inlet	1
21	PIPE	Broken-loop hot leg	5
22	STGEN	Broken-loop steam generator	12, 6
23	PIPE	Broken-loop pump suction	7
24	PUMP	Broken-loop pump	2
25	TEE	Broken-loop cold leg	3, 2
26	FILL	Broken-loop steam-generator feedwater	1
27	VALVE	Broken-loop steam line	2
28	BREAK	Broken-loop steam-generator-secondary pressure set point	1
34	TEE	Broken-loop steam-generator-secondary steam dome	2, 1
35	TEE	Broken-loop steam-generator-secondary downcomer	6, 1
40	FILL, BREAK	Fill for steady-state run, break for transient run	1
41	TEE	Broken-loop cold leg	2, 1
42	TEE	Broken-loop ECC line	2, 1
43	FILL	Broken-loop HPIS	1
44	VALVE	Broken-loop accumulator valve	2
45	ACCUM	Broken-loop accumulator	4

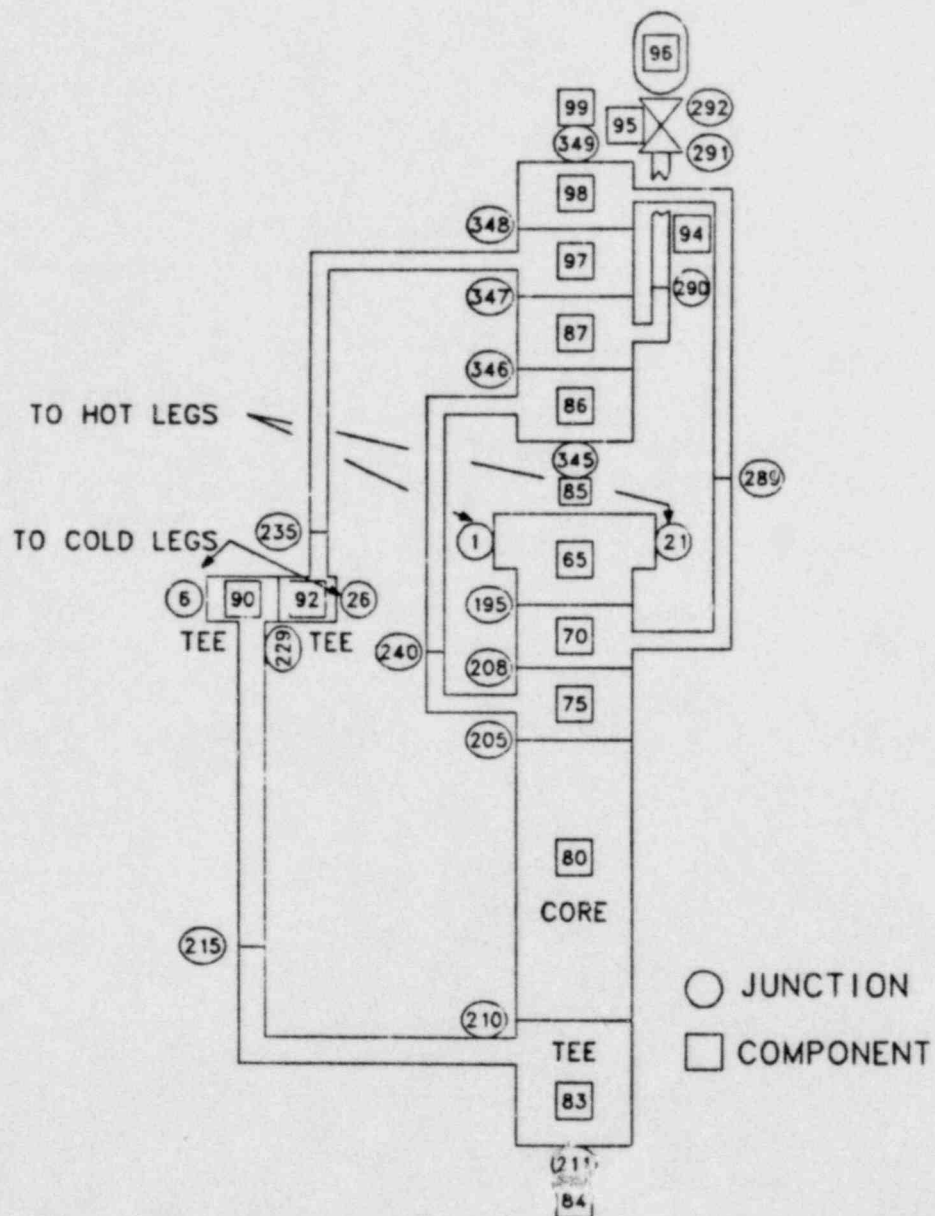


Fig. 53.  
TRAC downcomer and vessel noding for the Semiscale Mod-2A facility.



TABLE IV  
TRAC MODEL COMPONENTS

Component Number <sup>a</sup>	Component Type	Description	Number of Fluid Cells (Primary Side Secondary Side) <sup>b</sup>
1	TEE	Intact-loop hot leg	6, 3
2	STGEN	Intact-loop steam generator	12, 6
3	PIPE	Intact-loop pump suction	8
4	PUMP	Intact-loop pump	2
5	TEE	Intact-loop cold leg	5, 1
6	PRIZER	Intact-loop pressurizer	5
7	FILL	Intact-loop steam-generator feedwater	1
8	VALVE	Intact-loop steam line	2
9	BREAK	Intact-loop steam-generator-secondary pressure set point	1
10	TEE	Intact-loop ECC line	2, 1
11	VALVE	Intact-loop accumulator valve	2
12	ACCUM	Intact-loop accumulator	4
13	FILL	Intact-loop HPIS	1
14	TEE	Intact-loop steam-generator-secondary steam dome	2, 1
15	TEE	Intact-loop steam-generator-secondary downcomer	6, 1
16	FILL	Pressurizer inlet	1
21	PIPE	Broken-loop hot leg	5
22	STGEN	Broken-loop steam generator	12, 6
23	PIPE	Broken-loop pump suction	7
24	PUMP	Broken-loop pump	2
25	TEE	Broken-loop cold leg	3, 2
26	FILL	Broken-loop steam-generator feedwater	1
27	VALVE	Broken-loop steam line	2
28	BREAK	Broken-loop steam-generator-secondary pressure set point	1
34	TEE	Broken-loop steam-generator-secondary steam dome	2, 1
35	TEE	Broken-loop steam-generator-secondary downcomer	6, 1
40	FILL, BREAK	Fill for steady-state run, break for transient run	1
41	TEE	Broken-loop cold leg	2, 1
42	TEE	Broken-loop ECC line	2, 1
43	FILL	Broken-loop HPIS	1
44	VALVE	Broken-loop accumulator valve	2
45	ACCUM	Broken-loop accumulator	4

TABLE IV (cont.)

<u>Component Number<sup>a</sup></u>	<u>Component Type</u>	<u>Description</u>	<u>Number of Fluid Cells (Primary Side Secondary Side)<sup>b</sup></u>
65	TEE	Upper section of upper plenum	1, 1
70	TEE	Middle section of upper plenum	1, 2
75	TEE	Lower section of upper plenum and guide and core support tubes	1, 1
80	CORE	Core	9
83	TEE	Lower plenum and lower downcomer	3, 2
84	FILL	Bottom lower plenum	1
85	FILL	Bottom upper head	1
86	TEE	Lower section of upper head	1, 2
87	TEE	Lower mid section of upper head	1, 2
90	TEE	Intact-loop side downcomer inlet and downcomer	2, 10
92	TEE	Broken-loop side downcomer inlet and upper-head bypass	2, 1
94	PIPE	Upper-head injection tube	2
95	VALVE	Upper-head injection valve	2
96	ACCUM	Upper-head injection accumulated	4
97	TEE	Middle upper section of upper head	1, 2
98	TEE	Upper section of upper head	2, 2
99	FILL	Top upper head	1

<sup>a</sup>The total number of components is 49.

<sup>b</sup>The total number of cells is 198.

The TRAC-PF1 choked-flow model was used to calculate the break flow. The break orifice had a rounded entrance with a length-to-diameter ratio of 3.35 (length, 12.65 mm; diameter, 3.78 mm). Thus, the secondary side of break TEE 25 for this test was modeled using two cells with the second cell representing the break orifice.

Power tables were defined for the PIPE and TEE components representing the primary-loop piping to simulate the external heaters used during the test. A new pipe material was defined for the downcomer tube (TEE 90 secondary) and the vessel lower plenum (TEE 83) to simulate the thermal conductivity of a composite steel wall clad with honeycomb insulation. Primary-system heat losses to the environment were set to the values reported in Ref. 15. The intact and broken-loop steam generators were modified to reflect the geometry and heat-transfer characteristics of the Type-II steam generator installed in the Mod-2A facility.

The primary data base for the input model geometric specifications included the system design description,<sup>11,12</sup> the Semiscale Mod-3 drawings,<sup>16</sup> and the RELAP5 standard model description for the Semiscale Mod-2A system.<sup>17</sup> The data base for the initial and boundary conditions incorporated in the TRAC input model included the experiment data report,<sup>20</sup> the quick look reports,<sup>21,22</sup> and the experiment operating specification.<sup>23</sup>

## E. Results

The following sections present and discuss the results obtained during posttest predictions of Semiscale Mod-2A Tests S-UT-6 and S-UT-7. Results for Test S-UT-7 will be emphasized, and Test S-UT-6 results will be presented to highlight the primary differences in system response resulting from not using UHI.

1. General System Behavior. The initial conditions and specified test parameters for Test-S-UT-7 are presented in Table V. The pump speeds were set to yield primary-loop hot-leg temperatures close to those measured; the steam-generator-secondary pressures also were set to yield primary-loop cold-leg temperatures close to measured. Both the specified pump speeds and steam-generator secondary pressures differed from the measured values, with the largest deviations for the intact- and broken-loop pump speeds being 15% and

TABLE V  
TEST S-UT-7 INITIAL CONDITIONS

Parameter	Actual	Calculated
Core Power (MW) <sup>a</sup>	1.994	1.994 <sup>b</sup>
Pressurizer pressure (MPa)	15.5	15.5 <sup>b</sup>
Pressurizer liquid mass (kg)	10.4	10.2
Intact-loop mass flow (kg/s)	6.77	6.72
Intact-loop cold-leg temperature (K)	558.	559.2
Intact-loop hot-leg temperature (K)	599.	598.2
Broken-loop mass flow (kg/s)	2.1	2.1
Broken-loop cold-leg temperature (K)	559.	557.4
Broken-loop hot-leg temperature (K)	598.	598.2
Intact-loop pump speed (rad/s)	198.3	229.5 <sup>b</sup>
Broken-loop pump speed (rad/s)	974.3	1250. <sup>b</sup>
Intact-loop steam-generator-secondary pressure (MPa)	5.7	5.1
Intact-loop steam-generator-secondary feedwater temperature (K)	502.	502. <sup>b</sup>
Broken-loop steam-generator-secondary pressure (MPa)	5.9	5.5
Broken-loop steam-generator-secondary feedwater temperature (K)	497.	497. <sup>b</sup>

<sup>a</sup>Flat radial profile.

<sup>b</sup>Specified as input parameter.

28%, respectively. This suggests that further review of the Semiscale pump correlations and the steam-generator secondary-side heat-transfer correlations is warranted. The primary-system steady state calculated by TRAC matched the test conditions well.

Table VI presents the calculated event times for the base case and a parametric case. The latter varies from the former in the use of two multipliers on the critical-flow model. The first multiplier (value 2.1) increased the break flow during the subcooled and two-phase blowdown phases. The second multiplier (value 0.85) decreased the break flow for the remainder of the transient. The intent of the parametric study was to specify the measured break flow (or a close approximation) as a boundary condition. The multipliers are not interpreted to have a physical meaning (for example, discharge coefficients). Timing during the first 150 s of the transient was predicted quite well. The predicted timing of loop dynamics after was generally improved in the parametric study by matching closely the measured break flow. A partial core dryout was both measured and predicted with the largest cladding temperature increase calculated for Test S-UT-6 (no UHI). In each case the dryout resulted from the slow boil-off of liquid from the top of the core and the dryout was terminated following initiation of intact- and

TABLE VI  
TEST S-UT-7 EVENTS

Event	Time (s)		
	Actual	Base Case	Parametric Case
Blowdown initiated	0.	0.	0.
Pressure trip	8.6	7.5	7.1
Intact-and-broken loop main steam valves begin closing	10.8	9.6	9.3
Core power decay initiated	12.4	11.3	10.9
Intact-and broken-loop pump coastdown initiated	14.2	13.1	12.7
Upper-head injection begins	21.	21.9	21.4
Intact-and-broken loop main feedwater valves begin to close	34.	33.9	32.9
Broken-loop pump stops	77.	76.0	75.4
Intact-loop pump stops	136.	133.7	133.3
Intact-loop pump suction blows out	220.	289.	208.
Upper-head accumulator injection ends	296.	~366.	~284.
Intact-loop pump suction cleared of liquid	650.	no	no
Intact-and-broken loop accumulator injection begins	738.	745.	753.



broken-loop accumulator injection. The same dryout and rewet phenomena were observed in the test.

2. Break Flows. The calculated and measured instantaneous and integrated break flows for the base and parametric cases are shown in Figs. 54 and 55, respectively. A comparison of the measured and calculated instantaneous break flows showed that TRAC-PF1 underpredicted the rates of subcooled and two-phase break flow to ~225 s. The integral result of the underprediction is shown in Fig. 55. After 225 s the measured instantaneous break flow was reduced sharply because the loop seal in the intact-loop pump-suction pipe cleared and uncovered the break orifice to the passage of vapor only.<sup>22</sup> The calculated break flow between 225 and 450 s was too large. For the parametric study, the break flow was treated as a boundary condition; improved instantaneous and integrated break flows were calculated as shown in Figs. 54 and 55. There is a clear indication that the critical-flow model and the coupling of the model to upstream cells require additional review.

3. System Pressure. The calculated base-case, parametric-case, and measured system pressure responses for Test S-UT-7 are compared in Fig. 56. The calculated base-case pressure was overpredicted until ~450 s. This corresponds closely to the underprediction of integrated break flow shown in Fig. 55. The increased rate of system depressurization beginning at ~300 s for the base case was due to a steep drop in density upstream of the break following the initial clearance of the intact-loop pump-suction seal. An

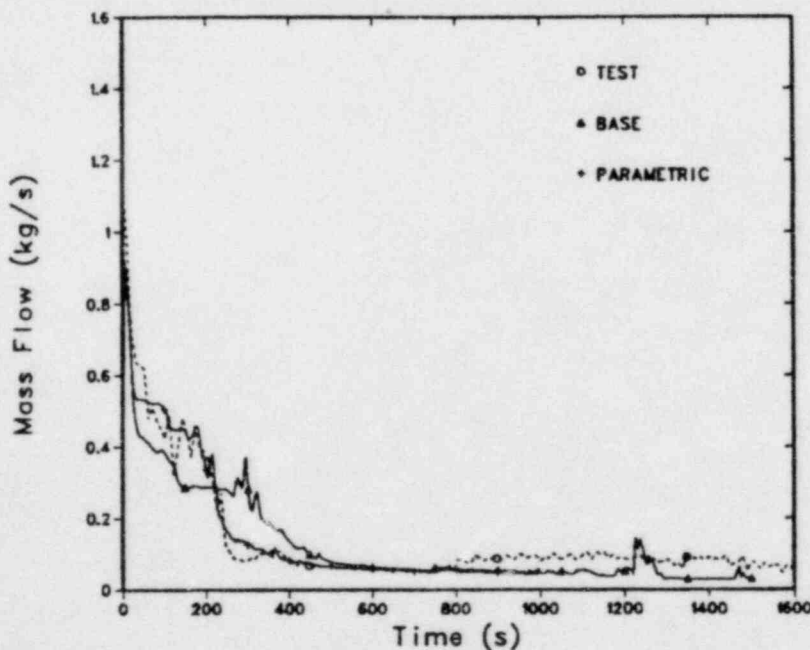


Fig. 54.  
Break flow for Test S-UT-7.

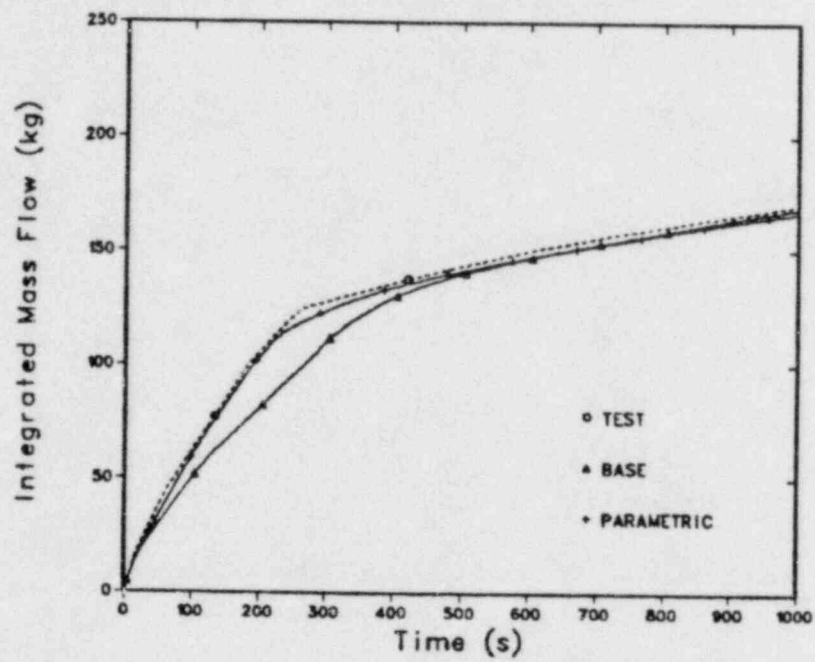


Fig. 55.  
Integrated break flow for Test S-UT-7.

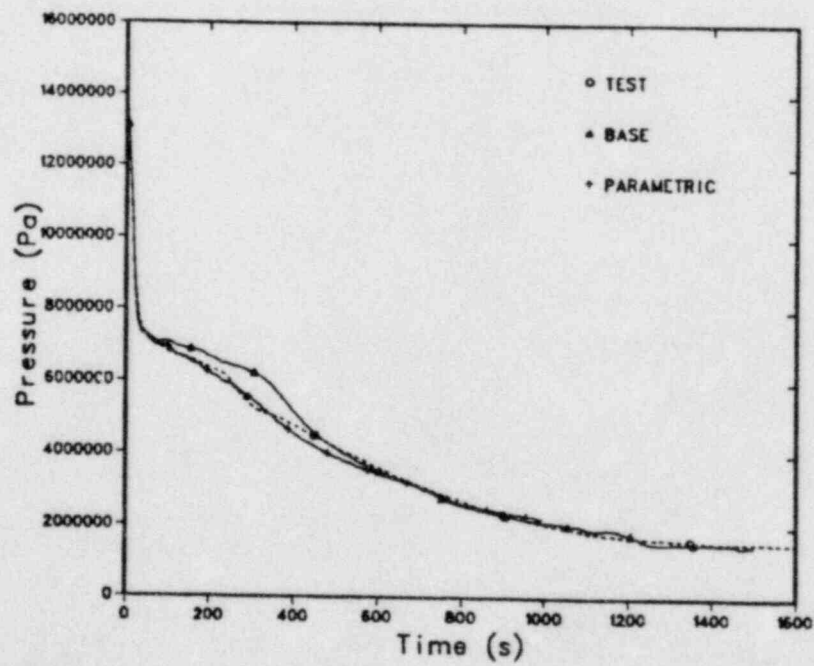


Fig. 56.  
System pressure response for Test S-UT-7.

improved pressure history was calculated for the parametric case, a direct result of more closely matching the measured break flow.

4. Loop Hydraulic Response. Predictions of loop hydraulic response generally displayed the correct qualitative behavior, but quantitative differences existed. The calculated and measured mixture densities in the broken-loop hot leg, broken-loop cold leg, and intact-loop cold leg are shown in Figs. 57-59. Both tangential and bottom gamma densitometer measurements are presented when available. The two-dimensional stratification of liquid and vapor in the horizontal pipe runs is clearly shown in Fig. 57. The rapid voiding of both the intact- and broken-loop cold legs was predicted to occur early.

The collapsed liquid levels in the intact-loop pump-suction downflow and upflow legs are shown in Figs. 60 and 61, where it can be seen that the initial clearance of the loop seal in both legs is delayed when compared to the test. It also can be observed that more liquid remained in each of the legs than was measured and that complete clearance of the intact-loop pump-suction seal was not calculated. The predicted initial clearance of the intact-loop pump-suction seal was improved in the parametric case but, again, the amounts of liquid remaining in each of the legs was similar to the base case.

Figures 62 and 63 show the calculated and measured mass flows in the hot and cold legs of the intact loop, respectively. Following establishment of the loop seal during the test, flow through the intact loop stopped. Flow was

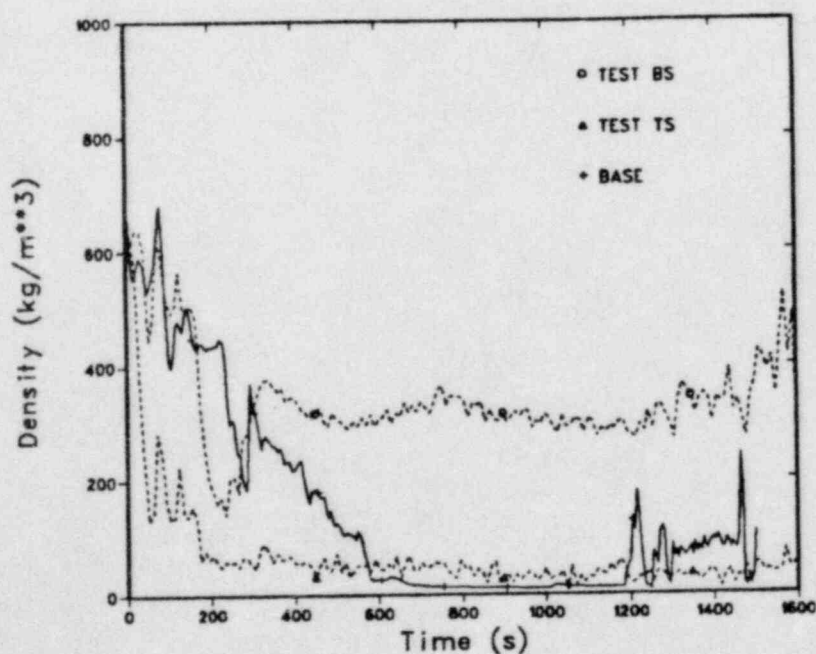


Fig. 57.  
Broken-loop hot-leg density for Test S-UT-7.

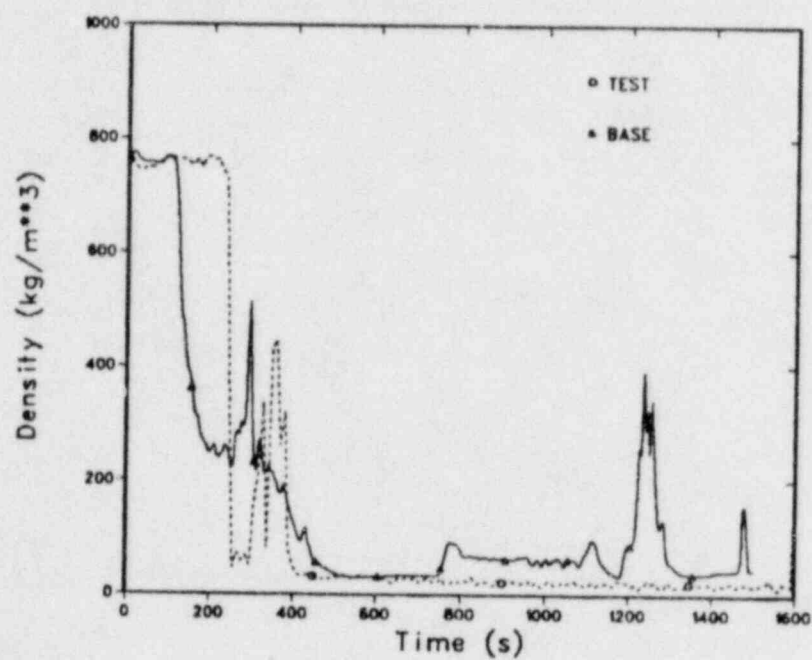


Fig. 58.  
Broken-loop cold-leg density for Test S-UT-7.

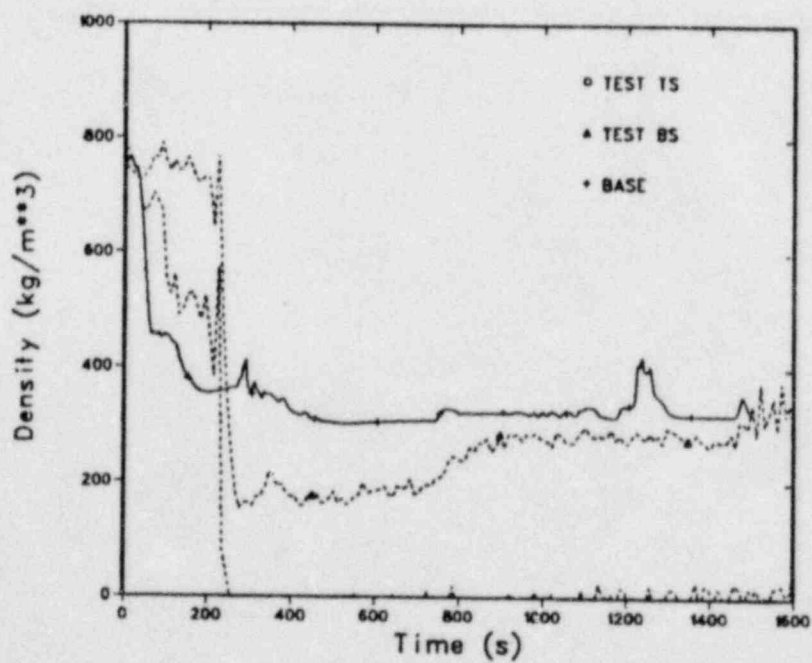


Fig. 59.  
Intact-loop hot-leg density for Test S-UT-7.



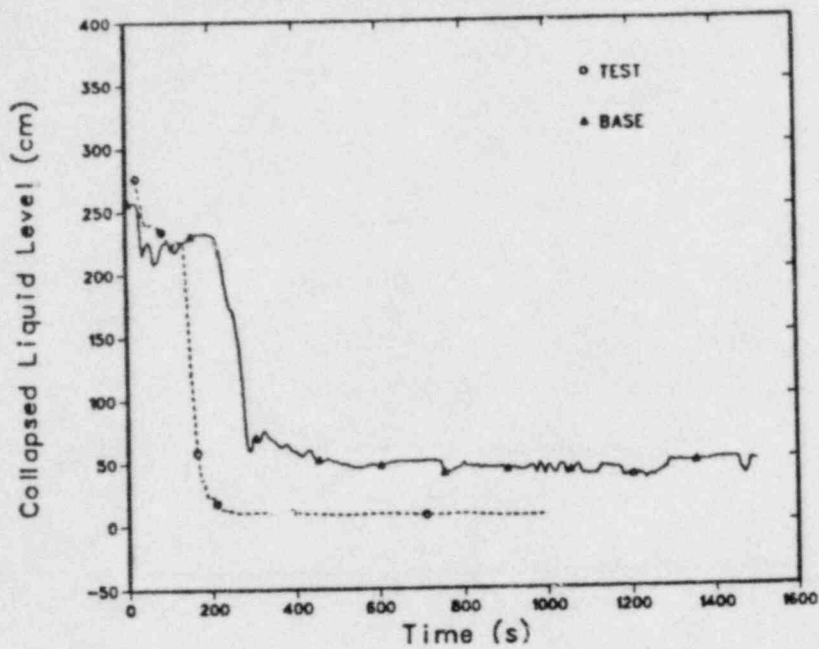


Fig. 60.

Collapsed liquid level in intact-loop pump-suction downflow leg for Test S-UT-7.

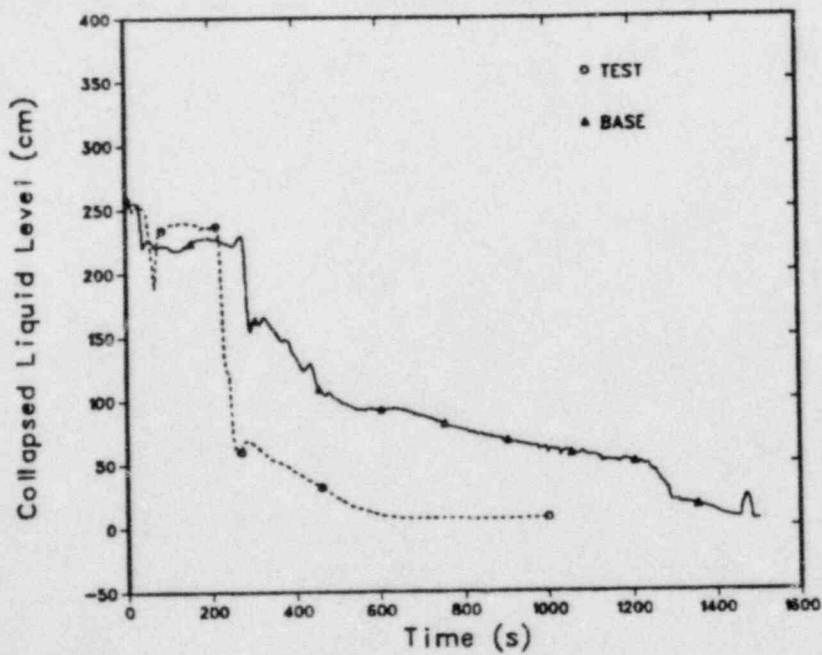


Fig. 61.

Collapsed liquid level in intact-loop pump-suction upflow leg for Test S-UT-7.

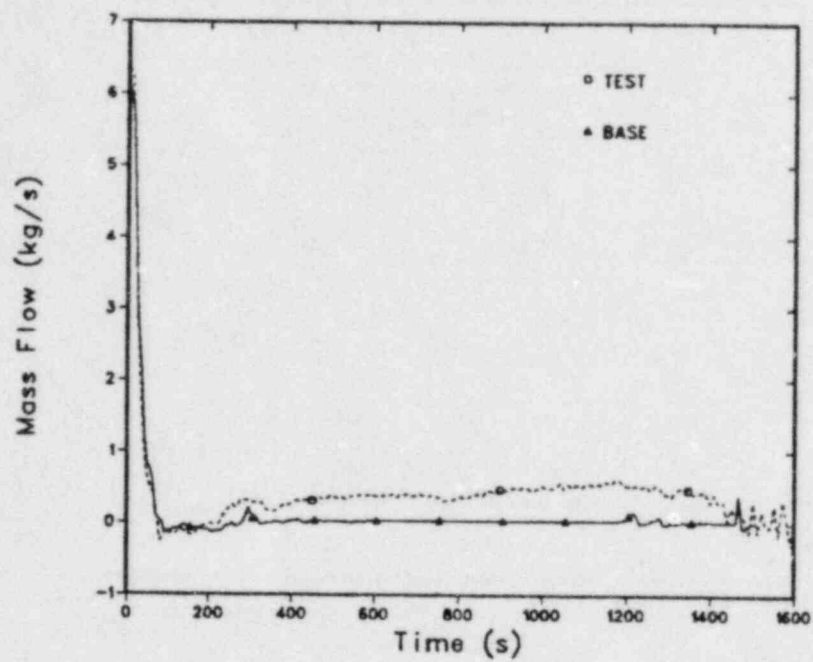


Fig. 62.  
Intact-loop hot-leg mass flow for Test S-UT-7.

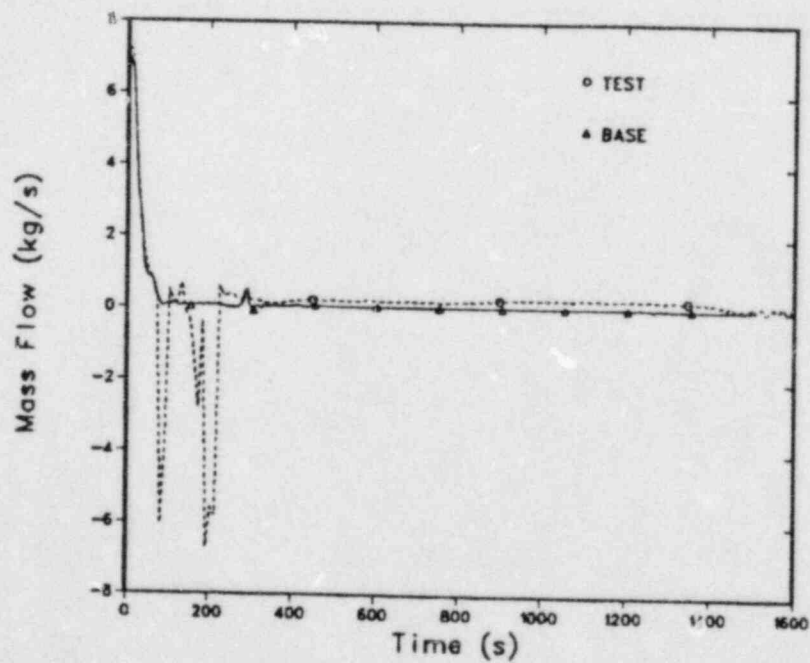


Fig. 63.  
Intact-loop cold-leg mass flow for Test S-UT-7.

reestablished following clearance of the loop seal. Because liquid remained in the upflow leg following the initial clearance of the loop seal, no such reestablishment of flow was calculated. The large flow surges in the intact-loop cold leg to ~200 s are not calculated.

The collapsed liquid levels in the broken-loop pump-suction downflow and upflow legs are shown in Figs. 64 and 65. In the downflow leg, the calculated clearance of the loop seal was slightly delayed. The data also show a slight refilling of the downflow leg between 400 and 1400 s that occurred over a longer time than calculated. In the upflow leg a more rapid initial clearance of the loop seal was calculated. Liquid remained in the upflow leg during the test while complete clearance was predicted by TRAC-PF1. Figures 66 and 67 show the calculated and measured mass flows in the hot- and pump-suction legs of the broken loop. The flow surges in the pump-suction leg to ~400 s were not calculated.

5. Core Behavior. The use of UHI did not radically affect the break flow, system pressure history, or loop hydraulics. However, its impact can be observed in the core behavior. The measured and calculated collapsed core liquid levels for Test S-UT-7 are shown in Fig. 68. Although the calculated liquid level does not display each turn of the data, the overall prediction is good. A minimum collapsed liquid level of approximately 180 cm was calculated and 170 cm measured. The calculated decrease in core liquid inventory terminated immediately following operation of the intact- and broken-loop accumulators, while a delay of ~60 s was observed in the test. The measured

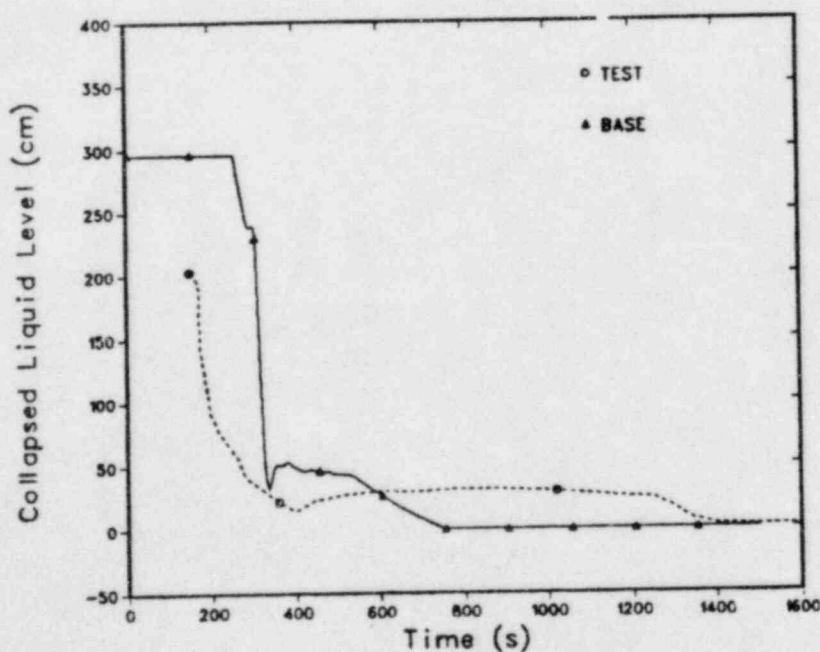


Fig. 64.

Collapsed liquid level in the broken-loop pump-suction downflow leg for Test S-UT-7.

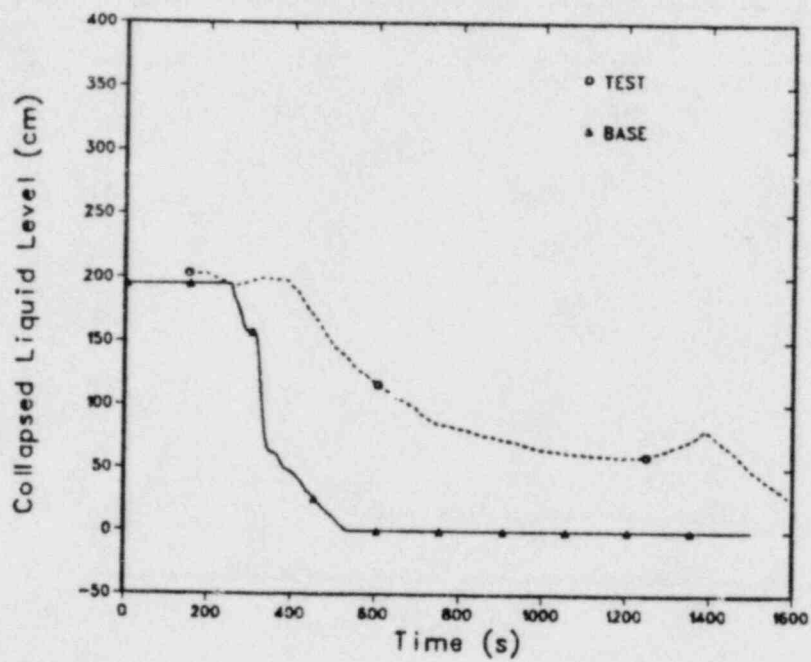


Fig. 65.

Collapsed liquid level in the broken-loop pump-suction upflow leg for Test S-UT-7.

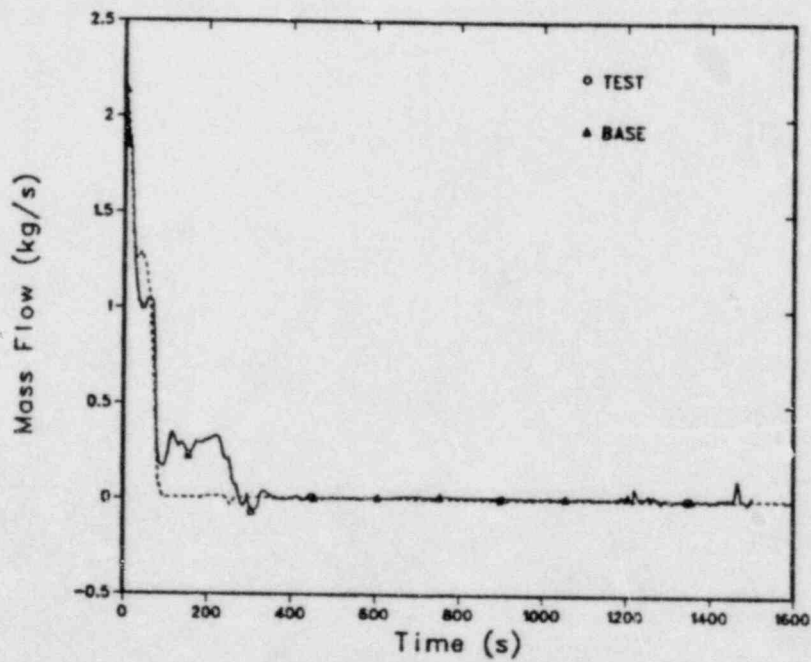


Fig. 66.

Broken-loop hot-leg mass flow for Test S-UT-7.



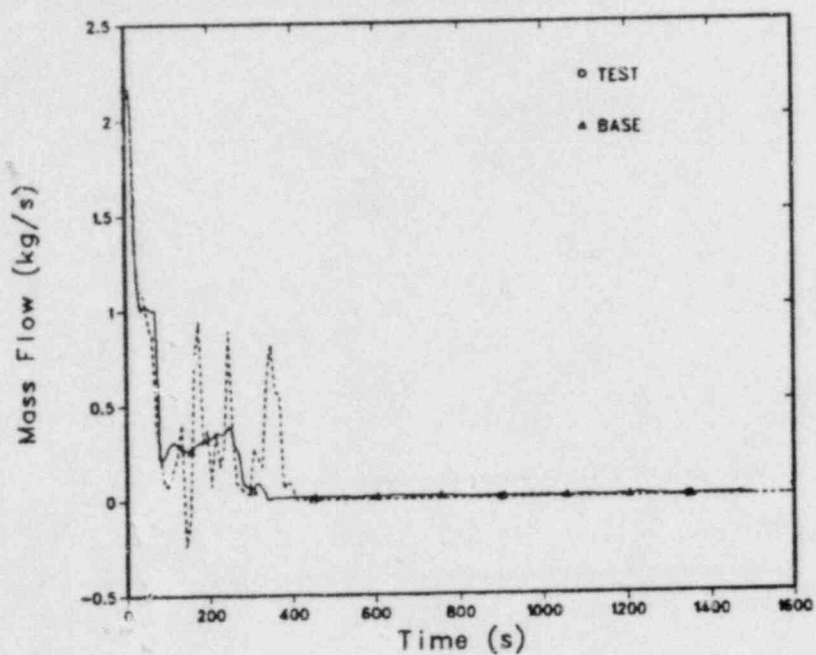


Fig. 67.  
Broken-loop pump-suction mass flow for Test S-UT-7.

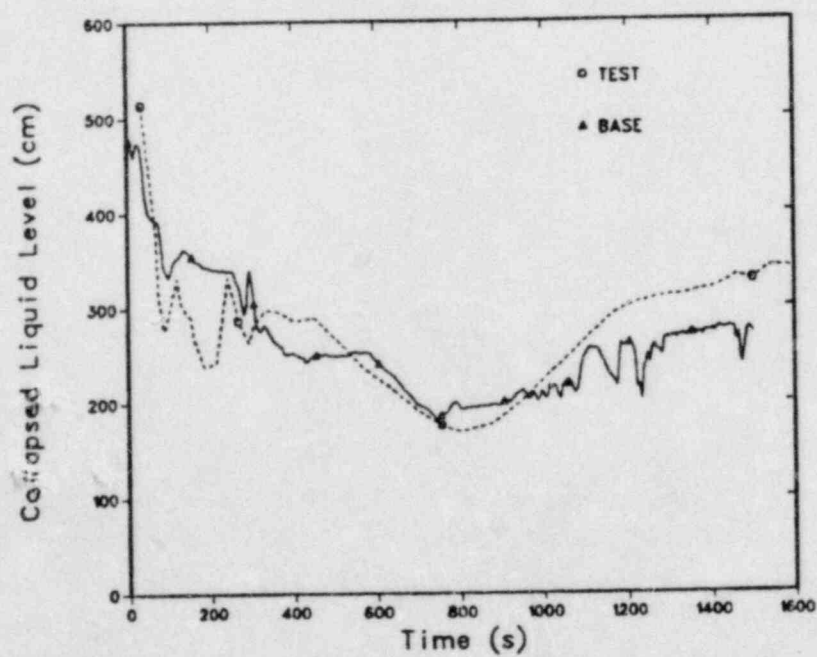


Fig. 68.  
Collapsed core liquid levels for Test S-UT-7.

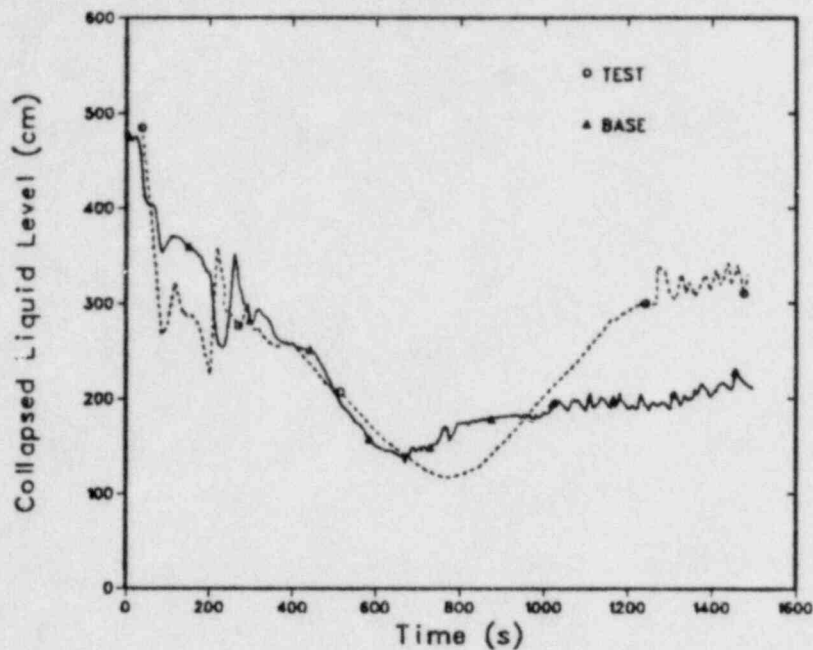


Fig. 69.  
Collapsed core liquid levels for Test S-UT-6.

and calculated core liquid levels for Test S-UT-6 are compared in Fig. 69. The calculated minimum collapsed liquid level of 133 cm occurred at 667 s, and the corresponding measured values were 118 cm at 790 s. The calculated refill is slower than measured in both tests and shows surges in and out of the vessel not observed in the test data. Thus, an increased margin against core heatup was both measured (0.52-m increase in collapsed liquid level) and calculated (0.47 m).

Figures 70 and 71 compare the calculated and measured core fluid densities for Tests S-UT-7 and S-UT-6 at a level 2.03 m above the bottom of the heated core.

Calculated and measured cladding temperatures at the 2.27-m, 2.53-m, and 3.21-m levels for Test S-UT-7 are presented in Figs. 72-74. A dryout is neither calculated or measured at the 2.27-m level, measured but not calculated at the 2.53-m level, and both measured and calculated at the 3.21-m level. At the 3.21-m level, the dryout was predicted to occur ~85 s early and the peak cladding temperature was overpredicted by ~8 K. Calculated and measured cladding temperatures at the same levels are presented for Test S-UT-6 in Figs. 75-77. TRAC-PF1 correctly predicts that the dryout has proceeded to lower core elevations for the non-UHI case as seen by comparing Figs. 72 and 75. At the 3.21-m level the dryout was predicted to occur ~100 s early and the peak cladding temperature was overpredicted by 50 K.

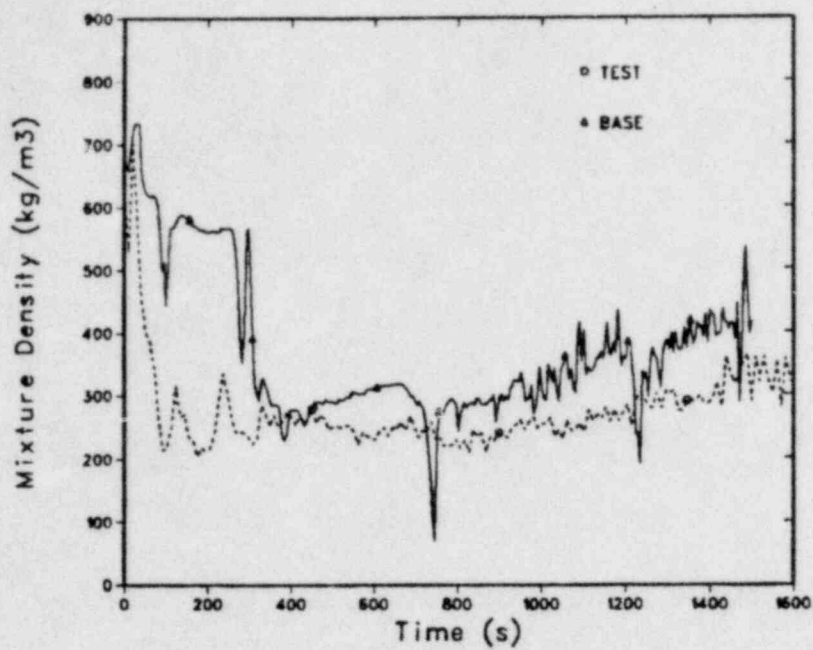


Fig. 70.  
Core density at the 2.53-m level for Test S-UT-7.

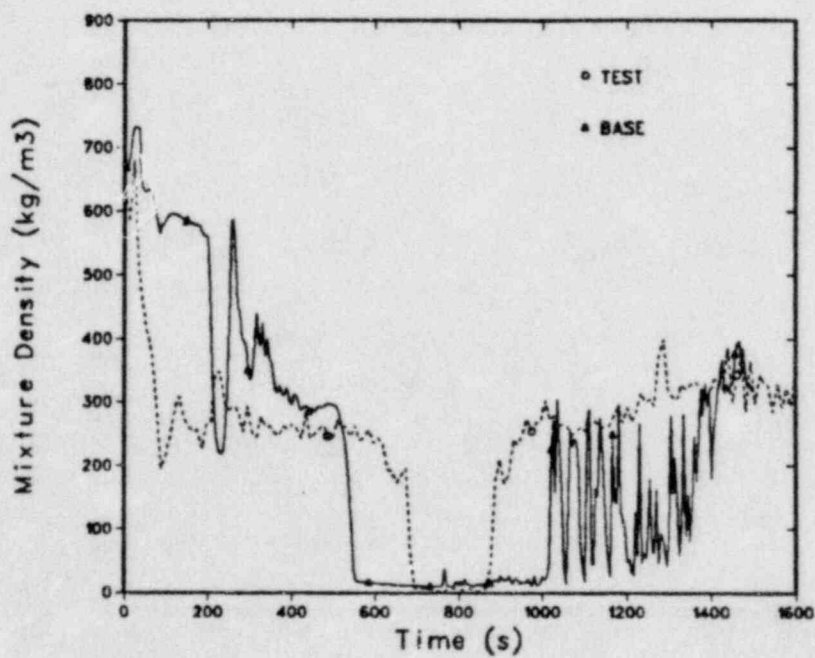


Fig. 71.  
Core density at the 2.53-m level for Test S-UT-6.

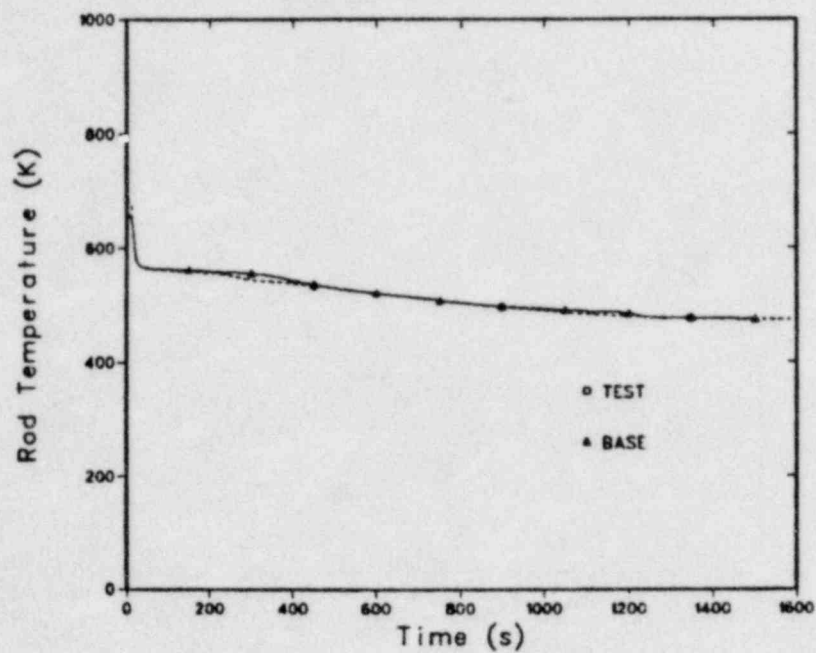


Fig. 72.  
Cladding temperatures at the 2.27-m level for Test S-UT-7.

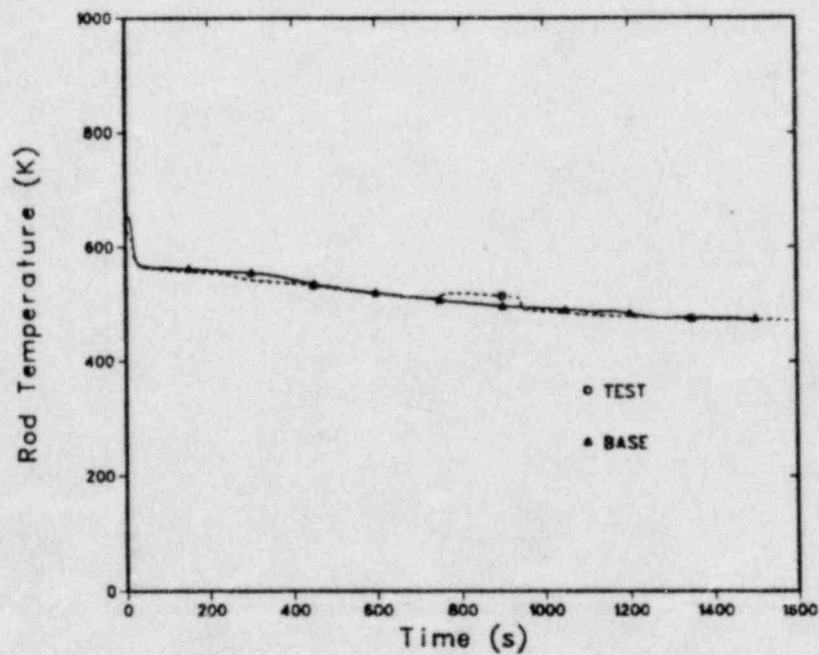


Fig. 73.  
Cladding temperatures at the 2.53-m level for Test S-UT-7.



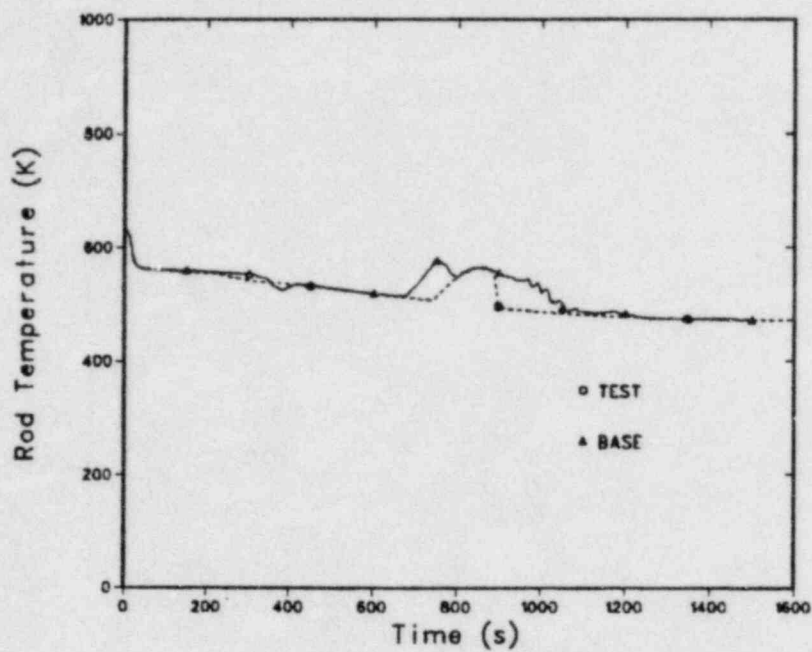


Fig. 74.  
Cladding temperatures at the 3.21-m level for Test S-UT-7.

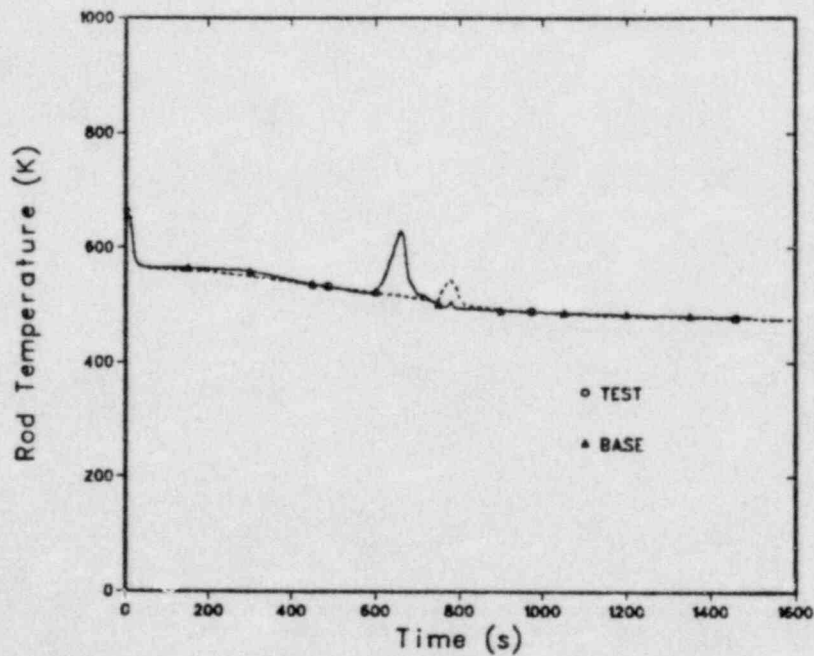


Fig. 75.  
Cladding temperatures at the 2.27-m level for Test S-UT-6.

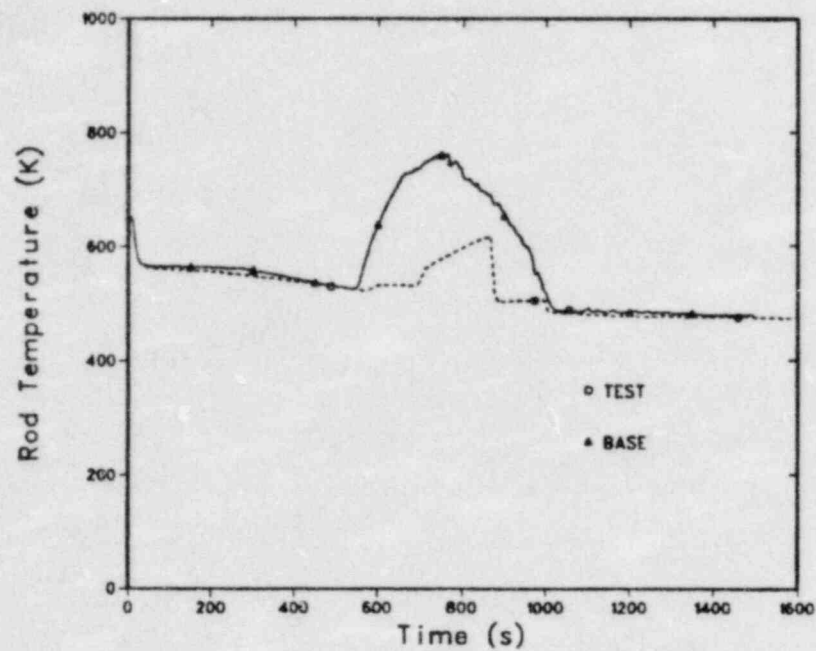


Fig. 76.  
Cladding temperatures at the 2.53-m level for Test S-UT-6.

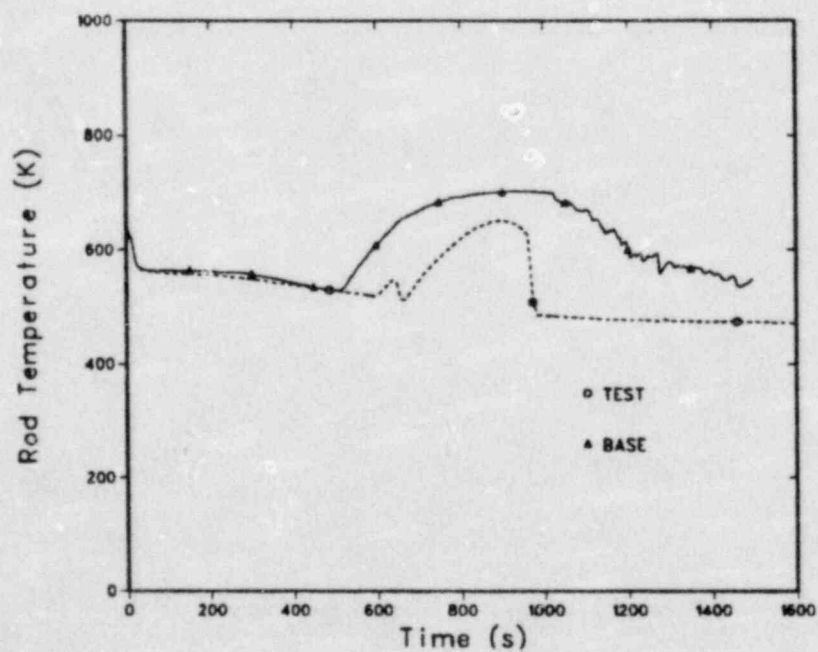


Fig. 77.  
Cladding temperatures at the 3.21-m level for Test S-UT-6.

6. Upper-Head Fluid Behavior. The behavior of the fluid in the upper head was not calculated well for Test S-UT-7. The initial flows for the bypass, guide, and core support tubes were 0.42 l/s, 0.32 l/s, and 0.10 l/s compared to measured values of 0.33 l/s, 0.242 l/s, and 0.088 l/s, respectively. The summed result of the various upper-head inflows and outflows is shown in Fig. 78 for Test S-UT-7, which displays the collapsed liquid level in the upper head. TRAC predicted an early initial drain of the upper head that was caused by calculated support tube flow exceeding the measured by a significant margin.

The prediction of fluid behavior in the upper head was improved for the non-UHI case, Test S-UT-6. The calculated and measured collapsed liquid levels in the upper head for Test S-UT-6 are presented in Fig. 79. It is evident that further review of the upper-head modeling is needed to improve the calculated dynamics of UHI in the upper-head region.

7. Timing Data. A complete transient was calculated for Test S-UT-7 only. The CDC-7600 CPU time required for the 4500 s transient was 18061 s. Thus, the ratio of CPU to real time for the transient was 4.01.

#### F. Conclusions

TRAC-PF1 predicted many of the features of Semiscale UHI Tests S-UT-6 and S-UT-7 well. The correct mode of core dryout was calculated, although predicted dryout times were early and predicted peak cladding temperatures were

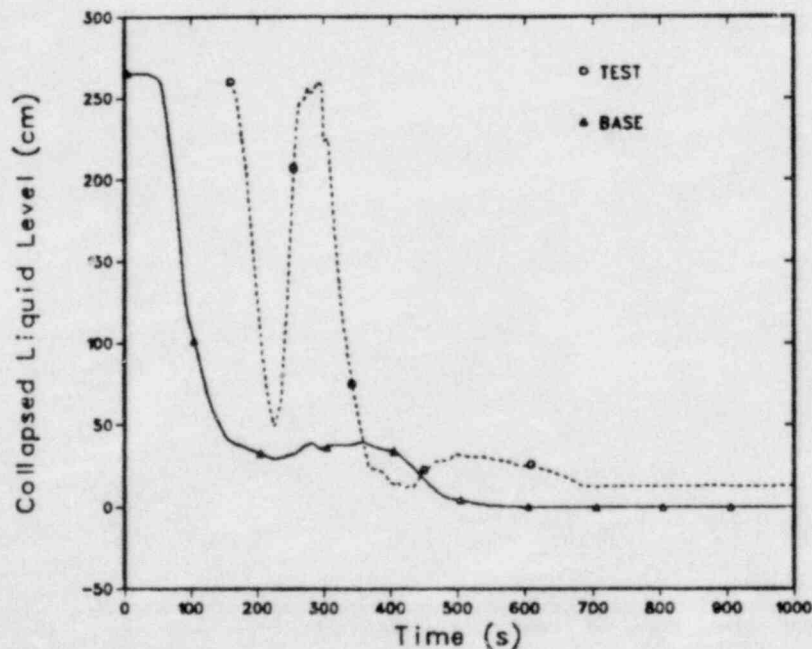


Fig. 78.  
Collapsed liquid level in the upper head for Test S-UT-7.

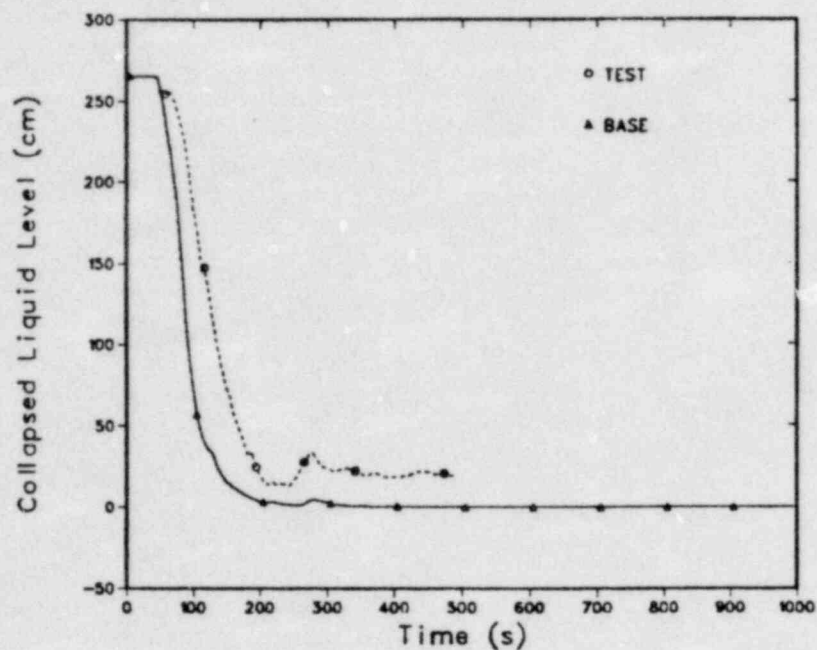


Fig. 79.  
Collapsed liquid level in the upper head for Test S-UT-6.

high. Given the small volume of the Semiscale core, the calculated results are considered to be acceptable.

This assessment has identified features of the code that should be studied further. First, to obtain the correct steady-state primary-loop hot-leg temperatures, it was necessary to specify pump speeds that exceeded those measured. Further review of the Semiscale pump correlations may be required, although these correlations generally are used only for assessment calculations. Second, to obtain the correct steady-state primary-loop cold-leg temperatures, it was necessary to set the steam-generator-secondary conditions at values different from those measured. This suggests a further review of steam-generator secondary-side heat transfer is required. Third, the critical-flow modeling and its coupling to the upstream nodes should be reexamined to determine why the subcooled and two-phase saturated blowdown rates were underpredicted.



## V. TRAC-PF1 POSTTEST ANALYSIS OF LOFT INTERMEDIATE-BREAK EXPERIMENTS L5-1 AND L8-2

Two experiments have been conducted at the LOFT (Ref. 24) at INEL. These tests investigated the thermal-hydraulic phenomena resulting from the rupture of a single 14-in.-diam accumulator injection line in a commercial four-loop PWR and evaluated the effect of primary-coolant-pump restart on core cooling when the primary-coolant system is in a highly voided condition. The data from these two experiments, designated as LOFT Experiments L5-1 and L8-2 (Ref. 25), were used to assess the analytical capability of the Transient Reactor Analysis Code.<sup>1</sup>

In this section, a brief description of the LOFT facility is presented, which is followed by a brief summary of the experimental conditions and test results. The TRAC-PF1 input model is discussed, and comparisons between code calculations and experiment results are presented. Conclusions are drawn regarding adequacy of the code to model LOFT intermediate breaks, and suggestions for future model development are provided.

### A. LOFT System Description

The LOFT facility is a 50-MW(t) PWR with instrumentation to measure the thermal-hydraulic conditions within the system. Operation of LOFT is representative of large commercial PWR operations. The LOFT facility consists of

1. a reactor vessel with a nuclear core;
2. an intact loop with an active steam generator, pressurizer, and two primary-coolant pumps connected in parallel;
3. a broken loop with a simulated pump, simulated steam generator, and two quick-opening blowdown valve (QOBV) assemblies;
4. a blowdown suppression system consisting of a header, suppression tank, and a spray system; and
5. an ECC injection system consisting of two low-pressure-injection-system (LPIS) pumps, two HPIS pumps, and two accumulators.

For LOFT Experiments L5-1 and L8-2, the broken-loop hot-leg components were blind flanged off just downstream of the reflood-assist bypass piping tee. The break nozzle in the broken-loop cold leg was scaled to that of a ruptured 14-in. accumulator line in a commercial PWR.

Figure 80 shows the LOFT major components. Additional information concerning the LOFT facility may be found in Refs. 24 and 25.

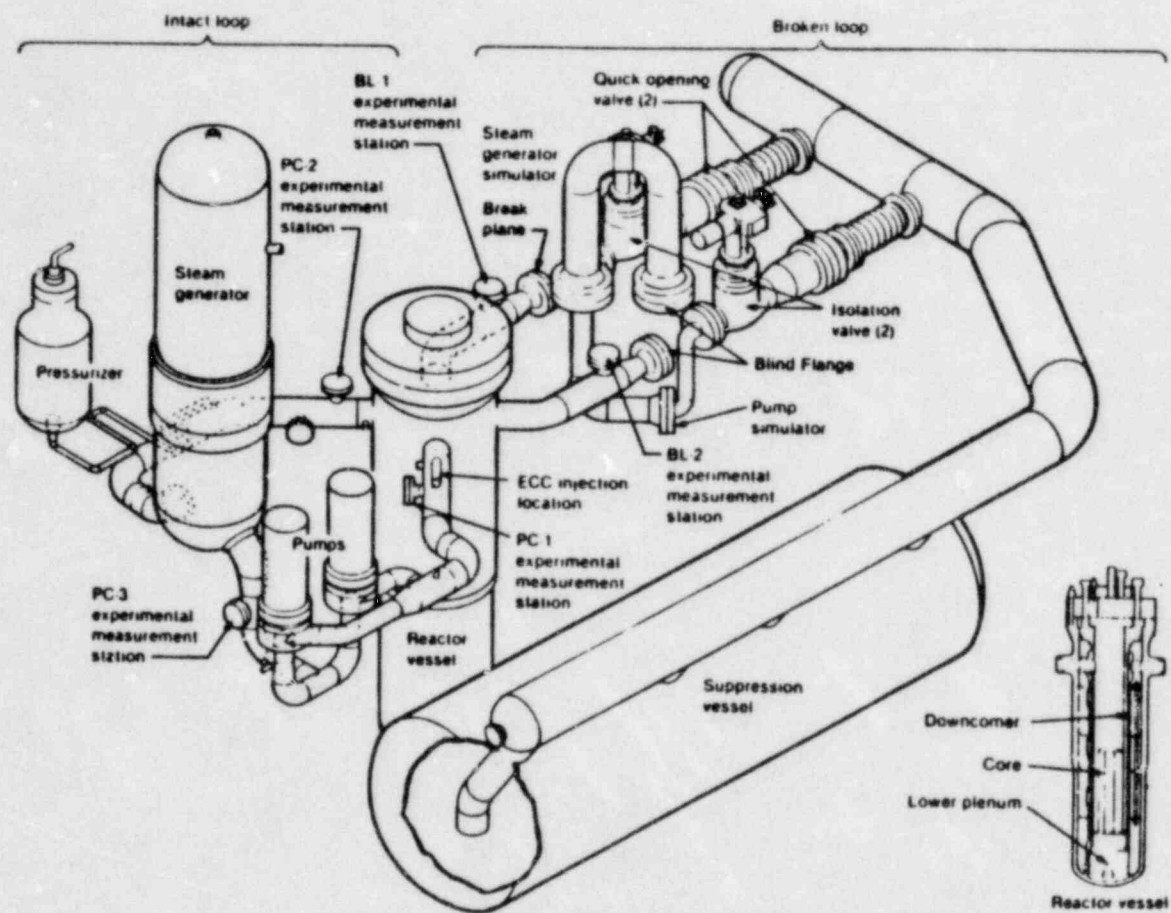


Fig. 80.  
LOFT major components (Ref. 24).

## B. Test Description

For LOFT Experiment L5-1, the plant was brought to the initial power level, temperature, and pressure approximately 40 h before experiment initiation. Experiment L5-1 was initiated when the cold-leg QOBV was opened. The reactor scrammed on low hot-leg pressure (14.19 MPa) at  $0.17 \pm .01$  s. When it was determined that the control rods were fully inserted, the primary-coolant pumps (PCPs) were tripped manually ( $4.0 \pm 0.5$  s) by terminating power to the pump motor-generator sets. The PCPs then coasted down under the influence of the generator-flywheel system until  $19.3 \pm 0.1$  s, when power to them was disconnected. One of the PCPs stopped fairly quickly, while the other continued to turn.

HPIS injection, initiated by a hot-leg pressure setpoint of 10.6 MPa, commenced at  $2.88 \pm 0.1$  s and delivered a scaled flow of  $0.5 \pm 0.2$  L/s into the intact-loop cold leg. The secondary main-feedwater pumps tripped on receipt of the scram signal, and the secondary steam-control valve commenced to close. The steam-control valve fully shut at  $12.1 \pm 0.2$  s. At  $0.2 \pm 0.1$  s, the reactor-vessel upper plenum reached saturation pressure and voiding began. The pressurizer emptied at  $15.5 \pm 0.5$  s. A thermal excursion began at the top of the active core region at  $108.4 \pm 1.0$  s and continued to move further down into the core until  $184.0 \pm 1.0$  s. At this time, the primary coolant system (PCS) pressure had decreased sufficiently ( $1.66 \pm 0.06$  MPa) to allow the accumulator injection system to commence core reflood. A maximum fuel-cladding temperature of  $715.0 \pm 3$  K was reached at  $198.0 \pm 2.0$  s. The core reflood was assisted by the scaled LPIS, which began injecting ECC water to the intact-loop cold leg when the PCS pressure had decreased to  $1.08 \pm 0.06$  MPa at  $201.0 \pm 0.5$  s. Core reflood was complete and the experiment was terminated at  $214.0 \pm 1.0$  s, when all fuel-cladding temperature measurements were at or below the saturation temperature.

The operating procedure and sequence of LOFT Experiment L8-2 essentially were identical to Experiment L5-1 until the time when the accumulator began injecting water in the PCS. In Experiment L8-2, the accumulators were isolated so that automatic coolant injection would not occur. The fuel-cladding-thermocouple temperature excursion began at  $112.0 \pm 0.5$  s, and progressed to the lowest thermocouple elevation by  $240.0 \pm 2.0$  s. The PCPs were restarted when the highest monitored fuel-cladding thermocouples reached the 811-K setpoint at  $234.5 \pm 0.5$  s. The highest fuel-cladding thermocouples reached  $950.0 \pm 3.0$  K at  $286.0 \pm 0.5$  s, whereupon the operators tripped the PCP power ( $291.0 \pm 1.0$  s) and initiated Accumulator-A injection ( $294.0 \pm 1.0$  s). Cladding temperatures continued to rise and at  $299.2 \pm 2.0$  s reached 978 K, at which time the test was terminated by the automatic safety system.

## C. TRAC Model

The code version for the analysis reported here was TRAC-PF1. The TRAC-PF1 LOFT input models were converted from TRAC-PD2 models for the same experiments. These were set up for both experiments using one- as well as three-dimensional representations of the LOFT reactor vessel. As the three-dimensional vessel models are more extensively run and analyzed, our discussion concerning the modeling details will concentrate on them.



Figures 81-83 show the TRAC-PF1 noding for LOFT Experiment L8-2. The noding for LOFT Experiment L5-1 was identical to L8-2 except for the modeling of ECC system B (components 71-76). The B system was not modeled in the L5-1 analysis because that system was not used during the L5-1 experiment.

Figure 84 shows a diagram of the break spool piece installed in the LOFT broken-loop cold leg for these two experiments. Figure 85 shows the TRAC-PF1 noding of this component for the final calculations.

As part of model development for these tests, several early calculations were performed to evaluate the relative merits of modeling the break orifice with a separate hydrodynamic fluid cell. It was found that if the saturated break discharge were overpredicted by a constant amount, the correct break flow could be predicted in both subcooled and saturated regimes by not modeling the break orifice explicitly and by using a saturated break-discharge coefficient of less than 1.0. As will be discussed in more detail in the next section, a nonconstant discharge coefficient is necessary to calculate the observed break flow accurately. Because of these difficulties in modeling the critical-flow processes through this component, it was necessary to control the break flow with a valve. Trips were used to adjust the valve area such that the calculated break flow approximated the measured break flow during the transient.

Table VII compares the key initial conditions for LOFT Experiment L5-1. The corresponding table of information for LOFT Experiment L8-2 is shown in Table VIII.

#### D. Results

In this section, results from three calculations will be discussed in detail: (a) an L5-1 base-case calculation where the break flow was not controlled to match the experiment results, (b) an L5-1 posttest analysis calculation, and (c) an L8-2 posttest calculation. The latter two cases employed a valve that controlled the break area such that the calculated break flow would approximate the measured break flow.

In performing the initial analysis of experiment L5-1, a one-dimensional vessel calculation was run. In these one-dimensional calculations, dryout of the core did not occur. The three-dimensional models were used in the final calculations to take advantage of the interphase sharpener model, which is available in the three-dimensional vessel component.

1. Base-Case Results. Figure 86 compares the calculated and measured break flow for the L5-1 base case. The calculated primary-system pressure declines much faster than the measured data for the majority of the experiment. Figure 87 shows the calculated break flow. The flow is significantly larger than the measured data for the majority of the transient and accounts for the too-rapid pressure decline. Figure 88 compares the calculated and measured fluid densities just upstream of the break to be in relatively good agreement for the majority of the period calculated. Figure 89 shows the calculated vapor fraction just upstream of the break, and Fig. 90 shows the calculated break flow plotted as a function of the calculated vapor fraction.



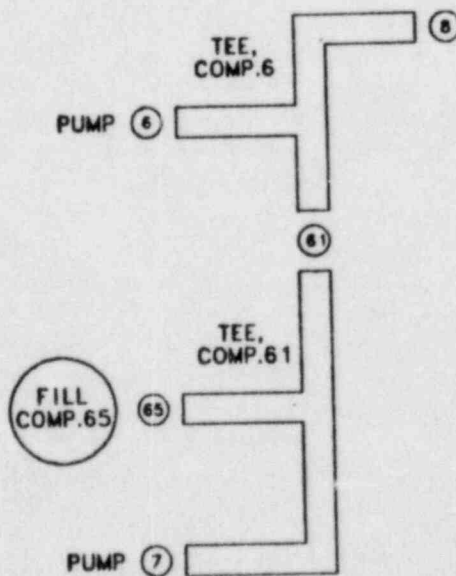
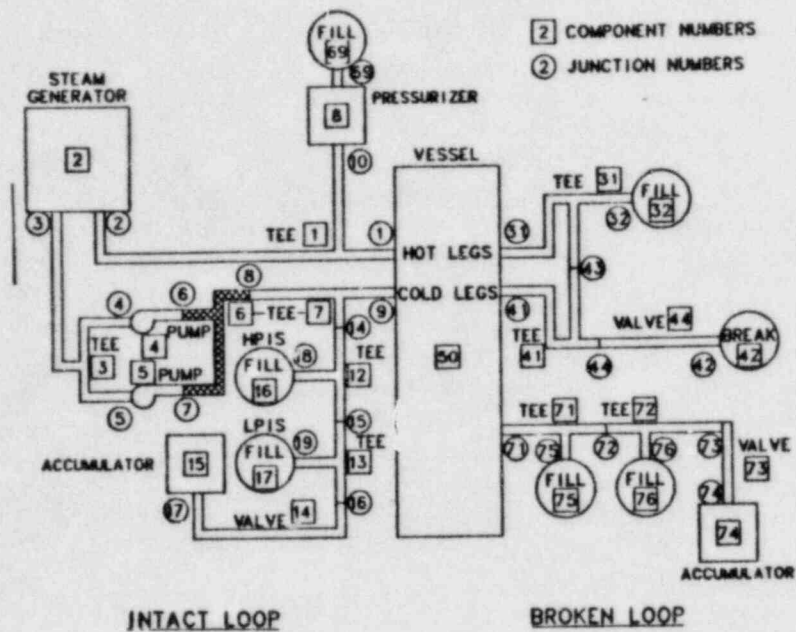


Fig. 81.  
TRAC noding for LOFT Experiment L8-2.

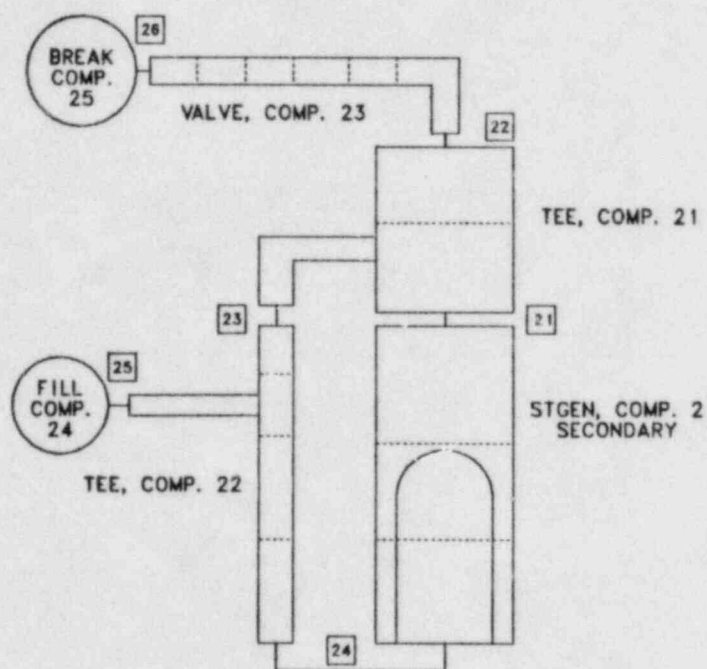


Fig. 82.  
TRAC noding for LOFT Experiment L8-2.

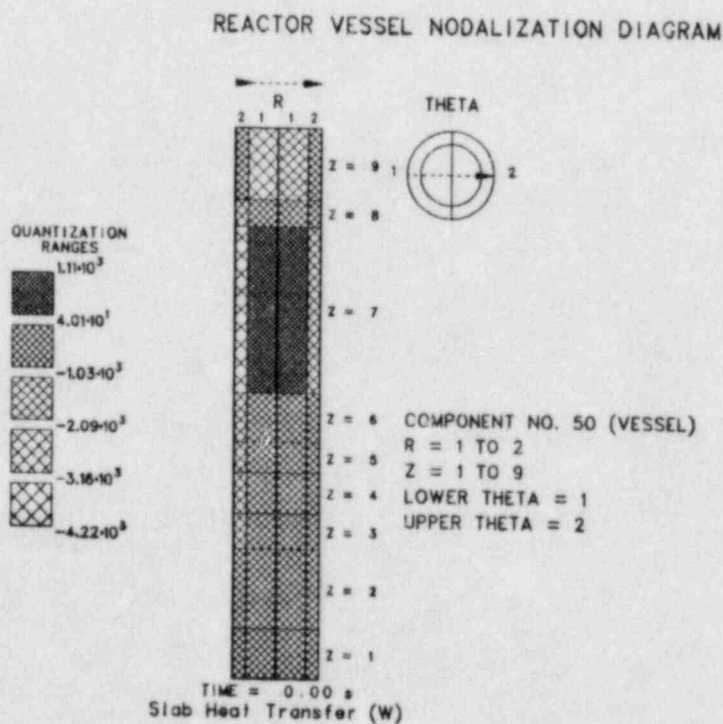


Fig. 83.  
TRAC reactor-vessel noding for LOFT Experiment L8-2.

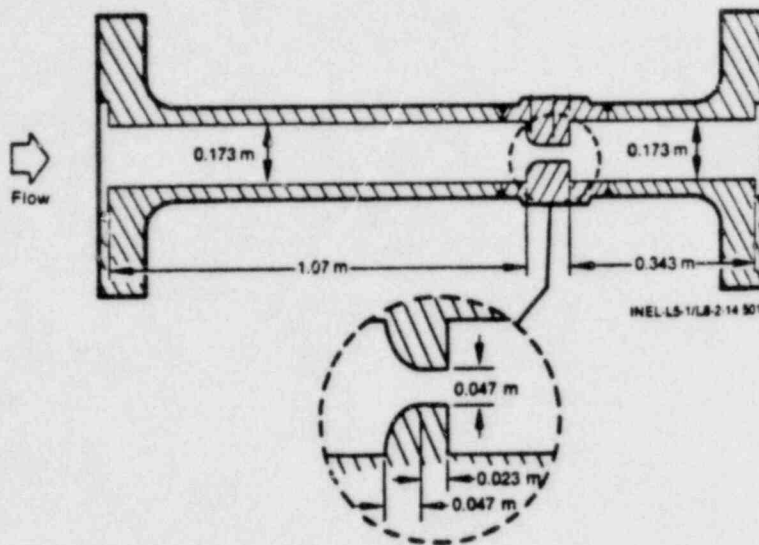


Fig. 84.  
LOFT broken-loop cold-leg spool piece (Ref. 24).

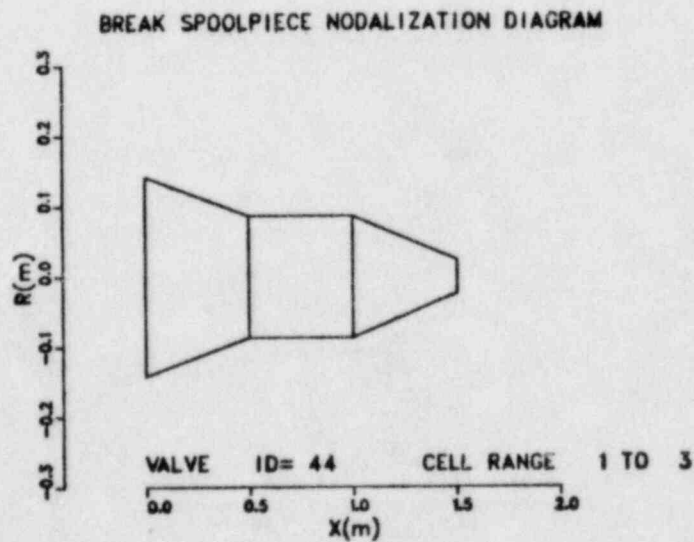


Fig. 85.  
LOFT break spool piece noding.

TABLE VII  
KEY INITIAL CONDITIONS FOR LOFT EXPERIMENT L5-1

<u>Initial Condition</u>	<u>LOFT</u>	<u>TRAC-PF1</u>
Intact-loop hot-leg temperature (K)	579.1 $\pm$ 0.9	580.8
Intact-loop cold-leg temperature (K)	552.3 $\pm$ 0.9	552.8
PCS mass flow (kg/s)	308.2 $\pm$ 4.0	305.2
Reactor power (MW)	45.9 $\pm$ 1.2	45.9
Hot-leg pressure (MPa)	14.93 $\pm$ 0.08	14.93
SGS steam dome pressure (MPa)	5.05 $\pm$ 0.06	5.09

TABLE VIII  
KEY INITIAL CONDITIONS FOR LOFT EXPERIMENT L8-2

<u>Initial Condition</u>	<u>LOFT</u>	<u>TRAC-FF1</u>
Intact-loop hot-leg temperature (K)	579.3 $\pm$ 0.8	579.9
Intact-loop cold-leg temperature (K)	552.4 $\pm$ 0.9	551.8
PCS mass flow (kg/s)	311.2 $\pm$ 4.0	305.9
Reactor power (MW)	46.0 $\pm$ 1.2	46.0
Hot-leg pressure (MPa)	14.86 $\pm$ 0.06	14.87
SGS steam dome pressure (MPa)	5.08 $\pm$ 0.06	5.01



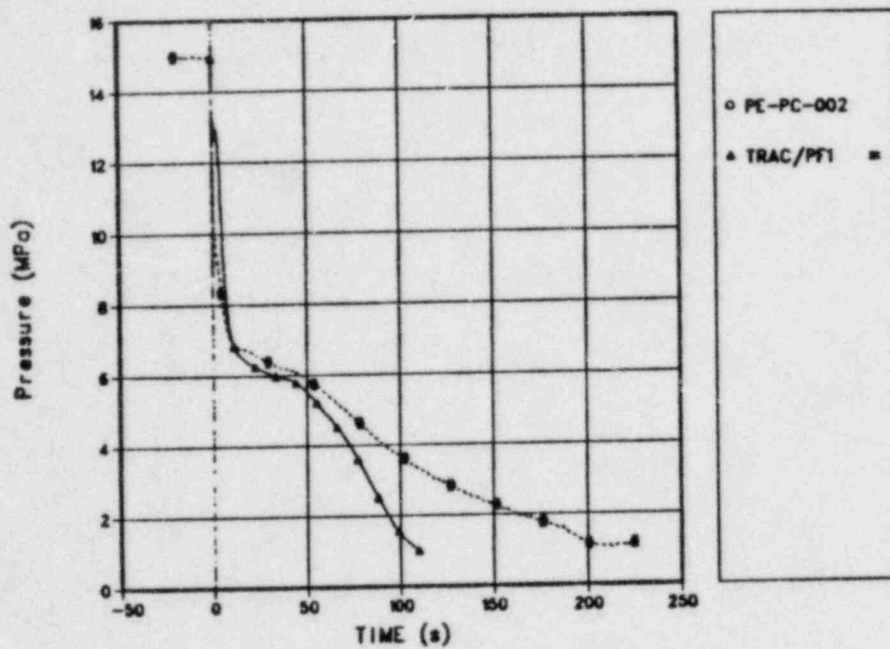


Fig. 86.  
Comparison of TRAC-calculated and measured primary-system pressures.

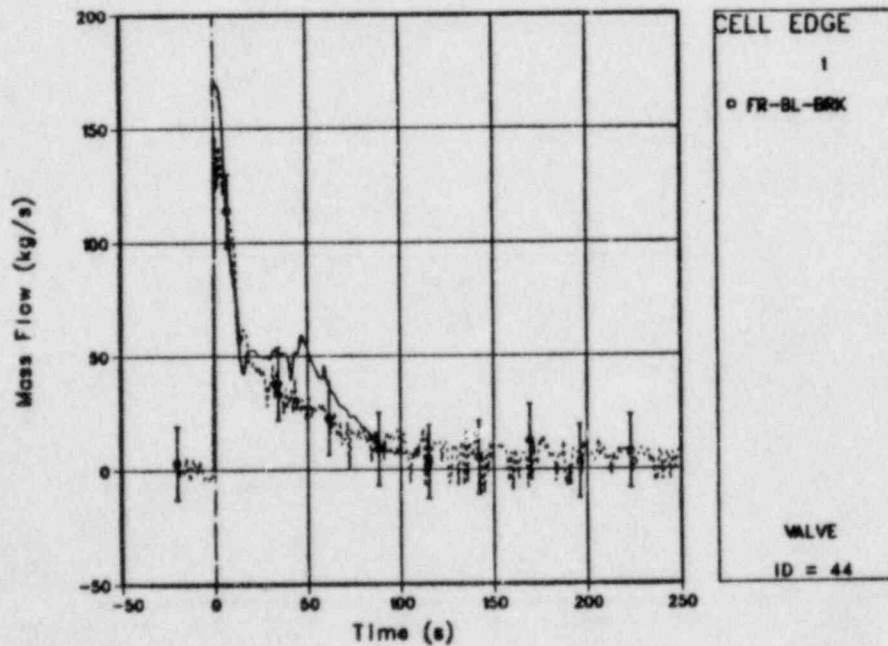


Fig. 87.  
Comparison of TRAC-calculated and measured break flows.

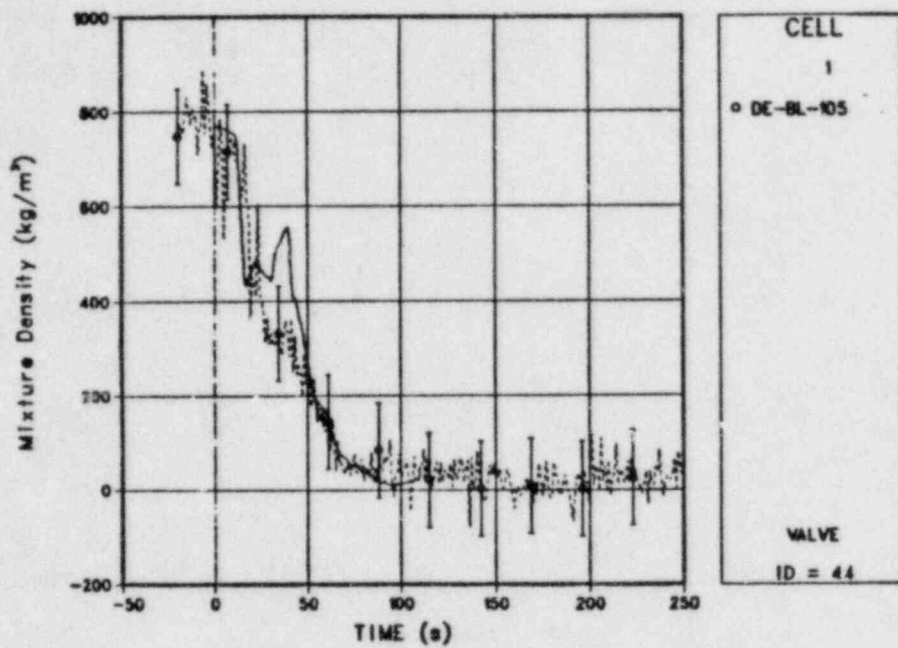


Fig. 88.  
Comparison of TRAC-calculated and measured break fluid densities upstream of the break.

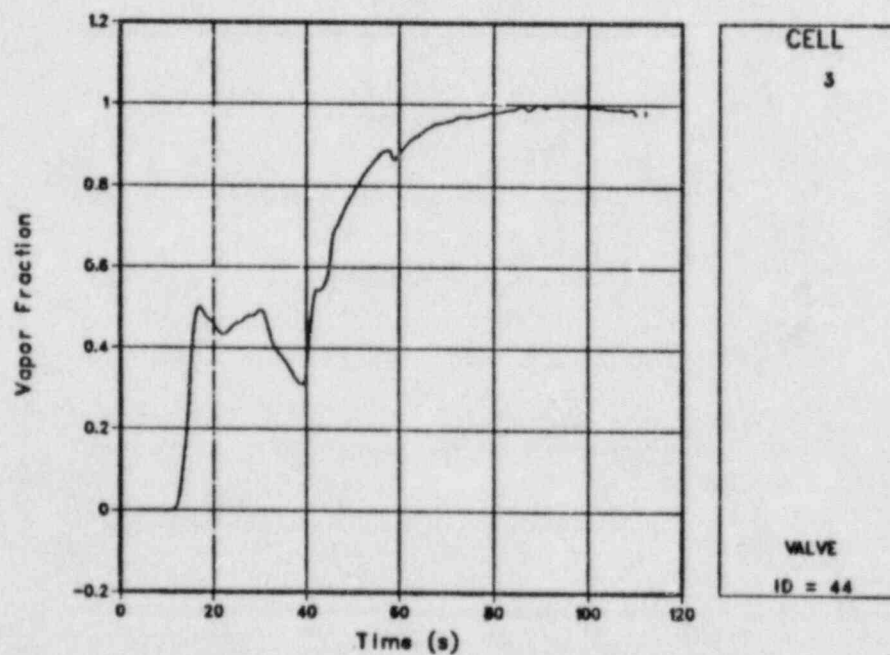


Fig. 89.  
Comparison of TRAC-calculated and measured vapor fractions upstream of the break.

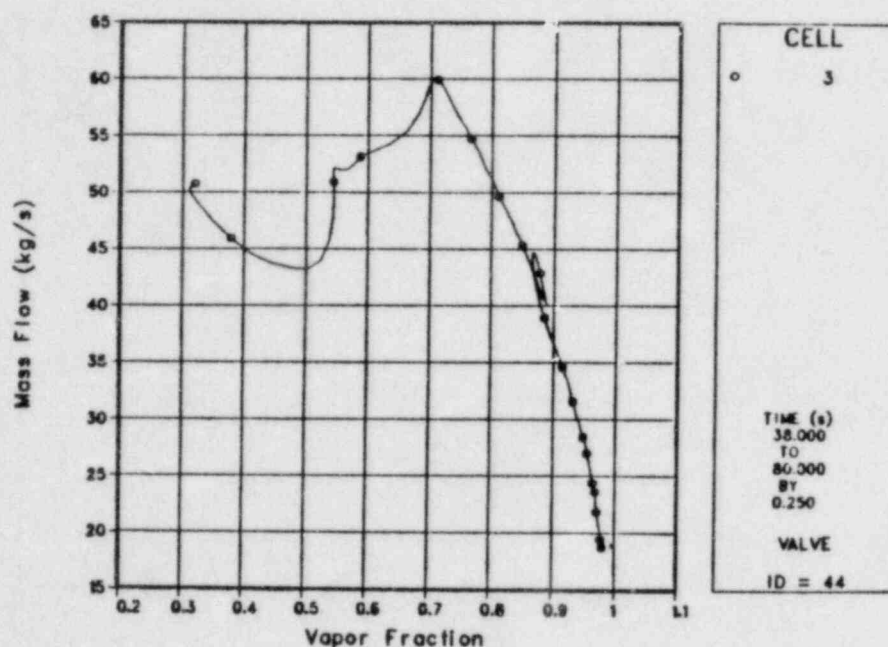


Fig. 90.  
TRAC-calculated break flow vs break vapor fraction.

Note that in Fig. 90 an increasing trend in calculated mass flow occurs between a vapor fraction of 0.5 and 0.7. During the period of increasing mass flow, fluid pressure declines. This result is nonphysical, and results in an unrealistic calculation. Not only is the pressure decline too rapid, but the core dryout occurs too rapidly, along with a too-rapid initiation of ECC. Because of this serious discrepancy in the calculation of break flow, it is difficult to interpret other features of the code comparisons to experiment results. Subsequent calculations, therefore, used the measured break flow to control the area of the valve just upstream of the break, such that the calculated break flow would be in better agreement with the experiment results. The break-flow model in subsequent versions of TRAC-PF1 has been modified and should correct the problems observed in these results.

2. L5-1 Posttest-Analysis Results. Figure 91 compares the predicted and measured break flows for LOFT Experiment L5-1. The valve at the break plane controls the minimum area at the break, shown in Fig. 92, to approximate the measured break flow. The calculated break flow is within the uncertainty of the data, but it is slightly higher than the mean of the data early in the transient and slightly lower later in the transient. This was done deliberately by altering the valve trip setpoints for the best match of time to core uncover and the measured depressurization. In the early analysis of this experiment, a valve was used that was controlled to the mean of the measured break flow; this resulted in more rapid depressurization in the calculations than in the experiment results, and the calculations resulted in delayed core uncover. The L5-1 posttest calculations were found to be extremely sensitive to small changes in break flow. When these occurred

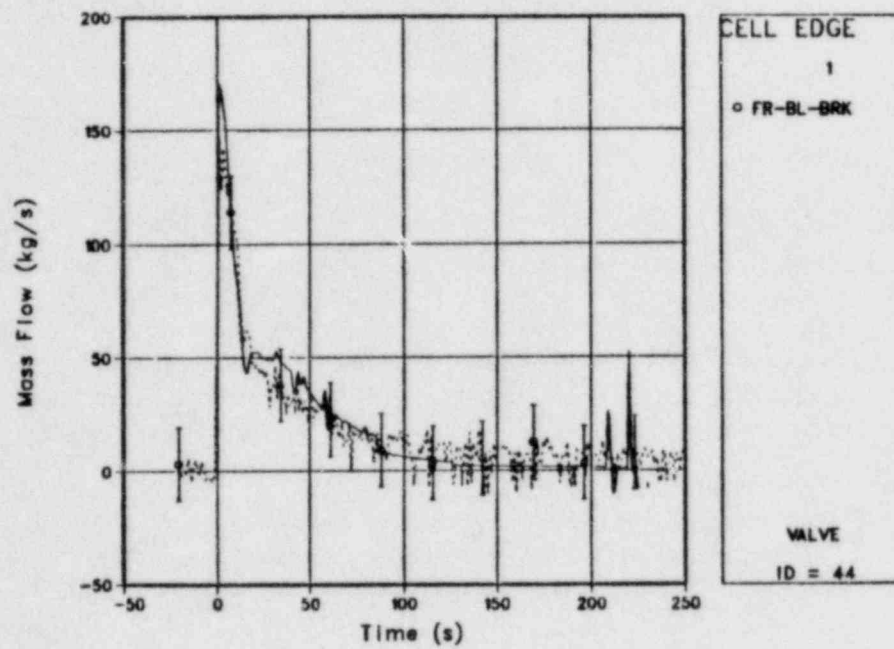


Fig. 91.  
Comparison of TRAC-calculated and measured break flows.

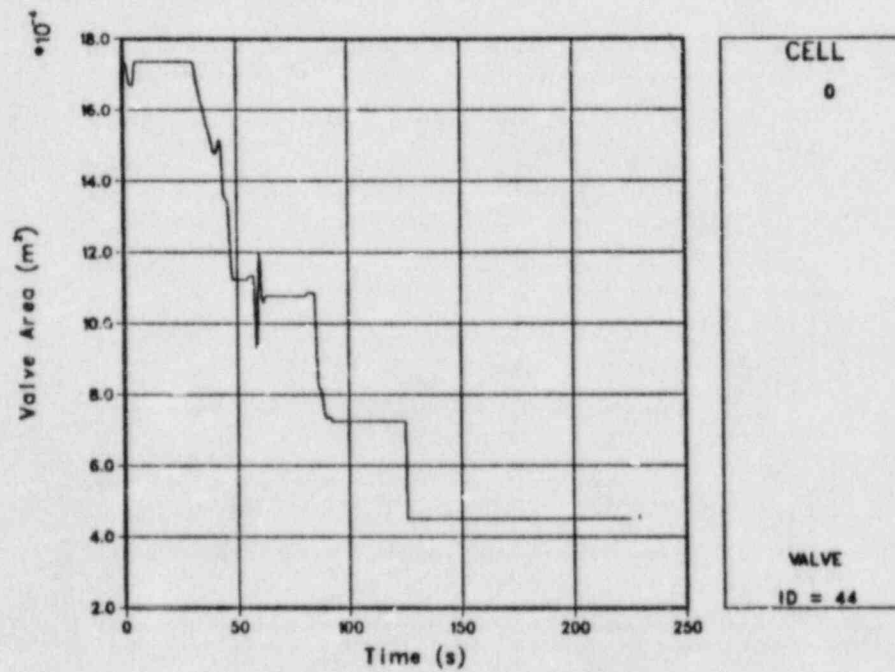


Fig. 92.  
Valve area at the break.



during the early portion of the experiment, when the break discharge was mostly liquid, significant differences resulted in the timing of the beginning of core uncover. Small changes in the break flow later in the transient, when the break discharge was mostly vapor, had significant effects on the rate of depressurization.

Figures 93-95 compare the predicted and measured pressures at different points in the LOFT system. The pressure in the primary system is somewhat higher than the data during the first 10.0 s of the transient, then falls below the experiment results. The calculated pressurizer pressure is in better agreement with the experiment results for the period of liquid discharge from the pressurizer; but as the pressurizer pressure approaches primary system pressure, the calculated results fall somewhat below the experimental results. The calculated pressure in the steam-generator secondary does not reach as high a peak as observed in the experiment results, nor does it decay as rapidly. The LOFT steam-generator secondary steam-control valve probably leaked during this transient and accounts for the more rapid than predicted pressure decay. Because the secondary is not important in breaks of this size, no attempt was made to model this probable leakage.

Figure 96 shows a comparison of the data shown in Fig. 93 on a smaller time scale. The TRAC-PF1-calculated primary-system pressure response during the early portion of the transient differs considerably from the measured results. Examination of the output revealed that the cause of this discrepancy is probably an underprediction of the rates of steam condensation

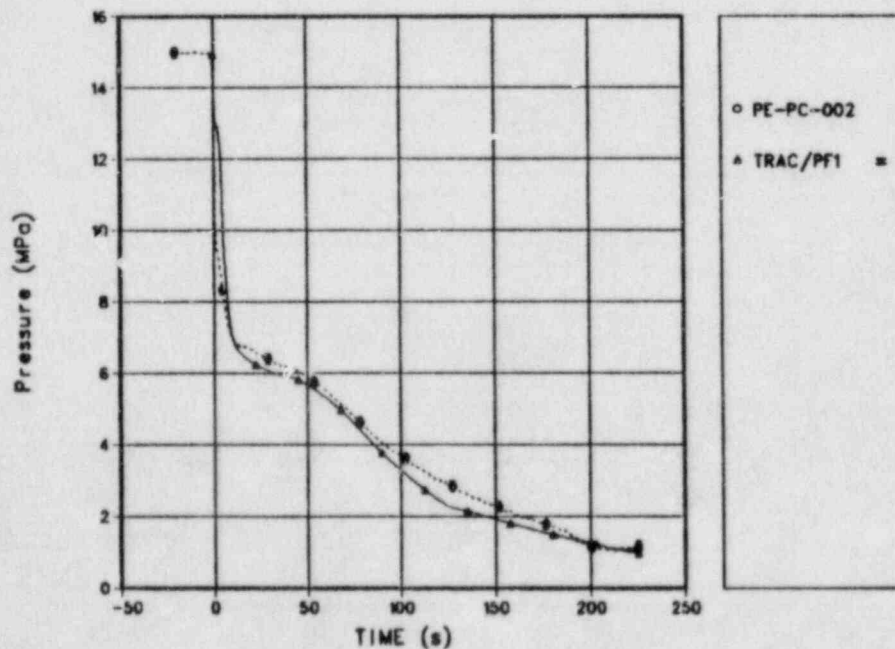


Fig. 93.  
Comparison of TRAC-calculated and measured primary-system pressures.

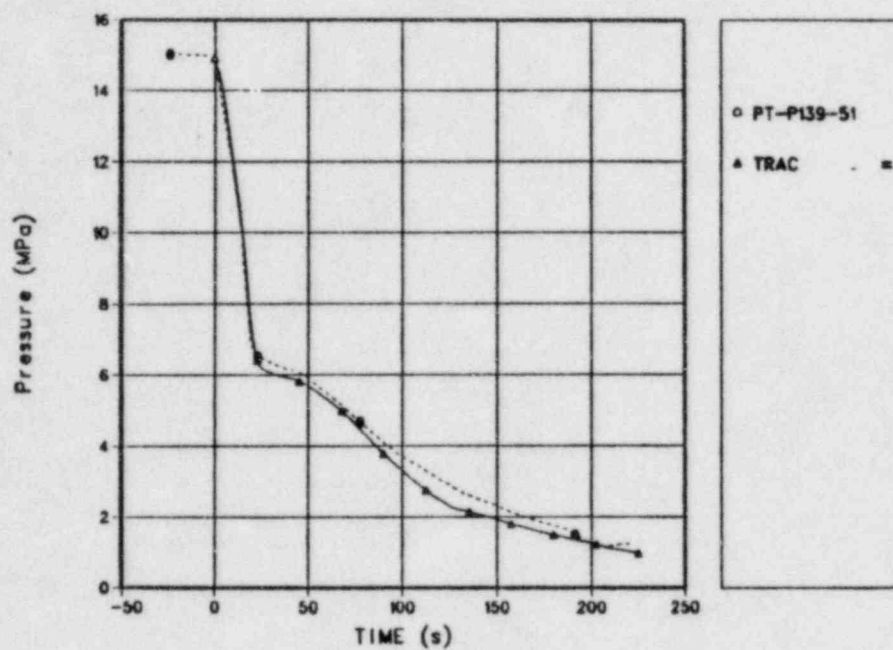


Fig. 94.  
Comparison of TRAC-calculated and measured pressurizer pressures.

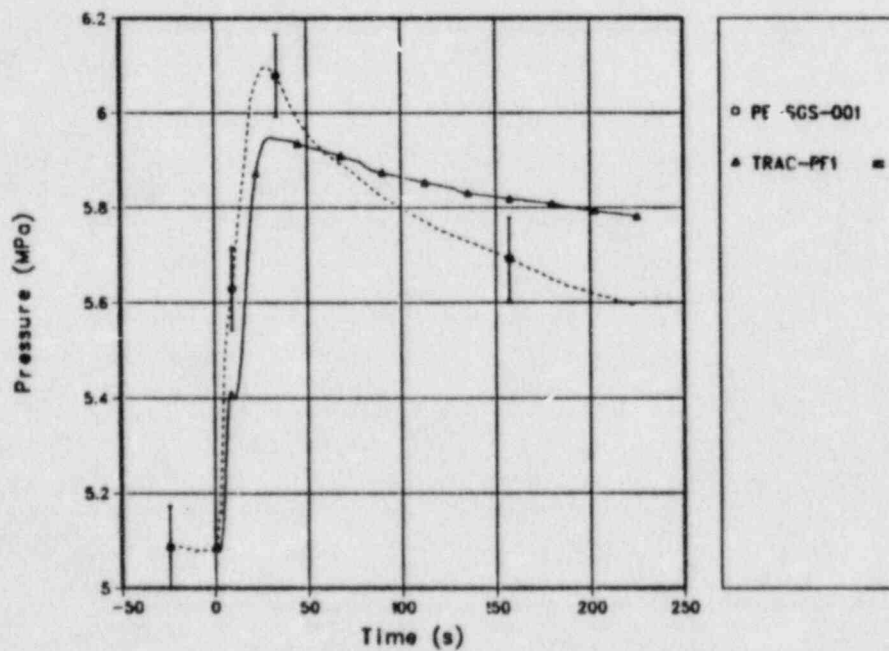


Fig. 95.  
Comparison of TRAC-calculated and measured steam-generator secondary-side steam-dome pressures.

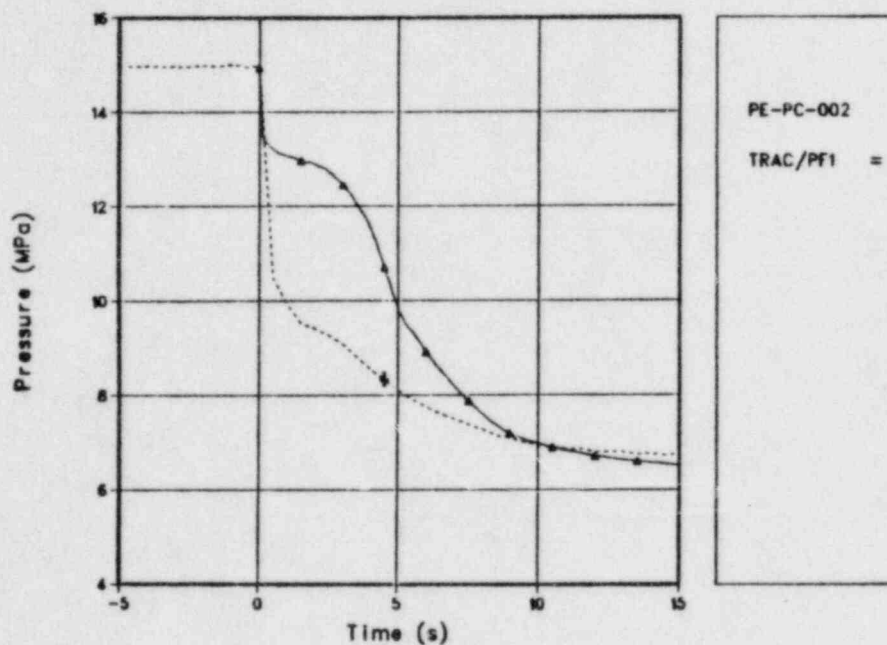


Fig. 96.

Comparison of TRAC-calculated and measured primary-system pressures during the early portion of the transient.

in the vessel. Almost immediately after the start of the transient, the average rods switch into a subcooled, nucleate-boiling heat-transfer mode, which starts vapor formation in a condition of a highly subcooled bulk fluid state. The vapor formed is slow to condense in the three-dimensional vessel component and apparently causes the overprediction of the early system pressure.

Figures 97-99 compare the calculated and measured fluid densities at several locations in the LOFT primary system. The calculated fluid density is within the uncertainty bands of the measured results for the majority of the transient. In the broken-loop cold leg, some core bypass was calculated late in the transient (Fig. 97) that was not observed in the experiment results.

Figure 100 shows a comparison of calculated and measured vapor velocities in the intact-loop cold leg. The calculated results are within the uncertainty bands of the experiment results for the majority of the transient. The sharp drop in the calculated velocity occurs when the break area is reduced sharply at 125.0 s.

Most of the LOFT fluid thermocouple data is subject to hot-wall effects during the transient. One measurement that did not show early hot-wall effects is the measurement in the broken-loop cold leg (shown in Fig. 101). The TRAC-PF1 calculations follow the general trends of the experiment results. Because the calculated primary-system pressure was lower than the experimental pressure and because the fluid temperature follows the corresponding

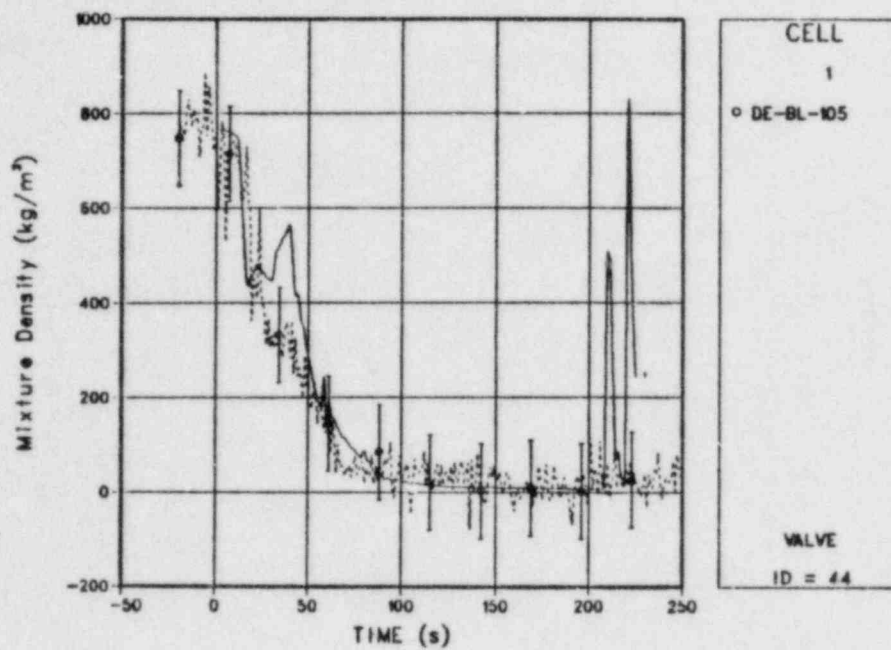


Fig. 97.

Comparison of TRAC-calculated and measured fluid densities upstream of the break.

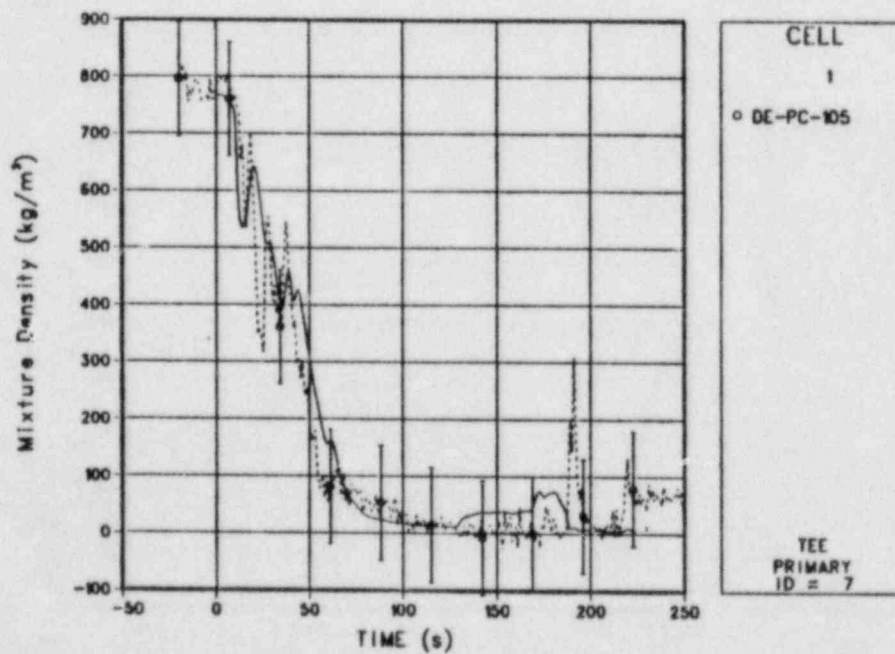


Fig. 98.

Comparison of TRAC-calculated and measured intact-loop cold-leg fluid densities.



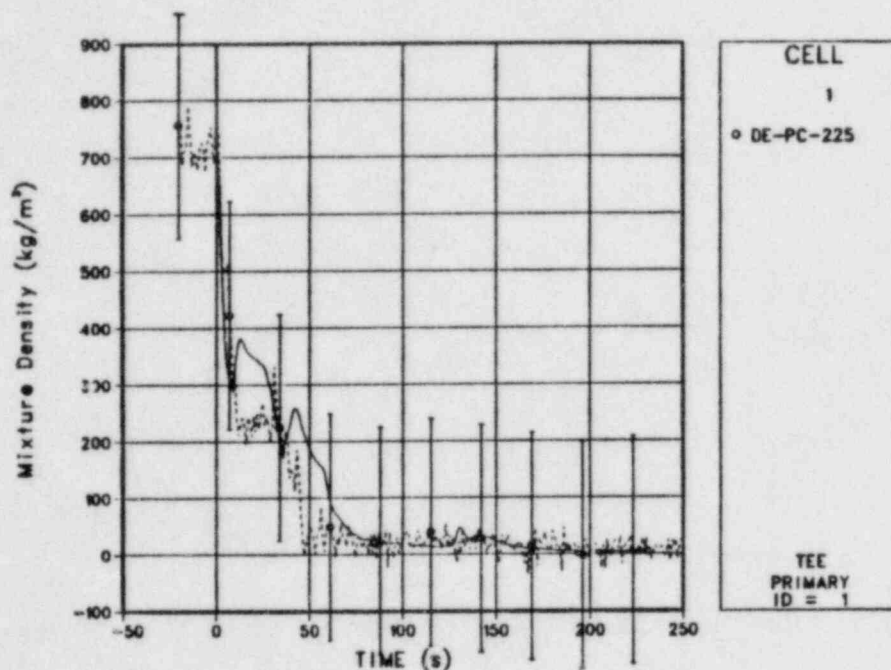


Fig. 99.

Comparison of TRAC-calculated and measured intact-loop hot-leg fluid densities.

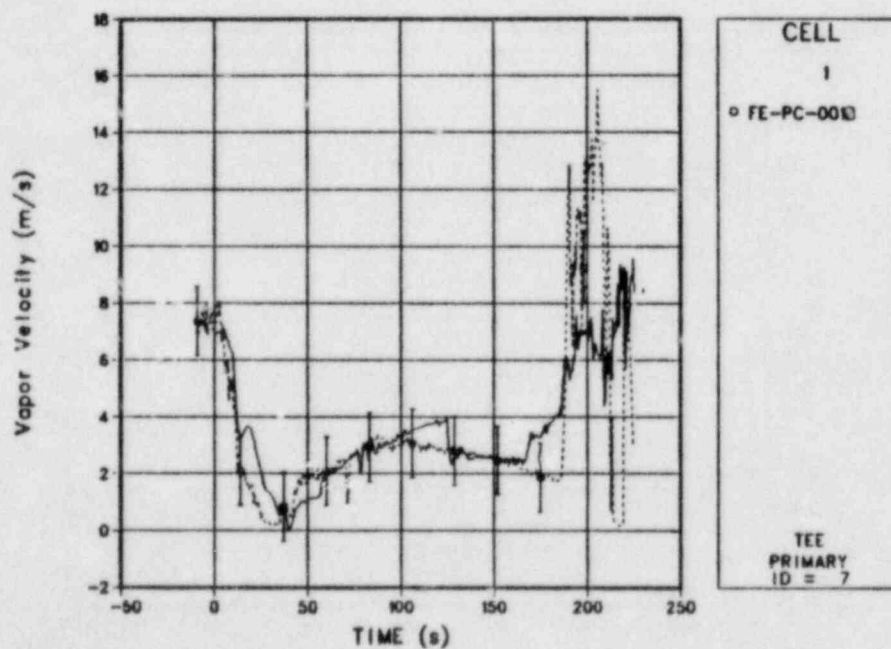


Fig. 100.

Comparison of TRAC-calculated and measured intact-loop cold-leg fluid velocities.

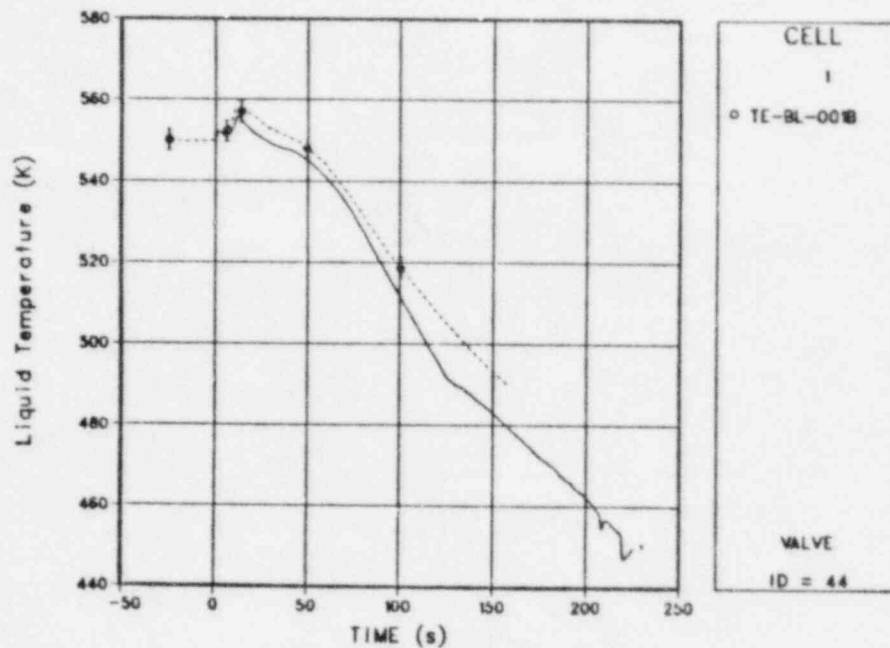


Fig. 101.

Comparison of TRAC-calculated and measured fluid temperatures upstream of the break.

saturation temperature, the calculated temperature was somewhat lower than the measured results. The early rise in measured fluid temperature, which was accurately characterized by TRAC-PF1, can be traced to fluid exiting the steam generator. Early in the transient, before the primary-side tubes void, heat-transfer effects couple the primary and secondary sides. As the pressure rises in the steam generator (due to the closure of the steam control valve), the fluid temperature in the secondary rises. This results in increased primary-system fluid temperature early in the experiment.

Figures 102-104 compare time history plots of the calculated fuel rod cladding for the average-, high-, and low-power rods, respectively. Dryouts and rewets of the rods occur when the void fraction in the adjacent fluid cell crosses 98% void fraction. The active core region was modeled fairly coarsely with four axial levels, so the dryouts and rewets occurred in groups corresponding to the locations of the fluid cells. Figures 105 and 106 show the axial temperature profile of the high-power rod during the blowdown and reflood portion of the transient, respectively. The unusual sawtooth pattern in the rod axial profile is caused by simultaneous dryout of all rods adjacent to a particular fluid cell, which is followed by temperature increases that are proportional to the axial power distribution.

No dryouts occurred in the lower portion of the core in the TRAC-PF1 calculation. This is contrary to the experiment results, where dryouts occurred to the very bottom of the heated core, as shown in Figs. 107-110. Figures 111-114 compare the rods in the next higher level within the core.

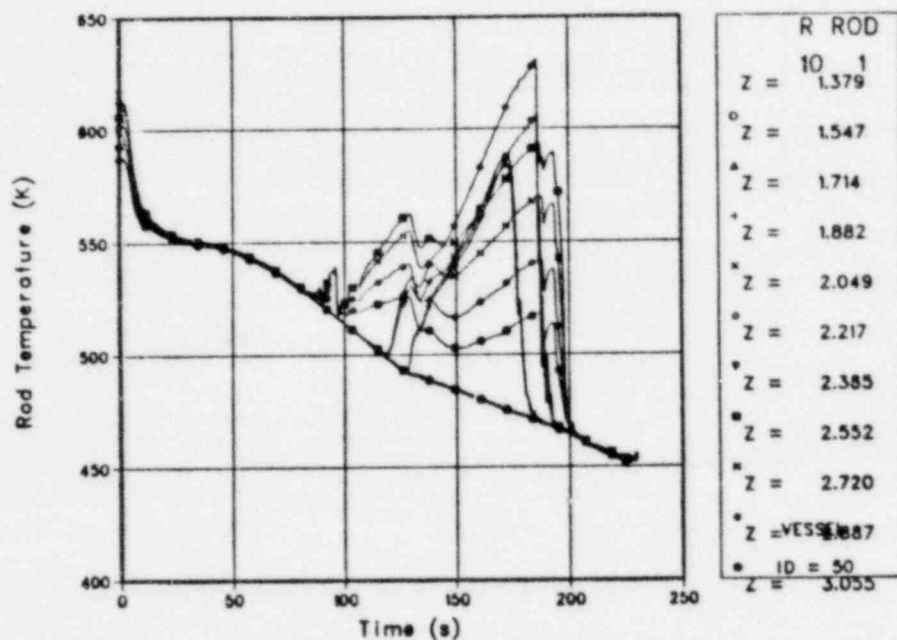


Fig. 102.

TRAC-calculated cladding temperatures for average-power rod at different axial elevations.

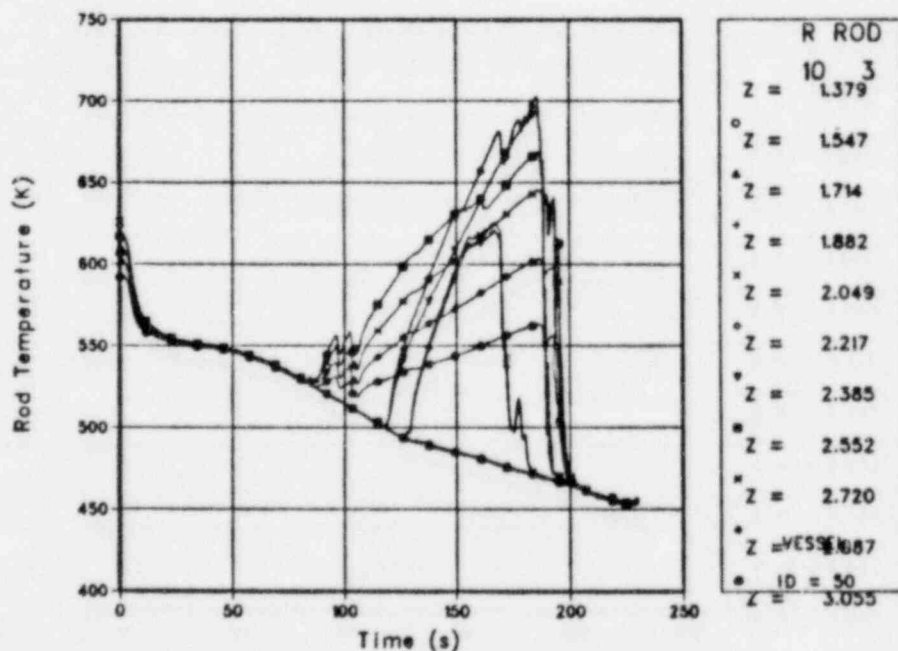


Fig. 103.

TRAC-calculated cladding temperatures for high-power rod at different axial elevations.

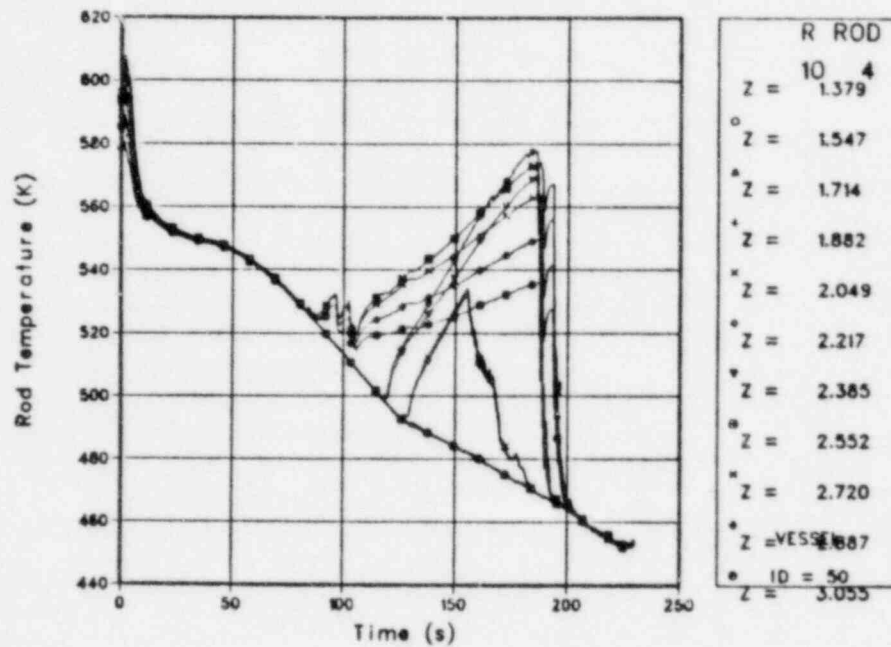


Fig. 104.  
TRAC-calculated cladding temperatures for low-power rod at different axial elevations.

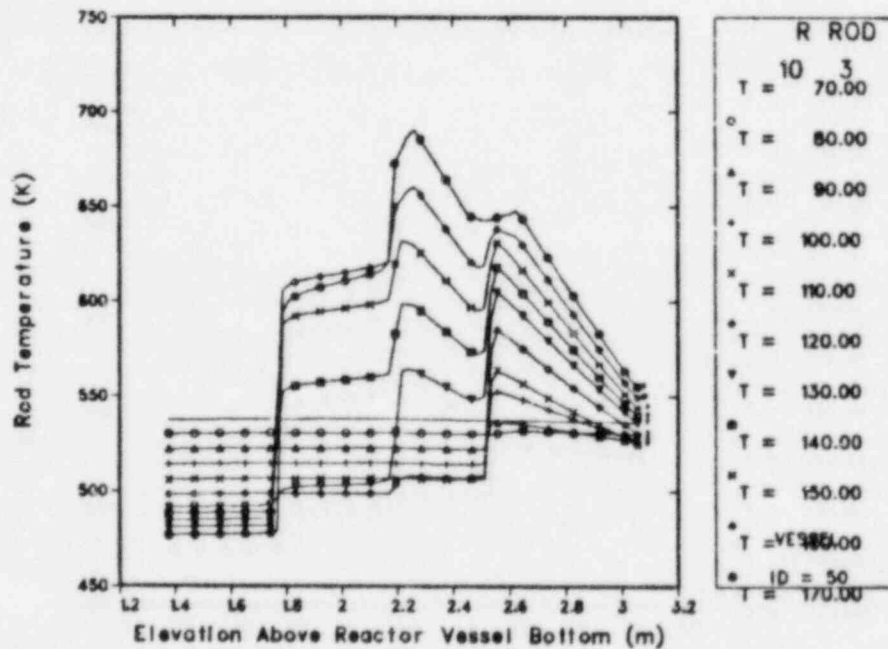


Fig. 105.  
Axial temperature profiles of high-power rod at different times during the blowdown portion of the experiment.



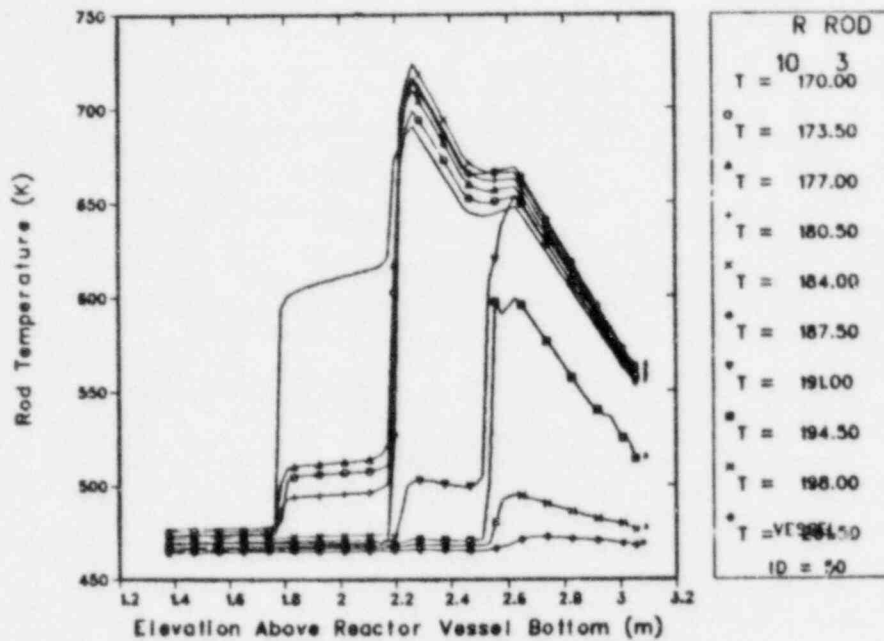


Fig. 106.

Axial temperature profiles of high-power rod at different times during the reflood portion of the experiment.

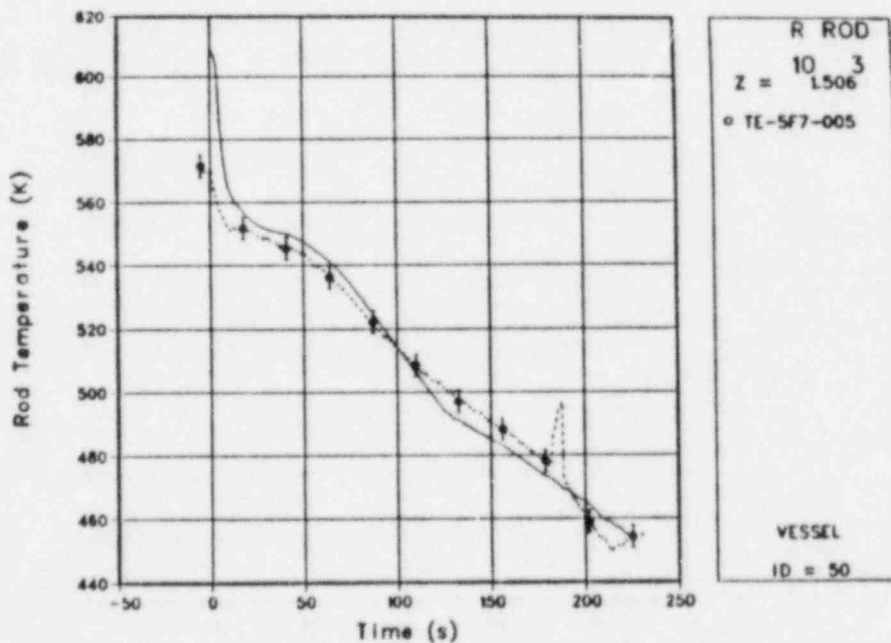


Fig. 107.

Comparison of TRAC-calculated and measured cladding temperatures at the 5-in. elevation for the high-power rod.

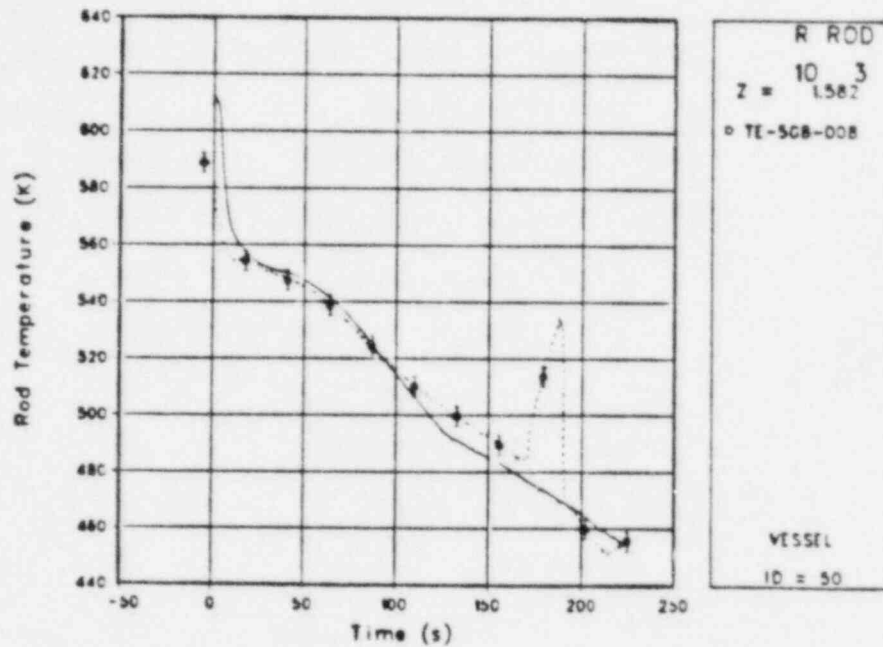


Fig. 108.

Comparison of the TRAC-calculated and measured cladding temperatures at the 8-in. elevation for the high-power rod.

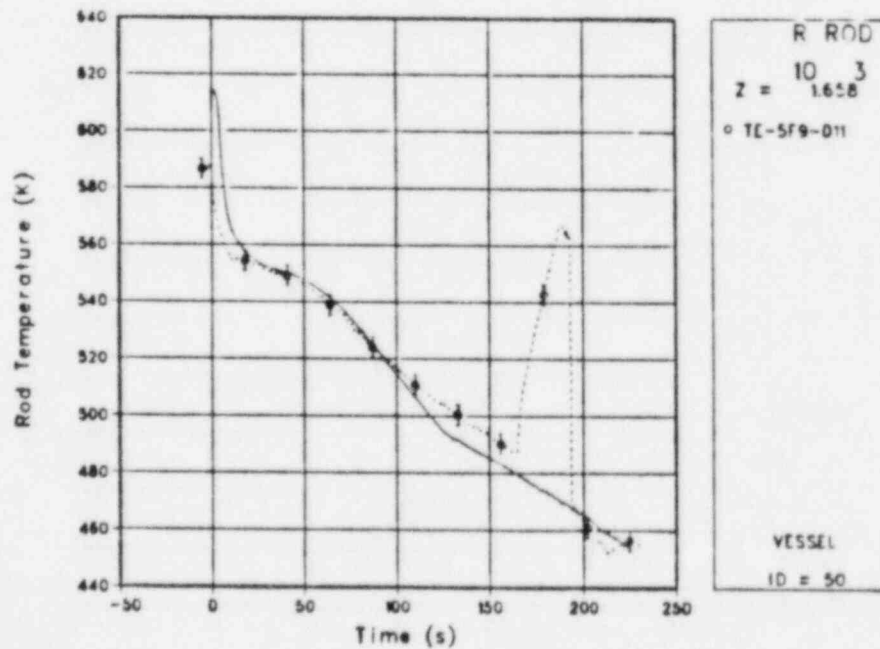


Fig. 109.

Comparison of the TRAC-calculated and measured cladding temperatures at the 11-in. elevation for the high-power rod.

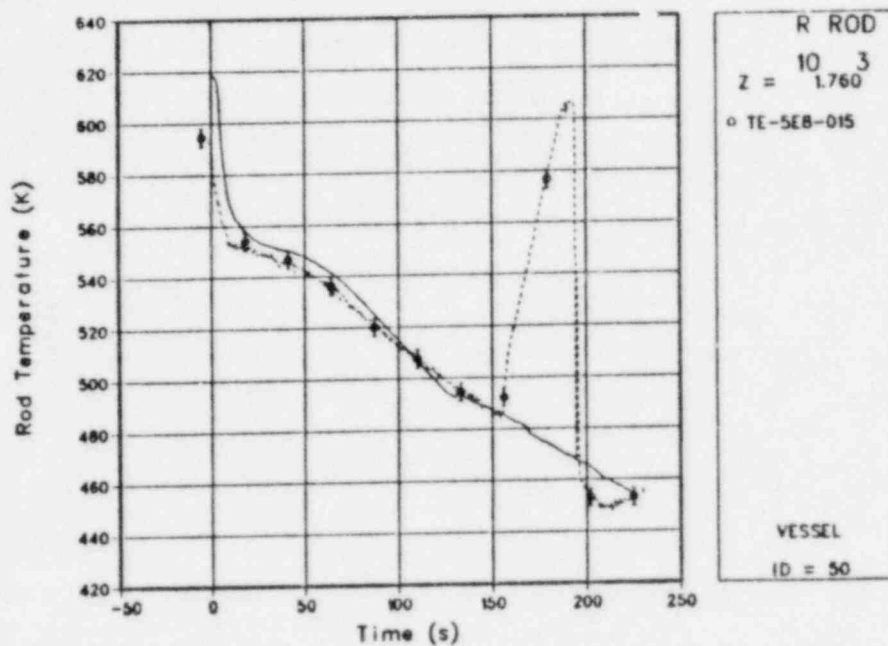


Fig. 110.

Comparison of TRAC-calculated and measured cladding temperatures at the 15-in. elevation for the high-power rod.

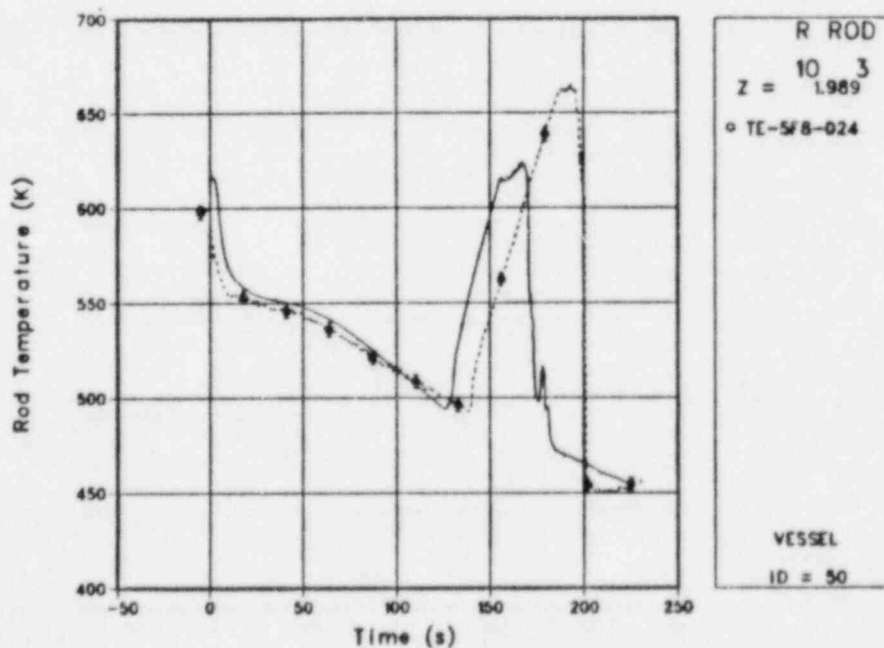


Fig. 111.

Comparison of TRAC-calculated and measured cladding temperatures at the 24-in. elevation for the high-power rod.

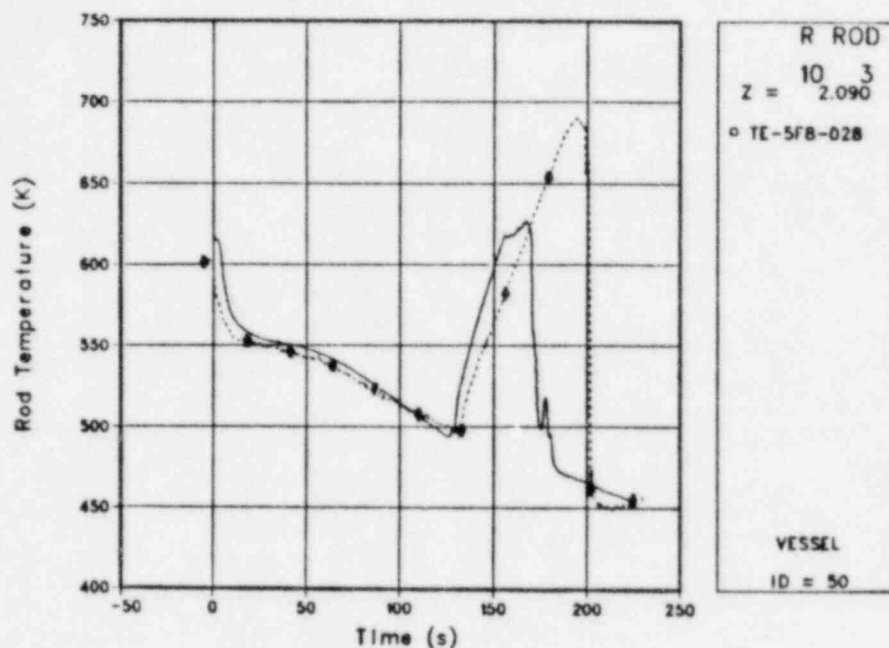


Fig. 112.  
Comparison of TRAC-calculated and measured cladding temperatures at the 28-in. elevation for the high-power rod.

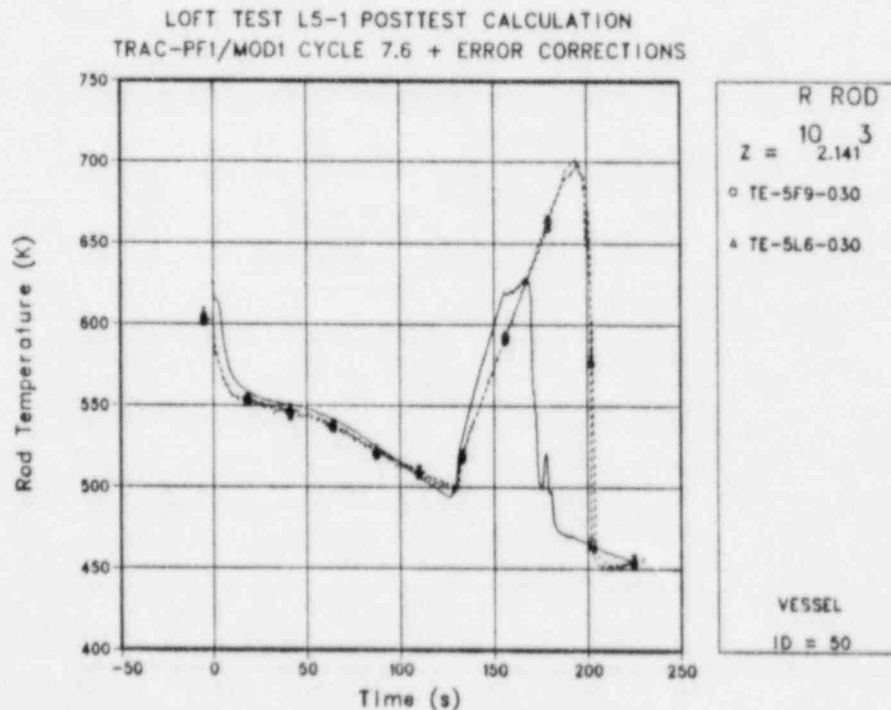


Fig. 113.  
Comparison of TRAC-calculated and measured cladding temperatures at the 30-in. elevation for the high-power rod.



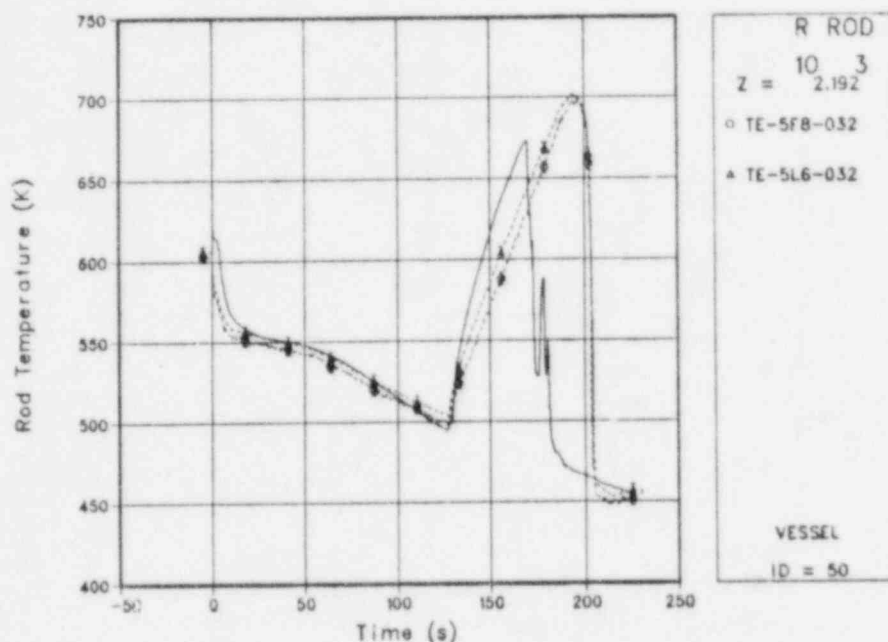


Fig. 114.

Comparison of TRAC-calculated and measured cladding temperatures at the 32-in. elevation for the high-power rod.

Both the dryout and quench occur early. Because the time the rods are uncovered is somewhat underpredicted, the peak temperatures are low relative to the experiment results. Figures 115-119 compare the calculated and measured fuel cladding temperatures for the region just above the core midplane. Both the calculation and the experiment cladding temperatures peaked in this region. The calculated peak temperature agreed well with the experimental value; however, the calculated peak temperature (shown in Fig. 115) occurred somewhat lower and earlier than that observed in the experiment (Fig. 117). Figures 120 and 121 compare the temperatures for the upper quarter of the core for the high-power fuel rods. The TRAC-PF1 calculations exhibited an earlier dryout than observed experimentally for this region of the core.

Figures 122-126 show the comparisons for the low-power fuel rods. Figures 127-131 show comparisons for the average-powered fuel rods. The comparisons are similar to those of the high-power rods. Very few radial differences were observed either in the calculation or in the experiment, except those due to the power profiles.

Figure 132 shows the time-step size for the LS-1 calculation. The calculation was very cost effective, requiring only 4641 s of CPU time for the 225.0-s simulation; and almost half of that CPU time was spent computing the last 30.0 s of the calculation. Table IX compares the key results for LOFT Experiment LS-1.

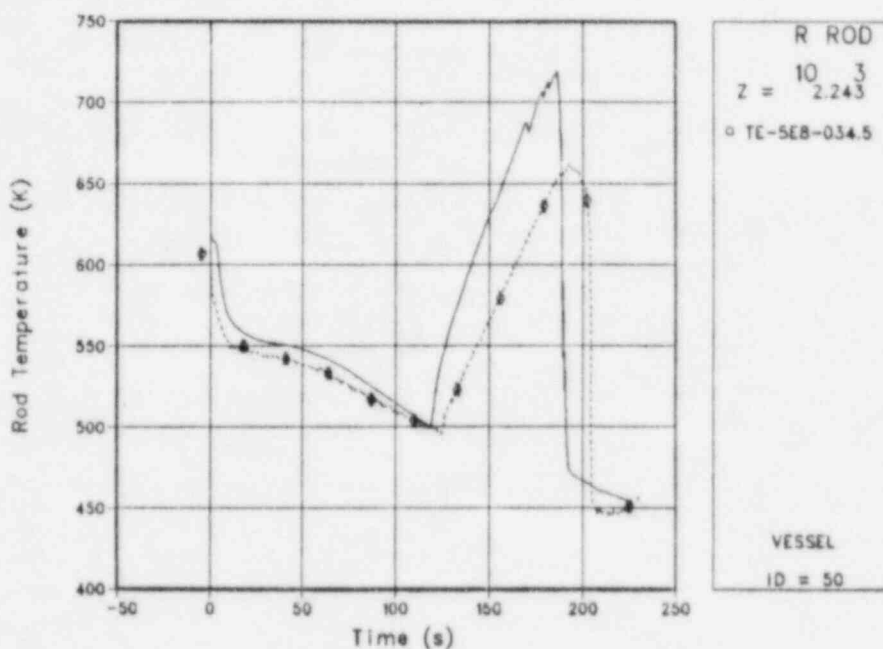


Fig. 115.  
 Comparison of TRAC-calculated and measured cladding temperatures at the 34.5-in. elevation for the high-power rod.

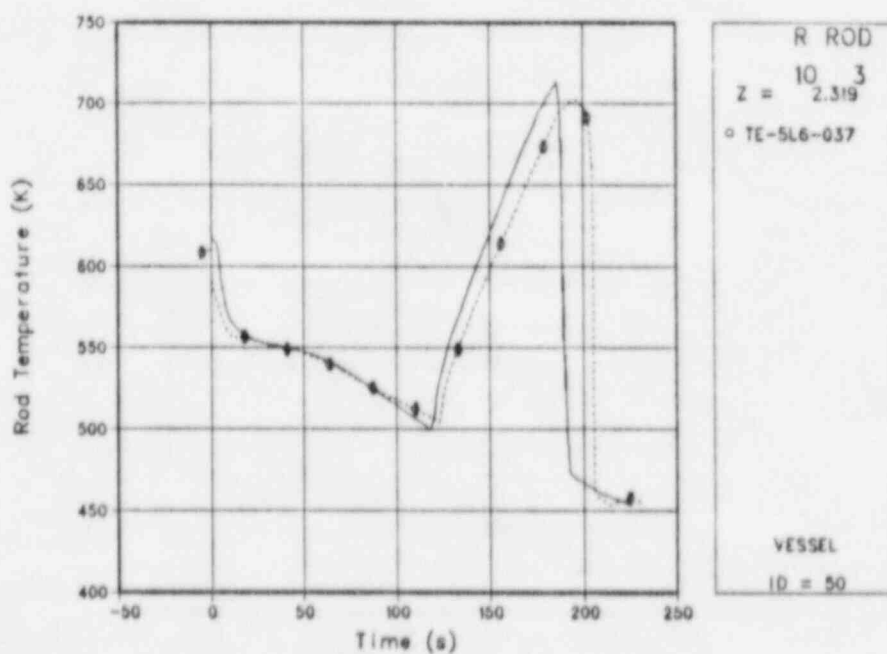


Fig. 116.  
 Comparison of TRAC-calculated and measured cladding temperatures at the 37-in. elevation for the high-power rod.

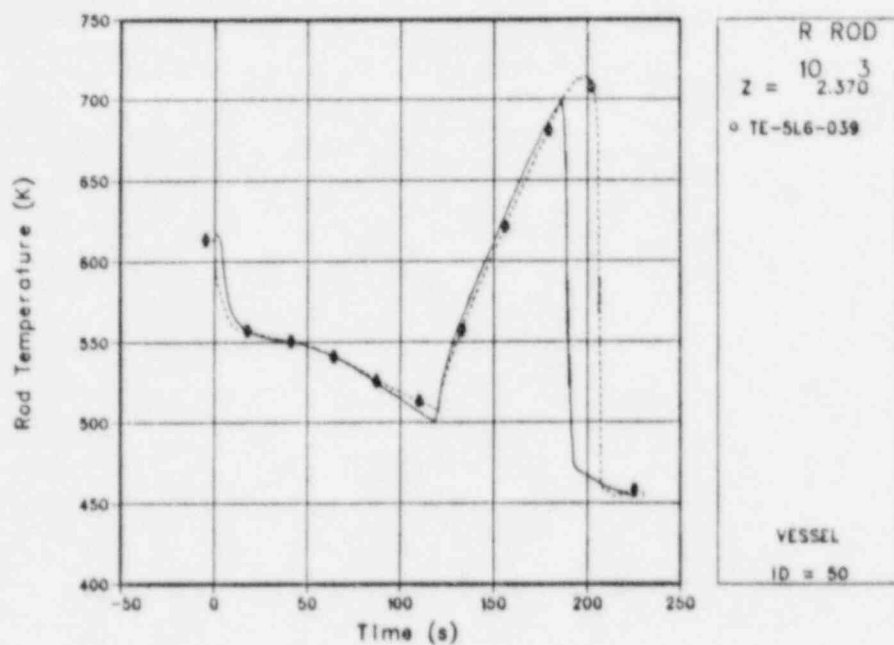


Fig. 117.

Comparison of TRAC-calculated and measured cladding temperatures at the 39-in. elevation for the high-power rod.

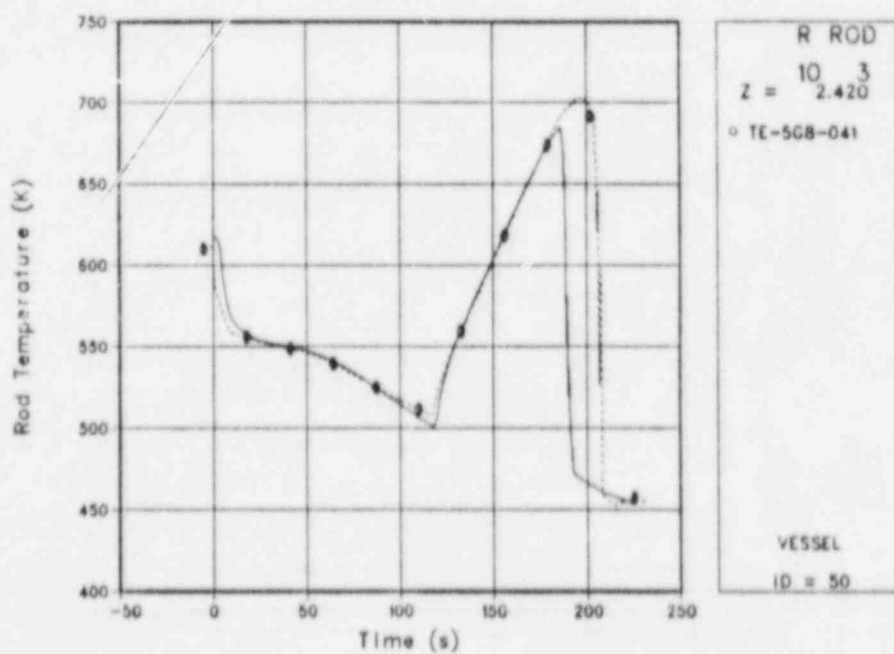


Fig. 118.

Comparison of TRAC-calculated and measured cladding temperatures at the 41-in. elevation for the high-power rod.

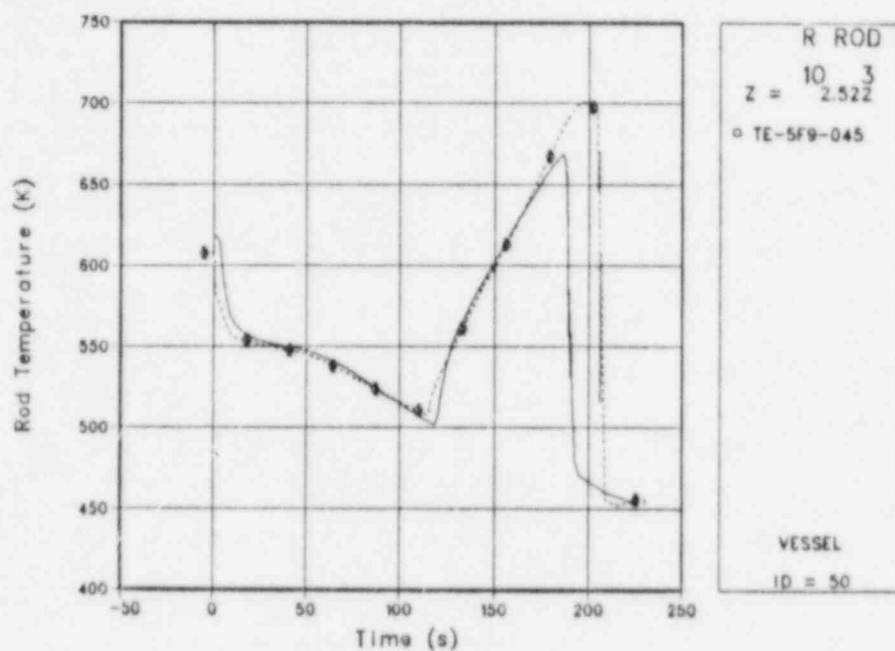


Fig. 119.  
 Comparison of TRAC-calculated and measured cladding temperatures at the 45-in. elevation for the high-power rod.

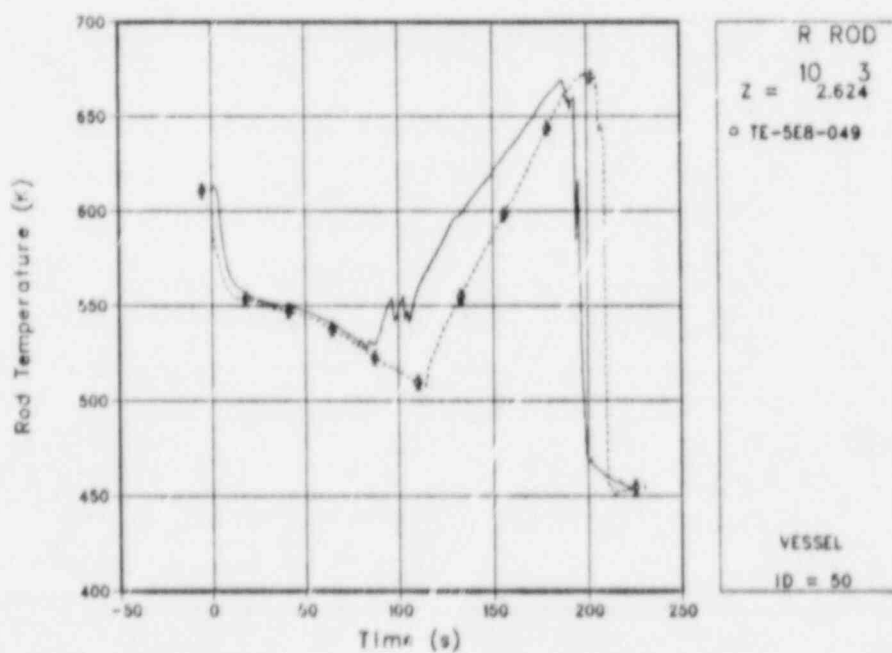


Fig. 120.  
 Comparison of TRAC-calculated and measured cladding temperatures at the 49-in. elevation for the high-power rod.



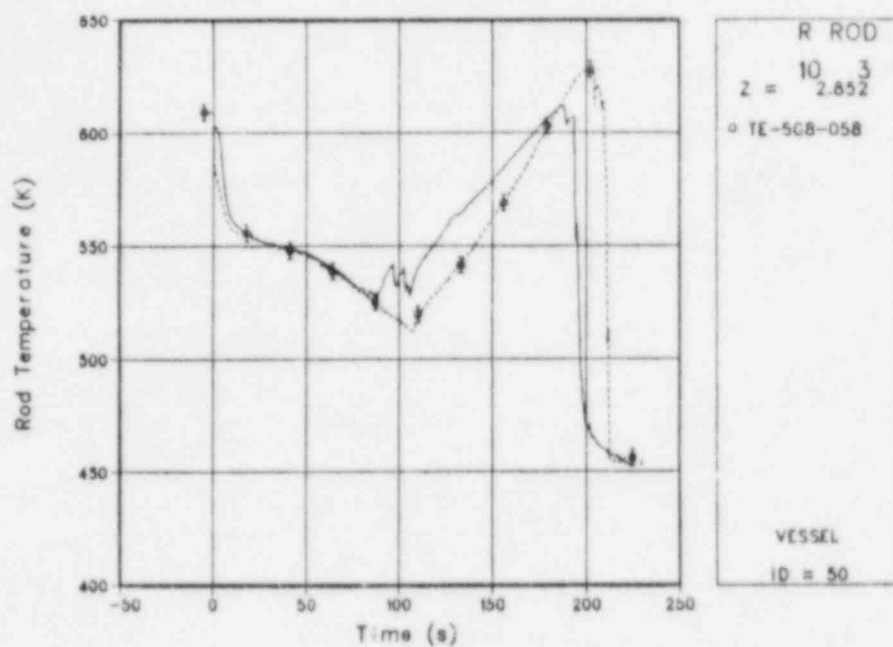


Fig. 121.

Comparison of TRAC-calculated and measured cladding temperatures at the 58-in. elevation for the high-power rod.

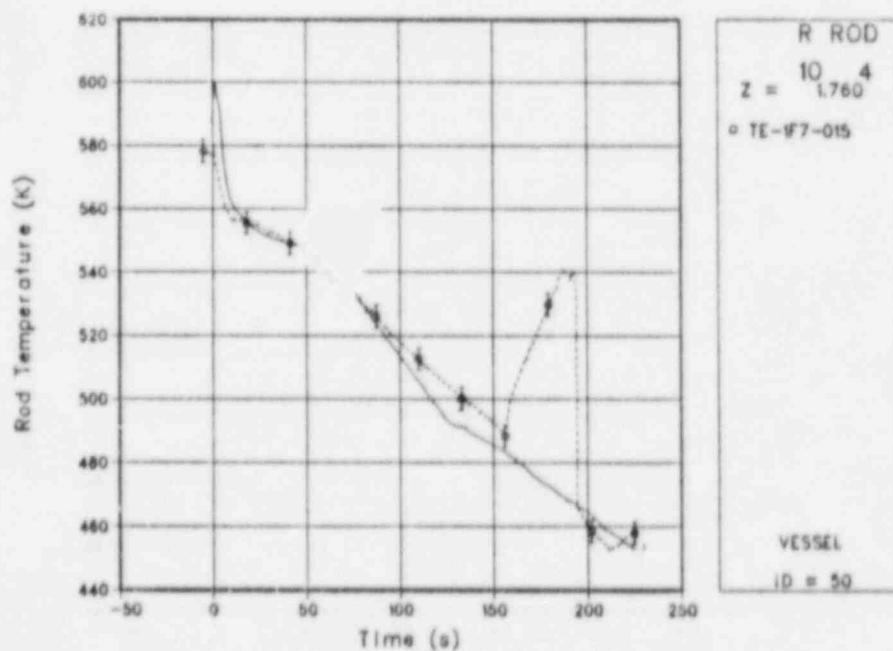


Fig. 122.

Comparison of TRAC-calculated and measured cladding temperatures at the 15-in. elevation for the low-power rod.

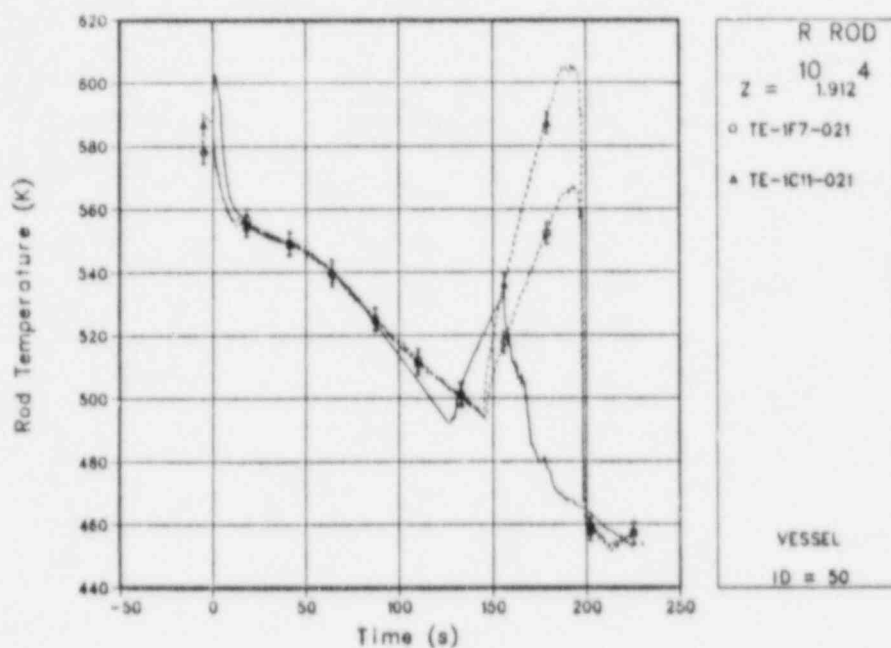


Fig. 123.  
 Comparison of TRAC-calculated and measured cladding temperatures at the 21-in. elevation for the low-power rod.

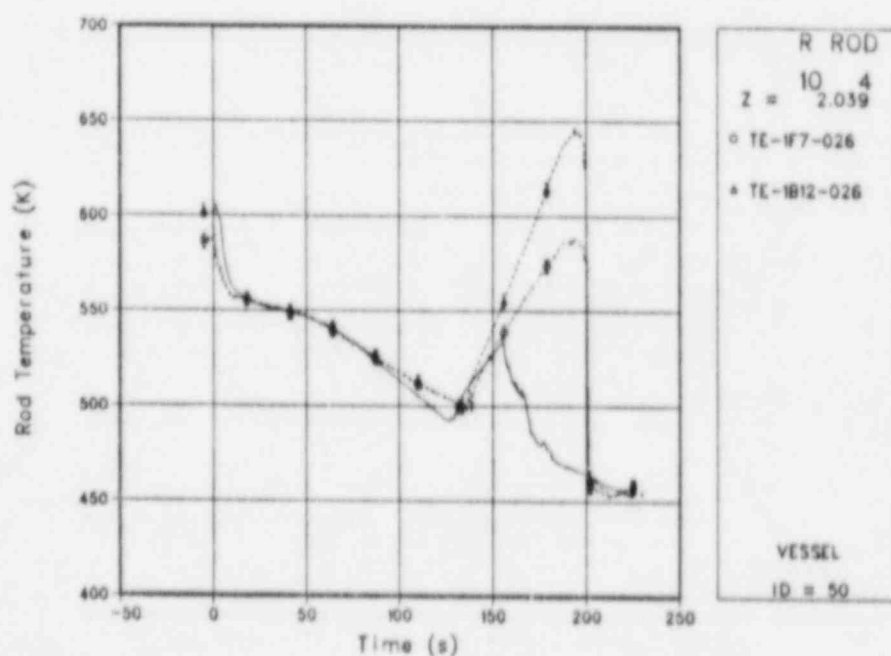


Fig. 124.  
 Comparison of TRAC-calculated and measured cladding temperatures at the 26-in. elevation for the low-power rod.

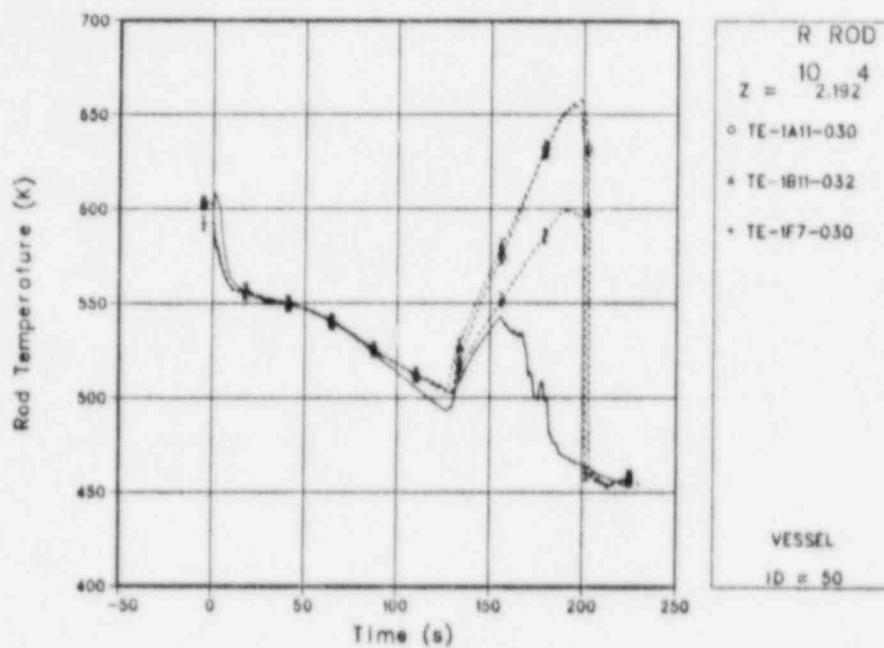


Fig. 125.

Comparison of TRAC-calculated and measured cladding temperatures at the 30-in. elevation for the low-power rod.

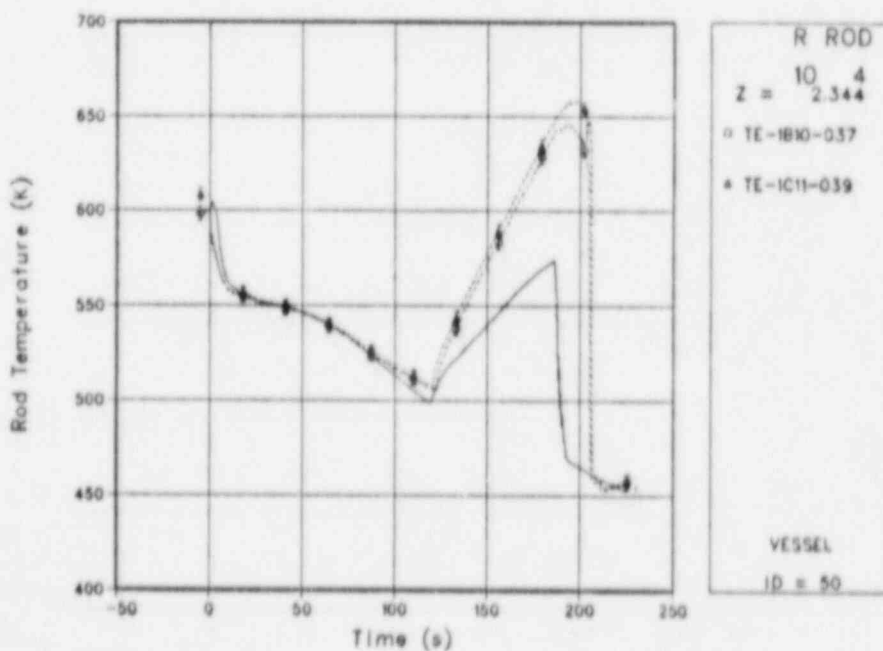


Fig. 126.

Comparison of TRAC-calculated and measured cladding temperatures at the 38-in. elevation for the low-power rod.

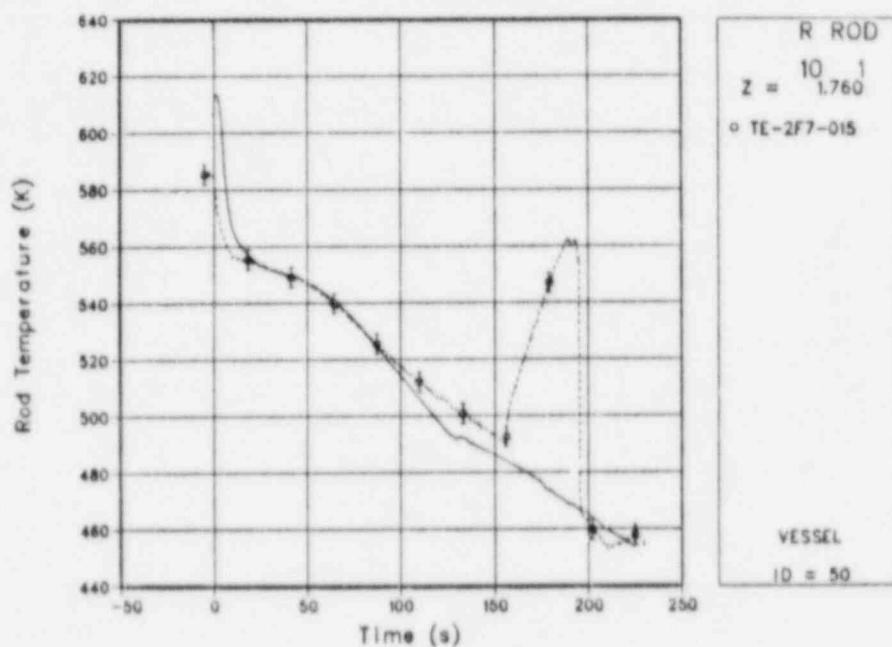


Fig. 127.

Comparison of TRAC-calculated and measured cladding temperatures at the 15-in. elevation for the average-power rod.

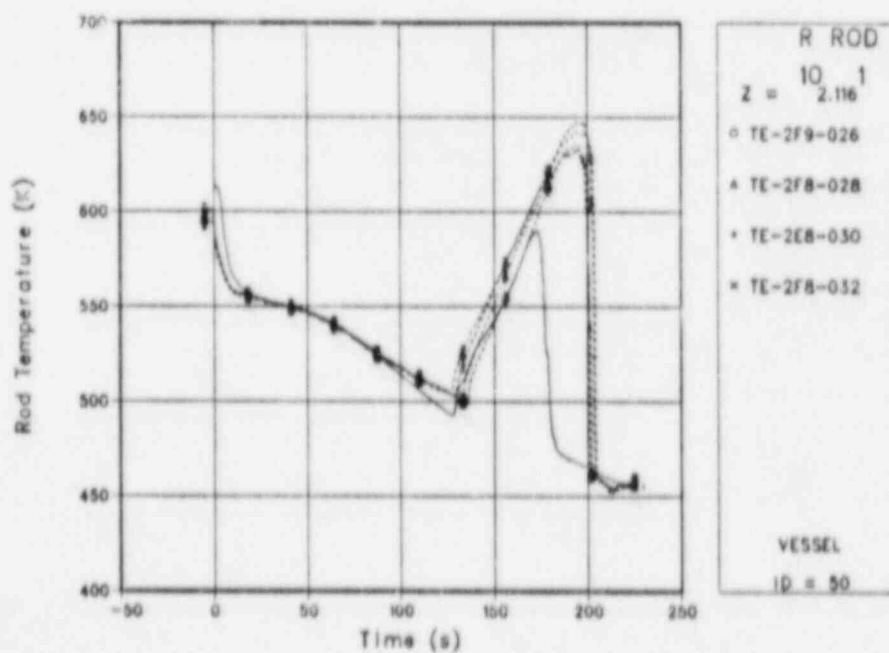


Fig. 128.

Comparison of TRAC-calculated and measured cladding temperatures at the 30-in. elevation for the average-power rod.



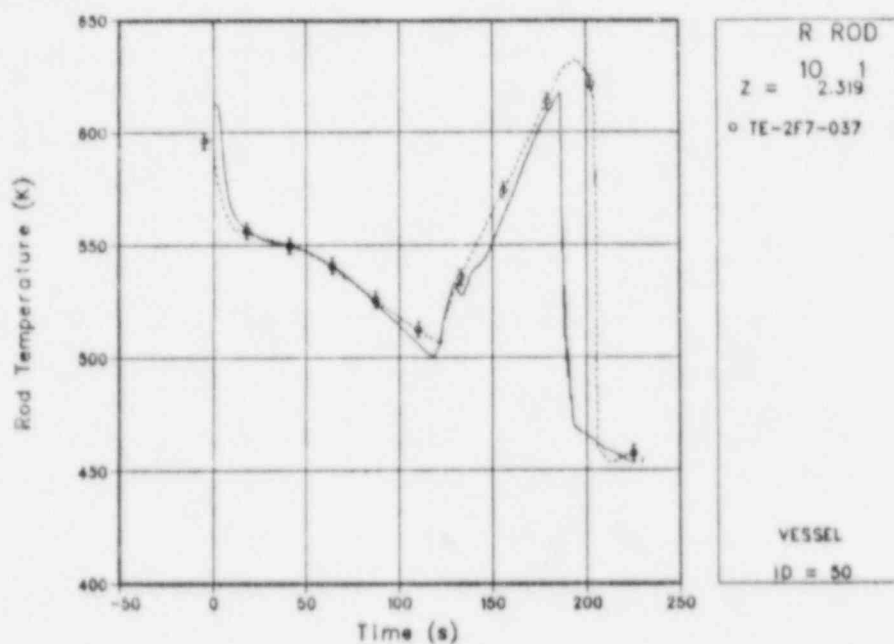


Fig. 129.

Comparison of TRAC-calculated and measured cladding temperatures at the 37-in. elevation for the average-power rod.

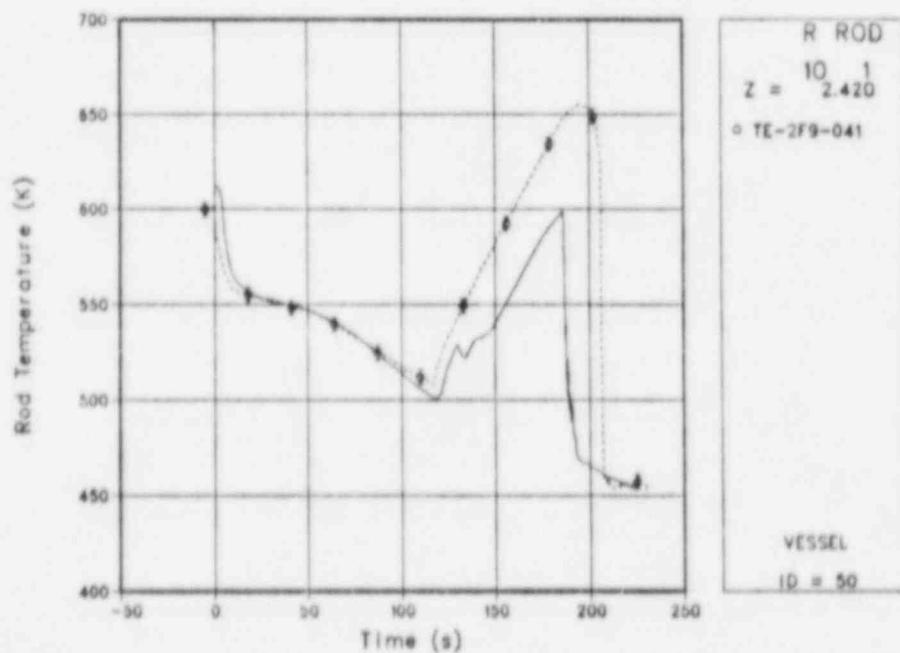


Fig. 130.

Comparison of TRAC-calculated and measured cladding temperatures at the 41-in. elevation for the average-power rod.

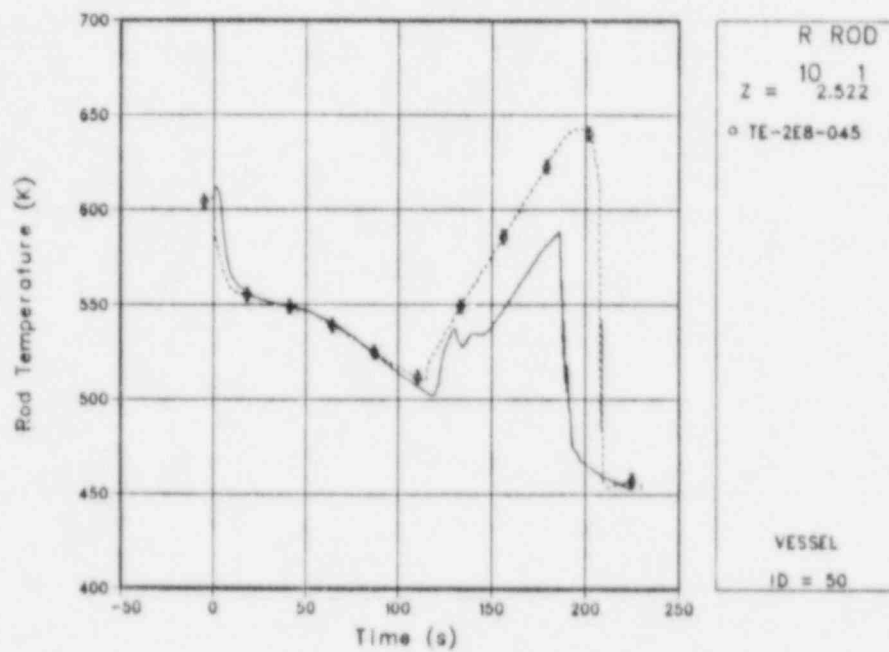


Fig. 131.  
Comparison of TRAC-calculated and measured cladding temperatures at the 45-in. elevation for the average-power rod.

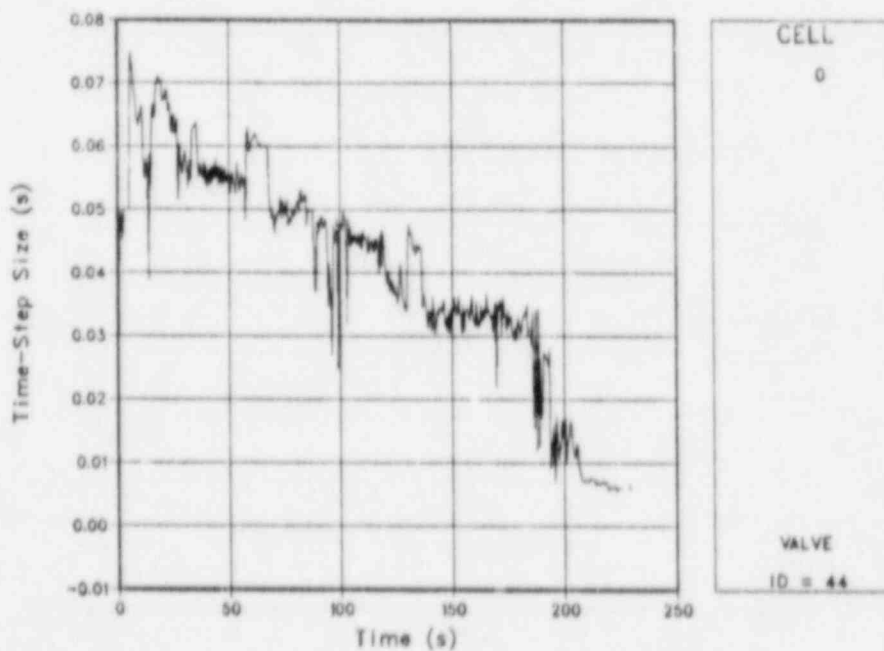


Fig. 132.  
Time-step size for LOFT L5-1 posttest calculation.

TABLE IX  
KEY PARAMETERS FOR LOFT EXPERIMENT L5-1<sup>a</sup>

Parameter	Experimental Results	TRAC-PF1
Peak cladding temperature (K)	715. $\pm$ 3.	699.
Time to dryout (s)	121.	118.
Time to quench (s)	207.5	192.5
Time to HPIS initiation (s)	2.9 $\pm$ .1	3.8
Time to accumulator initiation (s)	184. $\pm$ 1.	166.5
Time to LPIS initiation (s)	201. $\pm$ .5	201.

<sup>a</sup>The peak-cladding-temperature, time-to-dryout, and time-to-quench values are for the location of the peak temperature in the experiment. The corresponding values in the calculation are 720 K, 83 s, and 198 s, respectively.

3. L8-2 Posttest-Analysis Results. Figure 133 compares the calculated and measured break flows for the L8-2 posttest calculation. A valve controlled the break flow to approximate that in the L5-1 posttest analysis. The resulting break area is shown in Fig. 134.

Figures 135 and 136 compare the calculated and measured primary and secondary pressures. The comparison has many similarities to the L5-1 comparisons discussed earlier, including the overprediction of early primary-system pressure, followed by an underprediction of the long-term pressure response. The pressure spike in the primary-system pressure curves, both in the calculation and in the measurements, occurs when the ECC systems are initiated, followed by rapid quenching of the core. As was observed in the L5-1 comparisons, the apparent leakage of the steam-generator steam control valve caused the code to overpredict the long-term steam-generator pressure behavior.

Figures 137-140 compare the calculated and measured fluid densities at different points in the LOFT primary system. The calculated fluid densities are within the experiment measurement uncertainty bands for the majority of the transient.

Figure 141 compares the broken-loop cold-leg fluid temperatures. The comparison is similar to the L5-1 comparison discussed earlier. The experimental measurement is probably subject to hot-wall effects, which would account for the measurement departure from saturation temperature after 150 s. Because of the underprediction of primary-system pressure, the fluid-temperature measurements also are generally underpredicted.

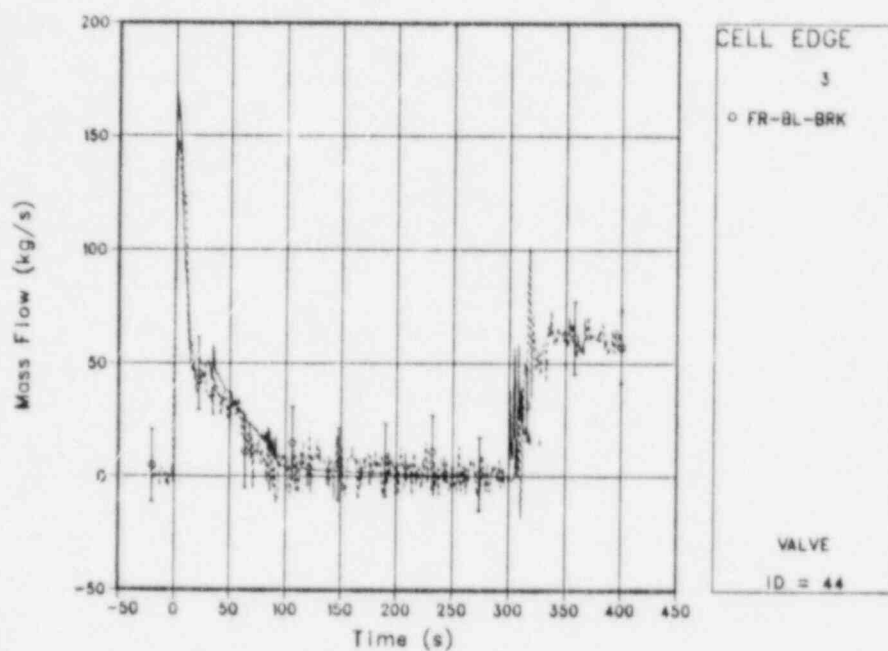


Fig. 133.  
Comparison of TRAC-calculated and measured break flows.

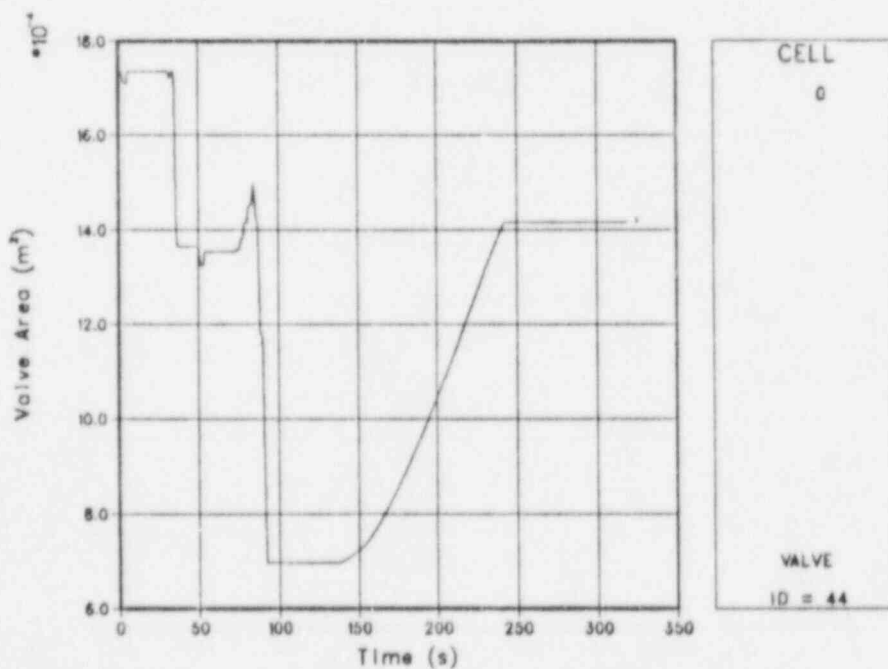


Fig. 134.  
Valve area at the break.

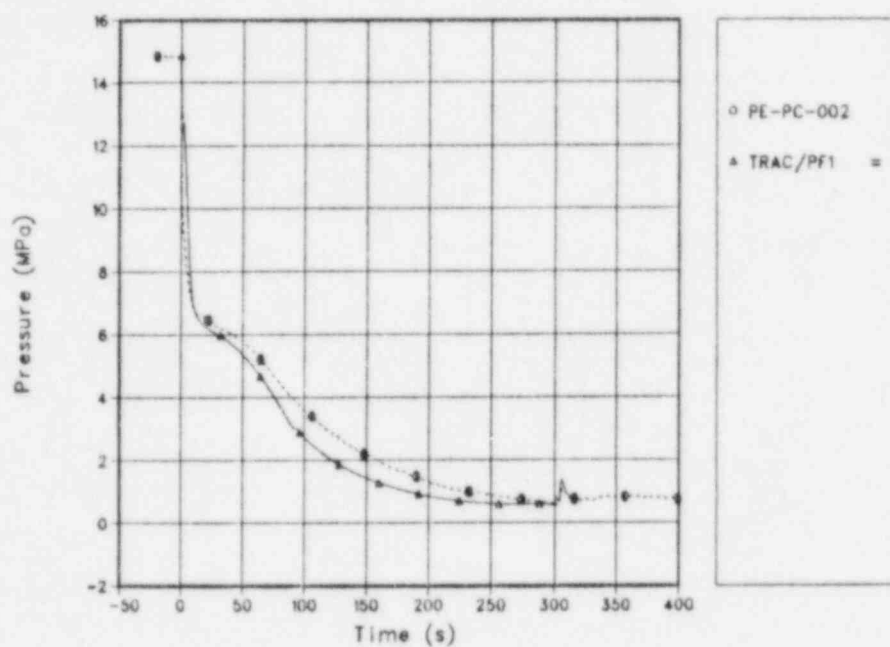


Fig. 135.  
Comparison of TRAC-calculated and measured primary-system pressures.

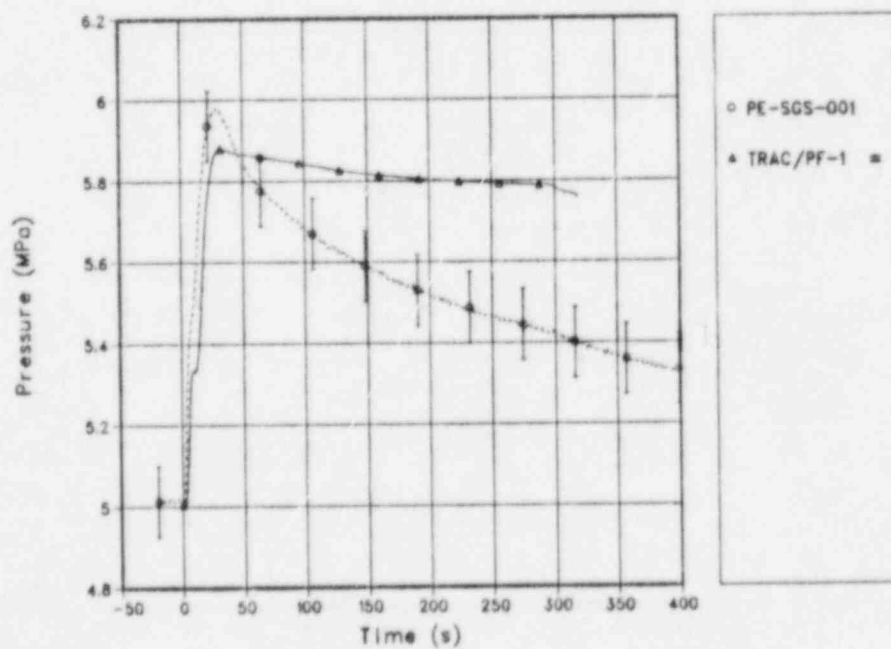


Fig. 136.  
Comparison of TRAC-calculated and measured steam-generator secondary-side steam-dome pressures.



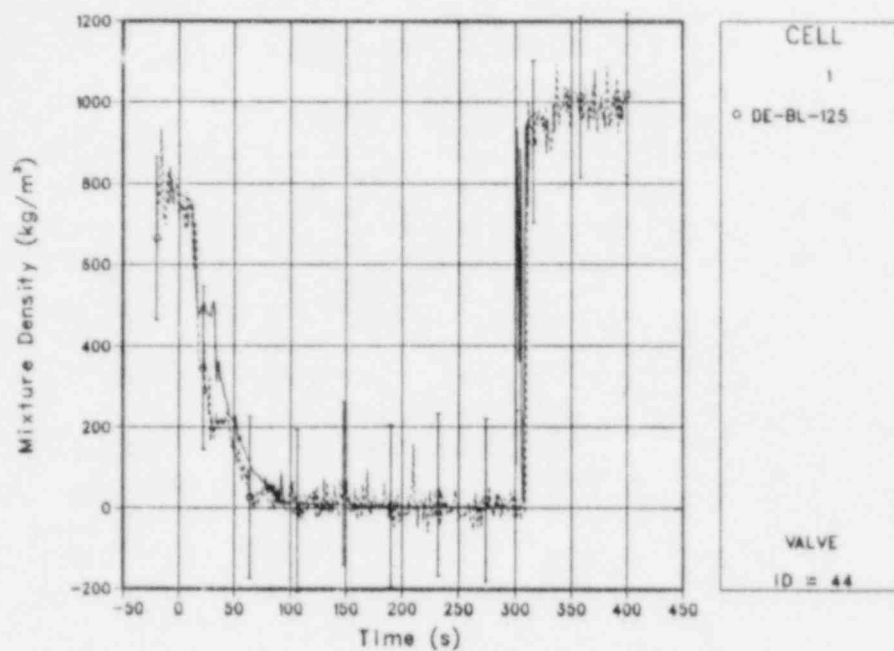


Fig. 137.  
Comparison of TRAC-calculated and measured average fluid densities in broken-loop cold leg.

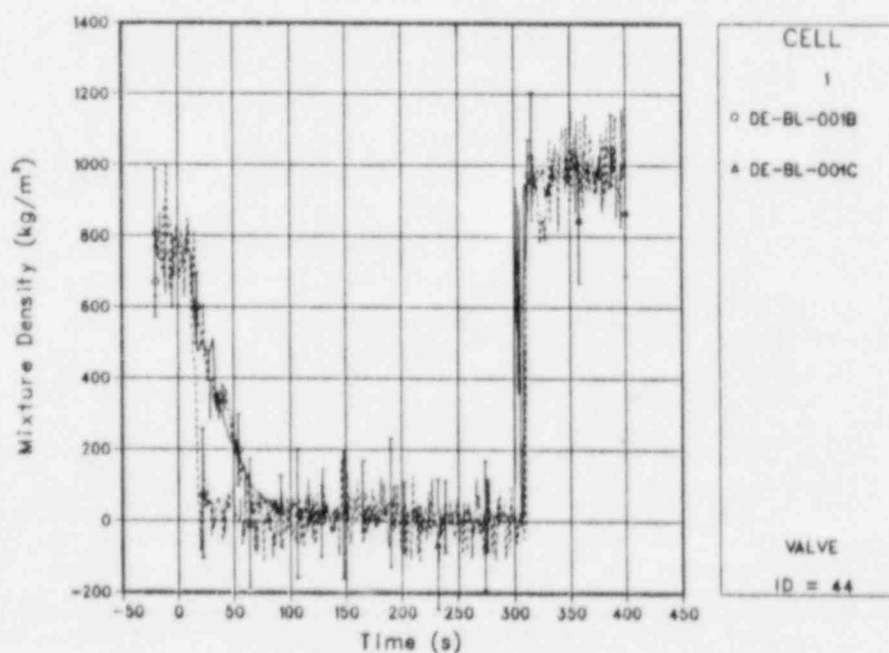


Fig. 138.  
Comparison of TRAC-calculated average density and measured average fluid density in the broken-loop cold leg.

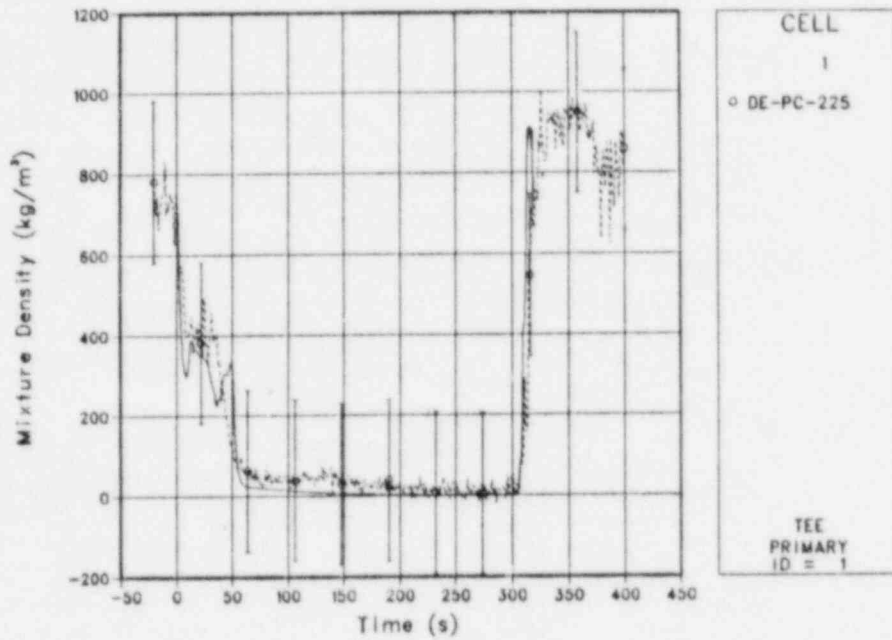


Fig. 139.

Comparison of TRAC-calculated and measured average fluid densities in intact-loop hot leg.

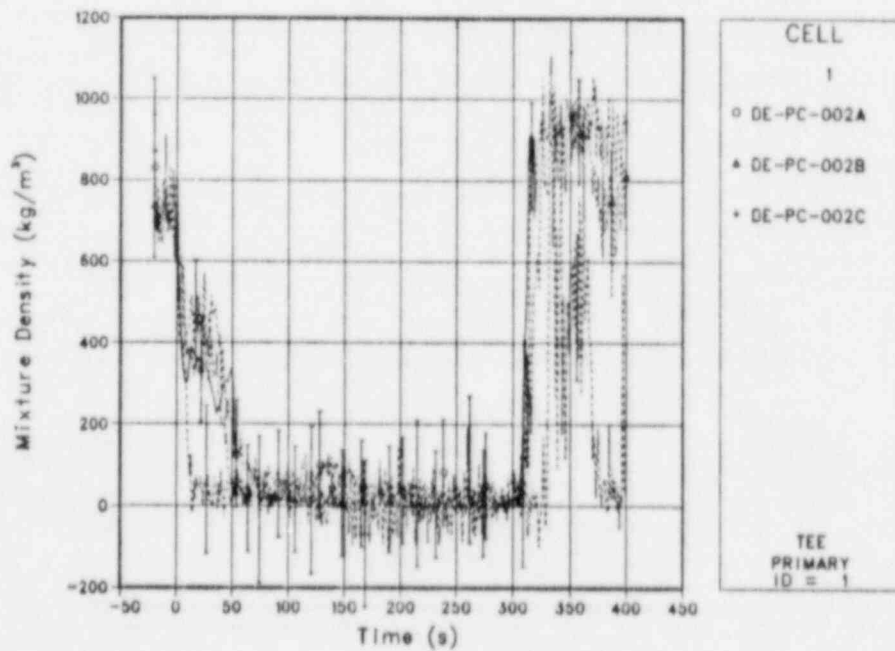


Fig. 140.

Comparison of TRAC-calculated average fluid density and measured average fluid density in the intact-loop hot leg.

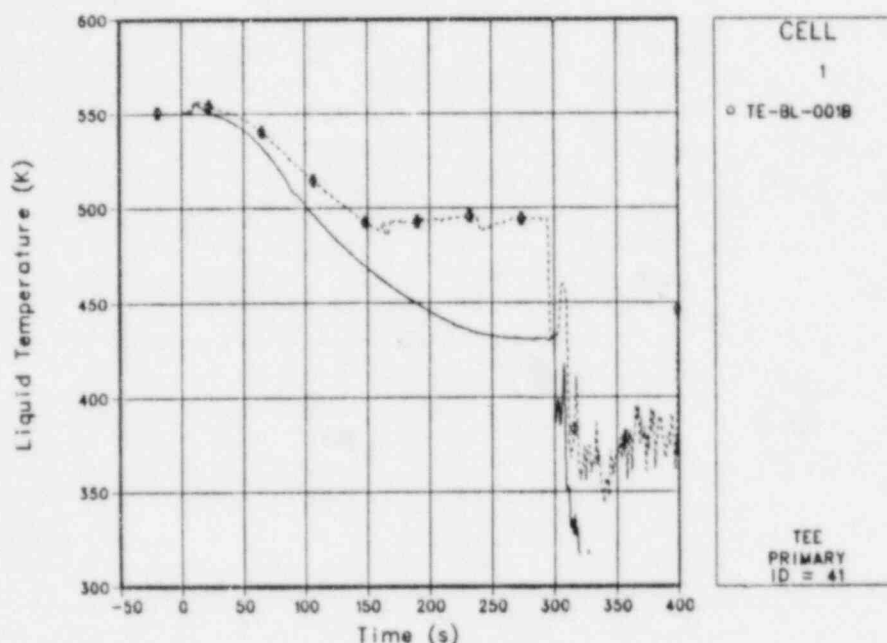


Fig. 141.

Comparison of TRAC-calculated and measured fluid temperatures in the broken-loop cold leg.

Figures 142 and 143 compare the calculated and measured pump speeds for the LOFT primary-coolant pumps. The approximate 5.0-s offset between calculations and measurements is caused by an input error. The pump speeds were input into TRAC-PF1 from a table that is used once a trip is set. The setpoints of the trip were such that the 5.0-s delay occurred between the start of the transient and the time of trip. As will be discussed later, the pump plays a relatively minor role in this transient, and this error was not judged to be significant enough to warrant repetition of the analysis.

Figure 144 shows the calculated fuel-rod-cladding surface temperature for an average-powered rod at different axial locations. As was seen in the LS-1 results, the dryouts and rewets occurred when the fluid conditions in the fluid cell adjacent to the rod crossed 98% void fraction. Contrary to the experiment results, the dryouts did not extend to the bottom of the heated rods. Figure 145 shows the void fraction in the vessel. The void fraction near the bottom reached a peak value of 85%, but was not high enough to dry the bottom 1/4 of the fuel rods.

Figures 146-149 compare the calculated and measured fuel-rod-cladding surface temperature for the high-power rod at different axial elevations up to the core midplane. The effects of the pump restart were slight, both on the calculations as well as on the experiment results.

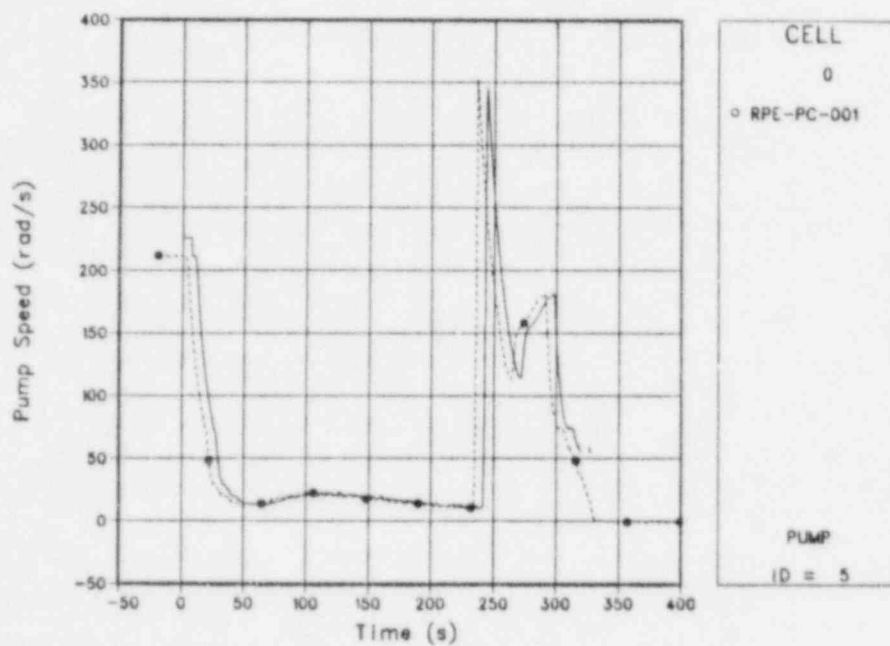


Fig. 142.  
Comparison of TRAC-calculated and measured pump speeds for pump 1.

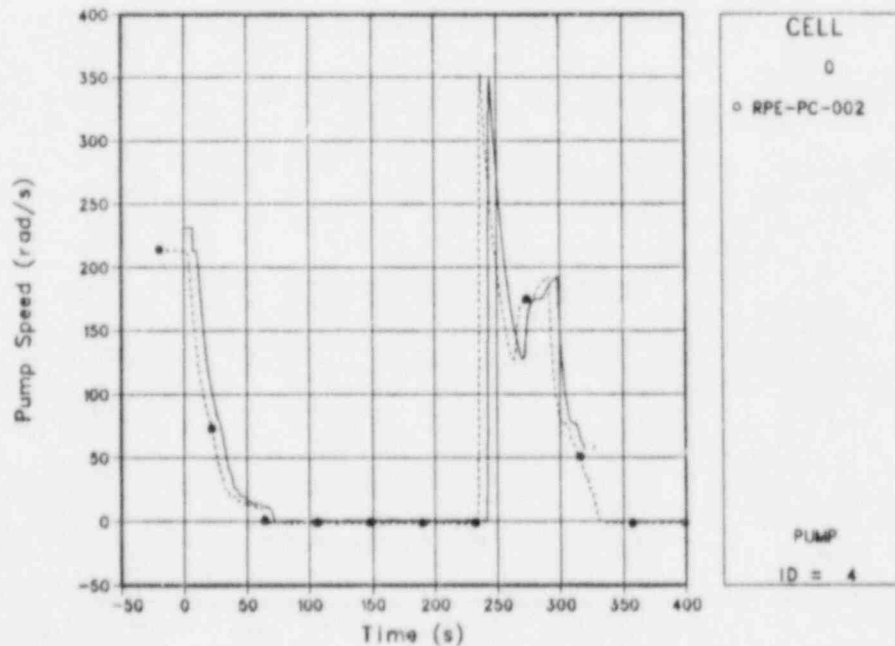


Fig. 143.  
Comparison of TRAC-calculated and measured pump speeds for pump 2.

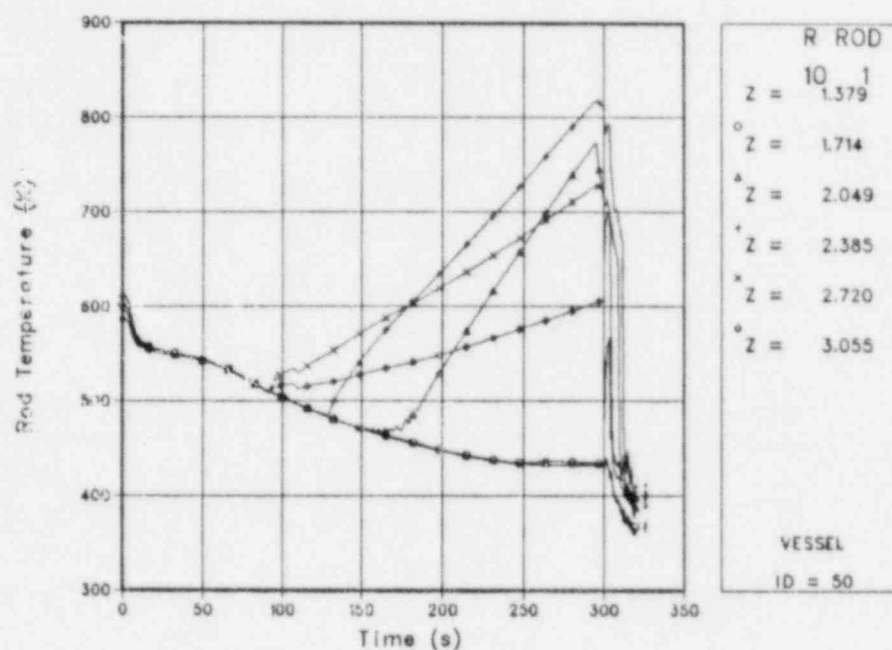


Fig. 144.  
TRAC-calculated fuel-rod-cladding temperatures at different axial elevations for average-power rod.

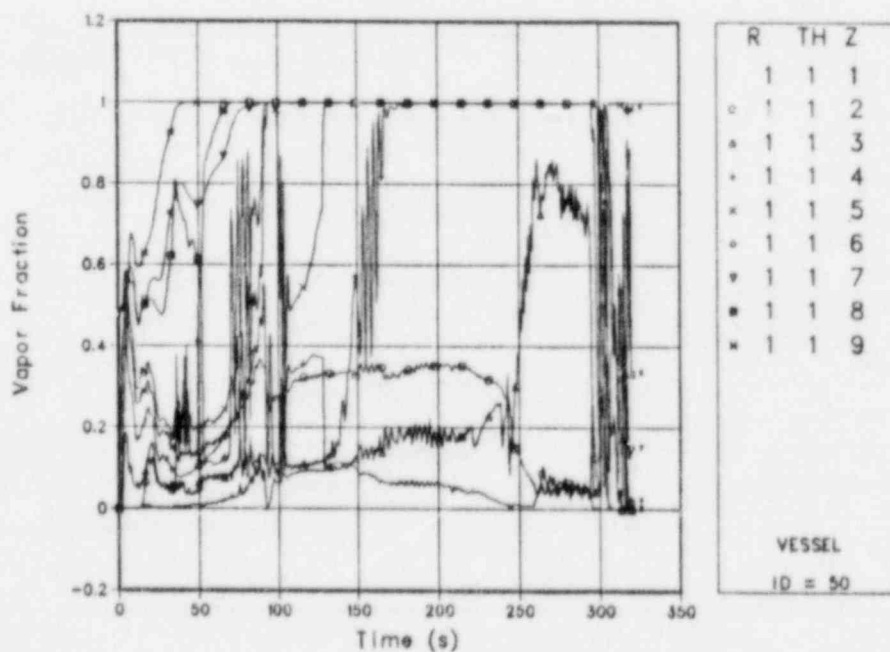


Fig. 145.  
TRAC-calculated reactor-vessel vapor fractions at different axial locations.



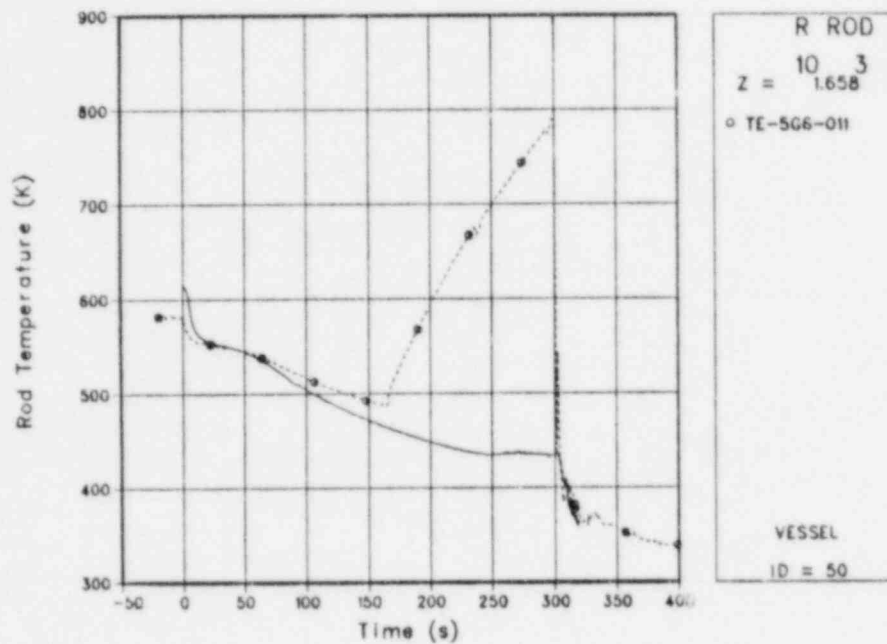


Fig. 146.  
 Comparison of TRAC-calculated and measured cladding temperatures at the 11-in. elevation for the high-power rod.

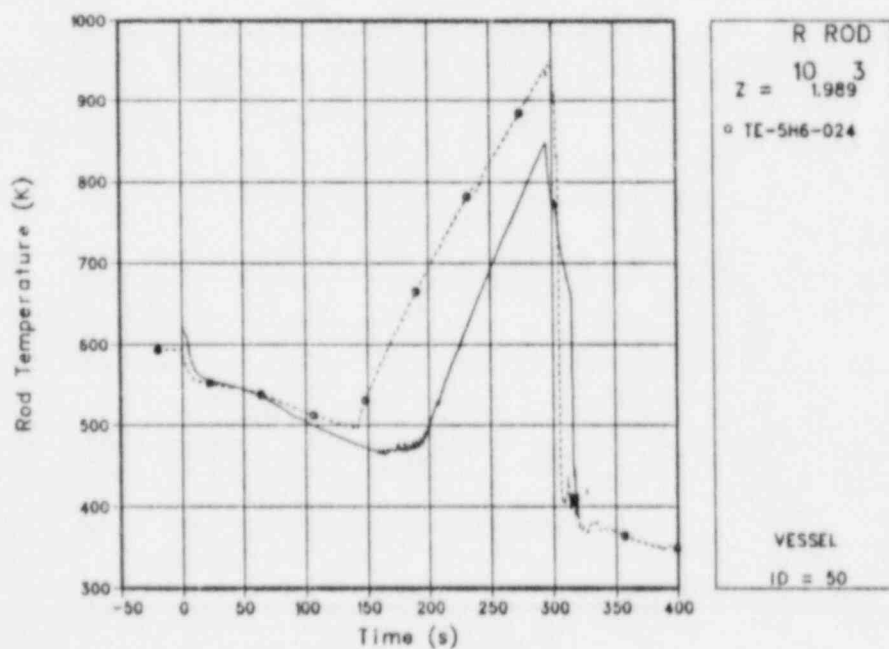


Fig. 147.  
 Comparison of TRAC-calculated and measured cladding temperatures at the 24-in. elevation for the high-power rod.

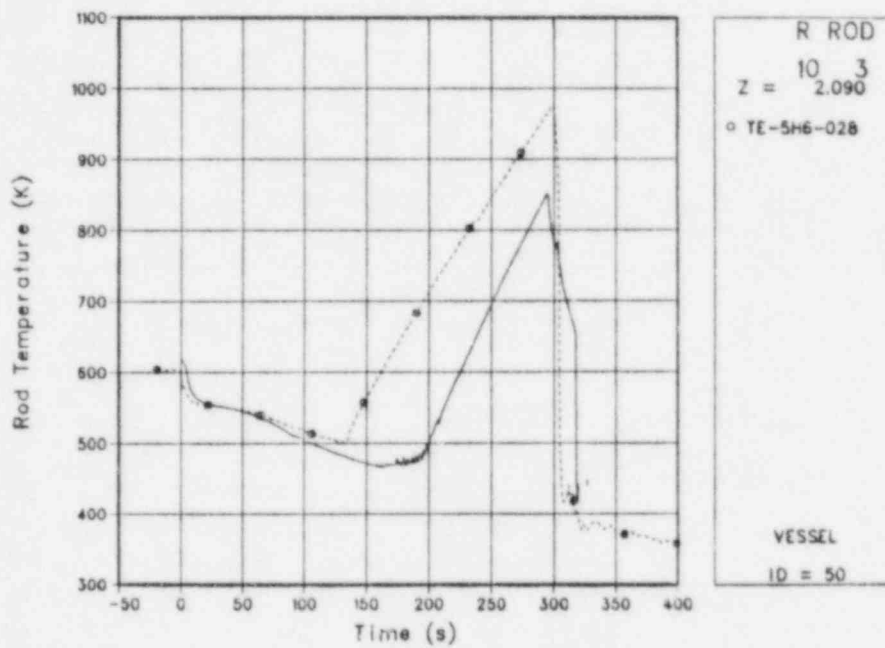


Fig. 148.  
 Comparison of TRAC-calculated and measured cladding temperatures at the 28-in. elevation for the high-power rod.

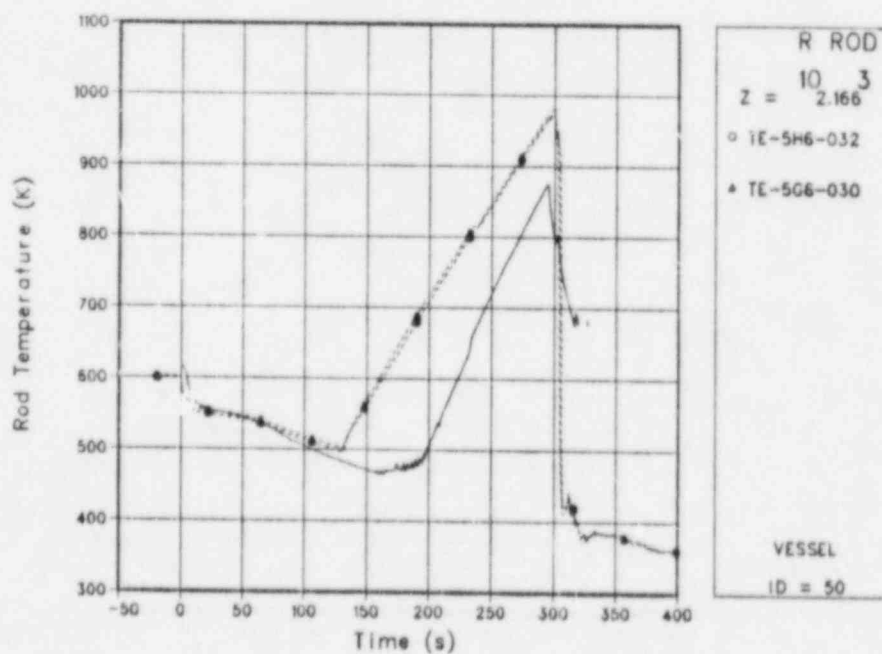


Fig. 149.  
 Comparison of TRAC-calculated and measured cladding temperatures at the 31-in. elevation for the high-power rod.

Figure 150 represents the maximum calculated cladding temperature, and is in reasonably good agreement with the experiment results. Figures 151 and 152 show comparisons at upper elevations along the high-power rod. Figures 153-155 show comparisons for the low-power rod at different axial elevations. Figures 156-162 show comparisons for the average-powered rod at different axial elevations. The differences between calculated and measured heating rates after dryout probably are due to differences in radial peaking factors between the actual fuel rod and the calculational rod. Figure 163 shows the time-step size for the L8-2 posttest calculation. This calculation was very cost effective in the early portion of the transient, requiring only 3781 s of CPU time for the simulation of the first 242 s. Table X compares the key parameters for LOFT Experiment L8-2.

### E. Conclusions

Using the three-dimensional vessel component, TRAC-PF1 modeled the LOFT intermediate-breaks L5-1 and L8-2 well. The results in some areas could be improved further through the code input. This would include such items as better modeling of the break flow, finer noding of the reactor vessel core in the axial direction for better simulation of the vertical void distribution, and use of the actual event times for the trips. The code ran relatively fast, considering the large number of fluid cells and heat conductors that were simulated. Early sensitivity studies revealed that the code results were remarkably insensitive to time-step size, and mass errors for all cases analyzed were negligible. In addition, the code never terminated abnormally,

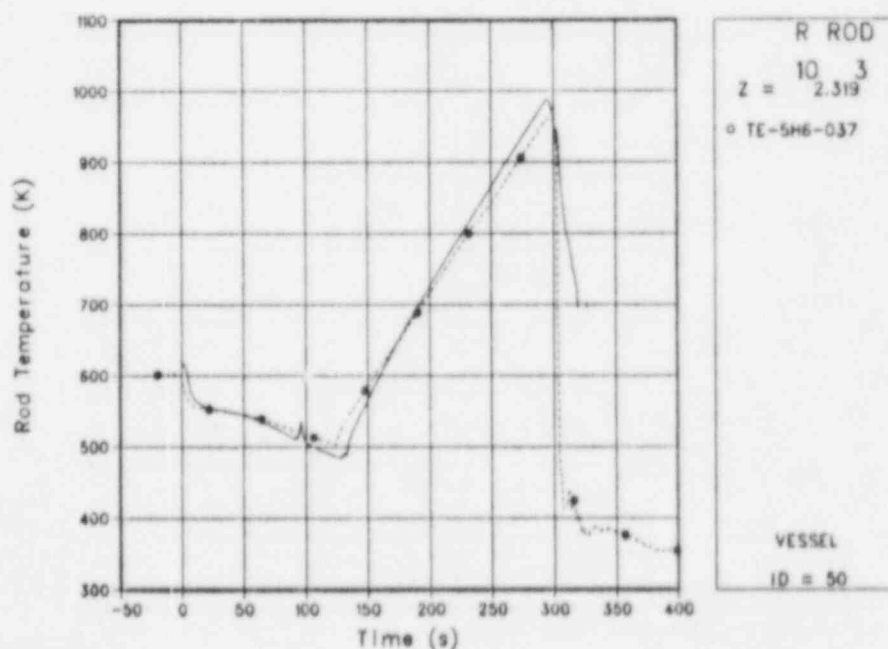


Fig. 150.

Comparison of TRAC-calculated and measured cladding temperatures at the 37-in. elevation for the high-power rod.

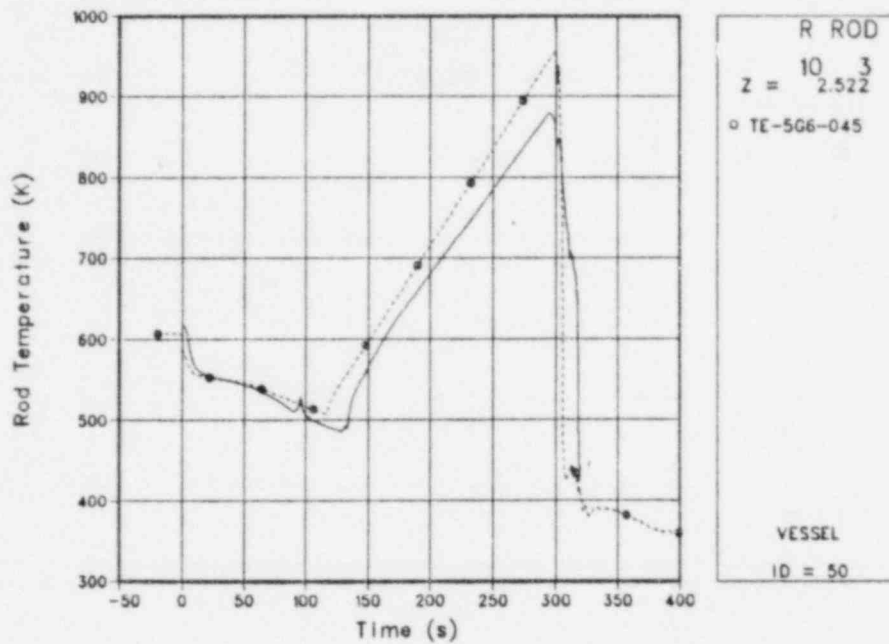


Fig. 151.  
 Comparison of TRAC-calculated and measured cladding temperatures at the 45-in. elevation for the high-power rod.

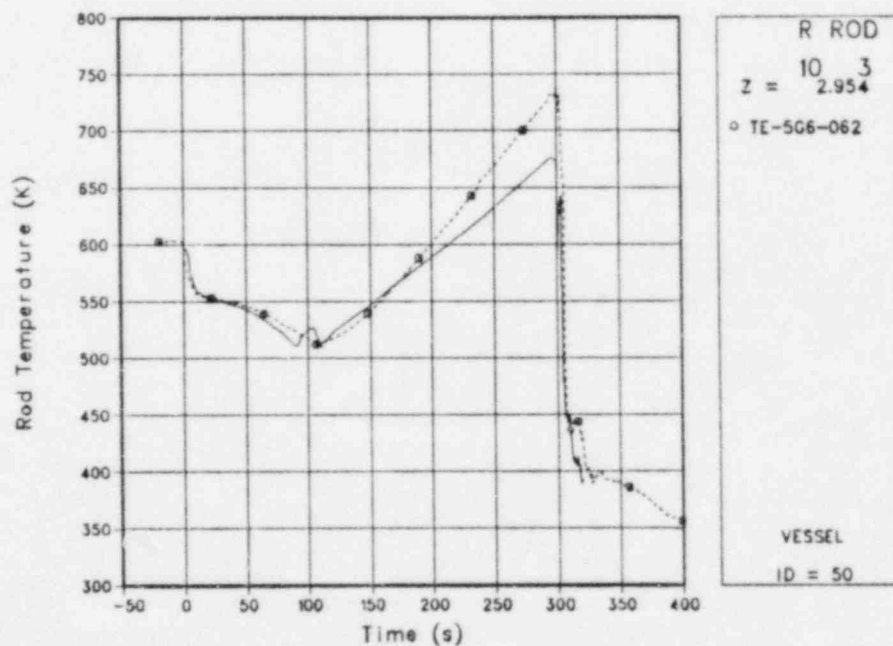


Fig. 152.  
 Comparison of TRAC-calculated and measured cladding temperatures at the 62-in. elevation for the high-power rod.

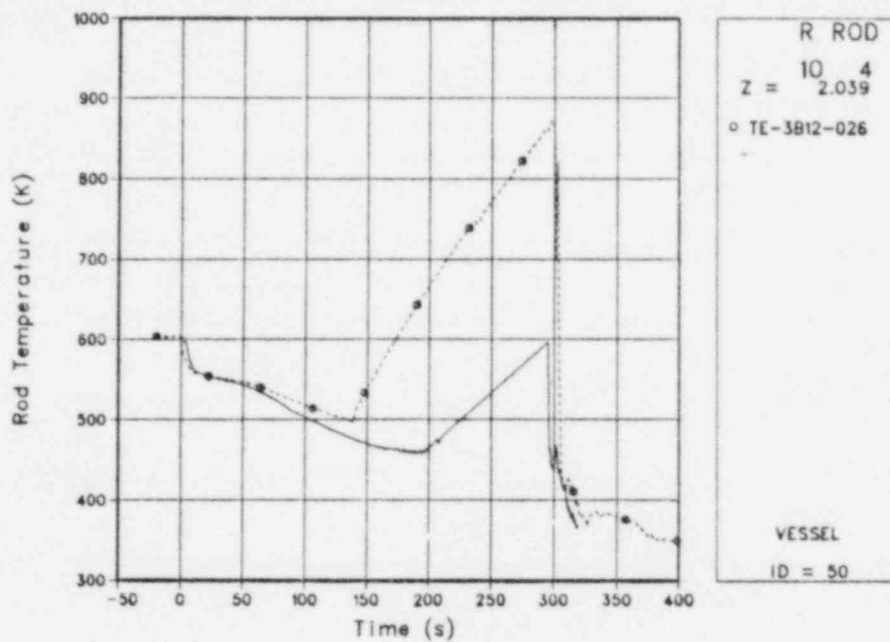


Fig. 153.

Comparison of TRAC-calculated and measured cladding temperatures at the 26-in. elevation for the low-power rod.

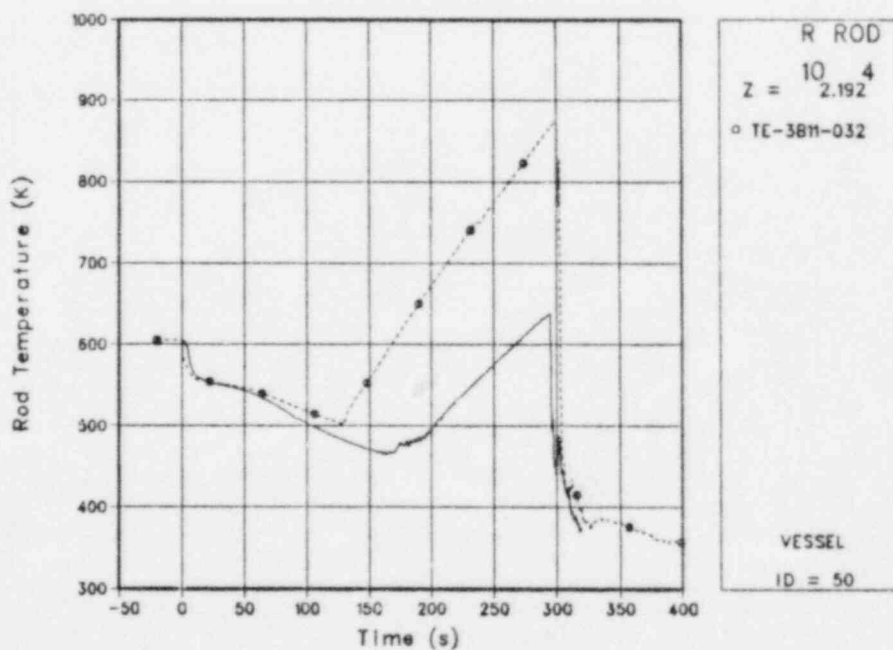


Fig. 154.

Comparison of TRAC-calculated and measured cladding temperatures at the 32-in. elevation for the low-power rod.



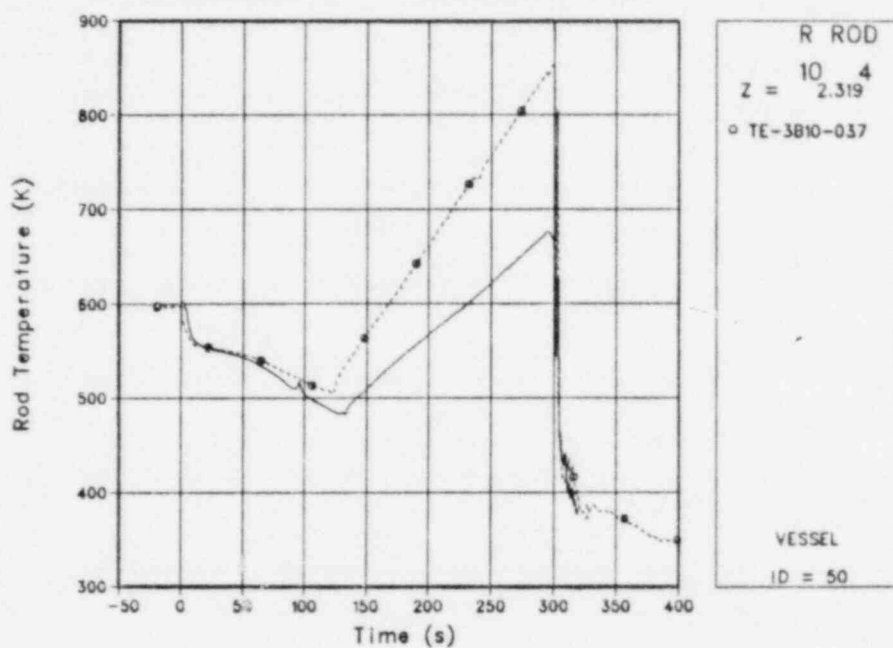


Fig. 155.

Comparison of TRAC-calculated and measured cladding temperatures at the 37-in. elevation for the low-power rod.

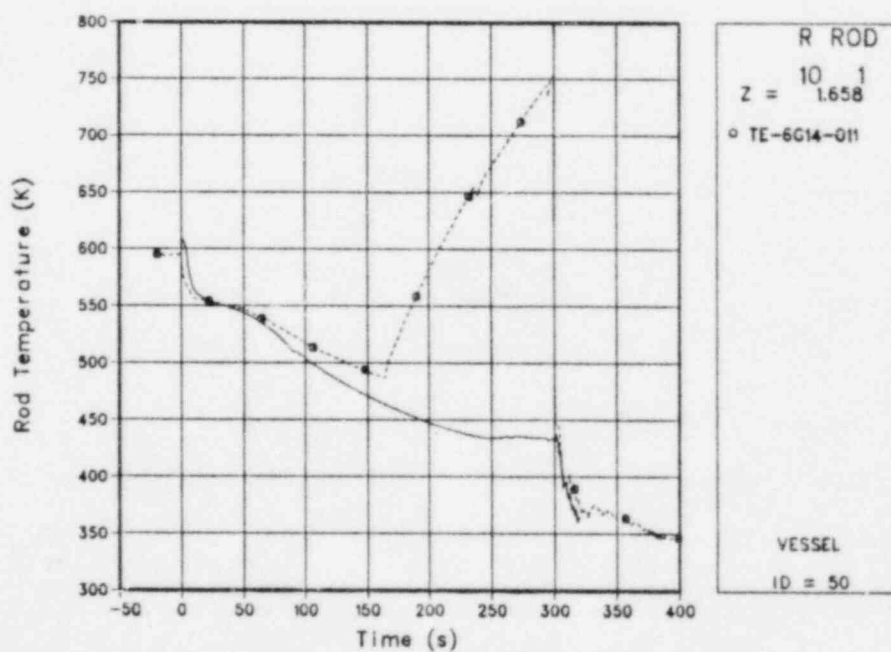


Fig. 156.

Comparison of TRAC-calculated and measured cladding temperatures at the 11-in. elevation for the average-power rod.

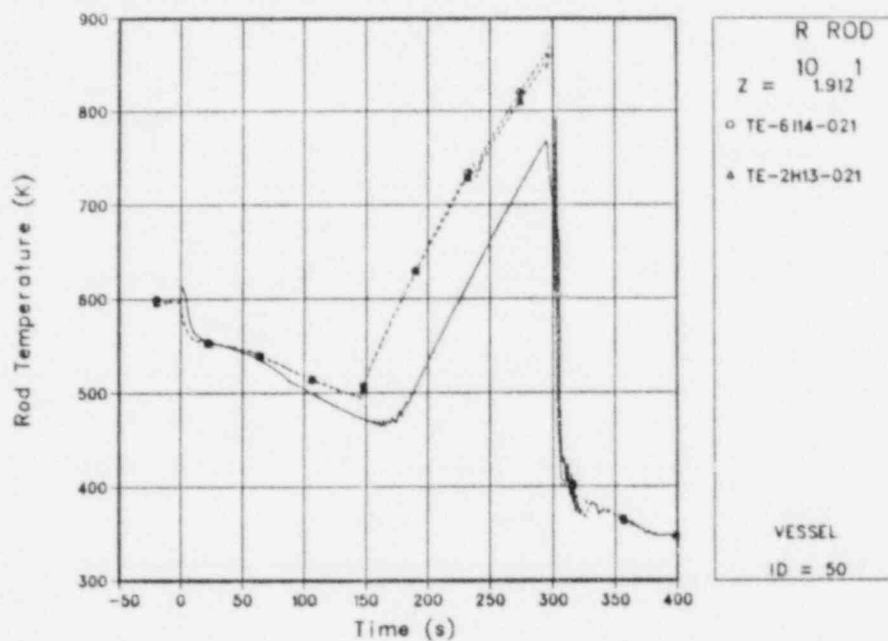


Fig. 157.

Comparison of TRAC-calculated and measured cladding temperatures at the 21-in. elevation for the average-power rod.

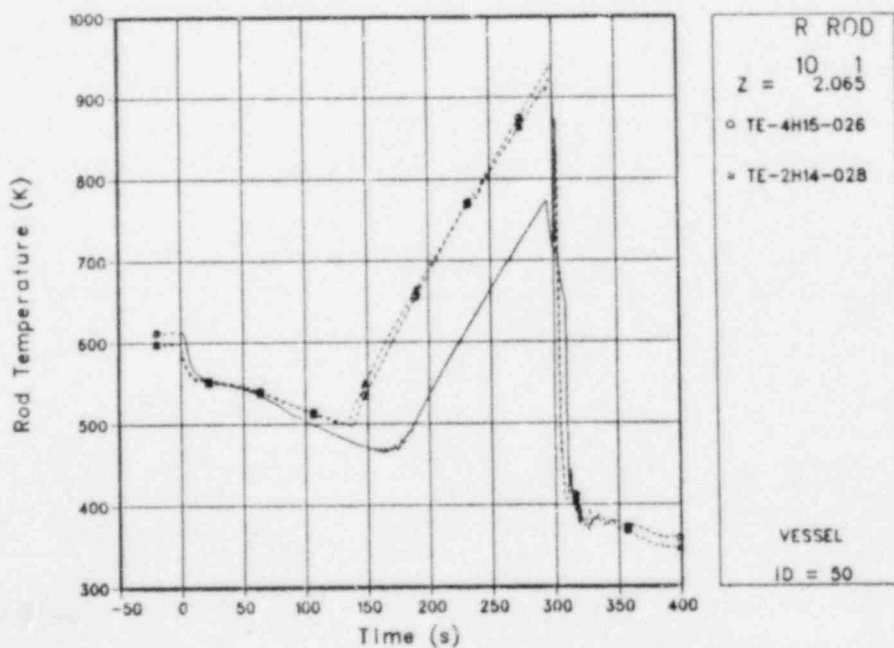


Fig. 158.

Comparison of TRAC-calculated and measured cladding temperatures at the 26-in. elevation for the average-power rod.

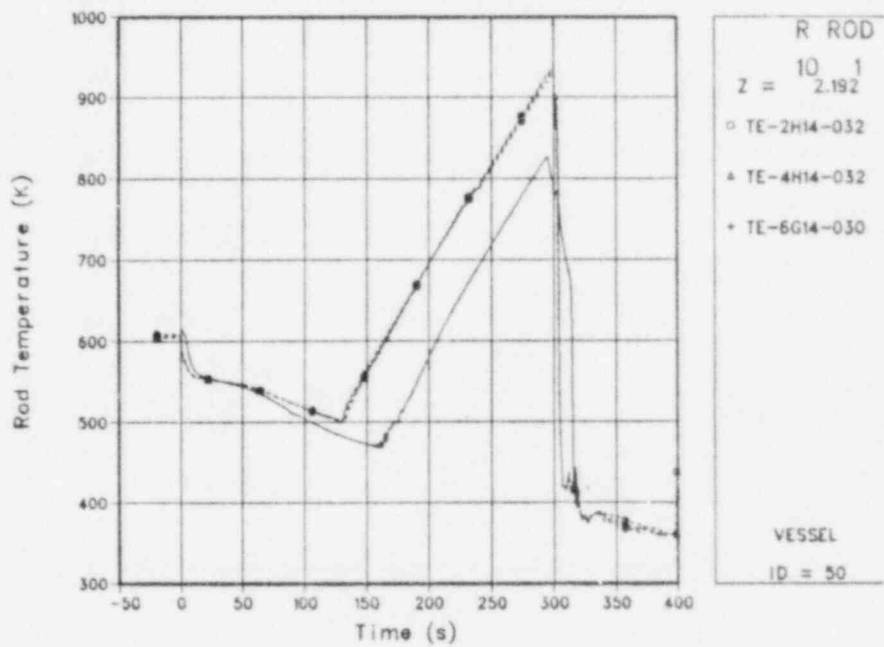


Fig. 159.  
 Comparison of TRAC-calculated and measured cladding temperatures at the 32-in. elevation for the average-power rod.

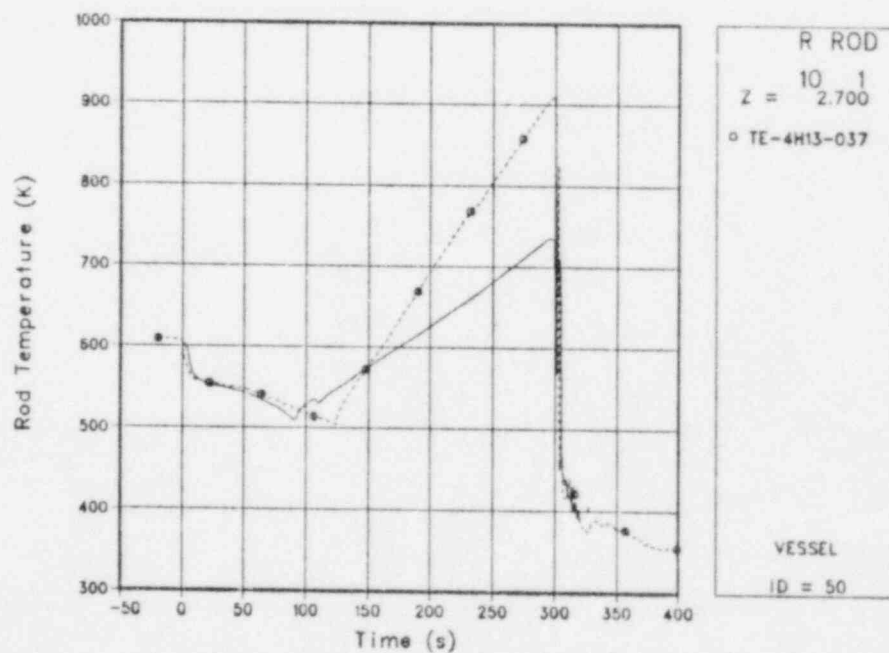


Fig. 160.  
 Comparison of TRAC-calculated and measured cladding temperatures at the 37-in. elevation for the average-power rod.

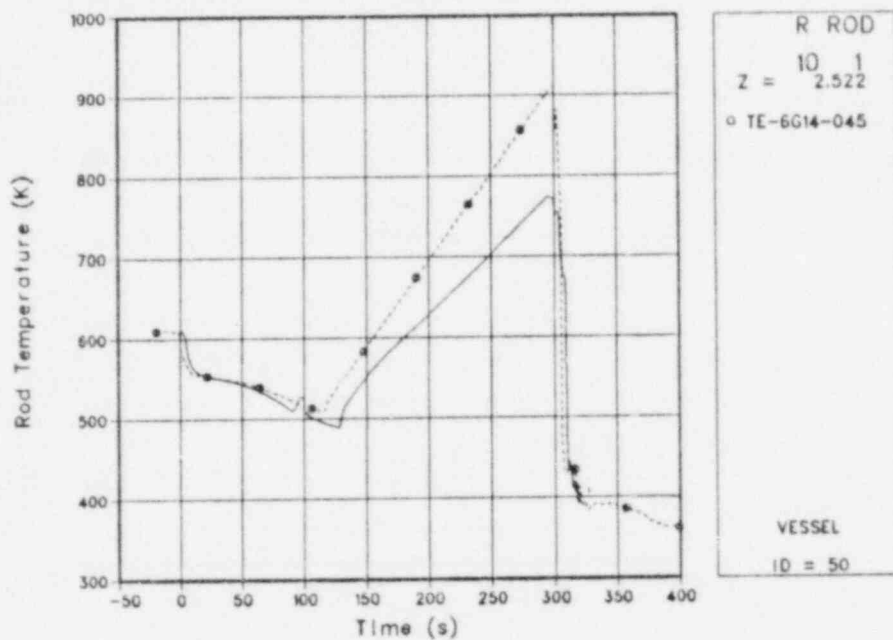


Fig. 161.

Comparison of TRAC-calculated and measured cladding temperatures at the 45-in. elevation for the average-power rod.

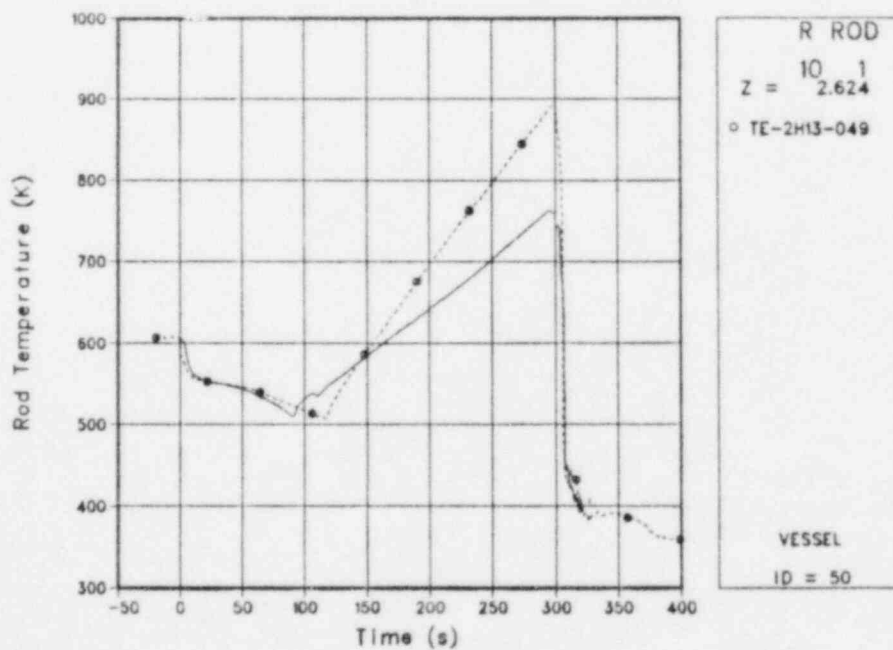


Fig. 162.

Comparison of TRAC-calculated and measured cladding temperatures at the 49-in. elevation for the average-power rod.

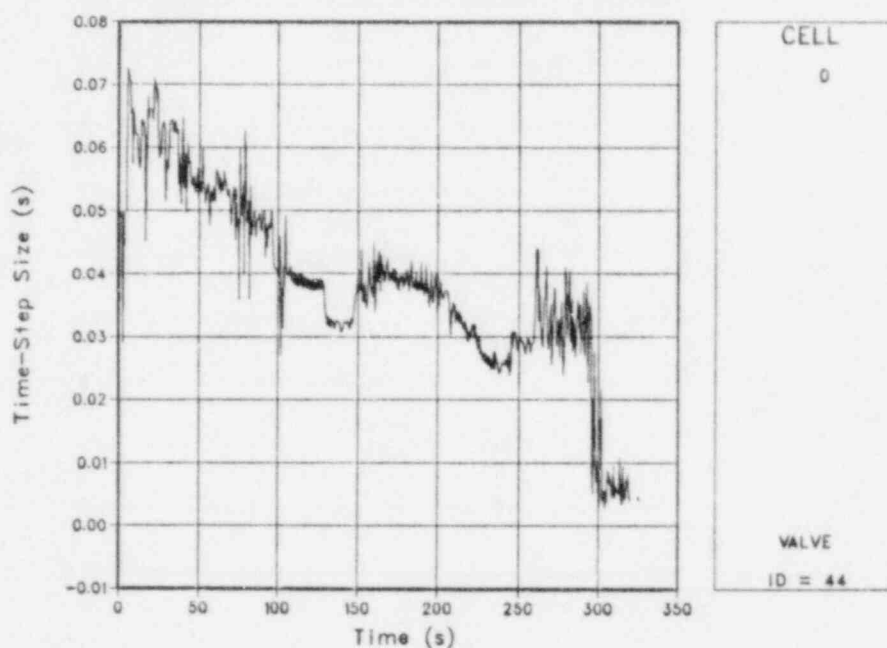


Fig. 163.  
TRAC-calculated time-step size.

except in a few cases during input processing, where the cause for the termination was easily determined.

The following items should be investigated.

1. The critical-flow model in subsequent versions of TRAC-PF1 is different from that used in this analysis. Thus, results from this new model should receive extensive independent assessment using a wide range of separate-effects experiments; if resources permit, analysis of integral experiments should be repeated where break-flow modeling is important to results such as those reported here.
2. In the present version, it is necessary to use a large number of fluid cells in the core region of the vessel for adequate tracking of the liquid-vapor interface if a sharp interface occurs. This would not be necessary, however, if the rod-to-fluid heat-transfer model used an interpolation algorithm to estimate the void profile along the fuel rod. We recommend that such an algorithm be put into the code and be evaluated against separate-effects and integral experiments.
3. The discrepancy in the early primary pressure response should be evaluated and corrected. The cause may be an underprediction of the condensation rates in the three-dimensional vessel component. The error in the calculation of primary-system pressure during subcooled blowdown is large, and while not significant to these



TABLE X  
KEY PARAMETERS FOR LOFT EXPERIMENT L8-2<sup>a</sup>

<u>Parameter</u>	<u>Experimental Results</u>	<u>TRAC-PF1</u>
Peak cladding temperature (K)	978.	875.
Time to dryout (s)	115.	161.
Time to quench (s)	303.	≥319.5
Time to HPIS initiation (s)	3.05 ± .1	3.42
Time to accumulator initiation (s)	294. ± 1.	293.75
Time to LPIS initiation (s)	303.0	311.25

<sup>a</sup>The peak-cladding-temperature, time-to-dryout, and time-to-quench values are for the location of peak temperature in the experiment. The corresponding values in the calculation are 990 K, 129 s, and 319 s, respectively. LOFT Experiment L8-2 was terminated by automatic-safety-system action at  $299.2 \pm 2$  s in a manner difficult to characterize analytically. The calculation was run beyond the time of experiment termination only to evaluate the code's capabilities to calculate the reflooding processes under very high flooding rates.

intermediate-break results, would become highly significant to the results where the calculation of accurate pressures was important.

4. It would be useful if an interphase sharpener were available in the one-dimensional core component. The one-dimensional core component has limited usefulness in transients such as L5-1 and L8-2, where the accurate tracking of a liquid-vapor interface is significant to the results. The interphase sharpener could be applied for other components as well, such as in the steam-generator secondary.
5. The velocity fluctuations in the three-dimensional vessel component require further investigation and correction.

## VI. TRAC-PF1 ANALYSIS OF LOFT STEAM-GENERATOR FEEDWATER TRANSIENT L9-1/L3-3

The LOFT L9-1/L3-3 data were compared to the TRAC-PF1 calculated results as part of the independent assessment of the TRAC code.<sup>1</sup> This experiment was a loss of steam-generator feedwater transient in which decay heat and pump operation caused the system to heat for a long period of time. The experiment was divided phenomenally into two time periods. In the first 100 s, the steam generator dried out and the resulting high primary-system pressure caused a reactor scram. To analyze this part of the transient, we had to calculate accurately the heat and mass transfer in the steam-generator secondary and the pressurizer. We obtained reasonably accurate calculations of this time period by varying the input description within the test-data limitations. During the rest of the transient, the decay heat and the pump operation caused the primary-system temperature to increase. The TRAC-PF1 program calculated this portion of the test well when its condensation heat-transfer coefficient (HTC) was modified.

### A. Test Description

LOFT L9-1/L3-3 simulated a loss-of-feedwater accident (anticipated transient) with a delayed reactor scram and no feedwater injection (multiple failures). Table XI lists a simplified sequence of events that occurred during the experiment.

Several essential phenomena occurred during the L9-1 phase of the experiment. When the feedwater was discontinued to the steam generator, the heat transfer from the primary-side fluid degraded. An increase in the temperature of the average primary-side fluid caused a fluid expansion that forced water into the pressurizer and increased the primary-side system pressure. The L3-3 phase of the experiment involved locking open the power-operated relief valve (PORV) and a pump trip. In response to the pressure increase, the pressurizer spray system was activated. This system temporarily controlled the increase in the system pressure, but eventually the steam-generator heat transfer degraded so severely that the primary-system pressure increase caused the reactor to scram. As a result of the scram signal, the reactor shut down and the steam-generator steam control valve began to close. After the valve closed the primary-system pressure increased until the pressurizer spray again controlled the primary-system pressure.

### B. TRAC-PF1 Input Model Description

Figures 164 and 165 show the TRAC-PF1 input model used for the intact and broken loops, respectively. The model included 43 one-dimensional components with a total of 150 fluid volumes. This input model was derived from one used to analyze LOFT L3-7 and L2-2 as part of the TRAC-PF1 developmental assessment.<sup>2</sup>

The major code-related difficulties encountered in this analysis pertained to the modeling of the trips, the steam generator, and the pressurizer. In the case of the trips, the main difficulty was in controlling the steam-generator-secondary liquid level and the steam control valve during the steady-state calculation. A quasi-steady state was obtained by regulating the inlet water with a liquid-level-dependent fill component and by reducing

TABLE XI  
SEQUENCE OF EVENTS FOR LOFT L9-1/L3-3

<u>Event</u>	<u>Time after Test Initiation (s)</u>
<u>L9-1 Phase</u>	
Main feed pump tripped off	0.0
Pressurizer spray-valve cycling initiated	30.0 ± 0.1
Reactor scrammed	65.4 + 0.2 - 0.0
Steam-generator steam control valve closed	77.2 + 0.0 - 0.2
Steam-generator liquid level reached the bottom of the measurement range (0.25 m above the tube sheet)	190 + 10 - 20
Pressurizer liquid level reached the top of the measurement range (1.83 m above the bottom of the pressurizer)	1090 ± 30
Pressurizer spray-valve cycling ended	1246.0 ± 0.1
PORV cycling initiated	1467.9 ± 0.1
<u>L3-3 Phase</u>	
PORV opened	3269.9 ± 0.1
PCPs tripped off	3284.8 + 0.2 - 0.0
PCP coastdown completed	3304.2 + 0.8 - 0.0
Upper-plenum fluid reached saturation pressure	3329.4 ± 0.2
PORV closed	4849.7 ± 0.1
Steam-generator-secondary refill initiated	5114.6 + 0.2 - 0.0
Primary-coolant-system natural circulation established	5205 + 10 - 5
Steam-generator-secondary refill completed	5746.4 + 0.2 - 0.0
Pressurizer liquid level reached the bottom of the measurement range (0.06 m above the bottom)	5915 ± 5
Steam-generator-secondary feed and bleed initiated	6712.2 + 0.2 - 0.0
Test completed (secondary feed and bleed ended)	9517.4 + 0.2 - 0.0

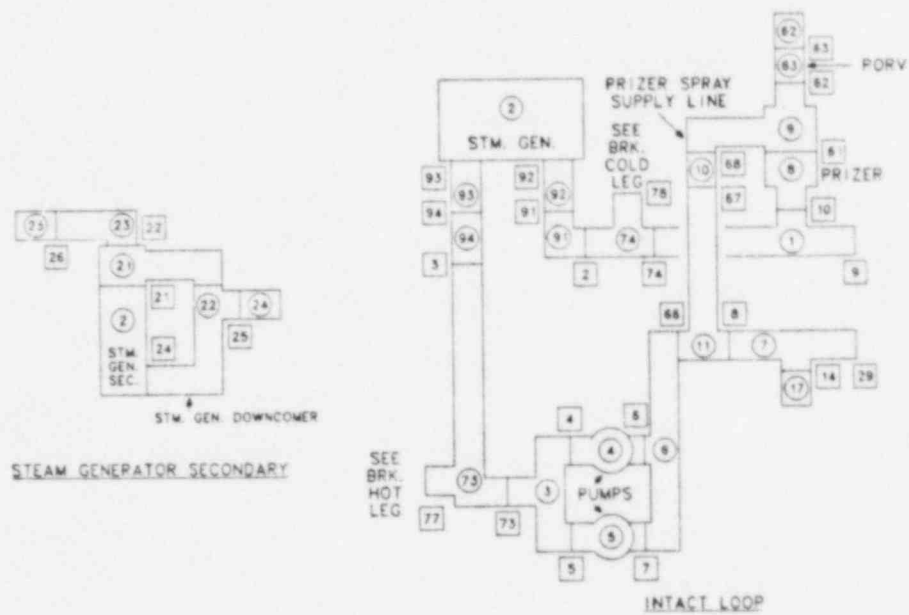


Fig. 164.  
TRAC-PF1 input model of the intact loop for LOFT L9-1/L3-3.

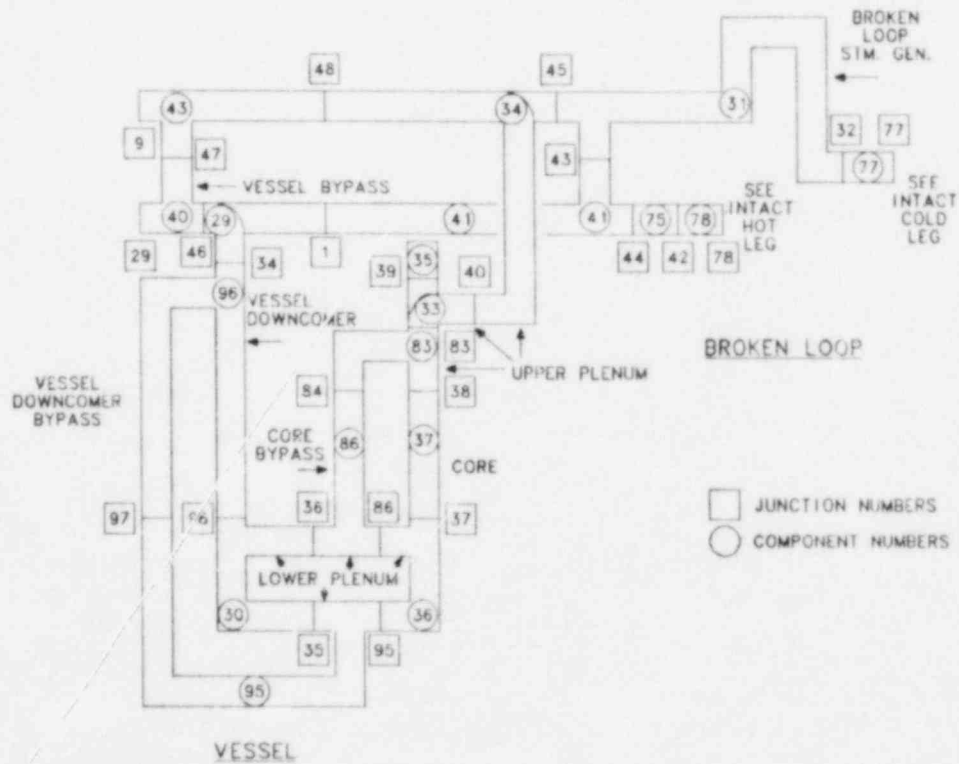


Fig. 165.  
TRAC-PF1 input model of the broken loop for LOFT L9-1/L3-3.

greatly the closing and opening rate of the steam control valve during the steady-state run. The proportional controllers in the newest version of the code, TRAC-PF1/MOD1, should alleviate this problem.

In the case of the steam generator, the phase-separation and heat-transfer processes that occur in the secondary side are very complicated. Accurate calculations for this type of transient require precise analysis of these heat-transfer processes.

The following example illustrates how an error in the calculation of these processes can cause problems in the remaining analysis. Scram initiation occurs on a high-pressure trip. The timing of that trip depends on the rate at which the primary-system pressure is increasing. The rate of pressure increase reflects two different phenomena: the primary-system heating resulting in the thermal expansion of the primary-system liquid, and the effectiveness of the pressurizer spray to counteract the pressure increase. If inadequate phase-separation models calculate an incorrect distribution in the steam-generator secondary, the heat transfer can degrade prematurely and cause an early, calculated reactor scram. Following scram, vaporization of the liquid after the scram removes heat from the primary system. This heat loss causes much lower primary-system pressures and affects the rest of the analysis.

In the pressurizer modeling we found that the expanding primary-system fluid forced cold fluid into the pressurizer. The resulting stratification effects were difficult for the pressurizer component to model. The new pressurizer model in TRAC-PF1/MOD1 was designed specifically to address these types of problems.

### C. Data Comparisons

The primary-system cold-leg temperature comparison was the most interesting in this analysis. Figure 166 compares the temperatures (at the steam-generator outlet). The test data and the calculated results agreed well until ~50 s when the test primary system heated more slowly than shown in the calculation. The heat-transfer or the phase-separation models in the steam-generator secondary side probably caused these discrepancies.

After the scram, both the test data and the calculated results (Fig. 166) showed approximately the same rate of temperature increase. This agreement implied that TRAC modeled the correct heat addition from the core and pumps; the correct amount of fluid in the system; and, most importantly, the correct heat transfer to the metal structure, piping, etc. When these tests were calculated initially, the predicted rate of temperature increase was 1/3 greater than the measured rate. To eliminate this discrepancy, we added bypass flow paths in the downcomer and core and more detailed modeling of the steam-generator inlet and outlet plenums; most importantly, we modified TRAC so that a  $50\text{-MW/m}^2$  HTC was used when the heat-transfer regime was condensation on the walls. More sophisticated changes to the condensation heat transfer are included in TRAC-PF1/MOD1. Discrepancies between the test and the calculated results after 3300 s may be attributed to differences between the analytical and the test PORV mass flow rates.



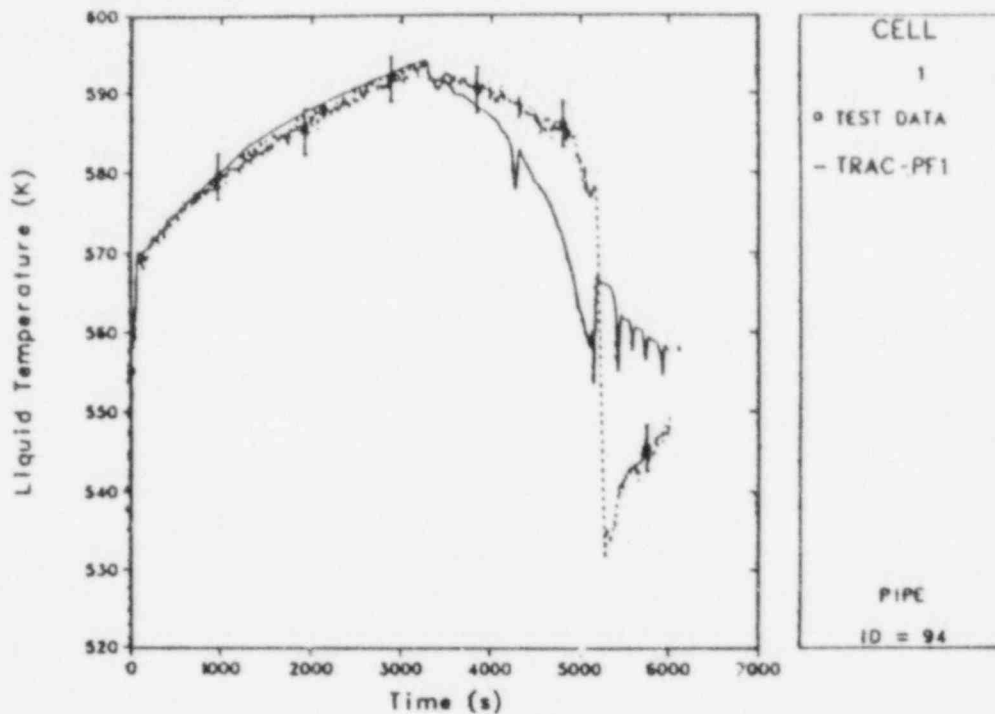


Fig. 166.

Comparison of TRAC-calculated and measured primary-system cold-leg temperatures for LOFT L9-1/L3-3.

Figure 167 compares the mass flow rates from the secondary steam flow control valve. The test data and the calculated results agreed fairly well. Differences between the initial flow rates were due to the different feedwater temperatures in the analysis and in the test. In subsequent analyses we used the same feedwater temperatures and obtained the same initial flow rates. Figure 168 compares the pressures on the steam-generator secondary side. As we discussed previously, heat-transfer changes in the steam-generator secondary caused temperature changes in the primary-system cold-leg fluid (Fig. 166). Figure 169 shows that the increased fluid temperature caused the primary fluid to expand into the pressurizer with a corresponding increase in pressurizer pressure. Although the measured and the calculated primary-system fluid-temperature increases correlated closely, note that the pressure traces diverged quickly. This discrepancy was due to the difficulties in modeling the complex heat- and mass-transfer processes in the pressurizer during the transient.

In Fig. 170 we see how the cycling pressurizer spray controlled the system pressure beyond 1000 s. The spray was discontinued and the pressure increased until the cycling PORV began to control the system pressure. This process continued until ~3260 s when the PORV remained open causing the system pressure to decrease. In general, the test and the analytical data agreed well towards the end of the transient. We stopped the analysis at 6000 s of problem time to reduce cost.

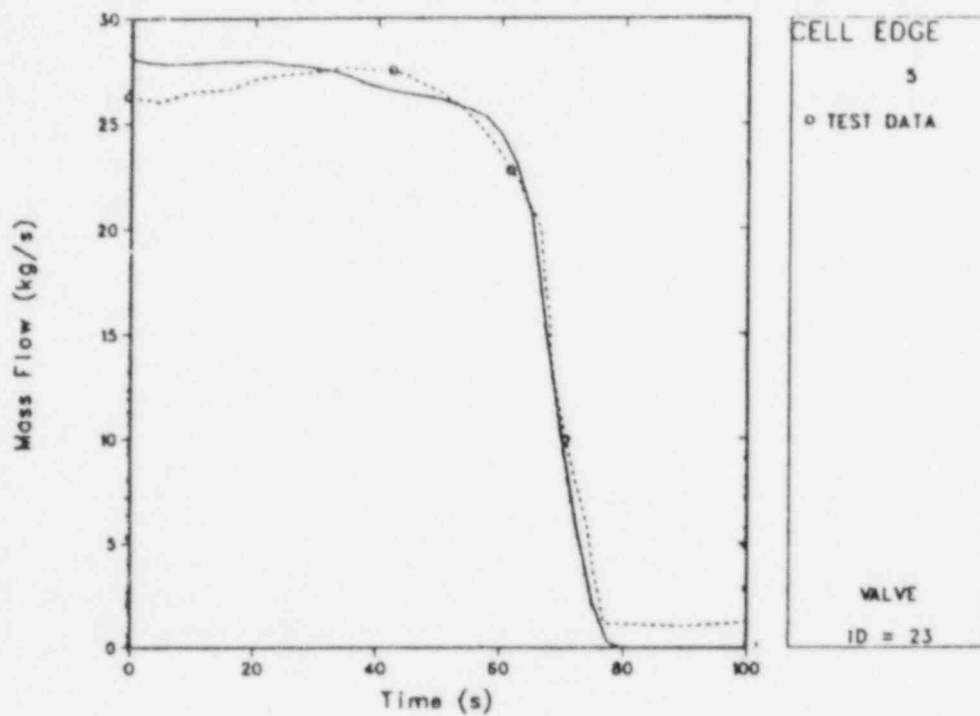


Fig. 167.

Comparison of TRAC-calculated and measured mass flows for LOFT L9-1/L3-3.

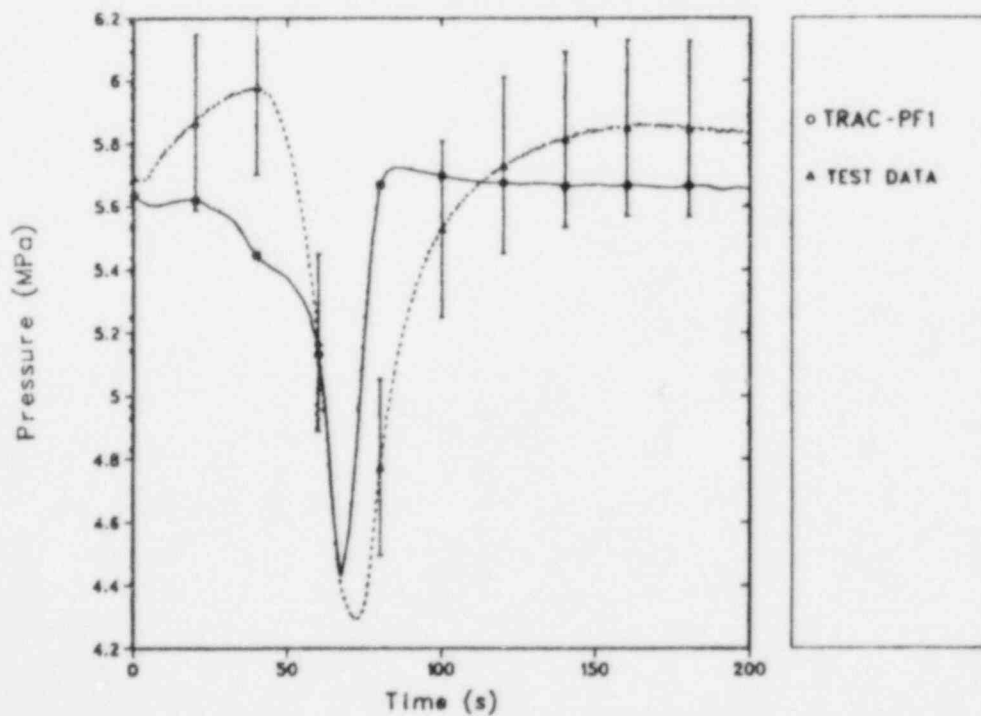


Fig. 168.

Comparison of TRAC-calculated and measured pressures on the steam-generator secondary side for LOFT L9-1/L3-3.

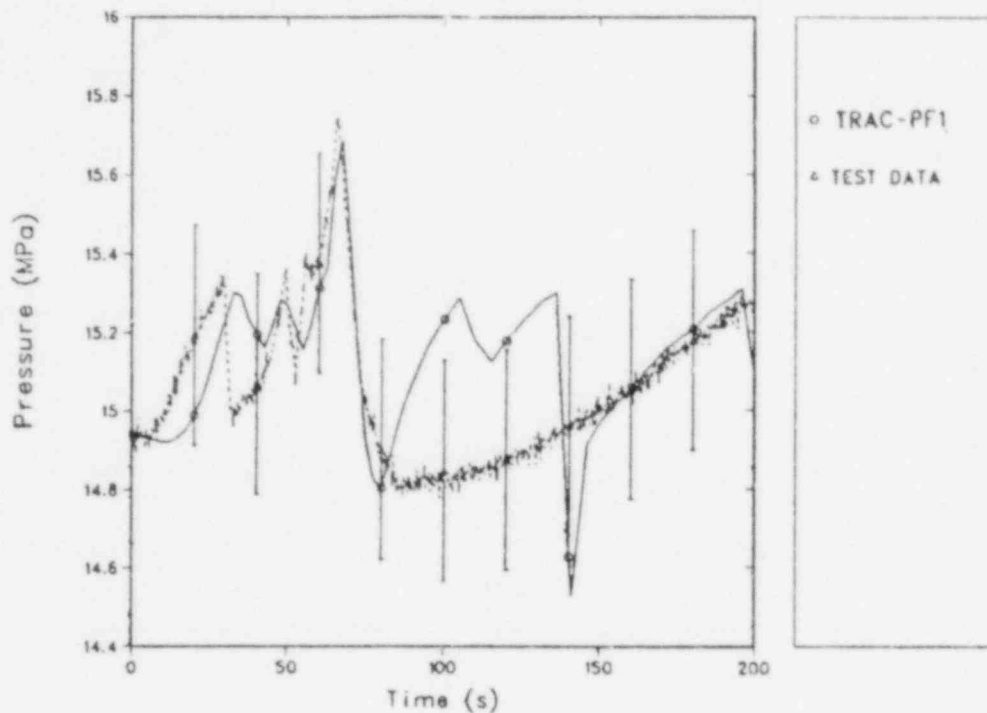


Fig. 169.  
Comparison of TRAC-calculated and measured pressurizer pressures for LOFT L9-1/L3-3.

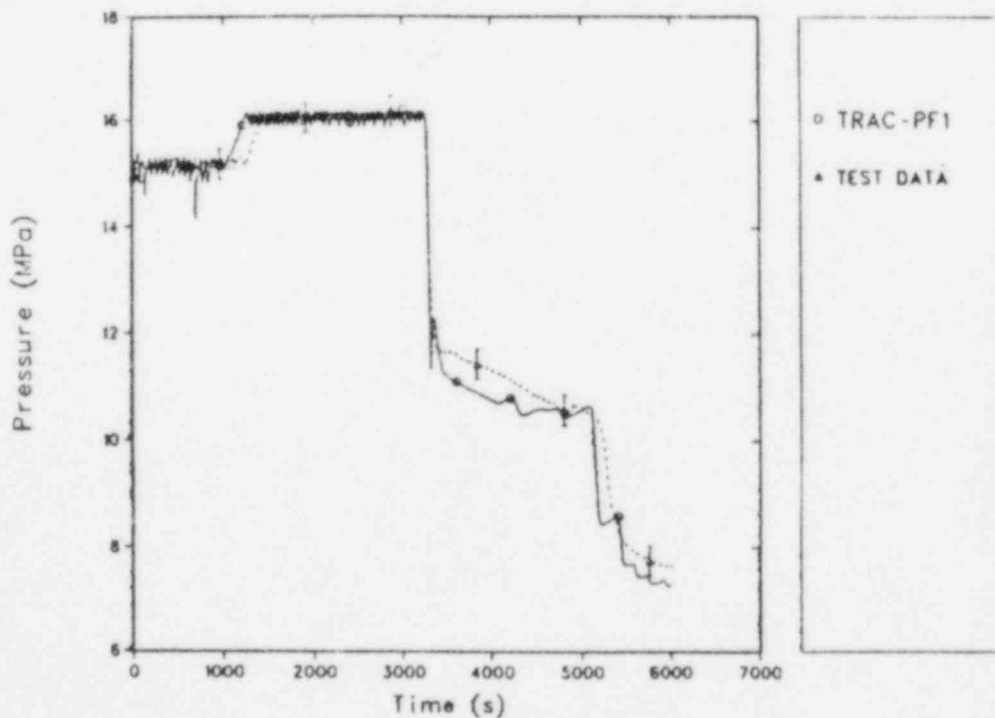


Fig. 170.  
Comparison of TRAC-calculated and measured pressures controlled by the pressurizer spray for LOFT L9-1/L3-3.

#### D. Conclusions

The code calculated the experiment well, given the uncertainties in the boundary conditions. The analysis indicates the need to model all the flow paths and heat structures and to improve the TRAC condensation heat-transfer model.

## VII. TRAC-PF1 ANALYSIS OF LOFT L6-7/L9-2

As part of our independent assessment of TRAC-PF1, we analyzed LOFT L6-7/L9-2 and compared the test data to the calculated results. Test L6-7 simulated a cooldown transient similar to the Arkansas Nuclear One Unit-2 turbine-trip transient.<sup>27</sup> During the L9-2 phase of the test, the primary-coolant pumps were tripped and natural circulation cooled the core while the plant cooldown continued. The TRAC results matched the test data well during the L6-7 portion of the transient (0.0-324 s). However, during the L9-2 portion, the calculated natural-circulation flow rate in the intact loop was much higher than the measured rate.

Other analysts<sup>28,29</sup> have encountered a similar problem in their calculations of this test, and they attribute the deficiency to a difference between the calculated and actual values of the LOFT locked-rotor pump resistance. However, the test data exhibit a multidimensional fluid-temperature distribution in the downcomer and imply a multidimensional flow field in the downcomer. We believe that the temperature distribution reduces the driving head for natural circulation.

The calculated vessel and valve leakage rates during natural circulation have large uncertainties. Also, significant uncertainties in the actual steady-state leakage rates, which were used as a basis for these calculations, probably compound the problem.

The primary-system pressure comparison is the most significant. From 300-400 s, the system pressure was very sensitive to the amount of water remaining in the pressurizer when the pumps tripped. After 500 s the system pressure was sensitive to the leakage rate in the reflood-assist bypass valves (RABVs) during the early portion of the transient. We obtained a reasonable match between the test and calculated results when we decreased the RABV leakage rate to 50% of the approximate values given by EG&G at the INEL.\* Otherwise, the comparison between the test data and calculated system pressure was good.

The analysis showed that very detailed noding is required in several locations to avoid numerical diffusion of liquid energy in the slowly moving liquid. It was important to calculate the correct distribution of energy in the system to obtain the correct distribution of vaporizing fluid.

The gradual system cooling during Test L9-2 led to a phenomenon that would not occur during a natural-circulation test at a constant temperature. During the later portion of the transient, the heat addition from the vessel walls was greater than that from the core. The complex flow patterns that probably resulted from this phenomenon indicate that a three-dimensional vessel model may yield better results than the one-dimensional model used in these calculations.

\*At the Semiscale/LOFT Modeling Workshop, August 19-20, 1981, EG&G Idaho indicated that the RABV leakage was ~1.4% of the total loop flow.



The details of the test, analysis, and data comparisons are presented in the following sections. There, we

- describe the test apparatus,
- describe the experiment and experimental phenomena,
- describe the TRAC input,
- present and discuss the data comparisons, and
- provide details of computer use.

#### A. Test Apparatus

The LOFT facility (shown in Fig. 171) is a 50-MW(t) PWR, detailed descriptions of which may be found in Refs. 25, 30, and 31. The description presented here will be limited to the particular configuration of the facility used for Experiment L6-7/L9-2, as well as specific details of the facility particularly important to this experiment.

The reflood-assist bypass lines (RABL), shown in Fig. 172, were particularly important in Test L6-7/L9-2. These lines connect the broken hot and cold legs of the LOFT system through the RABV. These valves leak at a rate such that fluid in the lines heats during steady state but only partially cools during the transient. This trapped hot fluid constitutes the major source of steam generation during the latter part of Test L9-2.

The leakage paths in the vessel were very important during this test because they influenced the flow fields and temperature distribution in the vessel. The two most important ones were: (1) the gap between the downcomer

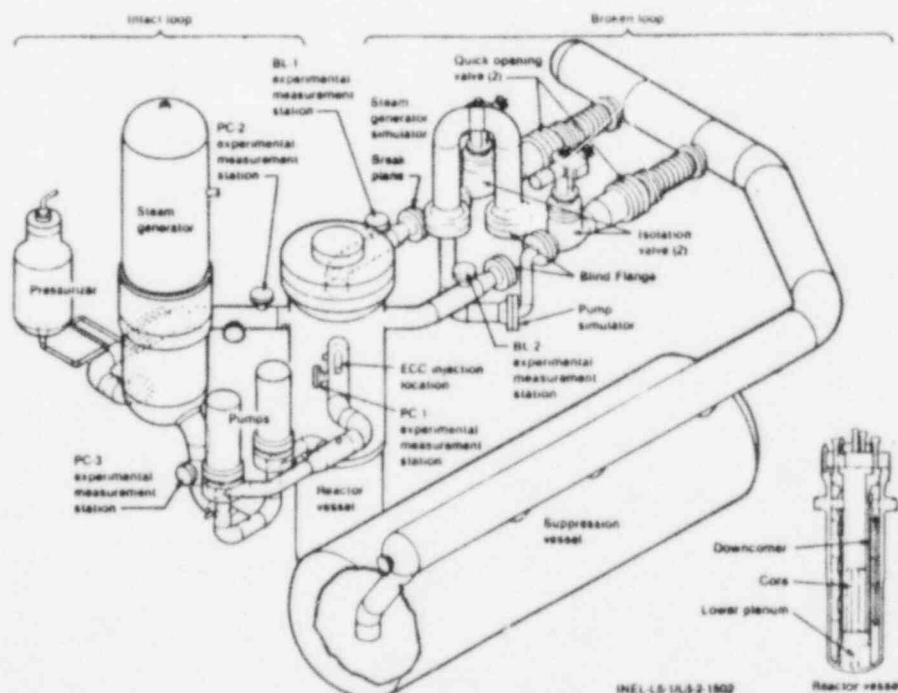


Fig. 171.  
LOFT major components (Ref. 31).

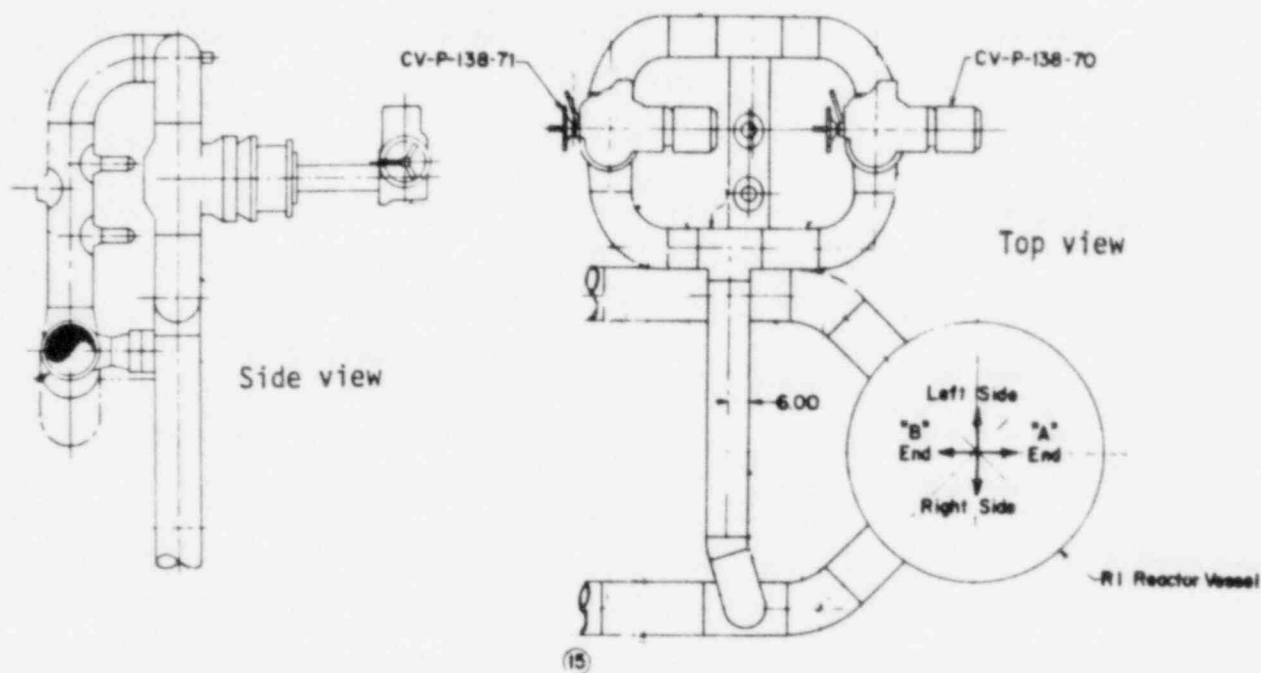


Fig. 172.  
Reflood-assist bypass lines (Ref. 25).

filler and pressure vessel (Fig. 173) in which we calculated the fluid to flow upward during natural circulation and (2) the leakage between the hot and cold legs (Fig. 174) carrying 5% of the primary-system flow during pump operation and as much as 20% of the system flow during natural circulation.

In this test, most of the broken hot leg was removed and the warm-up recirculation lines were closed.

#### B. Experimental Phenomena

A description of the important events and phenomena in these tests is presented below. Table XII lists the events for Test L6-7/L9-2. These events may be followed in the primary-system pressure trace of Fig. 175. The experiment begins as the operator manipulates the steam-generator secondary-side flow-control valve to give a predetermined rate of steam flow. After the reactor is manually scrammed at 7 s, this rate of flow cools the secondary-system fluid and consequently the primary-system fluid.

The fluid in the primary-system shrinks, drawing water out of the pressurizer and lowering the pressure in the primary system. This situation continues until the pressurizer almost empties and the primary-coolant pumps trip.

For future reference, note that there is small leakage through the RABV while the pump is running, resulting in cooled fluid in the broken loop and

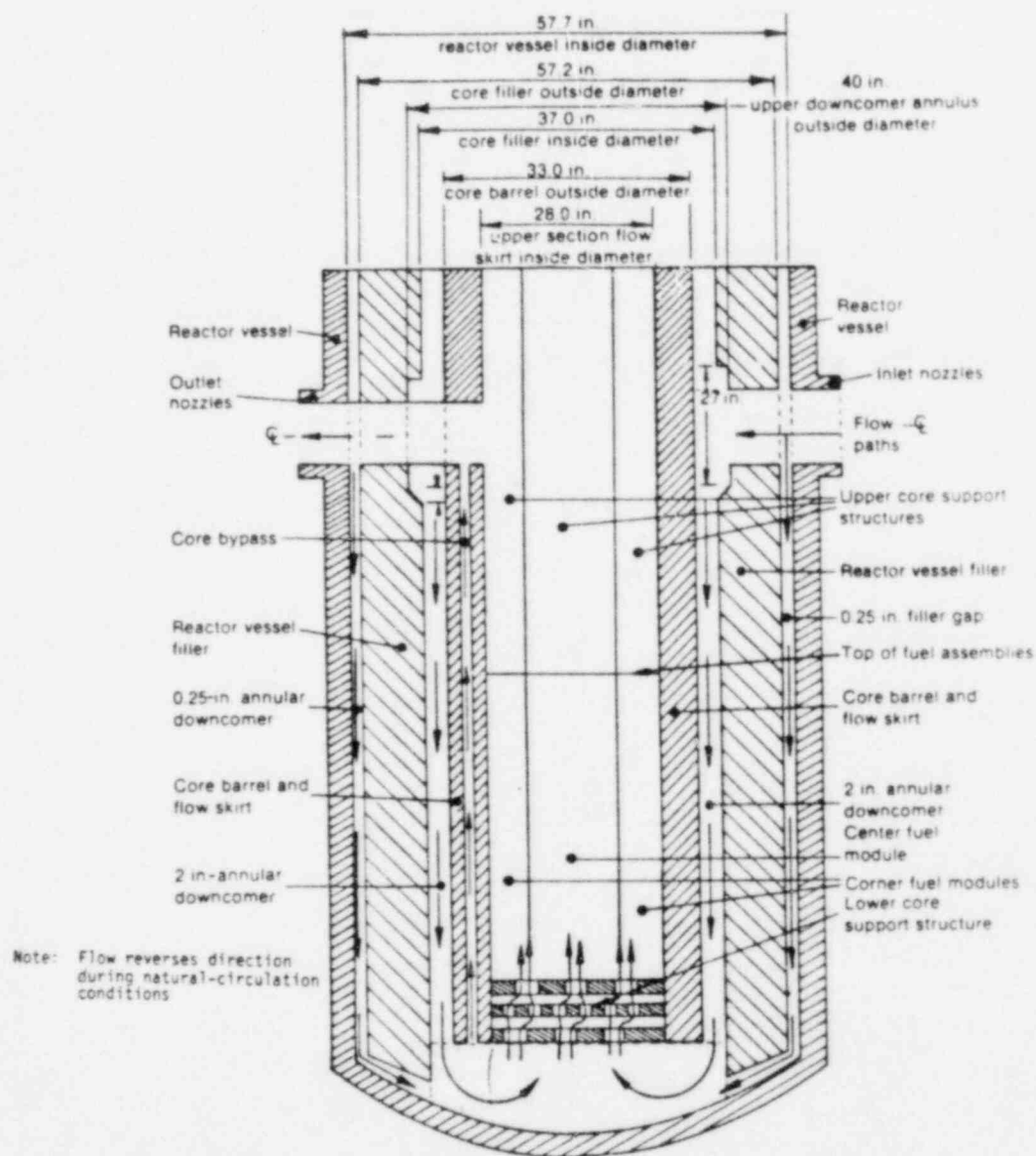


Fig. 173.  
Reactor-vessel schematic with flow paths (EG&G, Idaho, Semiscale LOFT Modeling Workshop, August 19-20, 1981).

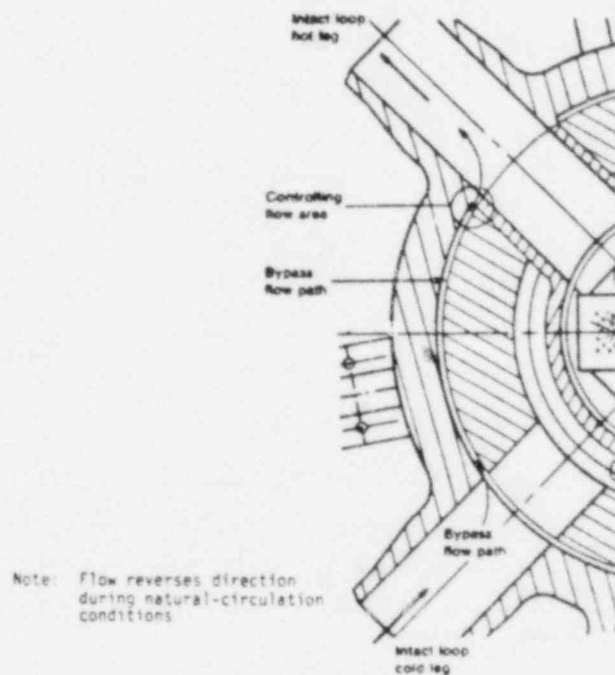


Fig. 174.

LOFT primary-system hot and cold legs (EG&G, Idaho, Semiscale LOFT Modeling Workshop, August 19-20, 1981).

TABLE XII

SEQUENCE OF EVENTS FOR EXPERIMENT L6-7/L9-2

<u>Event</u>	<u>Time after Experiment Initiation (s)</u>	
	<u>Measured</u>	<u>Calculated</u>
<u>Experiment L6-7</u>		
Experiment initiated	0.0	0.0
Reactor scrammed	$7.3 \pm 0.1$	7.3
Pressurizer liquid level reached bottom of range	$278 \pm 3$	272
<u>Experiment L9-2</u>		
Primary-coolant pumps tripped off	$324 \pm 2$	324
Natural-circulation flow first indicated	$341 \pm 5$	370
Coolant flashing outside the pressurizer first indicated	$595 \pm 2$	548

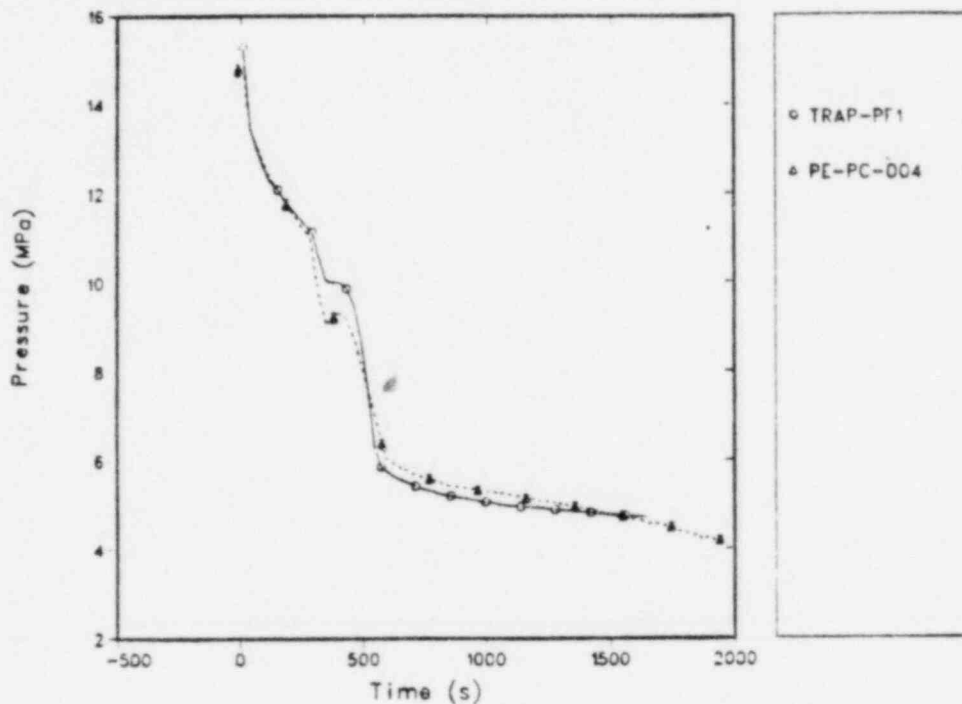


Fig. 175.  
Primary-system pressure.

RABL. Also, some fluid in the upper head is cooled as a result of fluid movement in the upper plenum.

As the hot, saturated fluid in the pressurizer is injected into the hot leg, it mixes with the colder fluid in the system. Therefore, when all the fluid in the pressurizer is injected, no saturated fluid in the primary system remains; and further vaporization is precluded. This causes the primary-system pressure to drop rapidly at ~280 s. Next, the flow rate in the intact loop drops with the coastdown of the pumps, resulting in a greater temperature difference across the vessel. This causes the temperature of the intact hot leg to rise temporarily, with a resulting temporary rise in the primary-system pressure. This temperature difference establishes natural circulation in the intact loop that limits intact-loop heating and eventually lowers the system pressure again at ~370 s.

The experiment data indicate that the natural-circulation patterns during this time are very complicated. For instance, thermocouples located in the downcomer show it to be as hot as the core. The TRAC calculation suggests the presence of significant mass flow in the various leakage paths within the vessel. Also, a heat balance across the vessel indicates that well over half of the heat added to the fluid passing through the vessel is from the metal structure. Note that if the fluid temperature in the system as a whole were not decreasing, the fluid and the structure would be the same temperature and the vessel flow patterns might be much different. The system pressure continues to fall as the primary-system fluid cools; then, at 550 s, liquid in



the upper head and then in the RABL starts to vaporize, stabilizing the pressure for the rest of the test.

### C. Description of TRAC Input

A component diagram of the input description is presented in Figs. 176 and 177.

The input description used for these analyses was derived from the one used for the L9-1/L3-3 analyses.<sup>32</sup> An important change was that the broken loop and RABL were noded much more finely. In the previous input description, only one or two volumes were used to model each of these sections of piping. Cold water from the main system, which slowly entered the broken loop because of RABV leakage, was quickly transported by numerical diffusion throughout the broken loop and RABL. In the actual test, this colder fluid appeared to remain near the entrance to the broken loop. By using much finer noding, we minimized this numerical diffusion. In the final description, 7 to 10 volumes were used to model each of these components. Other changes from the L9-1/L3-3 model were that the PORV, the warm-up recirculation valves, and much of the broken-loop hot leg were removed.

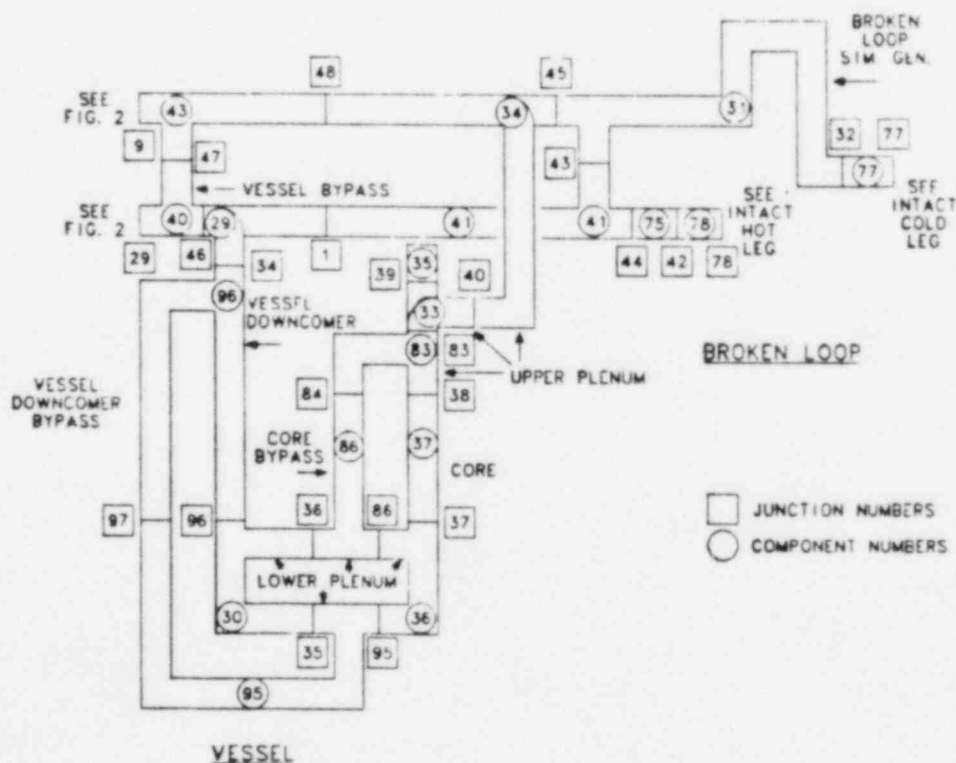


Fig. 176.  
Vessel and broken-loop component diagram.

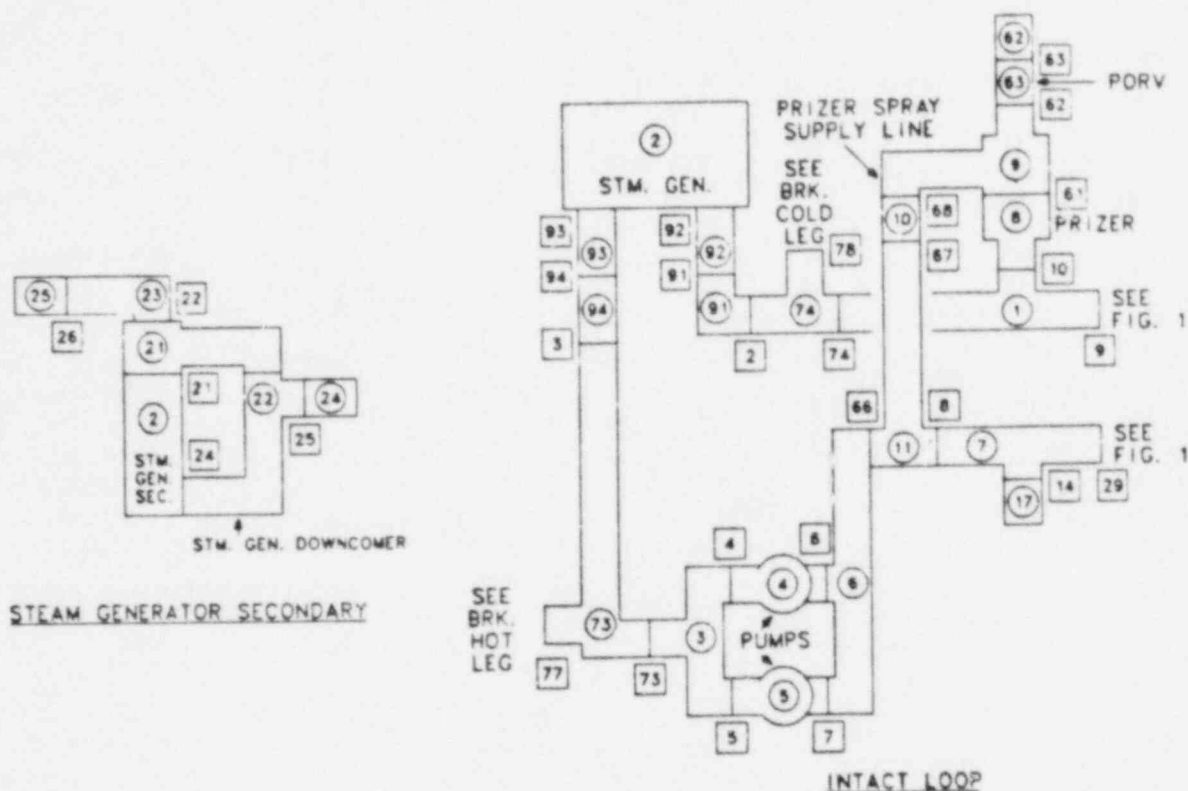


Fig. 177.  
Intact-loop component diagram.

To conserve computer time, the particular input description in these analyses uses a one-dimensional vessel description. The test data and the analytical results together indicate that important three-dimensional effects are present in the vessel, especially in the downcomer.

The primary boundary condition used in the analysis was that pressure in the steam-generator secondary side was controlled by a time-dependent break. Use of a fill to match the steam-generator secondary-side outlet mass flow was considered but rejected based on the superior accuracy of the pressure data.

The initial pressurizer liquid level was fixed at the lowest value within the error band of the test data.

Simulation of the leakage paths within the vessel presented special modeling problems. Because of the intricate geometry of these paths, they are modeled empirically; that is, a parameter within the TRAC input description is adjusted until TRAC calculations of the steady-state leakage rate match the INEL-supplied data. The three changeable parameters are the flow area, the hydraulic diameter, and the friction factor. A problem encountered in this test was that the range of flow rates in these leakage paths is many orders of

magnitude. Therefore, none of the above methods is likely to remain valid during the low flow rates that occur when natural circulation drives the system. Furthermore, the direction of the flow in several of the leakage paths reverses under natural-circulation conditions.

There is also some question as to whether the specified steady-state value of leakage for the RABV valves is applicable to this particular test. The calculations of Test L6-7/L9-2 were improved significantly when the leakage rate was halved. The way that INEL calculated the leakage rate is indicative of its large uncertainty; INEL used the core delta temperature, power, and intact-loop flow rate to estimate the overall leakage rate of fluid that was not flowing through the core during steady state. The INEL overall leakage rate, ~11%, is accurate to no more than 1-2% of the total loop flow. Then, based on the geometry of the various leak paths within the vessel, the individual leakage rates were calculated and subtracted from the overall leakage rate to obtain the INEL-specified RABV leakage rate of 1.4%.

In these tests, the one-dimensional vessel model presented a problem regarding the upper head. Because the upper head is modeled as a dead-end stub of pipe, there is little circulation between it and the rest of the system until it begins to flash. In the experiment, there is actually a small degree of circulation of fluid in the upper head caused by jets of fluid from the upper plenum, an additional indication of multidimensional behavior. This circulation lowers the temperature of the fluid in the upper head during the first 400 s of Test L6-7. To account for this temperature decrease in the calculation, the fluid in the upper head was set at a lower initial temperature than was recorded in the test data.

#### D. Presentation and Discussion of Data Comparisons

Figures 178-185 present data comparisons from this study. The designation in the box at the right of the curves TE-SG-002 indicates the LOFT transducer location. (See Ref. 31.) The TRAC component ID = 94 is listed at the bottom of the box.

The principal boundary condition used during this test was the pressure in the steam-generator secondary side. This then determined the temperature in the steam-generator secondary side, which in turn determined the temperature at the outlet of the steam-generator primary side. Not surprisingly, we see in Fig. 178 that the test and calculated results for the outlet temperature closely agree.

While the pump is running, all of the temperatures in the flowing loop essentially equalize after the reactor scrams. The intact-loop hot-leg temperature presented in Fig. 179 is typical of these. During Test L6-7, the experiment and the calculated results are the same.

The data comparisons of the fluid temperatures in the broken loop and RABL were influenced strongly by the leakage rate through the RABV. In the initial analysis of these tests in which the EG&G-recommended RABV leakage rate was modeled, the calculated rate of temperature decrease in the broken loop was twice that in the test data. Because EG&G has indicated that this

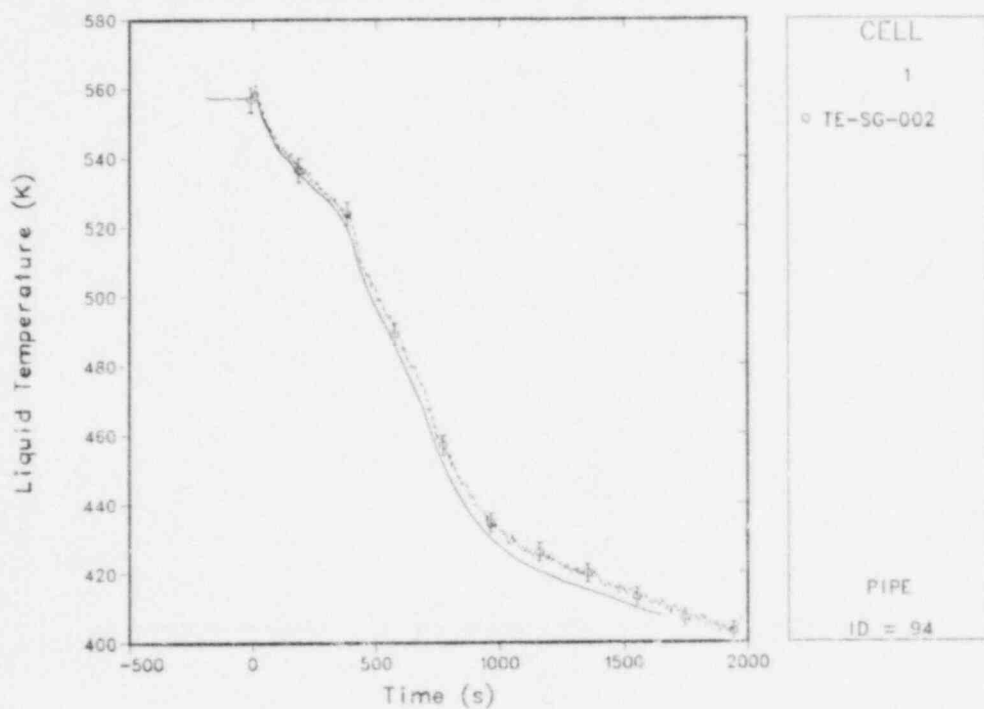


Fig. 178.  
Steam-generator outlet temperature.

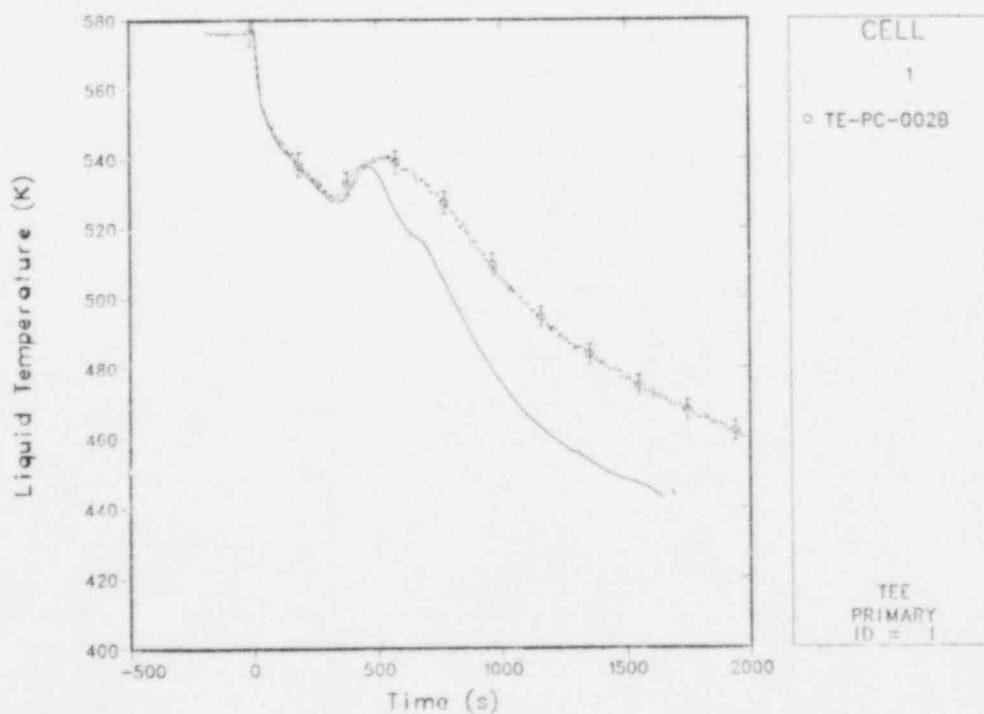


Fig. 179.  
Intact-loop hot-leg temperature.

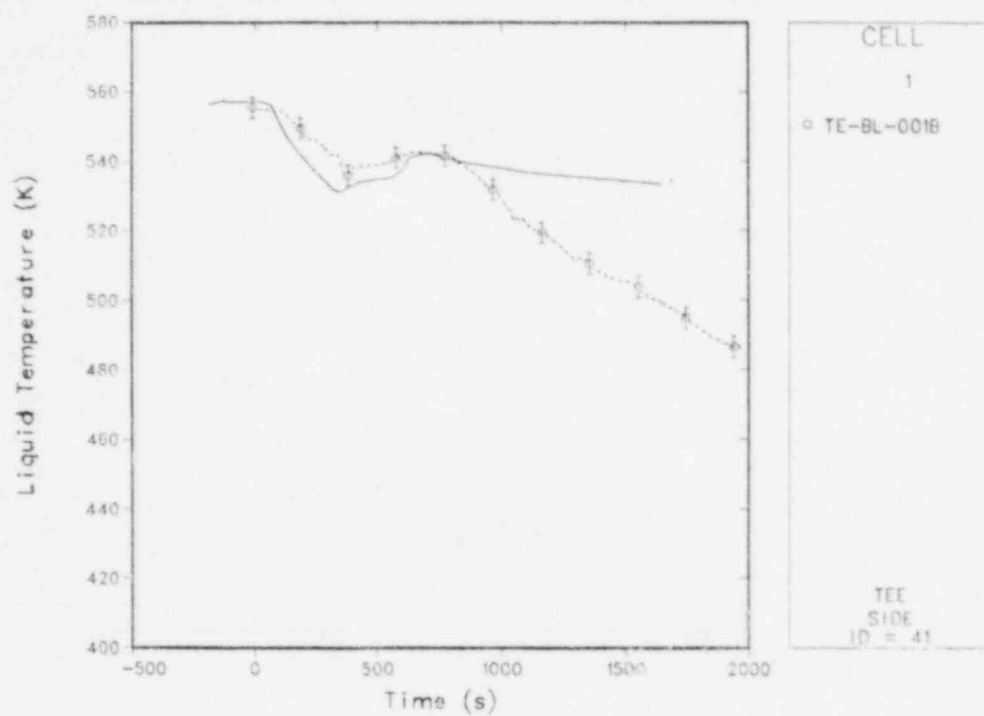


Fig. 180.  
Broken-loop cold-leg temperature.

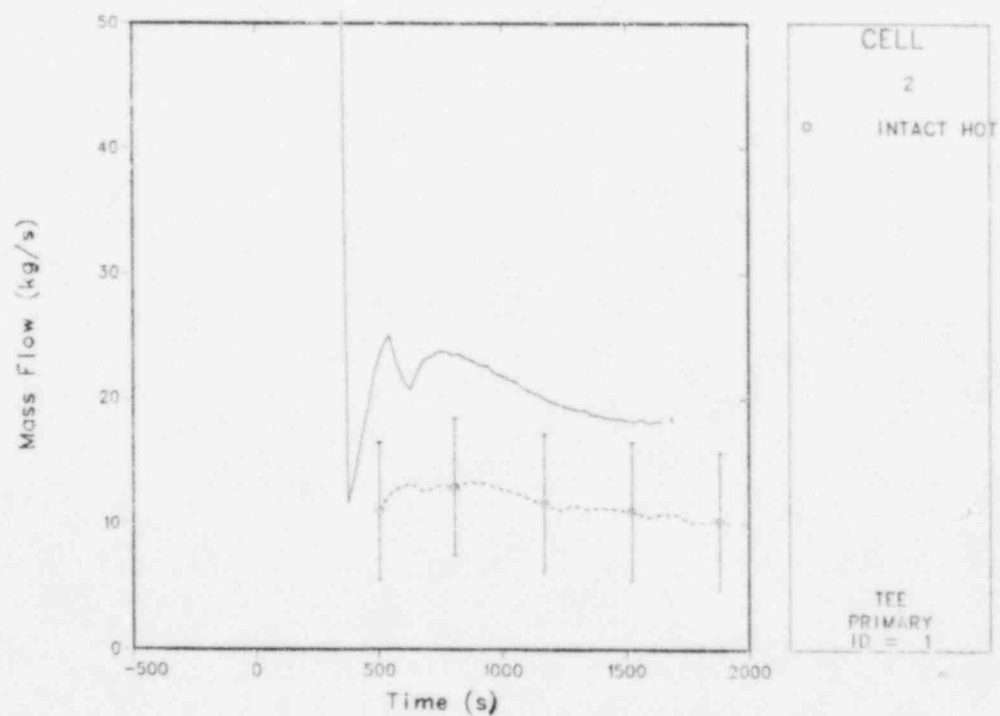


Fig. 181.  
Intact-loop mass flow rate.



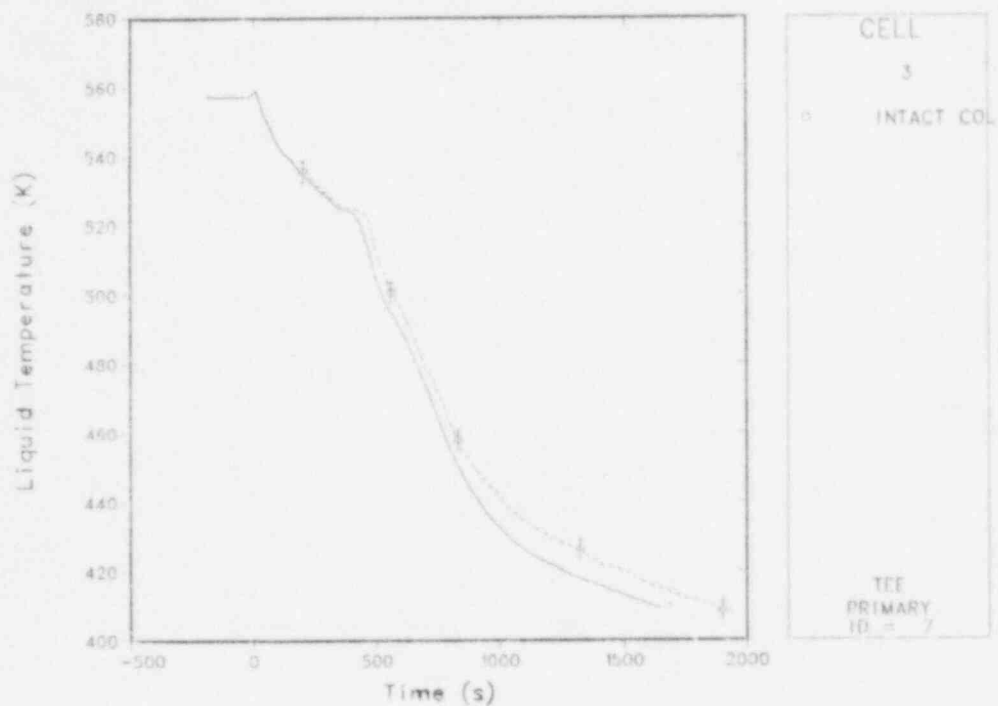


Fig. 182.  
Intact-loop cold-leg temperature.

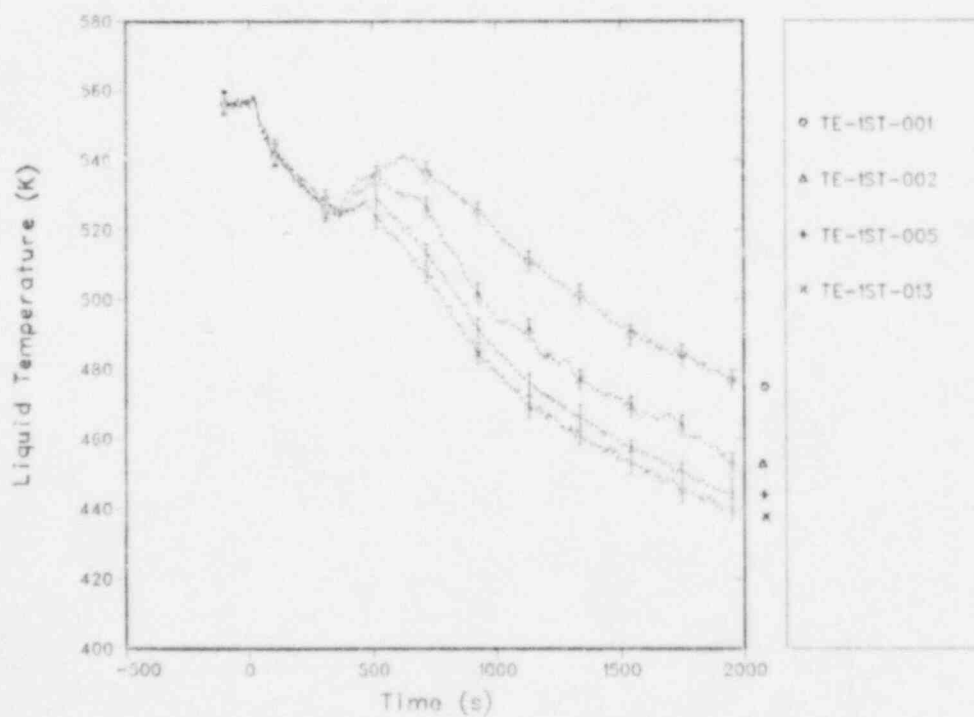


Fig. 183.  
Experiment downcomer temperatures (D. C. Stalk 1).

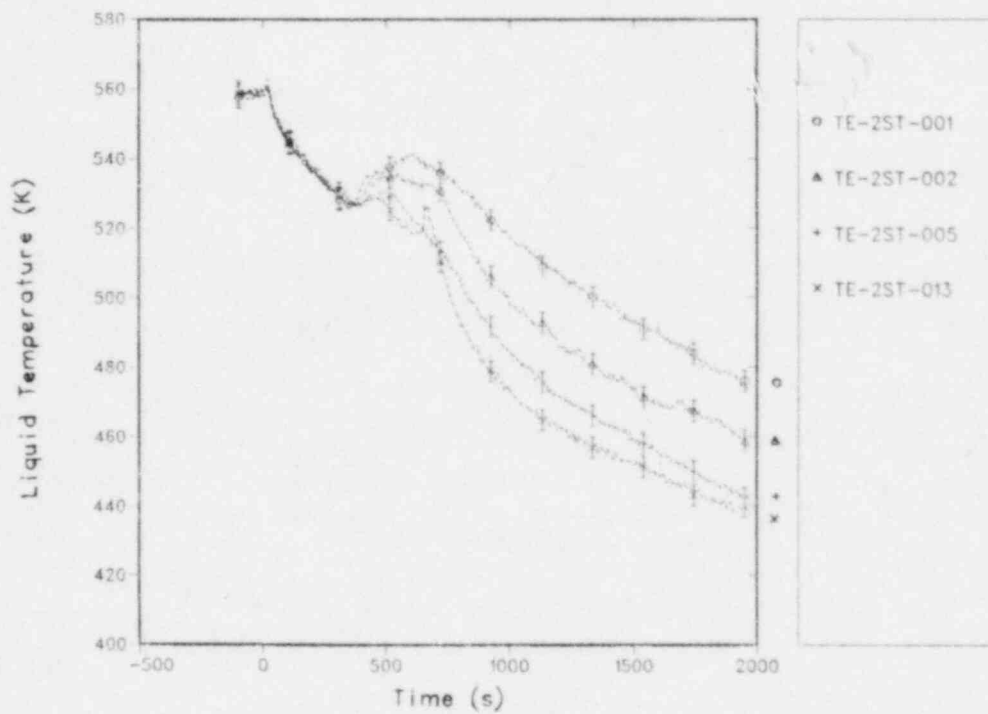


Fig. 184.  
Experiment downcomer temperatures (D. C. Stalk 2).

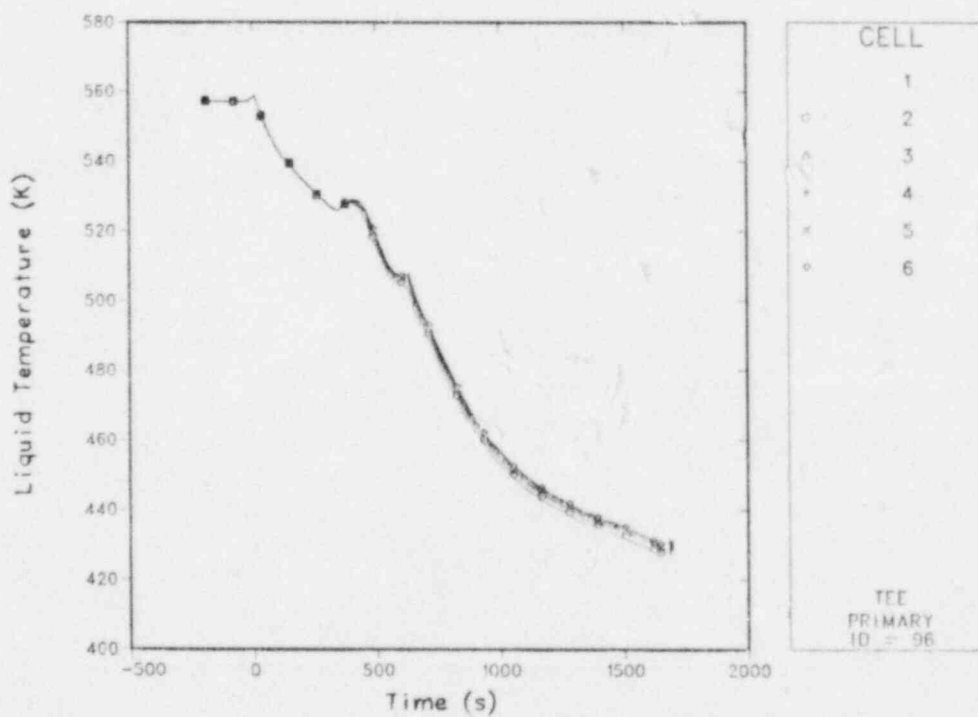


Fig. 185.  
Calculated downcomer temperatures.

leakage rate was very uncertain, the TRAC model was altered to reduce the rate by 50%. The results in Fig. 180 were from this run.

The primary-system pressure is presented in Fig. 175. The test and calculated results agree except in the 280-380-s interval. The sudden drop in pressure at ~280 s occurs when the pressurizer empties of liquid and no vaporizing liquid remains in the primary system to moderate the pressure decrease. The slight increase in pressure that occurs next results from the increase in temperature of fluid in the vessel and intact hot leg when the coolant pumps coast down. The difference between the test and calculated results from 280-350 s has been traced to three separate sources of roughly equal importance. The decline in pressure caused by the depletion of saturated liquid in the pressurizer occurs slightly earlier in the test than in the calculation. The change in the overall system density caused by a temperature decrease during this time period is slightly smaller in the calculation than in the test data. This is indicated by the slope of the system pressure just before 280 s. Finally, the TRAC steam-table values for  $d\rho/dT$  and  $d\rho/dP$  of liquid are somewhat inaccurate in this range of the pressure and temperature.

The relatively stable pressure after 600 s is, in large part, a result of vaporization of fluids in the RABL and broken loop. In initial calculations of this test using higher RABV leakage rates, the early temperature history in the RABL was underpredicted significantly. The primary-system pressure after 600 s also was underpredicted. When we roughly matched the fluid temperature in this loop by adjusting the RABV leakage rates, we obtained reasonably good agreement between the test and the calculated primary-system pressure. We believe vaporization of the high-temperature liquid in the upper head and downcomer also helped stabilize the system pressure. Because we could not match these temperature profiles with the one-dimensional model used in this analysis, we could not determine their significance.

Turning our attention to the natural-circulation-dominated part of the transient (Phase L9-2), we clearly see in Fig. 181 that the calculated mass flow in the intact-loop hot leg is much greater than in the test data. Correspondingly, we see that whereas the calculated steam-generator-outlet (Fig. 178) and intact-loop cold-leg (Fig. 182) temperatures match the test data, the calculated intact-loop hot-leg temperature (Fig. 179) is much lower than the test data show. When we examine Figs. 183 and 184, we also see that the measured axial fluid-temperature distributions near the broken-loop cold-leg nozzle and the intact-loop cold-leg nozzle, respectively, in the downcomer are far different than those calculated in the model (Fig. 183). In fact, the test data have an inverse temperature profile to that which we would expect, with the hottest fluid at the top of the downcomer (a stable thermal stratification). This is particularly surprising when one considers the small distance between the intact-loop cold-leg inlet and downcomer Stalk 2. Also, note that the temperature distributions measured by the two stalks are consistent.

A partial explanation for the inverse profile may be that much of the energy added to the fluid in the vessel is from the gap behind the downcomer, and the flow in this gap is from the bottom of the vessel to the top. Thus,

the hot fluid from the gap is dumped into the top of the downcomer. Because the TRAC model used in this analysis accounted for the downcomer gap flow and still did not calculate the correct temperature profile, we believe three-dimensional flow patterns and streaming of the cold fluid from the intact-loop cold leg also are responsible for the inverse temperature profile.

The actual flow profiles in the downcomer are not known. It is probable that they are much more complicated than those predicted by the one-dimensional method used for this analysis. Another significant observation is that the temperature profile in the downcomer is similar to that in the core and thus no natural-circulation driving potential is provided by the vessel. We feel this at least partially explains the difference between the test and calculated intact-loop flow rates.

An analysis of L6-7/L9-2 was performed using an alternate input description in which the locked-rotor resistance of the pump had been increased by a factor of 10. As expected, the intact-loop flow rate and temperature were brought into line with the test data; however, LOFT L6-2 (Ref. 33) indicates that the locked-rotor resistance is not substantially inaccurate. The primary-system pressure comparison was somewhat worse in the alternate-case downcomer.

#### E. Computer Use

The TRAC calculations of L6-7/L9-2 were performed on a Control Data Corporation 7600 computer. The steady state took 2700 s of CPU time; the transient took 8200 s.

# VIII. TRAC-PF1 ONE-DIMENSIONAL ANALYSIS OF THE CRYSTAL RIVER UNIT-3 PLANT TRANSIENT OF FEBRUARY 26, 1980

An automatic reactor shutdown occurred at the Crystal River Unit-3 Plant on February 26, 1980. Interruption of a power supply to the nonnuclear instrumentation caused erroneous signals to be supplied to the integrated control system (ICS). The ICS then reduced the feedwater, increased the reactor power, and opened the PORV. These actions produced a transient that partially depressurized the plant to the HPIS set point. Flow from the HPIS coupled with operator closing of the PORV repressurized the plant to the safety-relief-valve (SRV) trip level.

The transient was simulated using the TRAC-PF1 code.<sup>1</sup> Use was made of the fact that the TRAC-PF1 code has a one-dimensional core to construct a one-dimensional representation of the Crystal River Unit-3 Plant.

The plant data used in the TRAC-PF1 one-dimensional calculation was based primarily upon that used in the two previous TRAC-PD2 calculations<sup>34\*</sup> of the Crystal River incident. The TRAC-PD2 calculations were based upon a generic model of a Babcock and Wilcox (B & W) lowered-loop plant. The TRAC-PF1 one-dimensional calculations presented in this paper used modified plant boundary conditions appropriate to Crystal River Unit 3 obtained in part from Ref. 35. In particular, the TRAC-PF1 analysis included a once-through steam-generator (OTSG) model with aspirator flow.

There have been three analyses<sup>36-38</sup> of the Crystal River transient sequence of events. The first two reports<sup>36,37</sup> were issued shortly after the transient (that is, after approximately one month) and the third<sup>38</sup> approximately a year later. The latest analysis,<sup>38</sup> therefore, represents a better understanding of the sequence of events that occurred during the Crystal River Unit-3 incident. The plant boundary conditions and transient event data used in the present analysis were taken primarily from Ref. 38. The plant data from Ref. 37 were used in this report for comparison with the calculational results.

The major revised event assumptions available in the latter analysis<sup>38</sup> of the Crystal River Unit-3 plant transient were in the reduction of the steam-generator feedwater and in the flow rate through the PORV. Reference 38 determined, on the basis of pressure measurements, that the steam-generator feedwater was ramped down over a period of ~9 s rather than the period of ~60 s as indicated by the computer post-trip flow instruments. On the basis of flow measurements through a PORV similar to the one on the Crystal River pressurizer, the flow through the PORV was set to be 155% of the design flow. Also, Ref. 38 more accurately fixed the time of the PORV reclosing that was originally known only to within a 4-min period.

\*This information was provided by G. J. E. Willcutt, Jr., J. W. Bolstad, and M. W. Burkett, Los Alamos National Laboratory, Energy Division, Thermal-Hydraulics Group (February 1982).



Two calculations were carried out using the revised Ref. 38 boundary condition assumptions. Case 1 calculated the Loop-A secondary pressure based upon steamline relief capacities and primary-to-secondary forward and reverse heat transfer. Case 2 calculated the Loop-A secondary pressure in the same manner as Case 1 until 224 s. Between 224 s and 510 s, Case 2 ramped the Loop-A steam-generator secondary pressure down to the isolation pressure of 4.24 MPa (600 psig), as suggested in Ref. 38, and then maintained that value for the rest of the calculation. Both cases calculated well the system depressurization when compared to the plant data given in Ref. 37. (The agreement is particularly good when account is taken of the inconsistencies between the data given in the event synopsis and that in the figures of this reference.) Comparison with the upper-plenum temperature data obtained from subcooling alarms prior to 224 s and thermocouple data after that, demonstrated excellent agreement for both calculations. This indicates that the system's overall heat balance was well calculated in both calculations.

After the system repressurized, Case 1 was continued to 3000 s and Case 2 to 1700 s. During this period, no continuous flow was established in Loop A (in the calculations) because there was no steam-generator cooling to drive it. HPIS flow collected in the cold leg and because the HPIS injection location was close to the pump, the cold water flowed back through the pump to the loop seal producing intermittent gravity-driven reverse flows. HPIS water flow to the downcomer was thus reduced, and downcomer temperatures never fell below 440 K (332°F) for Case 1 and 490 K (422°F) for Case 2.

Section VIII.A of this report contains a description of the sequences of events that occurred during the Crystal River plant transient. Section VIII.B summarizes the TRAC-PF1 one-dimensional model of the Crystal River Unit 3, B & W lowered loop plant. Section VIII.C presents a description of the reactor initial conditions and the plant transient boundary conditions used in the two calculations. Section VIII.D contains the TRAC-PF1 calculational results and comparisons with actual plant data. A review of the application of TRAC-PF1 using a one-dimensional model to the Crystal River transient, together with the calculation timing statistics, is contained in Sec. VIII.E. Finally, Section VIII.F contains a summary and our conclusions.

#### A. Summary Description of Transient

There is a large uncertainty about when events actually occurred in the transient because so much instrumentation was lost, at least temporarily. The first TRAC-PD2 calculation\* was based on a B & W analysis of the transient,<sup>37</sup> which was completed only 11 days after the transient, plus a Nuclear Safety Analysis Center report completed the month after the transient.<sup>36</sup> Since then, there has been an improved understanding of what probably occurred.<sup>38</sup> Most of the analysis inherent in the TRAC-PF1 calculation is based on Ref. 38 with backup information and data comparisons from Ref. 37.

\*This information was provided by G. J. E. Willcutt, Jr., J. W. Bolstad, and M. W. Burkett, Los Alamos National Laboratory, Energy Division, Thermal-Hydraulics Group (February 1982).

The transient started when interruption of a power supply to the nonnuclear instrumentation caused erroneous signals to be supplied to the ICS (time = 0). The ICS then increased the steam flow to the turbines, reduced the feedwater flow, and increased the reactor power. These combined effects increased the reactor-coolant-system (RCS) pressure. The power-supply failure caused the opening of the PORV after 1 s, and it was held open because of the power-supply failure. Even with the PORV open, the RCS pressure reached the overpressure-trip set point of 15.96 MPa (2300 psig) sometime between 10 and 25 s, and both reactor and turbine trips occurred. The RCS pressure reached a peak of 16.10 MPa (2320 psig) and then decreased because of the combined effects of decreasing reactor power, post-reactor-trip cooling, and the open PORV.

At 201 s, the RCS pressure had decreased to 10.44 MPa (1500 psig), and the emergency-safeguards system (ESS) activated the HPIS with the full flow of three HPIS pumps injected into the RCS. At approximately 225 s, all four RCS pumps were tripped. Sometime between 280 and 520 s the operator shut a block valve (Ref. 38 estimated this occurred at 450 s). This stopped the PORV flow, and the RCS pressure increased until the SRV opened.

Reference 38 concluded from pressure data that the main feedwater to both steam generators was ramped down from full flow at 1 s to zero at 10 s. Previous estimates of the main feedwater reduction period were significantly longer than the 9 s evaluated in Ref. 38 and ranged from ~60 s, Ref. 38, to ~72 s (that is, from 13 s to 85 s), Ref. 37, Fig. III-33.\* The longer feedwater reduction period produced a greater cooling of the primary system during the initial period of the transient. The effect of this was observed in an early TRAC-PD2 calculation\* where the code-calculated depressurization was much faster than actually occurred.

## B. Model and Code Description

1. TRAC Noding. Figures 186 and 187 show a TRAC noding diagram for the B & W lowered-loop model representing Crystal River Unit 3. The model includes two identical loops except the pressurizer is connected to Loop A. Each loop includes a hot leg with candy cane, a steam generator, and two cold legs combined to increase calculational efficiency. Each combined cold leg includes a loop seal, a pump, and an HPIS connection. The RCS pumps were modeled using the LOFT pump characteristics built into TRAC, but scaled with TMI-2 pump data. Each steam-generator secondary is attached to a main-feedwater inlet by a secondary downcomer, a steam exit annulus, an auxiliary-feedwater inlet, and a long pipe to the steam outlet with a side connection to a safety valve that vents to the atmosphere. The TRAC-PF1 steam-generator model included an aspirator model whereas the previous TRAC calculations<sup>34\*</sup> using TRAC-PD2 did not.

\*This information was provided by G. J. E. Willcutt, Jr., J. W. Bolstad, and M. W. Burkett, Los Alamos National Laboratory, Energy Division, Thermal-Hydraulics Group (February 1982).

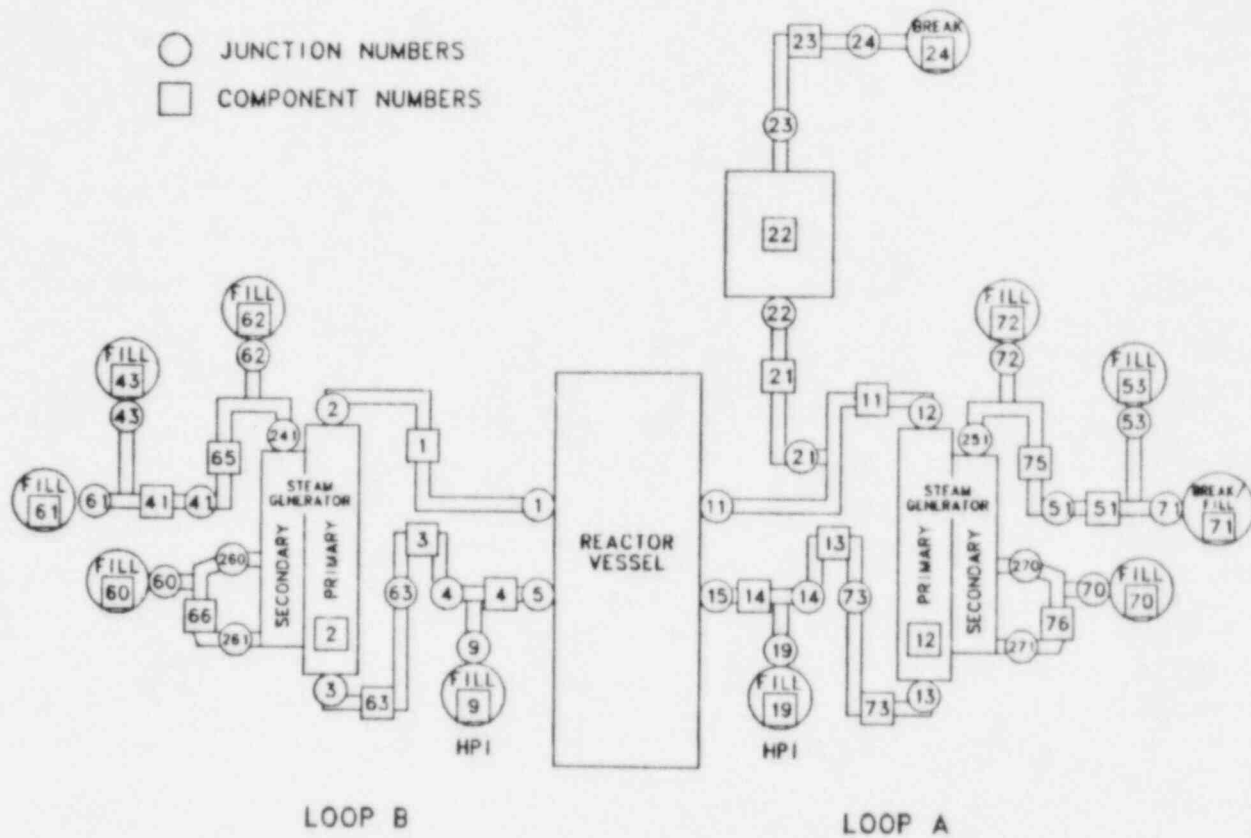
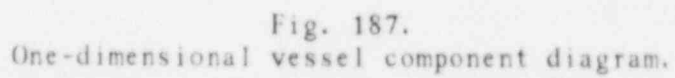


Fig. 186.  
Loop component diagram.



The model used in these calculations was based upon that developed for the previous TRAC-PD2 Crystal River calculations,<sup>34\*</sup> which in turn was based upon an input model developed for TMI-2.

In order to take advantage of the one-dimensional CORE component available in the TRAC-PF1 code, the reactor VESSEL was assembled from a selection of one-dimensional TRAC components as shown in Fig. 187. Two separate downcomers were used (this is usually referred to as a split downcomer) each connected to their respective intact loop cold legs. A downcomer bypass component was included in the model (Component 85) to permit fluid to flow from one cold leg to the other without having to flow through the lower plenum.

Because of the use of one-dimensional components in the TRAC-PF1 calculation, it was necessary to model both the VESSEL upper head recirculating flow and the VESSEL vent valves with external PIPE components. To do this, the region above the core was divided into three separate TEE components, that is, an upper-plenum and two upper-head regions. These then provided the necessary connections to model (1) the upper-head recirculation observed by B & W in their flow tests, and (2) the vent valve connections from the upper plenum to the split downcomer.

We adjusted the resistance in the upper-head recirculation TEE (component 91) in an attempt to obtain the B & W estimated flow split with 36% going through the upper head and 64% going directly from the upper plenum to the hot leg (Ref. 34).

Finally, the total hot-leg flow was split by a TEE component to provide flow to each of the individual hot legs.

Geometry and other plant data were obtained from that used for the previous TRAC-PD2 calculations<sup>34\*</sup> together with other Crystal River data sources (for example, Refs. 35 and 38).

In addition to the above, a 20-cell-pressurizer component was used to provide an accurate modeling of the refill process. The PORV and SRV models were coded to use the critical flow model available in TRAC-PF1 (a fine node model was required in TRAC-PD2<sup>34\*</sup> where no separate critical flow model was available). Preliminary calculations were used to calibrate these components so the nodings were not overly critical.

The noding of the once-through steam-generator secondaries was modified over that used in the TRAC-PD2 calculations,<sup>34\*</sup> to include the aspirator flow. The noding of the OTSG with aspirator flow was based upon that given in Ref. 35. The steam-generator-secondary downcomer noding was, however, modified over that to be found in Ref. 35 in an attempt to improve the recirculating flow. In particular, noding changes were made to decrease the

\*This information was provided by G. J. E. Willcutt, Jr., J. W. Bolstad, and M. W. Burkett, Los Alamos National Laboratory, Energy Division, Thermal-Hydraulics Group (February 1982).



subcooling of the water at the bottom of the steam-generator secondary-tube bundle.

2. TRAC Description. The TRAC-PF1 calculation of the Crystal River transient was performed as part of the independent assessment of the released TRAC-PF1/MOD 0 code (Ref. 1).

The code version used was TRAC-PF1/1A76A. This code was based upon the released version of TRAC-PF1/MOD 0, that is, version 7.0, but was updated to include error corrections to the released version. There were, however, no modeling changes made to the released version.

### C. Reactor Initial Conditions and Transient Boundary Assumptions

The boundary conditions for this analysis were primarily taken from Ref. 38. In particular, Ref. 38 suggested a steam-generator-secondary feedwater flow reduction period of 9 s; whereas previous analyses of the transient<sup>36,37</sup> had suggested a much longer flow rundown time. The feedwater was reduced linearly over a 9-s period in the calculation.

Also in line with Ref. 38, the PORV flow area was adjusted to allow a saturated steam flow of 19.57 kg/s at 15.96 MPa (155 000 lb/h at 2300 psig). Likewise, the SRV model was separately adjusted to permit a steam flow of 39.36 kg/s at 17.34 MPa (311 700 lb/h at 2500 psig) for saturated steam conditions; however, the SRV was opened and closed to maintain the observed RCS pressure of 16.65 MPa (2400 psig). It was found when performing the calculation that it was necessary to reduce the initial pressure set point for this valve from 17.34 MPa (2500 psig). Otherwise, a RCS pressure overshoot was calculated when the system repressurized.

The model used the correct Crystal River power of 2412 MW<sub>th</sub> and the 1979 ANS decay heat curve based on infinite irradiation excluding the actinide contribution. No allowance was made for the small increase in power that resulted from the withdrawal of the control rods at the start of the transient. Reactor trip was calculated using a RCS high-pressure trip; although the trip set point had to be reduced from the suggested value of 15.96 MPa (2300 psig) to avoid the calculation of a significant RCS pressure overshoot not seen by the reactor instrumentation. A trip set point of 15.66 MPa (2256 psig) was used.

Table XIII shows the total HPIS flow delivered vs pressure assuming three pumps running. This was based on Ref. 38 for pressures above 10.44 MPa (1500 psig) and on information provided by G. J. E. Willcutt, Jr., Los Alamos National Laboratory, for pressures below 10.44 MPa (1500 psig). Each loop received half of the HPIS flow. The HPIS was turned on when the RCS pressure decreased to 10.44 MPa (1500 psig).

Based on Ref. 38, feedwater to both loops was ramped to zero between 1 and 10 s in the transient. After 10 s, no main or auxiliary feedwater was supplied to Loop A for the remaining period modeled. After the RCS pumps tripped, the Loop-B feedwater was restarted at 226 s with 76.2 kg/s (1400 gpm) and remained on until the auxiliary feedwater was started at 510 s and the

TABLE XIII  
TOTAL HPIS FLOW VS PRESSURE

<u>Pressure</u>		<u>Flow Rate</u>	
<u>MPa</u>	<u>psig</u>	<u>kg/s</u>	<u>gal/min</u>
0.10	0	96.6	1530
3.55	500	87.2	1380
7.00	1000	76.8	1215
10.44	1500	71.6	1132
11.13	1600	69.2	1095
12.51	1800	64.0	1012
13.89	2000	57.8	915
15.27	2200	51.2	810
16.65	2400	44.2	700
17.34	2500	39.2	620

main feedwater was then turned off.<sup>38</sup> After the Loop-B auxiliary feedwater was started at 510 s, it remained on at 46.5 kg/s (740 gpm).<sup>38</sup>

The turbine stop valves were closed at the same time as the reactor trip. After the turbine stop valves closed, the secondary pressure-relief system was modeled by a flow vs pressure table (Table XIV) combining the

TABLE XIV  
SECONDARY PRESSURE RELIEF CAPACITY

<u>Pressure</u>		<u>Flow Rate</u>	
<u>MPa</u>	<u>psig</u>	<u>kg/s</u>	<u>lb/h</u>
0.00	0	0.0	0
7.00	1000	115.8	919000
7.35	1050	238.5	1893000
7.49	1070	378.7	3006000
7.62	1090	554.0	4397000
7.69	1100	799.4	6345000

turbine-bypass capacity with the relief-valve capacity. The flow vs pressure table was used as the boundary condition to Loop B throughout the transient.

Two calculations were performed. These were identical except for the boundary conditions applied to the secondary side of the Loop-A steam generator. Case 1 modeled the steam-generator secondary pressure in Loop A using a relief rate based on the secondary relief capacity, including the turbine-bypass capacity, as given in Table XIV, and the primary-to-secondary forward and reverse heat transfer. Case 2 calculated the Loop-A secondary pressure in the same manner as Case 1 until 225 s; between 225 and 510 s, Case 2 ramped the Loop-A secondary pressure down to the isolation pressure of 4.24 MPa (600 psig) and then maintained that value for the rest of the calculation.

Reference 38 provides evidence to suggest both that the pressurizer spray valve was closed during the transient, and that the pressurizer heaters were inoperable. Neither of these was modeled, therefore, in the TRAC-PF1 calculations.

Also, Ref. 38 indicated that during the transient, there was a total letdown flow of only 25 gal (95 kg), that is, 48 gpm ( $\sim 3$  kg/s) for 31 s. Because of the small quantity of this letdown flow, it was not modeled in the TRAC-PF1 calculations.

#### D. Computational Results

In this section of the report, we present the results of the two transient calculations together with the results from the steady-state calculation. The two transient calculations were initialized from the same steady-state calculation.

1. Steady-State Calculation. The results of the steady-state calculation at the point of transient initialization are presented in Table XV for the primary circuit and Table XVI for the steam-generator secondaries. Comparative plant data are presented where available. The calculated primary circuit average temperature  $T_{av}$  of 577.6 K (580°F) is 1 K (2°F) higher than the estimated plant value just prior to the plant transient while the calculated Loop  $\Delta T$ s are within 0.5 K (1°F) of the average Loop  $\Delta T$ s for the plant. The primary circuit loop flow necessary to obtain the 24.1 K (43.4°F) Loop  $\Delta T$  was 8823 kg/s ( $7.0 \times 10^7$  lb/h), whereas the plant RCS flows were 4.5% higher at 9217 kg/s ( $7.3 \times 10^7$  lb/h). The calculated upper head/upper plenum to hot leg flow split in the TRAC-PF1 calculation was 31.8% upper head, 68.2% upper plenum, compared to the B & W estimated flow split of 36% upper head and 64% upper plenum. Table XVI provides a comparison of the steady-state results, for the TRAC-PF1 once-through steam-generator model including aspirator flow, with experimental data from various sources. The data in Table XVI were obtained from the Crystal River incident reports,<sup>36-38</sup> the Crystal River FSAR,<sup>35</sup> and generic data on the performance of B & W, once-through-steam generators.

TABLE XV  
STEADY-STATE CONDITIONS FOR CRYSTAL RIVER UNIT-3 PLANT  
PRIMARY REACTOR SYSTEM

	<u>TRAC-PF1 Calculation</u>		<u>Crystal River<sup>a</sup> Plant Data</u>	
Power	2418 MW		98.6% of 2452 MW	
RCS Pressure	15.0 MPa (2160 psig)		14.98 MPa (2157 psig)	
Upper head				
T <sub>H</sub> Loop A	589.7 K	601.7°F	588.2 K	599°F
T <sub>H</sub> Loop B	589.7 K	601.7°F	588.8 K	600°F
T <sub>C</sub> Loop A	565.6 K	558.3°F	564.9 K	557°F
T <sub>C</sub> Loop B	565.6 K	558.3°F	564.3 K	556°F
ΔT Loop A	24.1 K	43.4°F	23.3 K	42°F
ΔT Loop B	24.1 K	43.4°F	24.4 K	44°F
T <sub>av</sub> Loop A	577.65 K	580. °F	576.5 K	578°F
T <sub>av</sub> Loop B	577.65 K	580. °F	576.5 K	578°F
Mass Flow (Pump)				
Combined (Total Flow)				
Loop A	8824 kg/s	6.988×10 <sup>38</sup> lb/h	9217 kg/s	7.3×10 <sup>7</sup> lb/h
Loop B	8823 kg/s	6.988×10 <sup>38</sup> lb/h	9217 kg/s	7.3×10 <sup>7</sup> lb/h
Flow Split Combined Loops				
	Calculation		B & W Estimated <sup>b</sup>	
% Flows Upper head	31.8%		36%	
% Flows Upper head	68.2%		64%	

<sup>a</sup>Plant data taken from Ref. 38.

<sup>b</sup>Reference 34.

TABLE XVI  
ONCE-THROUGH STEAM-GENERATOR SECONDARY-SIDE  
STEADY-STATE CONDITIONS

<u>Loop A</u>	<u>TRAC-PF1 Calculation</u>		<u>Crystal River Plant Data</u>	
Feedwater Mass Flow Rate	650 kg/s	$5.148 \times 10^6$ lb/h	631 kg/s	$5 \times 10^6$ lb/h <sup>a</sup>
Feedwater Temperature	508.2 K	455°F	508.2 K	455°F <sup>b</sup>
Recirculating Flow Rate	65.76 kg/s	$0.521 \times 10^6$ lb/h		
Total Flow Rate Tube Bundle	715.76 kg/s	$5.669 \times 10^6$ lb/h		
Steam Exit Temperature	571.2 K	568.4°F	572 K	570°F <sup>b</sup>
Steam Superheat	18.1 K	32.6°F		
Exit Pressure	6.378 MPa	910 psig	6.38 MPa	911 psig <sup>a</sup>
Feedwater Inlet Pressure	6.55 MPa	935 psig	6.79 MPa	970 psig <sup>a c</sup>
Mass Inventory				
Downcomer	$6.208 \times 10^3$ kg	$13.66 \times 10^3$ lb		d
Tube Bundle	$9.079 \times 10^3$ kg	$19.97 \times 10^3$ lb		d
Total	$15.287 \times 10^3$ kg	$33.63 \times 10^3$ lb		d
<u>Loop B</u>				
Feedwater Mass Flow Rate	650 kg/s	$5.148 \times 10^6$ lb/h	631 kg/s	$5 \times 10^6$ lb/h <sup>a</sup>
Feedwater Temperature	508.2 K	455°F	508.2 K	455°F <sup>b</sup>
Recirculating Flow Rate	65.76 kg/s	$0.521 \times 10^6$ lb/h		
Total Flow Rate Tube Bundle	715.76 kg/s	$5.669 \times 10^6$ lb/h		



TABLE XVI (cont.)

ONCE-THROUGH STEAM-GENERATOR SECONDARY-SIDE  
STEADY-STATE CONDITIONS

<u>Loop B</u>	<u>TRAC-PF1 Calculation</u>		<u>Crystal River Plant Data</u>	
Steam Exit Temperature	571.2 K	568.4°F	573 K	570°F <sup>b</sup>
Steam Superheat	18.1 K	32.6°F		
Exit Pressure	6.378 MPa	910 psig	6.370 MPa	909 psig <sup>a</sup>
Inlet Pressure	6.55 MPa	935 psig	6.78 MPa	968 psig <sup>a c</sup>
Mass Inventory				
Downcomer	$6.208 \times 10^3$ kg	$13.66 \times 10^3$ lb	d	
Tube Bundle	$9.081 \times 10^3$ kg	$19.98 \times 10^3$ lb	d	
Total	$15.289 \times 10^3$ kg	$33.64 \times 10^3$ lb	d	

<sup>a</sup>Data taken from Ref. 38.

<sup>b</sup>Data taken from Crystal River FSAR<sup>35</sup> and appropriate to nominal full-load conditions.

<sup>c</sup>The physical location of the experimental inlet pressure measurement position is not known and, therefore, may not be the same as the one in the calculation.

<sup>d</sup>Reference 38 gives steam-generator levels as Loop A, 67% of operating range; Loop B, 65% of operating range.

An inlet flow to each steam generator of  $650 \text{ kg/s}$  ( $5.148 \times 10^6 \text{ lb/h}$ ) was used in the TRAC-PF1 calculation. The FSAR<sup>15</sup> value is  $707 \text{ kg/s}$  ( $5.6 \times 10^6 \text{ lb/h}$ ); whereas, Ref. 37, Fig. III-33 shows the flow (for the 6 mins prior to the incident) to each loop oscillating between 630 and 663 kg/s ( $5.0 \times 10^6$  and  $5.25 \times 10^6 \text{ lb/h}$ ).

The feedwater temperature was set to the FSAR value of  $508.2 \text{ K}$  ( $455^\circ\text{F}$ ). The steam temperature calculated by TRAC-PF1 was  $571.2 \text{ K}$  ( $568.4^\circ\text{F}$ ). This compares well with the FSAR value of  $572 \text{ K}$  ( $570^\circ\text{F}$ ) and corresponds to  $18.1 \text{ K}$  ( $32.6^\circ\text{F}$ ) degrees of superheat. This agreement was very good in spite of the fact that the TRAC-PF1 code underestimated the steam/water interface condensation. The low condensation rates calculated by TRAC-PF1 resulted in the calculated water temperature in the bottom node of the steam-generator secondary being  $4.8 \text{ K}$  ( $8.6^\circ\text{F}$ ) subcooled, whereas in the plant the water would be saturated.

The TRAC-PF1 calculation produced a recirculating flow of  $65.7 \text{ kg/s}$  ( $0.520 \times 10^6 \text{ lb/h}$ ) so that the total flow through the steam-generator tube bundle was  $715.7 \text{ kg/s}$  ( $5.67 \times 10^6 \text{ lb/h}$ ).

The total inventory of each of the steam-generator secondaries was  $15.29 \times 10^3 \text{ kg}$  ( $33.64 \times 10^3 \text{ lb}$ ) with  $6.21 \times 10^3 \text{ kg}$  ( $13.66 \times 10^3 \text{ lb}$ ) residing in the steam-generator-secondary downcomer and  $9.08 \times 10^3 \text{ kg}$  ( $19.98 \times 10^3 \text{ lb}$ ) in the steam-generator-secondary tube bundle.

The conditions given in Tables XV and XVI were those appropriate to the start of the transient calculation. The steady-state calculation was run as a transient for approximately 400 s. A true steady state was not totally achieved with the feedwater flow of  $650 \text{ kg/s}$  ( $5.148 \times 10^6 \text{ lb/h}$ ) used. At the time the transient was initiated, the primary circuit average coolant temperature was increasing at a rate of approximately  $0.25 \text{ K/100 s}$ . However, it is also obvious from the plant data that the plant was not in a "true" steady-state.

2. Transient Calculations. Table XVII summarizes the significant transient events for the two cases calculated using TRAC-PF1, together with plant data where available. In addition, Figs. 188 to 192 compare the calculated results with plant data from Ref. 37. Only a limited data comparison was possible because the Crystal River plant transient was initiated by a partial loss of the nonnuclear instrumentation.

The nonnuclear instrumentation failure caused the PORV to open after 1 s, and the feedwater to both steam generators to be reduced from full flow at 1 s to zero at 10 s. The reduced feedwater flow caused an increase in RCS pressure, a high-pressure reactor trip, and a coincident turbine trip. In the TRAC-PF1 calculations, the reactor was tripped on high primary RCS pressure with a trip set point of  $15.66 \text{ MPa}$  ( $2256.2 \text{ psig}$ ). This was approximately  $0.3 \text{ MPa}$  ( $44 \text{ psi}$ ) less than the suggested trip set point<sup>38</sup> of  $15.96 \text{ MPa}$  ( $2300 \text{ psig}$ ). However, in the calculations, a pressure overshoot of  $0.55 \text{ MPa}$  ( $80 \text{ psi}$ ) was observed (that is, the RCS pressure continued to increase after the reactor trip) when a trip set point of  $15.96 \text{ MPa}$  ( $2500 \text{ psig}$ ) was used. Therefore, in order to calculate approximately the correct peak RCS pressure of  $16.1 \text{ MPa}$  ( $2320 \text{ psig}$ ), the lower trip set point was used. Employing a

TABLE XVII  
TRANSIENT EVENT SEQUENCE TIME (s)

<u>TRAC-PF1 Case 1 Calculation</u>	<u>TRAC-PF1 Case 2 Calculation</u>	<u>Plant<sup>a</sup> Data</u>	<u>Event</u>
0	0	0	Nonnuclear instrumentation failure.
1	1	1	PORV open. Feedwater begins to ramp down to both steam generators.
10	10		Feedwater completely off.
17.6	17.6	25 (25.5 <sup>b</sup> )	Reactor trip.
207.1 189.5 <sup>d</sup>	207.1 189.5 <sup>d</sup>	201 <sup>c</sup> (176 <sup>d</sup> ) <sup>c</sup> 235 <sup>e</sup> (210 <sup>d</sup> ) <sup>e</sup>	HPIS trip. System pressure falls below 10.44 MPa (1500 psig).
224	224	224-227 (199-202 <sup>d</sup> ) 224 <sup>b</sup>	Reactor-coolant-pump trip.
224-229	224-229	224	Feedwater reestablished to Loop-B steam-generator secondary.
245	245		Initial void formation, primary coolant saturated.
320			Loop-A flow stalls on high void fraction in candy cane.
335			Two-phase flow out of PORV
395			Pressurizer liquid solid.
450	450	280-520 450 <sup>b</sup>	Closure of PORV block valve.

TABLE XVII (cont.)

510	510	510 <sup>b</sup>	Main feedwater turned off and auxiliary feedwater turned on to Loop-B steam generator.
671	685	591 <sup>f</sup> 595-610 <sup>g</sup> ~620 <sup>h</sup>	SRV open first time (system repressurized).

<sup>a</sup>Plant data from Ref. 37 unless otherwise indicated.

<sup>b</sup>Reference 38.

<sup>c</sup>Times taken from Ref. 37, Event Synopsis.

<sup>d</sup>Times with respect to Reactor Trip.

<sup>e</sup>Times taken from Ref. 37, Fig. III-3.

<sup>f</sup>Reference 37, Event Synopsis  
Reactor-Coolant-System pressure 16.38 MPa (2361 psig).

<sup>g</sup>Reference 37, Event Synopsis SRV opened.

<sup>h</sup>Reference 37, Fig. III-3 and III-4.

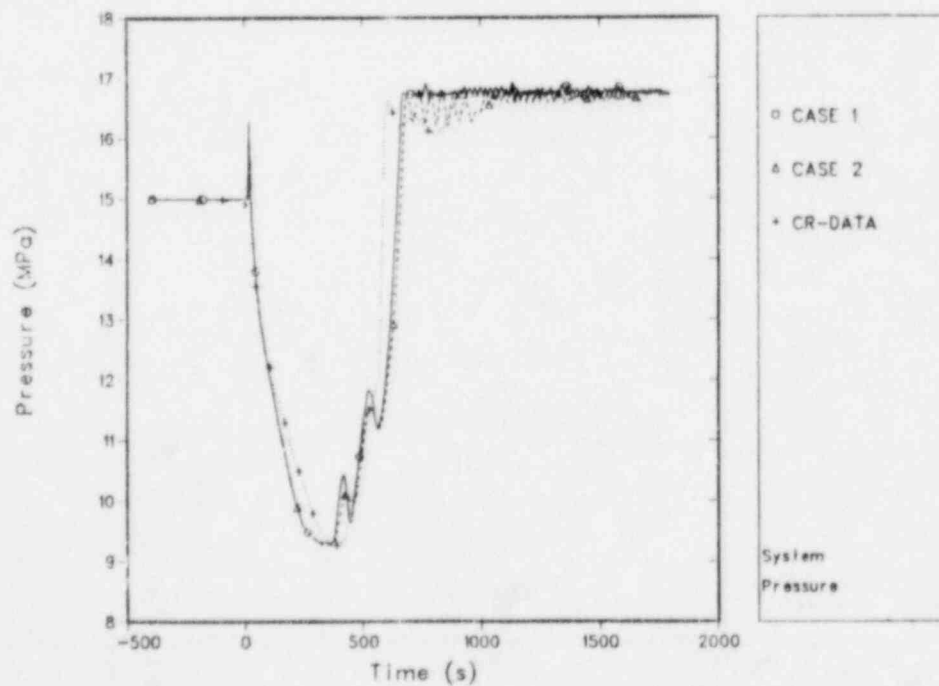


Fig. 188.  
Comparison of TRAC-calculated and measured system pressures.

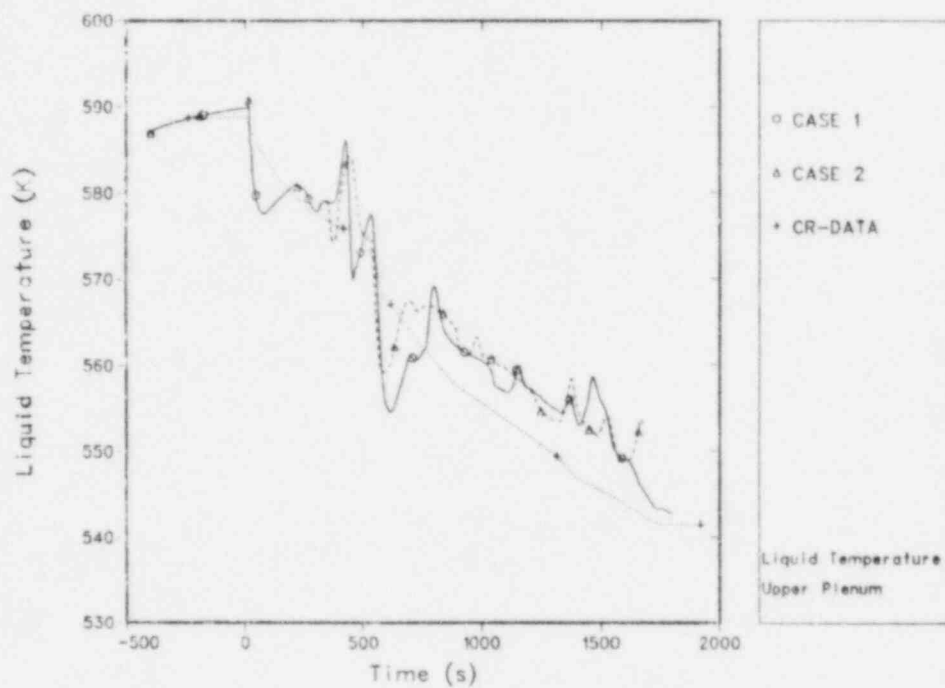


Fig. 189.  
Comparison of TRAC-calculated and measured upper-plenum temperatures.

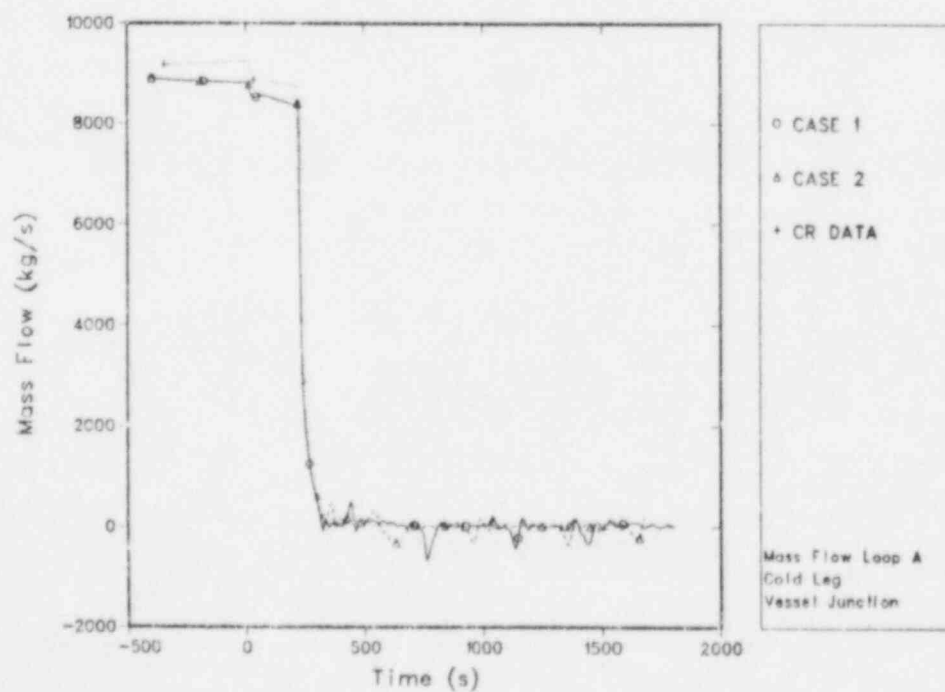


Fig. 190.  
Comparison of TRAC-calculated and measured plant Loop-A mass flows.



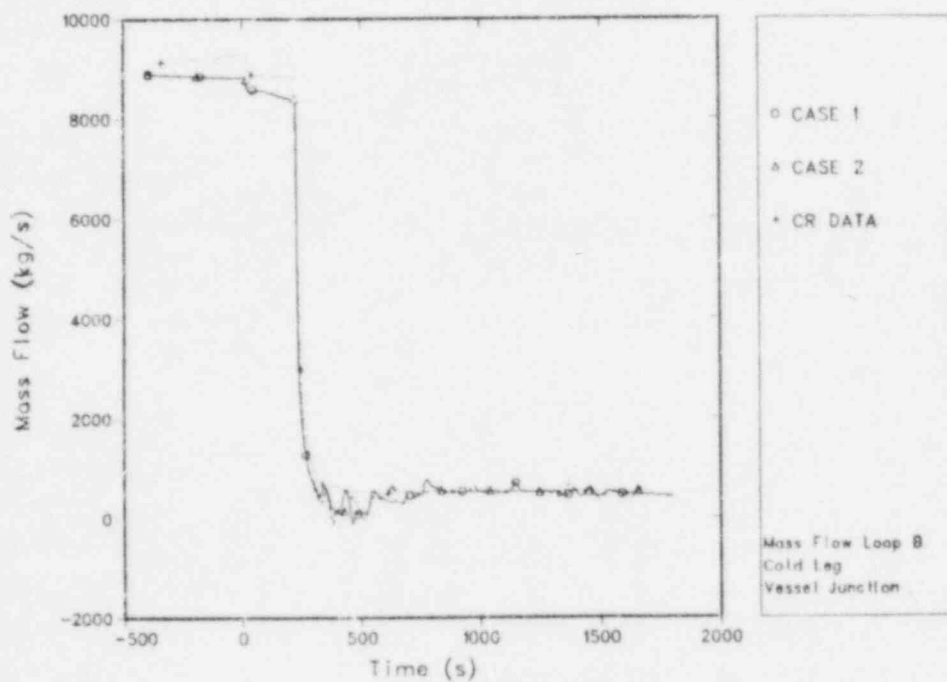


Fig. 191.  
Comparison of TRAC-calculated and measured plant Loop-B mass flows.

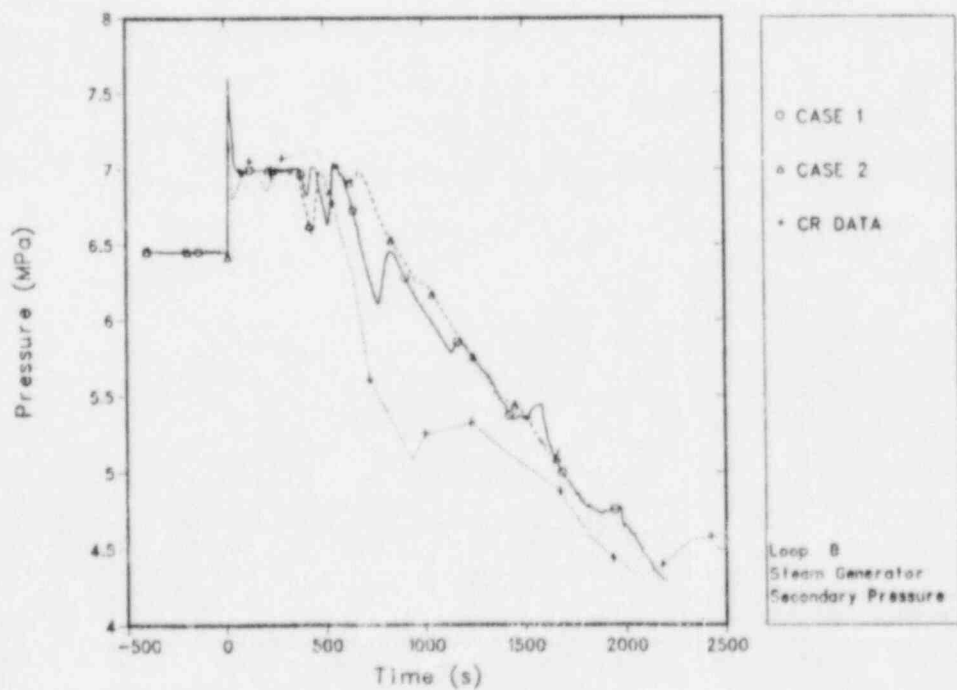


Fig. 192.  
Comparison of TRAC-calculated and measured plant Loop-B steam-generator secondary-side pressures.

reactor trip set point of 15.66 MPa (2256.2 psig) produced a calculated trip time of 17.6 s; this compares well with the estimated plant trip time of between 10 and 25 s, Ref. 37 or 24.5 s, Ref. 38.

The rise in RCS pressure is strongly controlled by the rate of the reduction of feedwater to the steam-generator secondaries, and therefore, any "error" associated with the reactor trip time is most likely to be a result of the use of an incorrect feedwater reduction rate. For example, the feedwater was ramped down linearly over a period of 9 s in these calculations, in line with the analysis in Ref. 38; however, an earlier calculation\* used a 72-s period as indicated by the flow readings on the computer post-trip review, Ref. 37, Fig. III-33.

Steam lost through the PORV depressurized the system as shown in Fig. 188. The TRAC-PF1 calculations used a PORV model adjusted to provide a steam flow rate of 19.57 kg/s (155 000 lb/h) at 15.96 MPa (2300 psig) for saturated steam conditions. This number was obtained by the Electric Power Research Institute testing of a valve similar to the one in the Crystal River Unit-3 plant.<sup>38</sup> It is, however, 155% of the design flow for the valve. As can be seen from Fig. 188, use of this high value for the PORV flow rate led to a slight overestimation of the system depressurization rate. A RETRAN analysis<sup>38</sup> of this transient also used this PORV flow rate and again overestimated the depressurization rate. An earlier TRAC-PD2<sup>34</sup> analysis of this transient using a PORV calibrated to give a 13.89 kg/s (110 000 lb/h) flow rate underestimated the system depressurization rate.

The primary system continued to depressurize until the system pressure fell below 10.44 MPa (1500 psig) at which time the HPIS was turned on. In the plant transient, the RCS pumps were tripped upon HPIS initiation in line with the USNRC small break guidelines. In the TRAC-PF1 calculations, HPIS initiation occurred at 207 s; however, a pump trip was imposed upon the calculation at a time of 224 s in line with the pump trip observed in the plant transient. There was, therefore, a 17-s delay in the TRAC-PF1 calculations between HPIS initiation and pump trip. After the RCS pump trip, the Loop-B main feedwater was reestablished.

In the TRAC-PF1 calculations, the HPIS flow was initiated immediately upon receipt of the HPIS trip signal (that is, with zero-time delay).

In the original event sequence, Ref. 37, the event synopsis shows that the RCS pressure decreased to 10.44 MPa (1500 psig), i.e., the ESS HPIS set point, 176 s after reactor trip (which is 194 s on the calculated time scale used in this analysis), and the RCS pumps were turned off after a delay of ~24 s, that is, at a time of between 199 and 202 s after reactor trip (217 to 220 s on the TRAC-PF1 calculational time scale). However, the plant system pressure data taken from Fig. III-3 of the same reference (shown in Fig. 188) shows that the system pressure fell below 10.44 MPa (1500 psig), that is, the HPIS set point at (3-1/2 min) 210 s after the reactor (high-pressure) trip.

\*This information was provided by G. J. E. Willcutt, Jr., J. W. Bolstad, and M. W. Burkett, Los Alamos National Laboratory, Energy Division, Thermal-Hydraulics Group (February 1982).

There is, therefore, an inconsistency in the plant data as given in Ref. 37. The event synopsis gives HPIS initiation at 176 s; whereas, Fig. III-3 gives HPIS initiation at 210 s (both times with respect to reactor trip). Reference 38 quotes a time of 223 s for the RCS pump trip; this time is from the initial closure of the PORV and is 198.5 s after their interpretation of reactor trip. This, therefore, is in close agreement with the event synopsis time (Ref. 37) of 199 s to 202 s for RCS pump trip (time again with respect to reactor trip). If Ref. 38 is to be taken as correct, then it must be assumed that there is a timing error in the plant pressure curve (that is, Fig. III-3, Ref. 37). The timing error is in the direction to increase the depressurization rate and would, therefore, enhance the agreement between the TRAC-PF1 calculation and the data. For example, with respect to the event synopsis, the TRAC-PF1 calculation predicts HPIS initiation 190 s after reactor trip compared to a plant data time of 176 s (these times are TRAC-PF1 207 s and plant data 201 s when the timing is taken from the start of the transient).

The pump-trip time of 223 s (Ref. 38) is equivalent to 224 s from the initiation of the transient (that is, the failure of the nonnuclear instrumentation) and was the time used in the TRAC-PF1 calculations.

Following the RCS pump trip, the system continued to depressurize until the liquid became saturated and voids began to form. Figure 189 shows the transient cooling rate, namely, the upper-plenum liquid temperature. Figures 193-195 show the void fraction at the three primary circuit high points, that is, at the top of the Loop-A candy cane (Fig. 193), at the top of

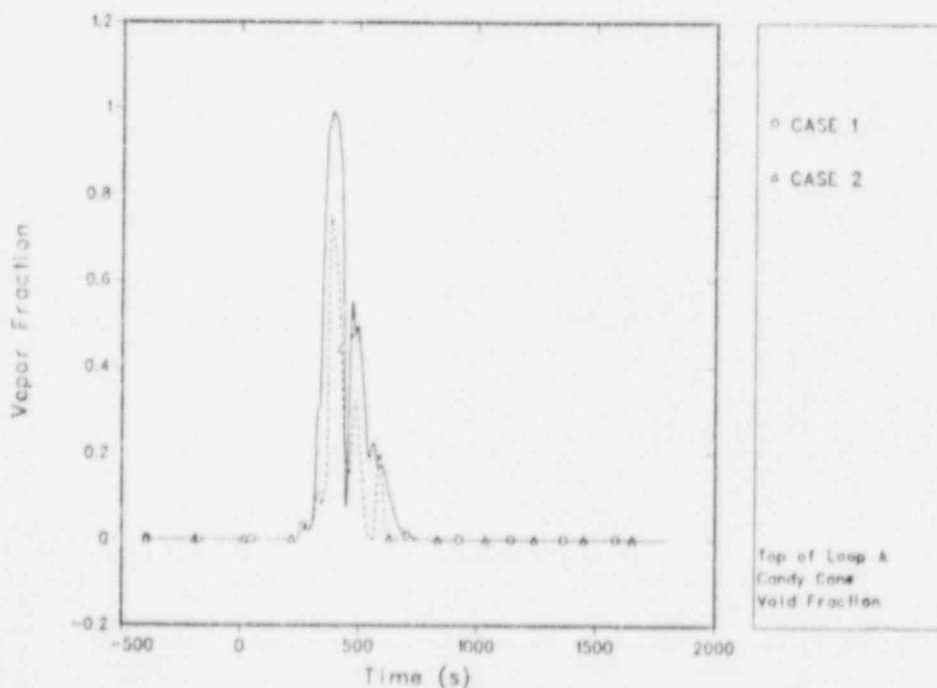


Fig. 193.  
Void fraction at the top of Loop-A candy cane.

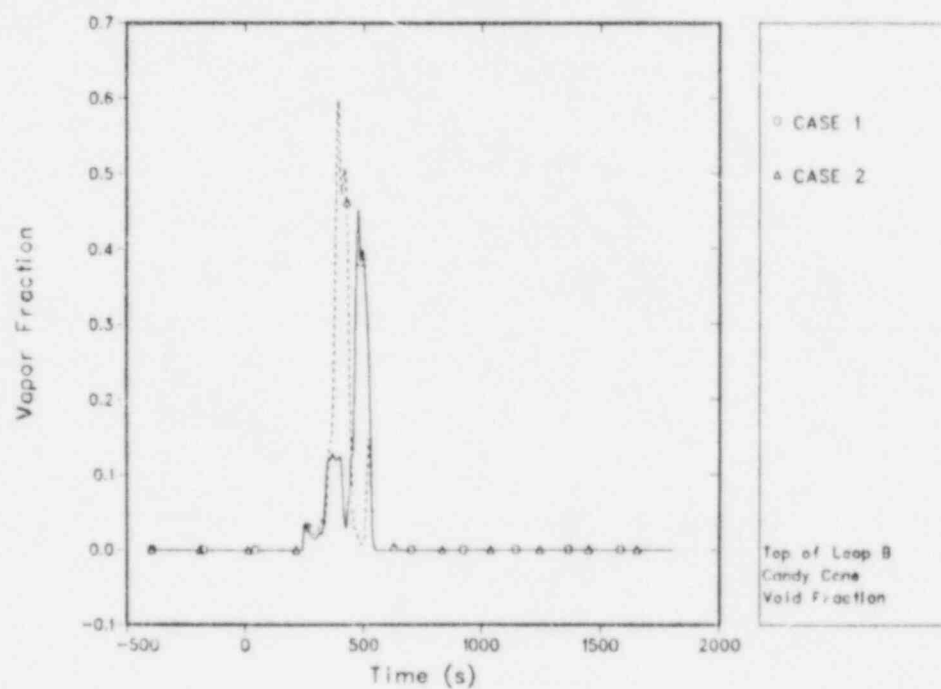


Fig. 194.  
Void fraction at the top of Loop-B candy cane.

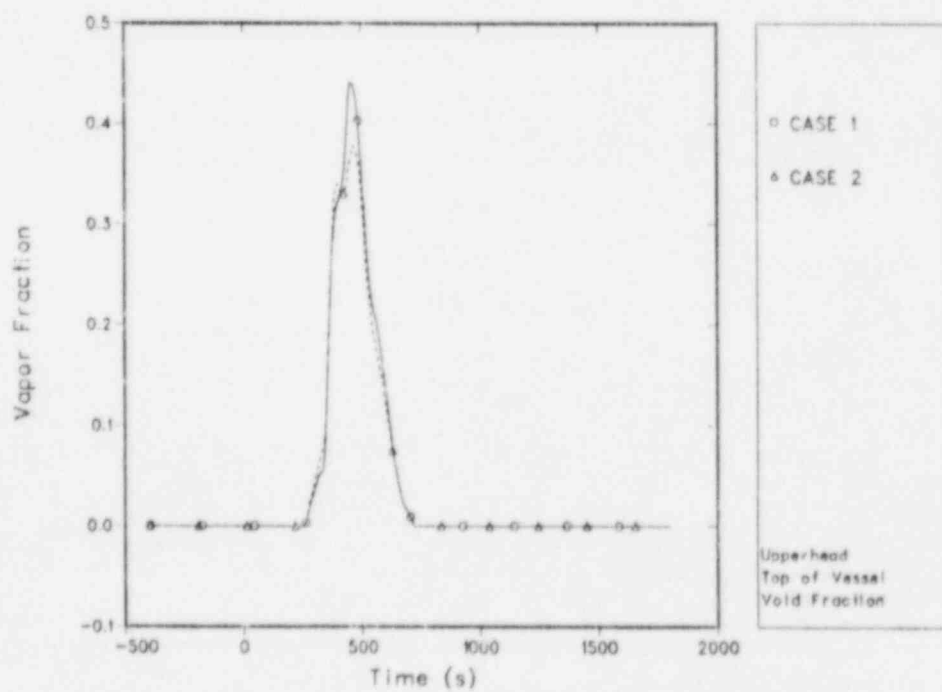


Fig. 195.  
Void fraction in vessel upper head.

the Loop-B candy cane (Fig. 194), and at the top of the upper head (Fig. 195). Void formation began at approximately 245 s. At this time, the depressurization slowed down as the liquid flashed. During this period, natural-circulation flow was established in Loop B (Figs. 191 and 196) because of the secondary cooling initiated in the Loop-B steam generator following the primary-coolant-pump trip. Figures 191, 196, and 197, respectively, show the Loop-B mass flow (Fig. 191) and the Loop-B steam-generator-primary inlet and outlet temperatures for calculation 1 (Fig. 196) and calculation 2 (Fig. 197). The Loop-A flow was reduced almost to zero at approximately 320 s (Fig. 190). Note the data used for Figs. 190 and 191 were taken from Fig. III-13 of Ref. 37. We assume the data labeling was switched in that figure because it shows the Loop-A flow continuing when the Loop-B flow stopped even though Loop B was cooled and Loop A was not. Void formation continued and the voids collected at the top of the Loop-A candy cane (Fig. 193), Loop-B candy cane (Fig. 194), and at the top of the vessel upper head (Fig. 195).

The Loop-A candy cane void fraction for Case 1 increased to about 1.0 at ~385 s (Fig. 193). For Case 2, ramping the Loop-A secondary pressure down to 4.24 MPa (600 psig) between 225 s and 510 s (Fig. 198) provided a small amount of additional cooling that increased slightly the Loop-A primary flow and, therefore, reduced the peak Loop-A candy cane void fraction to less than 0.8. (Again, this occurred between 380 and 385 s.) The subsequent Loop-A steam-generator-secondary pressure decrease for Case 1 was caused by secondary-to-primary cooling.

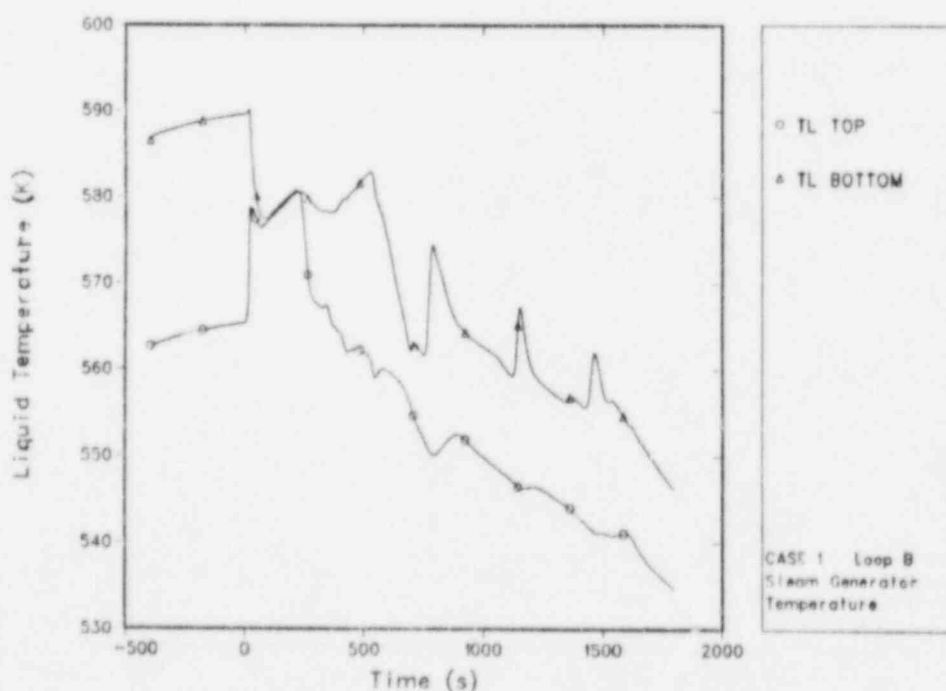


Fig. 196.  
Loop-B Case 1 steam-generator primary inlet and outlet temperatures.



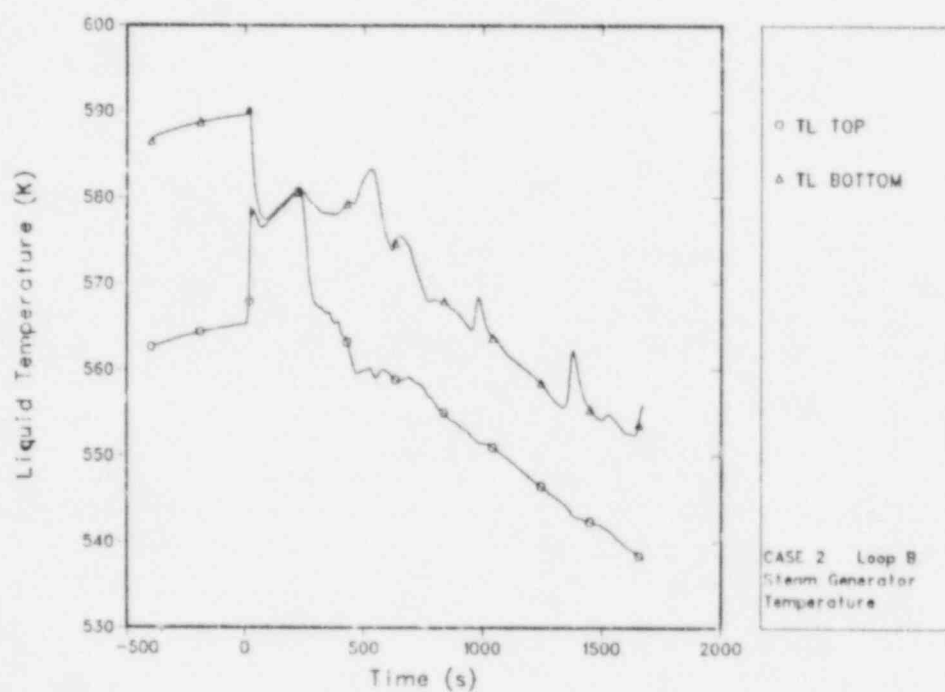


Fig. 197.  
Loop-B Case 2 steam-generator primary inlet and outlet temperatures.

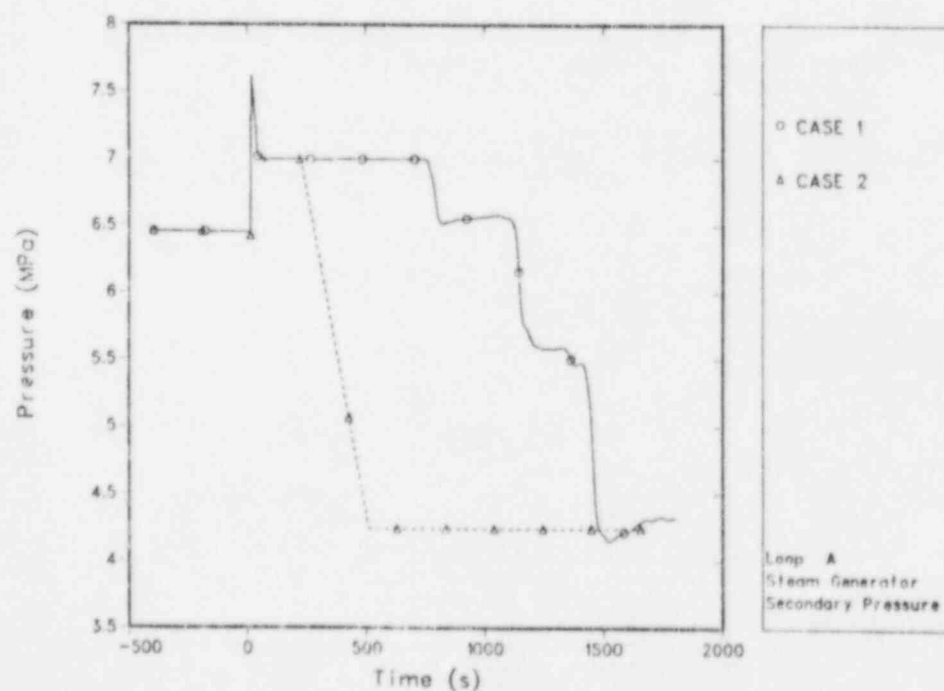


Fig. 198.  
Loop-A steam-generator secondary-side pressures.

Figures 199 and 200, respectively, show the pressurizer collapsed water level, the flow rate of water and steam exiting the pressurizer first through the PORV and then the SRV. The pressurizer level and PORV flow rate increased initially at the start of the transient calculation as the primary circuit pressurized. Following the reactor trip, both the pressurizer level and the steam flow rate out of the PORV decreased as the primary circuit began to depressurize. For the first ~50 s following the reactor trip, the circuit cooled, hence depressurization (due to liquid contraction, that is, density increase) was greater than the pressure reduction in the pressurizer due to the steam flow out of the PORV. Water, therefore, flowed out of the pressurizer into the primary circuit enhancing the fall in the pressurizer liquid level. After ~80 s, the pressurizer pressure fell below that in the primary circuit, and liquid began to flow from the primary circuit into the pressurizer. The pressurizer level, therefore, began to rise slowly (Fig. 199). The rate of rise of the pressurizer level increased significantly twice: first, at ~210 s following the initiation of HPIS, and second at ~250 s following the saturation of the primary coolant and the production of voids in the primary circuit.

After ~250 s the pressurizer water level increased rapidly until the pressurizer became full at somewhere between 350 s and 400 s. In the TRAC-PF1 calculation, as liquid entered the top cell of the pressurizer, a two-phase mixture was discharged through the PORV. This can be observed at 335 s in Fig. 200 as an increase in the PORV mass-flow rate. Therefore, to model accurately the pressurizer discharge, a small cell was used at the top of the pressurizer. The TRAC-PF1 pressurizer became liquid solid at ~395 s.

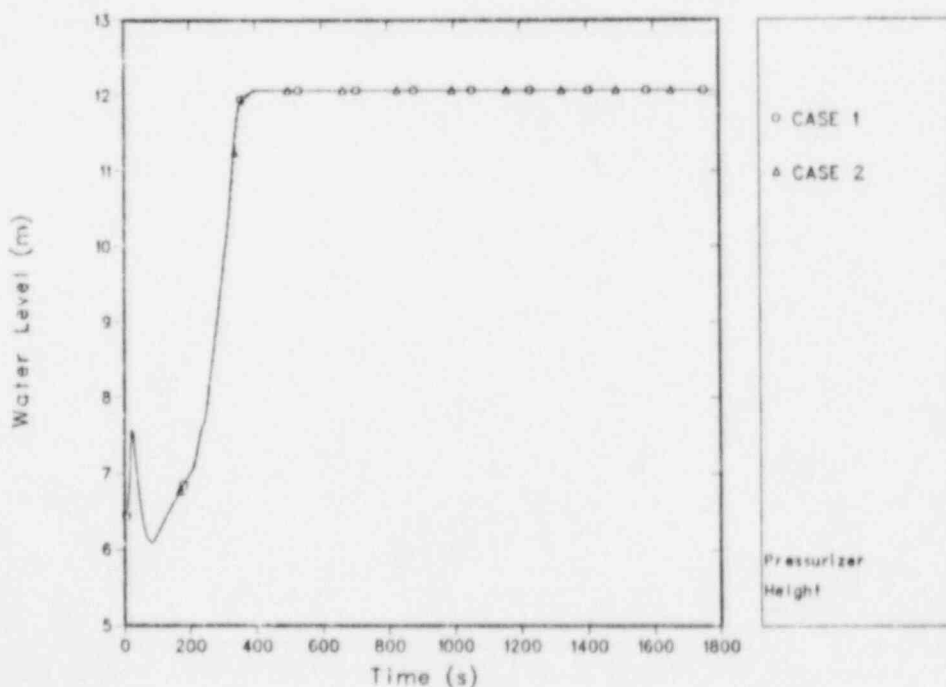


Fig. 199.  
Pressurizer collapsed liquid level.

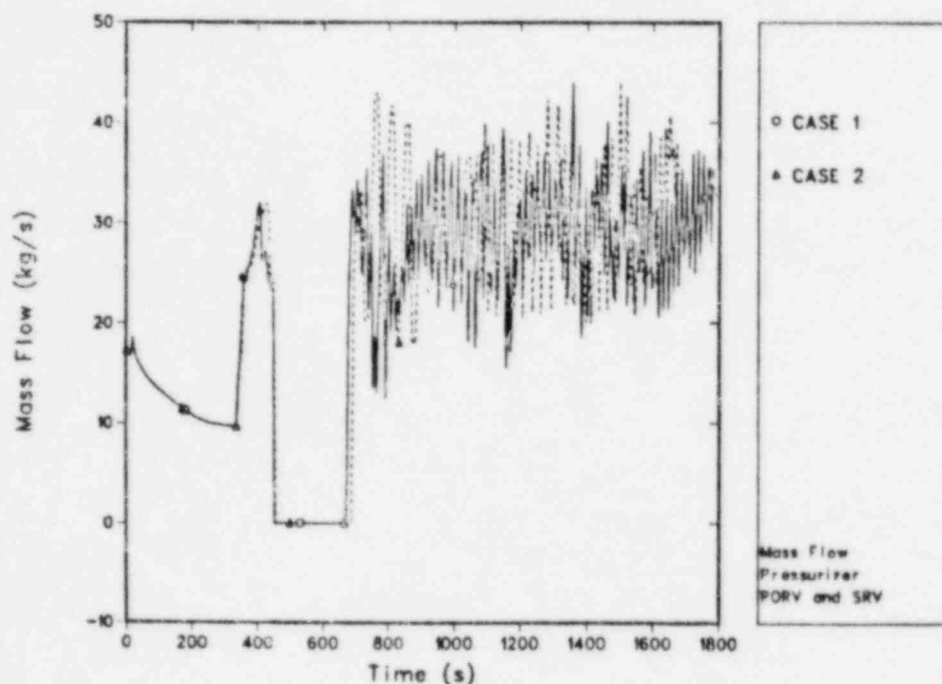


Fig. 200.  
Pressurizer mass flow through PORV and SRV.

As the water level approached the top of the pressurizer, the HPIS flow (Figs. 201 and 202) into the primary circuit of  $\sim 72 \text{ kg/s}$  ( $0.57 \times 10^6 \text{ lb/h}$ ) exceeded that out of the primary circuit into the pressurizer. Once the pressurizer was full, the flow into the pressurizer from the primary circuit equaled that out of the PORV, that is, a flow of  $25\text{--}30 \text{ kg/s}$  ( $0.198 \times 10^6\text{--}0.238 \times 10^6 \text{ lb/h}$ ).

Following the filling of the pressurizer (at  $\sim 380 \text{ s}$ ), the primary system began to repressurize (Fig. 188) as the HPIS flow continued to exceed the PORV liquid critical discharge. As the system began to repressurize, flashing of the primary coolant stopped as the coolant became subcooled.

The system repressurization was enhanced by the closing of the PORV. The PORV was closed in the TRAC-PF1 calculations at  $450 \text{ s}$  in line with Ref. 38. Earlier investigation<sup>36,37</sup> put the closure of the PORV (through the operator closing of the PORV block valve) at between  $280 \text{ s}$  and  $520 \text{ s}$ .

The TRAC-PF1 calculated system repressurization was marked by two oscillations in the system pressure (Fig. 188), which were accompanied by similar oscillations in the upper-plenum liquid temperature (Fig. 189). These oscillations occurred as a result of a "two-stage" repressurization process. For example in Case 1, immediately following the filling of the pressurizer, the primary system pressurized by compressing the voids without significant void collapse, that is, vapor condensation. Void collapse in Loop A was then calculated resulting in the first pressure decrease beginning at  $415 \text{ s}$ . The

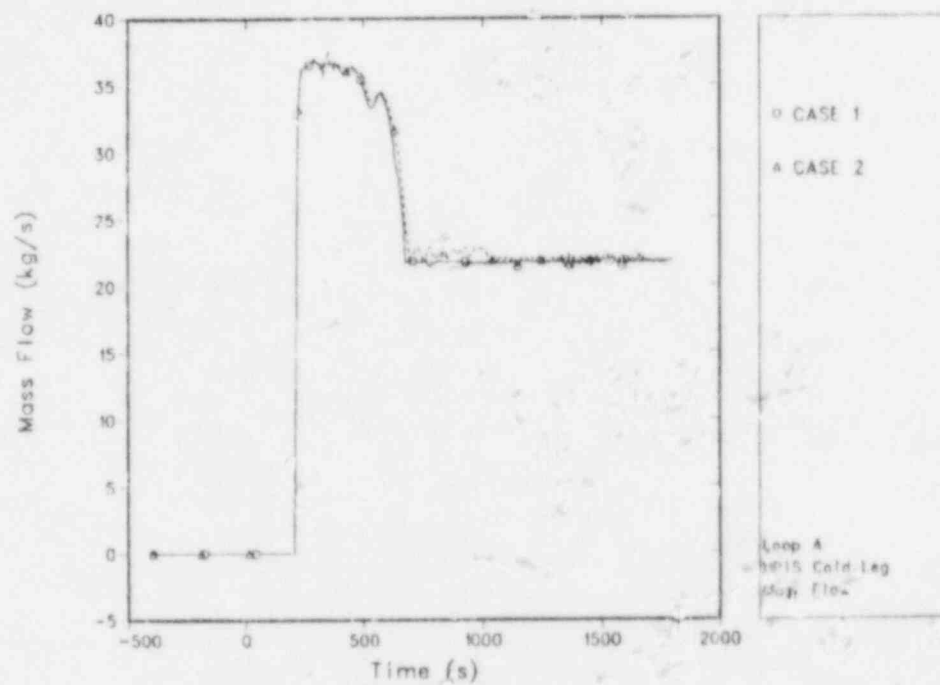


Fig. 201.  
Loop-A HPIS mass flows.

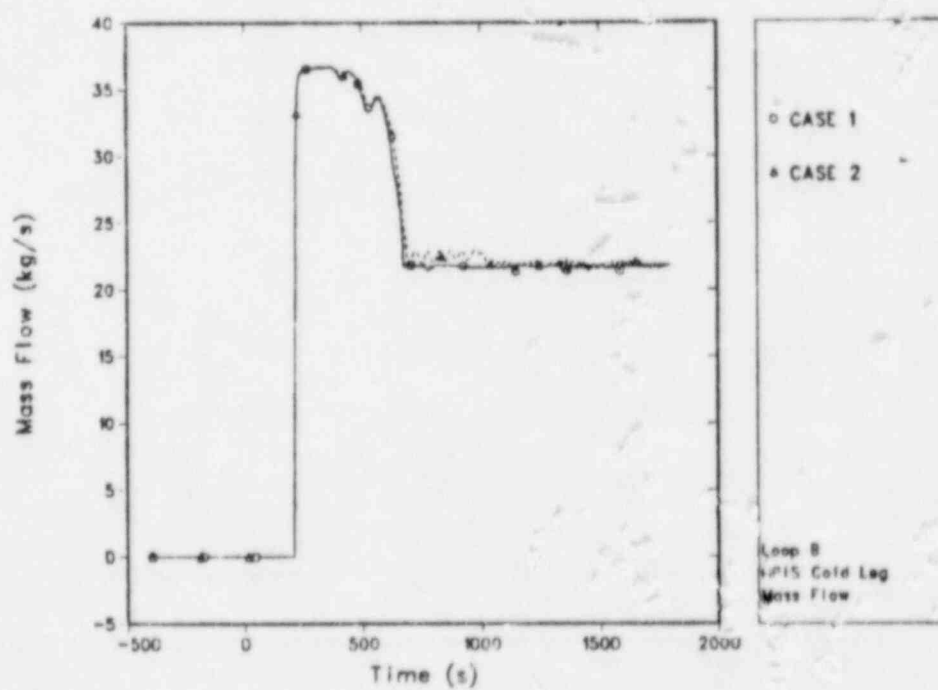


Fig. 202.  
Loop-B HPIS mass flows.

closing of the PORV at 450 s halted this pressure fall. During this period, the loop flows circulated some of the upper-head voids to the top of the Loop-A and Loop-B candy canes, increasing significantly the void fraction at the top of the Loop-B candy cane. The system then repressurized until ~520 s when the collapse of the voids in the Loop-B candy cane resulted in the second fall in pressure. The pressure began increasing again at ~560 s following the complete collapse of all voids in Loop B at ~545 s.

Just before the second pressure oscillation, that is, at 510 s, the main feedwater to the Loop-B steam generator was turned off, and the auxiliary feedwater turned on. The auxiliary feed into the steam generator is from the top (Fig. 186), and therefore cools the whole of the steam-generator tube bundle. The additional cooling of the steam generator caused by the establishment of the auxiliary feed was partly responsible for increasing the primary circuit flow in Loop B in the TRAC-PF1 calculation, which in turn caused the collapse of the voids in the Loop-B candy cane beginning at ~520 s.

The TRAC-PF1 calculated "two-stage" repressurization process is similar but opposite to a previous analysis that used the RETRAN code.<sup>38</sup> In the RETRAN calculation, void collapse was calculated before the system repressurization because of the equilibrium nature of RETRAN.

The remaining voids in Loop A and the upper head continued to condense and collapse as the primary circuit repressurized to the SRV set point. With an SRV set point of 16.65 MPa (2400 psig) for Case 1, the SRV first opened at 671 s. For Case 2, a SRV set point of 16.55 MPa (2385 psig) was used; and in this instance, the SRV first opened at 685 s. As can be seen from Fig. 188 and Table XVII, the calculated system repressurization was slightly delayed (that is, between 50 s and 90 s) with respect to the plant data. The SRV set points used in the TRAC-PF1 calculations were similar to that given in Ref. 38, which was ~0.69 MPa (100 psig) less than the design set point of 17.34 MPa (2500 psig).

For the remainder of the TRAC-PF1 calculated transients, the SRV was modeled to open and close to maintain an approximately constant system pressure of 16.65 MPa (2400 psig) (Fig. 188). The response of the SRV in performing this task can be seen in Fig. 200 for both cases. The flow out of the SRV oscillated about an approximate mean value of 28 kg/s ( $0.222 \times 10^6$  lb/h).

Figure 189 shows the calculated core outlet temperature, that is, the upper-plenum (component 88, Fig. 187) temperature for both cases compared with the plant data (Ref. 37, Fig III-8). Although the data are shown as a continuous line, there were no thermocouple readings available until the RCS pump trip at 224 s because of the partial loss of the nonnuclear instrumentation. Plant data, therefore, was obtained from subcooling alarms until the RCS pump trip at 224 s and from thermocouple data following that. The overall primary cooling was well predicted by both TRAC-PF1 calculations. The plant data, however, does not show either the temperature oscillations that occurred during the repressurization period (that is, those associated with the repressurization oscillations at approximately 425 s and 540 s) or the oscillations following repressurization (that is, after 700 s) that arose from Loop-A density flow oscillations.



The fall in the core-outlet temperature at ~540 s was well predicted by TRAC-PF1 and corresponds to the collapse of the voids in the Loop-B candy cane.

After 700 s the TRAC-PF1 calculated cooling rate agrees well with the data except that the calculated coolant temperature was ~5 K (9°F) higher than the data. The correct calculation by TRAC-PF1 of the overall cooling rate demonstrates that the code accurately calculated the primary system energy balance between decay-heat production and heat loss through the Loop-B steam generator.

Figure 192 shows that the TRAC-PF1 calculated Loop-B steam-generator-secondary pressure agrees well with plant data from Ref. 37, Fig. III-26. The pressure rose initially to the secondary-pressure relief valve set point of 7.0 MPa (1000 psig). The relief valves maintained this pressure until the reestablished feedwater began to cool the steam-generator secondary. The pressure began to fall in both the calculation and data at ~450 s. However, in the TRAC-PF1 calculation, the pressure rose again at ~510 s when the main feedwater was turned off and the auxiliary feedwater turned on. The subsequent fall in the plant pressure (hence, temperature, because the tube bundle contains saturated steam and water) was well matched by the TRAC-PF1 calculation.

After the system repressurized to the SRV set point, the calculations were continued to determine how cold the cold leg and downcomer water would get. Case 2 was terminated at 1700 s just before the ramp down of the HPIS (see Ref. 37). Case 1 was continued to 3000 s. However, at ~2200 s, feedwater was reestablished to the Loop-A steam generator (see Ref. 37 event synopsis) and so provided a natural circulation flow in Loop A. The boundary conditions for Case 1 were not modified to include either the HPIS ramp down or reestablishment of feedwater to Loop A. The results presented (after ~2200 s), therefore, represent what might have happened had flow not been reestablished in Loop A.

After 700 s for both cases, the Loop-B flow continued because of steam-generator cooling, so there was no significant HPIS cooling of the Loop-B cold leg, hence downcomer, fluid. Figures 203 and 204, respectively, show the coolant temperatures at the top of the Loop-B downcomer and the Loop-B cold leg at the point of HPIS injection. We do see, however, that the two flow stalls in Loop B during the period of repressurization caused two slugs of relatively cold water ~500 K (440°F) to pass through the downcomer.

The Loop-A flow, however, was nearly zero for long periods (Fig. 205) because there was no steam-generator cooling to drive it. Figure 205 shows in detail the Loop-A mass flow for Case 1 between 600 s and 3000 s. During these quiescent periods, the HPIS water entered the cold leg and started spreading both ways from the injection location. When this cold high-density water reached the pipe leading down into the loop seal (Fig. 206), the density difference produced a flow back through the loop and out the hot leg to the vessel. This reverse flow rapidly damped out as warm water from the vessel entered the cold leg and mixed with the HPIS flow to remove the driving force. Figures 207 and 208 illustrate this density-variation driving "force" by showing the density times gravitational constant times height products (that

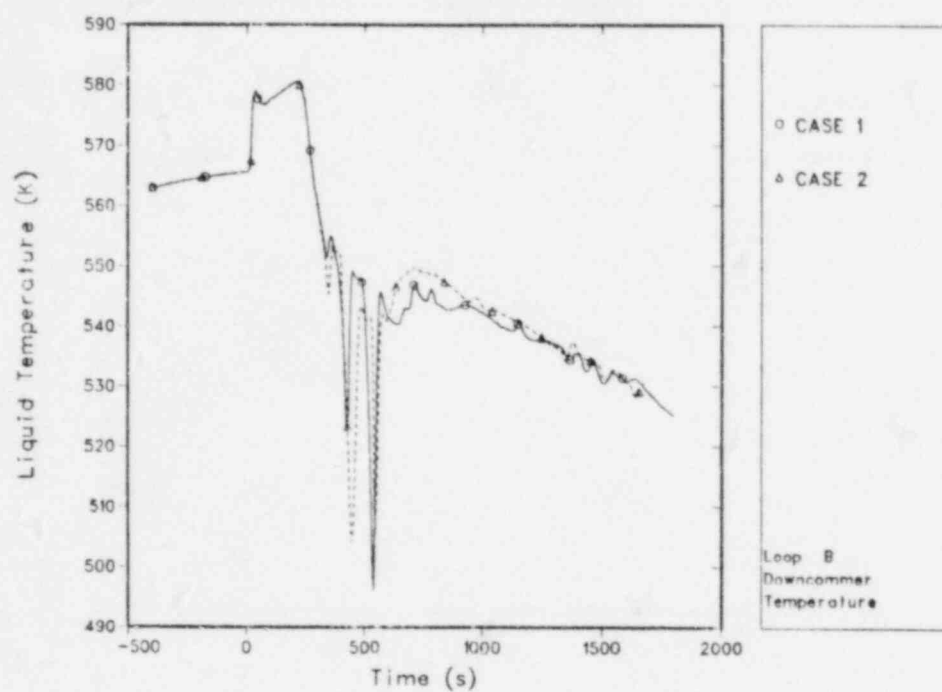


Fig. 203.  
Loop-B downcomer temperatures (cell below cold-leg connection).

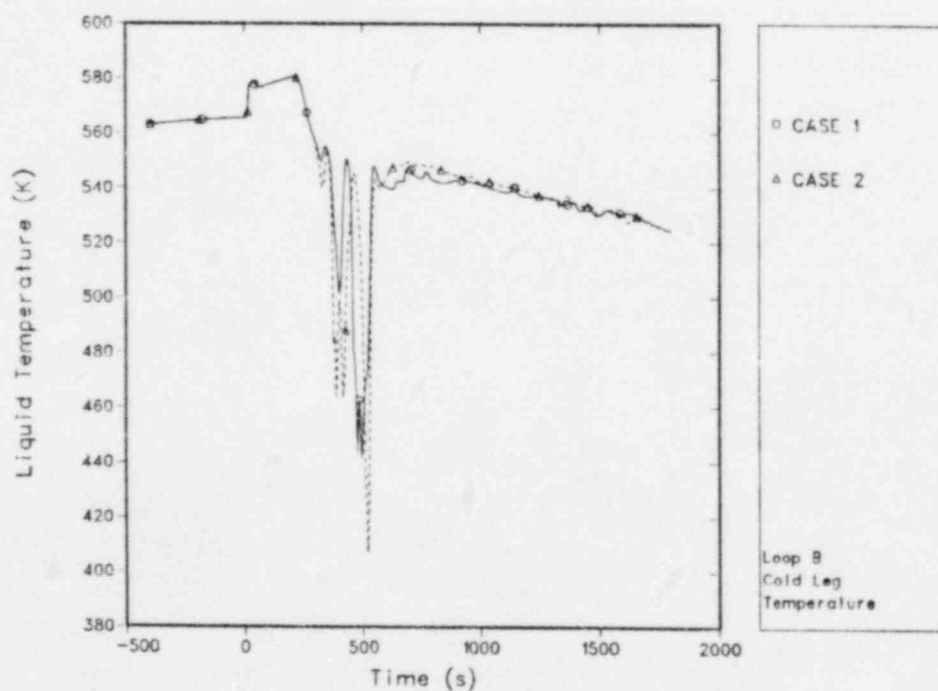


Fig. 204.  
Loop-B cold-leg temperatures (at HPIS connection).

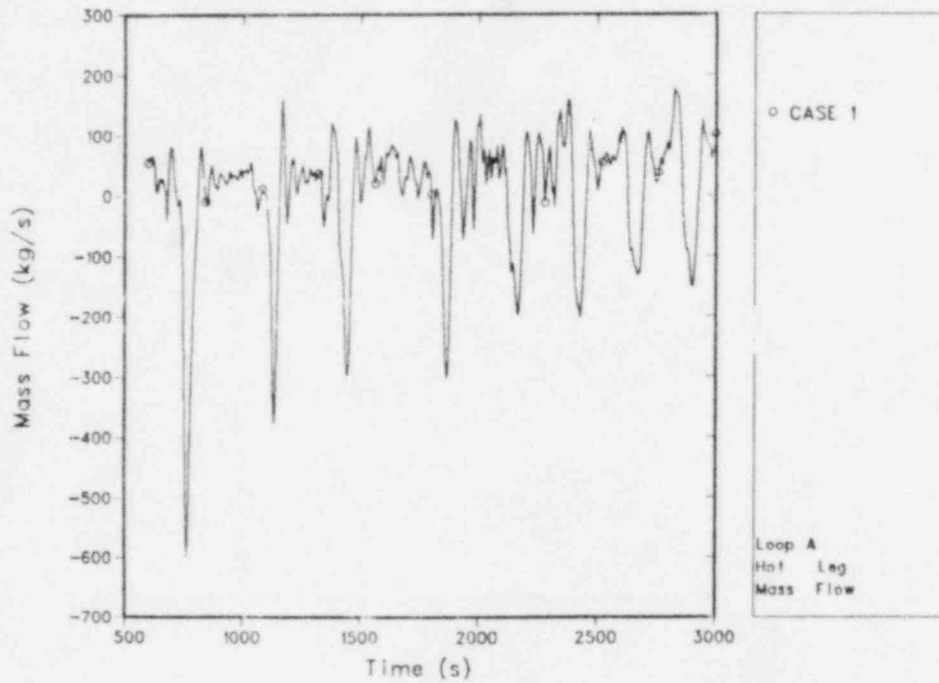


Fig. 205.  
Loop-A mass flows.

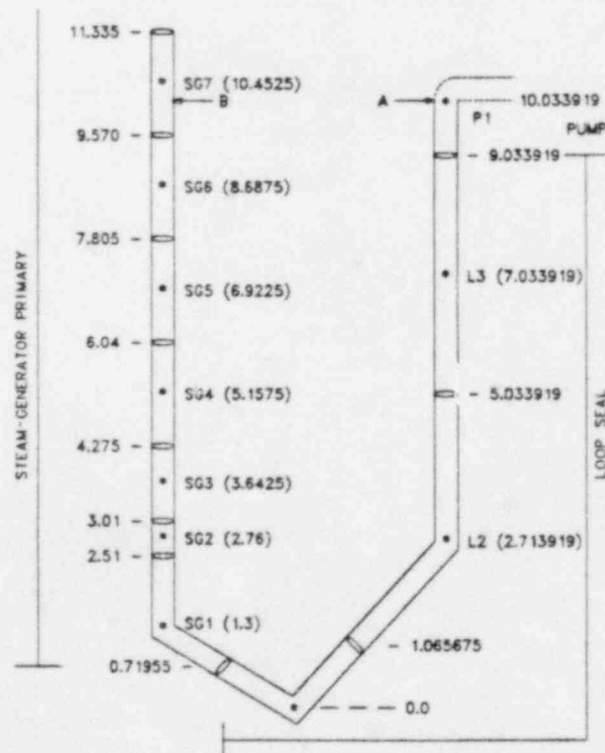


Fig. 206.  
Loop seal--steam-generator primary-side geometry.

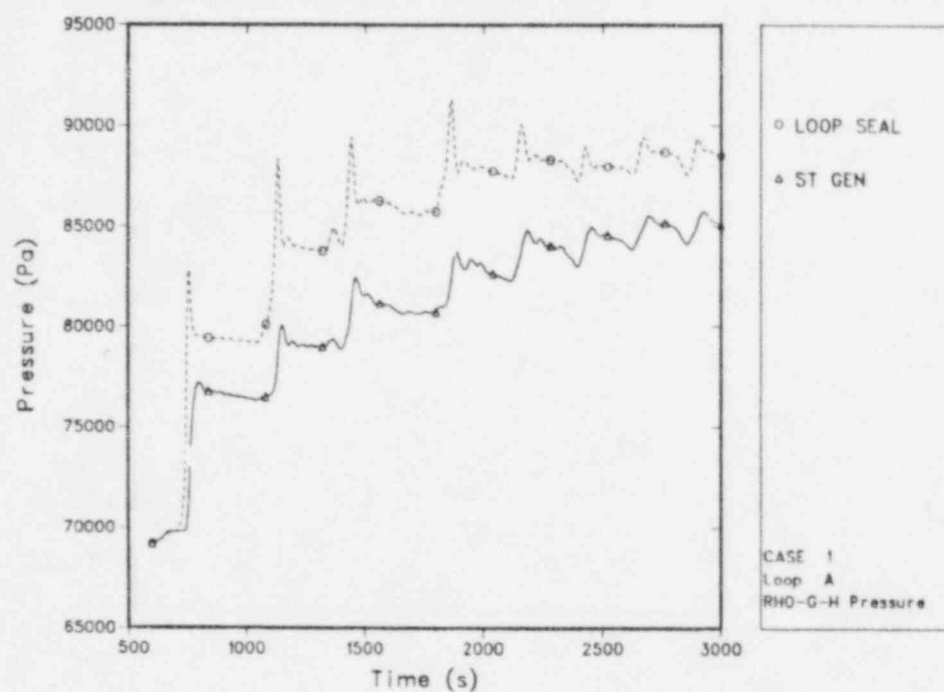


Fig. 207.  
RHO-G-H pressure difference in Loop A between bottom of the loop seal and (1) top of loop seal and (2) equivalent height in steam-generator primary.

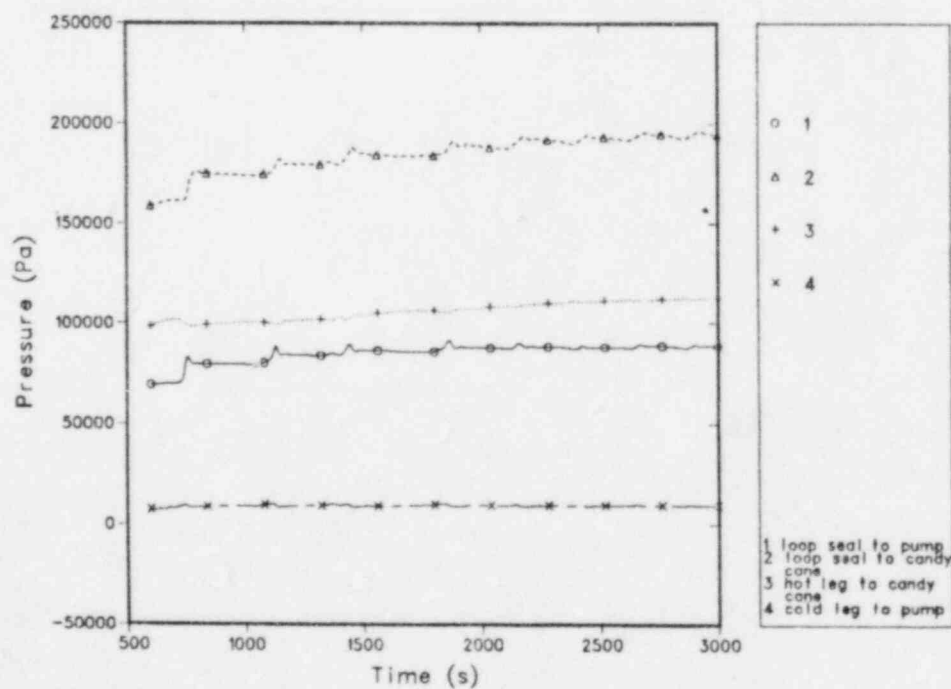


Fig. 208.  
RHO-G-H pressure drop terms around Loop A.

is,  $\text{RHO-G-H}$  in pressure units of pascals) for the fluid at various locations around Loop A. Figure 207 shows the " $\text{RHO-G-H}$ " products from the bottom of the loop seal to (1) the top of the loop seal (position A, Fig. 206) and (2) to an equivalent height location in the steam generator (position B, Fig. 206). Figure 208 shows the " $\text{RHO-G-H}$ " products for (1) the loop-seal low point to the pump midpoint, (2) the loop-seal low point to the candy-cane high point, (3) the hot-leg horizontal section to the candy-cane high point, and (4) the cold-leg horizontal section to the pump midpoint. This intermittent flow prevented cold unmixed HPIS water from reaching the vessel; thus the downcomer temperatures remained above 440 K (333°F) Case 1, and 490 K (423°F) Case 2 (Fig. 209), even though temperatures in the Loop-A cold leg adjacent to the HPIS location were as low as ~320 K (116°F) during the quiescent periods (Fig. 210) for both cases.

We see for Case 1 that this intermittent flow continued well past the time when in-the-plant feedwater was reestablished to the Loop-A steam generator. After ~1800 s, however, even though the density-driven oscillations continued, the time-averaged fluid temperature in the loop seal remained constant at ~450 K (350°F) (Fig. 211).

Another factor besides the intermittent reverse flow in Loop A that kept the downcomer from getting very cold was the flow through the vent valves, that is, between the upper plenum/upper head and the tops of the downcomers. Figures 212-214, respectively, show the fluid temperature entering the vent valves, and the mass flow rate through the vent valves to the "Loop-A" and "Loop-B" downcomers (that is, components 95 and 96, Fig. 187).

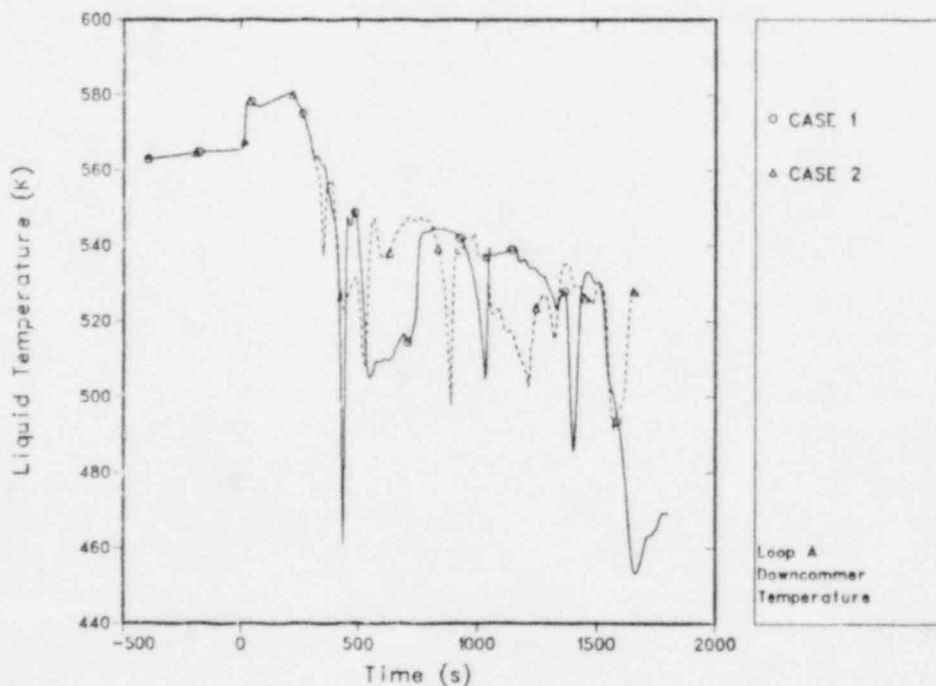


Fig. 209.  
Downcomer temperature, immediately below Loop-A cold-leg connection.



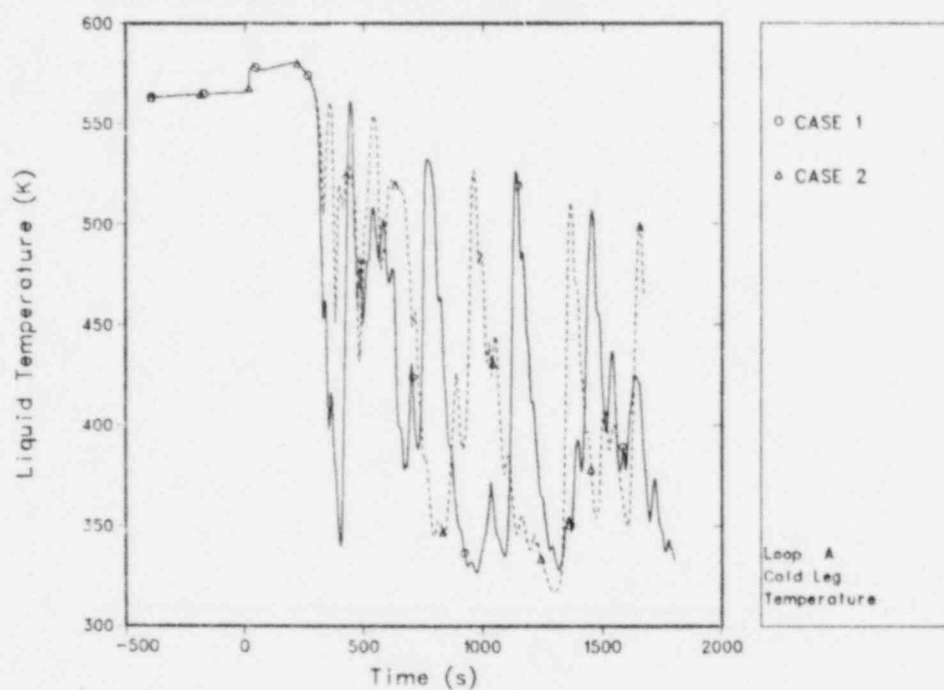


Fig. 210.  
Loop-A cold-leg temperature opposite HPIS injection location.

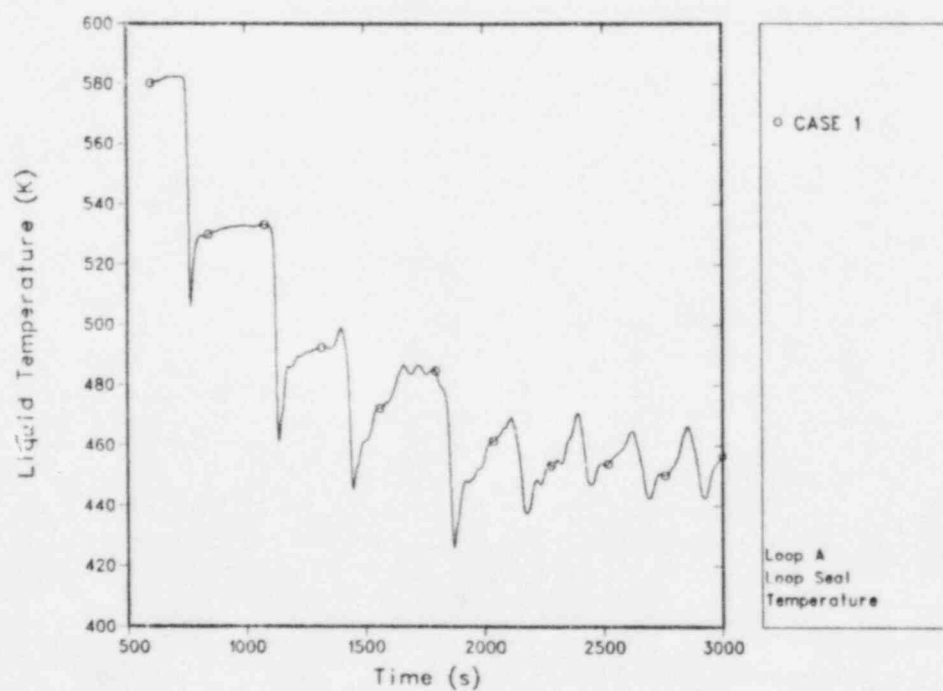


Fig. 211.  
Water temperature in Loop-A seal.

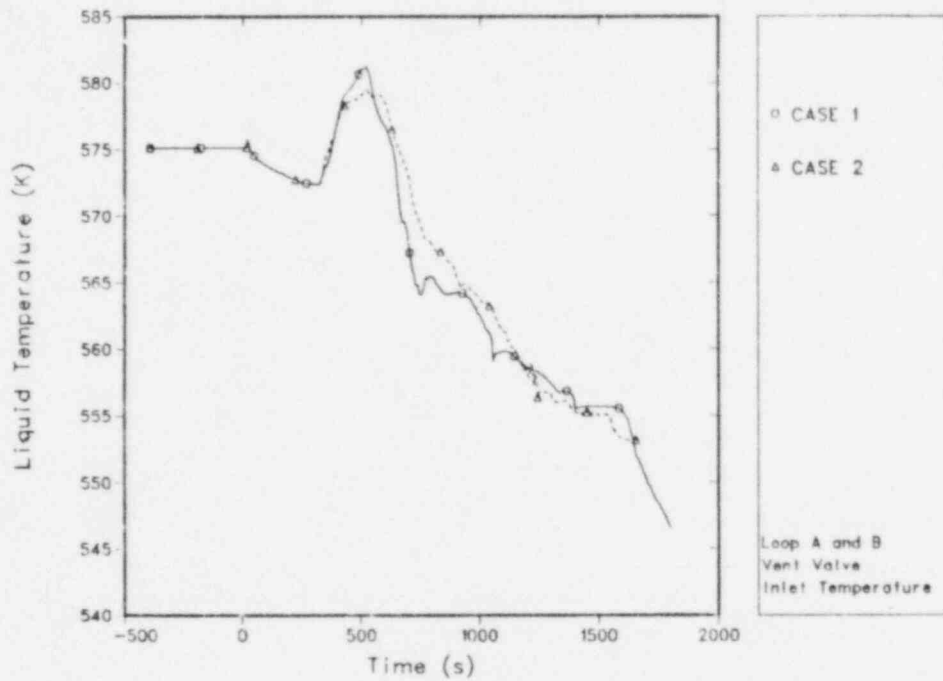


Fig. 212.  
Water temperature at inlet to vent valves.

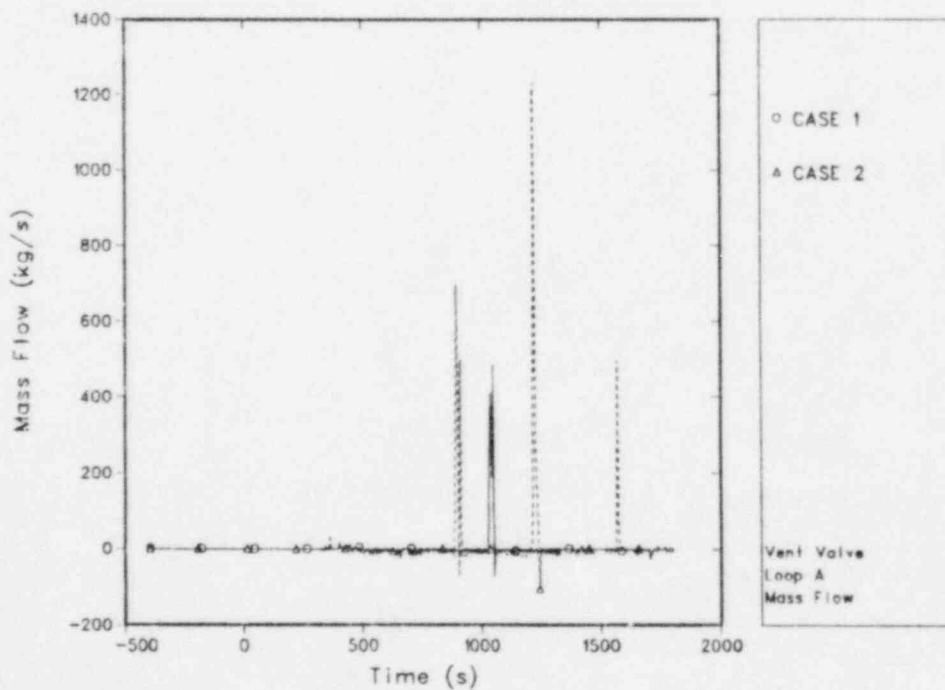


Fig. 213.  
Mass flow through Loop-A vent valve.

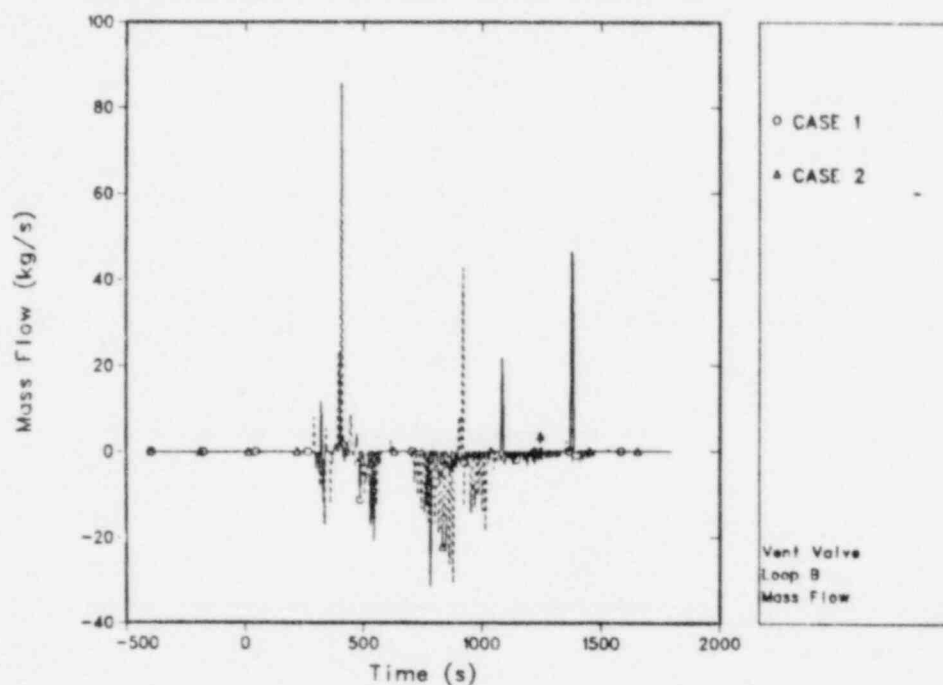


Fig. 214.  
Mass flow through Loop-B vent valve.

#### E. User Experience and Calculation Timing Statistics

The TRAC-PF1 calculation of the Crystal River transient using a one-dimensional core and vessel simulation can be compared with the similar, most recent TRAC-PD2<sup>34</sup> analysis using a three-dimensional vessel.

For this transient, no limitations were observed in the use of a one-dimensional core/vessel. In fact, because of the use of both more recent plant modeling (namely, OTSG complete with aspirator flow) and transient boundary conditions, the TRAC-PF1 calculation better calculated the system depressurization, repressurization, and plant cooldown. More pronounced pressure oscillations were seen during the system repressurization with TRAC-PF1 than with TRAC-PD2. This difference is attributed to the change in condensation modeling between the two codes and not to the use of a one-dimensional (TRAC-PF1) or three-dimensional (TRAC-PD2) input model. The advantage of the use of TRAC-PF1 with a one-dimensional core/vessel was that CPU/transient time ratio was half of that for the TRAC-PD2 transient.

To improve the primary-to-secondary heat transfer during the steady-state calculation, a 6-mm hydraulic diameter, based upon the tube separation distance, was used for the steam-generator tube bundle nodes.

The timing statistics for both of the TRAC-PF1 calculations are presented in Figs. 215 and 216 and in Table XVIII. For the majority of the TRAC-PF1 calculations, a 1.0 s maximum time step was used. Figure 215 shows the "total CPU time" for both calculations, that is, for a transient time of 3000 s for Case 1 and for a transient time of ~1700 s for Case 2. Figure 215 shows the corresponding "total numbers of time steps" for both calculations. Both calculations were run on the Los Alamos National Laboratory CDC 7600 computers.

From Table XVIII, we see that the average CPU/transient time ratio was ~2.8 for both calculations and that the "average time step", that is, (the CPU time)/(total number of time steps) was 0.739 s for Case 1 and 0.727 s for Case 2. This is close to the maximum imposed time step limit of 1.0 s.

Both figures show that for both calculations, the calculations ran very quickly between ~500 s and 1300 s with a CPU/transient time ratio during that period of ~1.0.

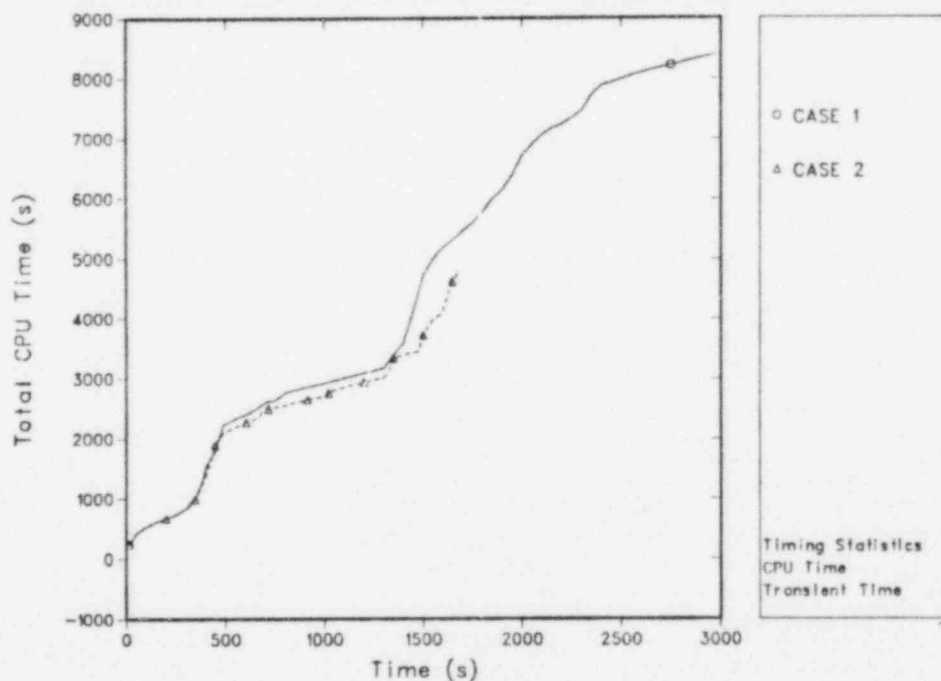


Fig. 215.  
CPU time for Crystal River transients, run on a CDC 7600 computer.

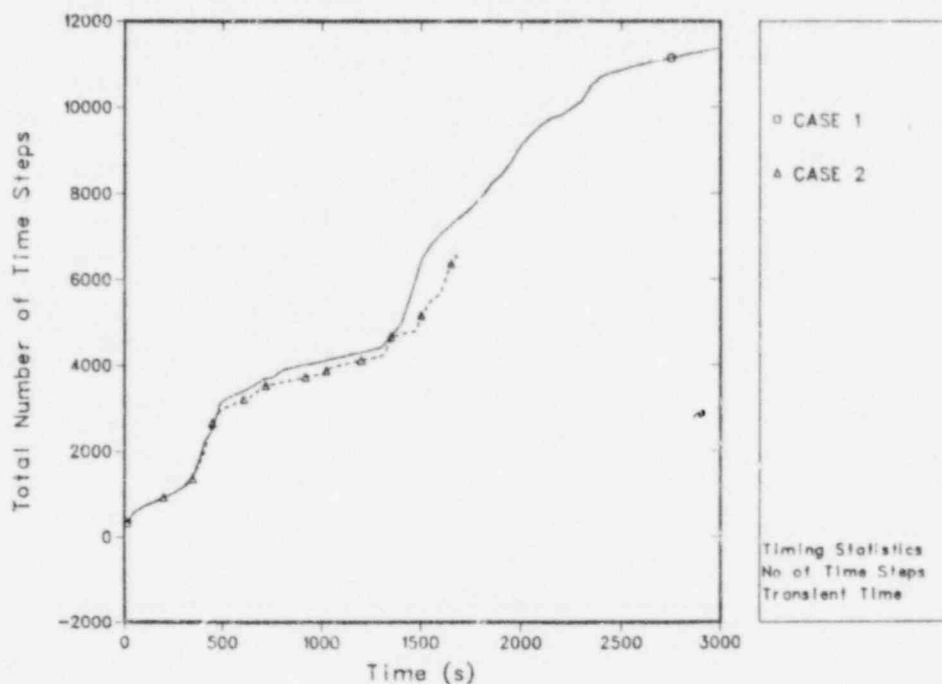


Fig. 216.  
Total number of time steps for Crystal River transients.

TABLE XVIII

TIMING STATISTICS FOR CRYSTAL RIVER  
TRAC-PF1 ONE-DIMENSIONAL CALCULATIONS

	Case 1	Case 2
Transient Time	3000. s	1677.8 s
CPU Time	8416.5 s	4756.7 s
Total Number of Time Steps	11393	6540
CPU Time/Transient Time	2.8055	2.8351
Cells	208	208
<u>CPU/Transient</u> Cell	0.013488	0.013630
"Average time step" i.e., CPU/No. of Time Steps	0.7387 s	0.7273 s
<u>CPU/No. of Time Steps</u> Cell	$3.552 \times 10^{-3}$ s	$3.497 \times 10^{-3}$ s



## F. Summary and Conclusions

This was the first application of TRAC-PF1 using a one-dimensional core and vessel to a full reactor transient.

Because the Crystal River Unit-3 transient was initiated by a partial loss of the nonnuclear instrumentation, only a limited data comparison was possible.

Using the one-dimensional CORE component of TRAC-PF1, a one-dimensional model of the Crystal River Unit-3 plant, that is, a B & W lowered loop plant, was constructed. The model included a representation of the B & W once-through-steam generators with aspirator flow.

A reactor steady state was obtained that agreed very well with the limited plant data available. The modeling of the once-through-steam generators with aspirator flow permitted the calculation of steam superheat at the exit of the steam-generator secondaries. The calculated exit steam temperature of 571.2 K (568.4°F) was in excellent agreement with the FSAR<sup>35</sup> value of 572 K (570°F). The water at the inlet to the steam-generator tube bundle was, however, slightly subcooled. This subcooling resulted from the low steam/water condensation rate calculated by the TRAC-PF1 code.

The Crystal River Unit 3 transient boundary conditions were taken primarily from Ref. 38. Using these boundary conditions, the TRAC-PF1 calculations showed a reactor trip because of high primary system pressure at 17.5 s. The system then depressurized due to the flow of fluid out of the PORV and the contraction of the liquid in the primary circuit as the primary-coolant temperature fell. The RCS pressure fell to the HPIS set point of 10.44 MPa (1500 psig) at 207 s. This was in excellent agreement with the time of 201 s for HPIS initiation taken from the event synopsis of Ref. 37.

A discrepancy was discovered between the depressurization rate as given by the event synopsis of Ref. 37 and the pressure time curve of Fig. III-3, Ref. 37.

Reactor-coolant-pump trip was initiated at 224 s together with the establishment of feedwater to the Loop-B steam-generator secondary.

Two separate calculations were performed for the period following 224 s. In Case 1, the Loop-A steam-generator-secondary pressure was determined by the steam valve relief capacity and the primary-to-secondary heat transfer. In Case 2, the Loop-A steam-generator pressure was ramped down to the isolation pressure of 4.24 MPa (600 psig) between 224 s and 510 s and kept at that value for the remainder of the transient.

Following the reestablishment of cooling to the Loop-B steam generator, natural circulation was established in Loop B in both of the TRAC-PF1 calculations.

The RCS pressure fell to saturation at ~245 s and the resultant voids produced collected at the three primary circuit high points, that is, at the top of the Loop-A candy cane, at the top of the Loop-B candy cane, and at the top of the vessel.

Following the production of voids, the pressurizer rapidly filled with water. Once the pressurizer became liquid solid (at ~395 s), the primary system began to repressurize as the HPIS flow of 72 kg/s ( $0.570 \times 10^6$  lb/h) into the primary circuit exceeded the flow of 27 kg/s ( $0.214 \times 10^6$  lb/h) out of the PORV. The primary circuit repressurization was enhanced by the closing of the PORV at 450 s.

Two pressure oscillations were observed during the TRAC-PF1 calculated primary system repressurization. The oscillations occurred as a result of a "two-stage" repressurization process in which the RCS pressure first increased as the primary system voids were compressed and then decreased as a fraction of the voids collapsed (condensed). This process occurred twice and was observed in both calculations.

The primary circuit continued to pressurize until it reached the SRV trip set point of 16.65 MPa (2400 psig). This occurred at 671 s for Case 1 and 685 s for Case 2. The plant data (Ref. 37) indicated that the SRV opened somewhere between 595 s and 620 s. The TRAC-PF1 calculated repressurization was, therefore, delayed by between ~50 s and 90 s when compared with the plant data.

Comparison of the TRAC-PF1 calculated upper-plenum temperature with plant data demonstrated that the overall cooling was well predicted.

After the system repressurized, Case 1 was continued to 3000 s and Case 2 to 1700 s. In Case 1, no account was taken of the fact that in the plant transient the HPIS was reduced at ~1750 s and that feedwater was reestablished to Loop A at ~2200 s. For long periods of time, the flow in Loop A was very small as there was no steam-generator cooling to drive it. The HPIS water, therefore, collected in the cold leg, spreading out in both directions. Because the HPIS injection point was close to the pump, cold high-density water flowed back through the pump into the loop seal producing gravity-driven reverse flows through Loop A. The flow of the cold HPIS water to the downcomer was thus reduced, and the Loop-A downcomer coolant temperature never fell below 440 K (333°F) Case 1, and 490 K (423°F) Case 2, even though the cold-leg fluid temperature reached a value as low as 320 K (116°F) for both Case 1 and Case 2.

The TRAC-PF1 code, therefore, did an excellent job of calculating the sequence of events during the Crystal River Unit-3 plant transient. The reactor trip on high pressure, the primary system depressurization and repressurization, and the overall cooling of the primary coolant were all very well calculated.

No major parameter variations in plant boundary conditions were performed using TRAC-PF1. It is obvious, however, from an examination of this and previous TRAC calculations<sup>3,4\*</sup> that the improved calculation contained in this report was as a result, at least in part, of the improved understanding of the way the transient progressed is reflected in the analysis contained in Ref. 38. The two most influential transient boundary conditions used in the TRAC-PF1 calculations and taken from Ref. 38 were (1) the increase in the size of the PORV (the size of the PORV was increased to permit a steam flow rate of 155% of the design value), and (2) the reduction of the steam-generator-secondary feedwater from full flow to zero over a period of ~9 s rather than the previously estimated longer period of ~60 s. Using these transient boundary conditions, the system depressurization, in particular, was extremely well calculated with only a 6 s difference between the TRAC-PF1 calculation and the plant data for the initiation of the HPIS [that is, the RCS pressure equal to 10.44 MPa (1500 psig)].

The formulation of the TRAC-PF1 condensation model influenced two aspects of the calculations. First in the steady-state calculation, low values of the steam/water condensation were responsible for the water entering the steam-generator-secondary tube bundle being subcooled. Second during the transient repressurization, low values of the steam/water condensation at low flow rates (that is, small liquid velocities) contributed to the calculated pressure oscillations.

Following the system repressurization for the first calculation, that is, Case 1, there was almost no flow in Loop A for a period of ~1600 s, as there was no cooling of the Loop-A steam-generator secondary to drive it. During this period, gravity-driven reverse flows in Loop A prevented the cold HPIS water from reaching the vessel downcomer so that the downcomer temperature never fell below 440 K (333°F).

---

\*This information was provided by G. J. E. Willcutt, Jr., J. W. Bolstad, and M. W. Burkett, Los Alamos National Laboratory, Energy Division, Thermal-Hydraulics Group (February 1982).

## IX. TIMING STATISTICS

Many questions have been raised in the past concerning the CPU requirements for running TRAC calculations. Therefore, we have summarized in Table XIX statistics that bear on the question of computer usage. Most of the calculations listed in the table are described in this report. The LOFT L2-2 and L3-7 calculations are described in the TRAC-PF1 developmental-assessment report.<sup>2</sup> All of the calculations were run on one of the Los Alamos CDC 7600 computers.

Included in the table are small-break, intermediate-break, and large-break LOCAs. The noding varies from reasonably coarse to moderately fine; we have run calculations with ~1000 cells. The VESSEL nodings are not particularly detailed. We have used vessels with as many as five radial rings and eight azimuthal segments. Clearly as the number of cells increases, the total CPU time requirement increases.

The last column in the table lists the CPU time per cell per time step, a quantity commonly referred to as grind time. The calculations with the very coarse VESSEL nodings (the intermediate breaks) are more efficient in terms of grind time than are the calculations with more detailed VESSEL noding. The calculations with the coarsely noded VESSEL component use the direct-matrix-inversion option in TRAC-PF1 (set IITMAX to 0 on Main Control Card 4). The LOFT L2-2 calculation with a more detailed VESSEL component uses the iterative solution of the VESSEL matrix. The iterative technique is slower than the direct inversion, but the iterative technique can solve a much larger matrix. The maximum VESSEL size for which we have used direct inversion is 76 cells. The maximum VESSEL size for which the direct inversion can be used is dependent on the available small-core memory.

The grind time also reflects differences in the iteration counts required to converge the solution. Increasing the convergence criteria may permit a calculation to run marginally faster, but the increased speed must be weighed against the solution accuracy. Reduction in the number of cells is a more effective way to reduce CPU time, with VESSEL cells more important than one-dimensional component cells (if for no other reason than VESSEL cells tend to be removed in fairly large blocks). Again, the improved run time must be weighed against the accuracy of the calculation. Normally, changing the noding by a few percent is not significant.

The user can affect the CPU time, sometimes dramatically, by watching the short-edit information to determine what is controlling the time-step size. For example, if the Courant limit is controlling the time step consistently at a VESSEL connection or an internal VESSEL interface, one can make the calculation run faster by increasing the cell lengths, with a corresponding reduction of perhaps only a few cells.

The column in Table XIX that gives the ratio of CPU time to transient time is interesting. The LOFT L3-7 calculation ran ~2 times real time. The Semiscale small-break calculations ran between 3.5 and 5.5 times real time. The one-dimensional LOFT L2-2 calculation is an order of magnitude faster than the corresponding three-dimensional calculation.

TABLE XIX  
CODE TIMING STATISTICS<sup>a</sup>

Test	Code	Cells <sup>b</sup>	Heat Slabs <sup>c</sup>	Transient Time (s)	CPU Time (s)	Time Steps	CPU Transient	CPU/Trans Cell	CPU/Trans/Cell Slab	CPU/Cell Time Step (ms)
LOFT L2-2	PF1	334/192	398	70.00	21 412.0	10 983	305.8857	0.9158	0.0023	5.8370
LOFT L2-2	PF1	168/0	153	70.01	2 013.2	2 964	28.7559	0.1712	0.0011	4.0430
LOFT L3-7	PF1	114/0	86	10 800.	21 265.9	49 267	1.9691	0.0173	0.0002	3.7864
Semiscale S-UT-2	PF1	198/0	105	1 494.72	8 243.4	12 793	5.5150	0.0279	0.0003	3.2544
Semiscale S-UT-6	PF1	198/0	105	1 500.06	5 791.7	8 618	3.8610	0.0195	0.0002	3.3942
Semiscale S-UT-7	PF1	198/0	105	1 000.02	3 460.2	5 117	3.4601	0.0175	0.0002	3.4152
LOFT L5-1	PF1	116/36	94	225.61	4 640.9	8 609	20.5705	0.1773	0.0019	4.6472
LOFT L8-2	PF1	128/36	94	319.53	7 461.6	12 463	23.3518	0.1824	0.0019	4.6773

<sup>a</sup> To conserve space, the following equivalences exist: Trans = total transient time  
Cell, Cells = number of hydraulic cells  
Slab, Heat Slabs = number of heat slabs

<sup>b</sup> Cells are given as total cells/vessel (3-D) cells.

<sup>c</sup> Heat Slabs are heat surfaces. The count includes the rods, with each fixed axial node (without the fine mesh turned on) in each rod counted as one heat slab.



Figures 217-224 show the cumulative CPU time as a function of transient time for the calculations in Table XIX. For these calculations, the void-fraction changes are the principal actor in setting the time-step size. For those calculations with core dryouts, the portions of the transient during which the cladding rewets exhibit some control based on changes in pressure, fluid temperatures, structure temperatures, and iteration counts. For those calculations with the VESSEL component, the Courant limit determined the time-step size only occasionally. Figures 217 and 218 are typical of transients with refloods. After some time-step limitation during the subcooled decompression of the primary system, the calculation accelerates during the blowdown; when the accumulators begin to inject subcooled liquid, the condensation effects cause void-fraction changes and flow oscillations that slow the calculation down. Normally, the reflood process represents the slowest portion of the transient, and then as the core quenching slows (in LOFT, the accumulators empty at ~50 s), the calculation accelerates. Figures 223 and 224 show a similar behavior for the LOFT intermediate-break LOCA calculations. Figure 219 indicates that the code ran the first 2000 s of Test L3-7 much faster than real time. After the termination of the high-pressure injection in this calculation, void-fraction changes reduce the time-step size and the calculation slows. After the first hour of the transient, the operators control the facility; matching the facility control requires restriction of the time-step size.

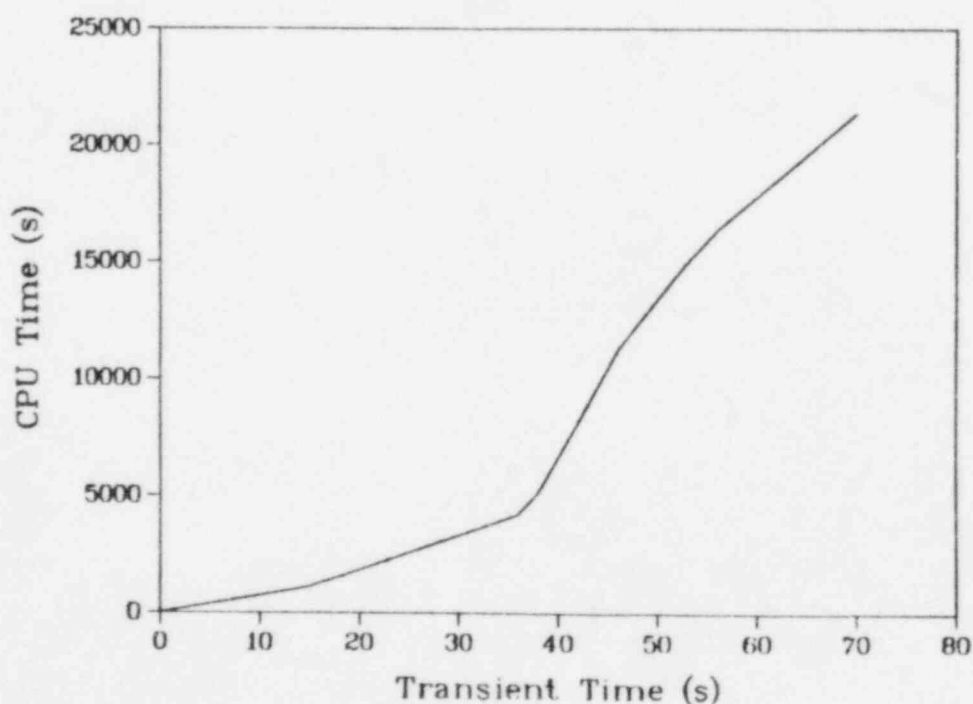


Fig. 217.  
CPU-time utilization for the LOFT L2-2 calculation  
with the three-dimensional VESSEL component.

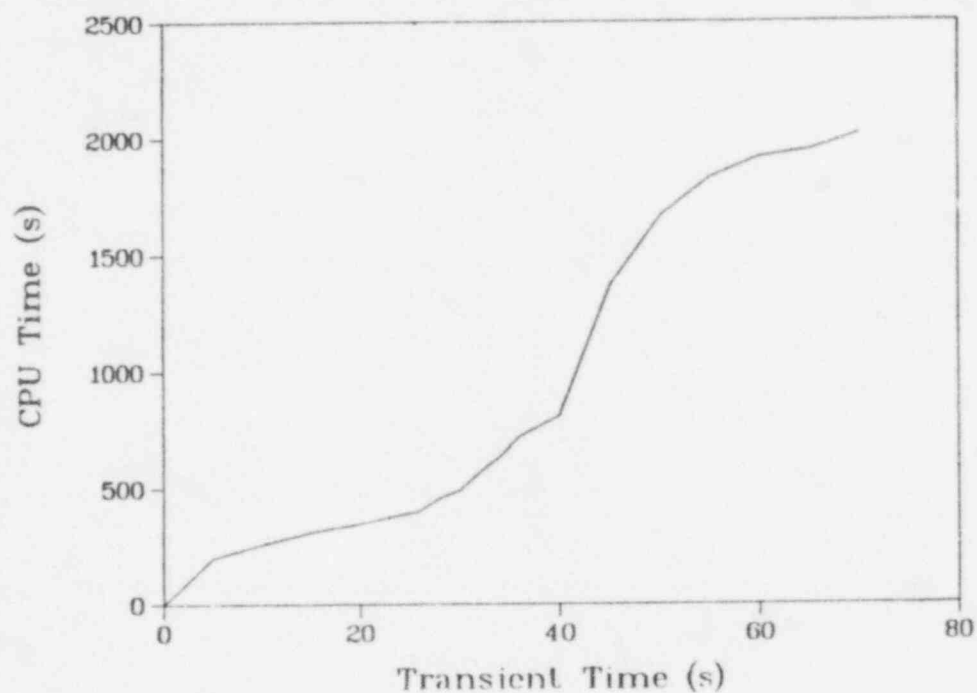


Fig. 218.  
CPU-time utilization for the LOFT L2-2 calculation  
with the one-dimensional vessel representation.

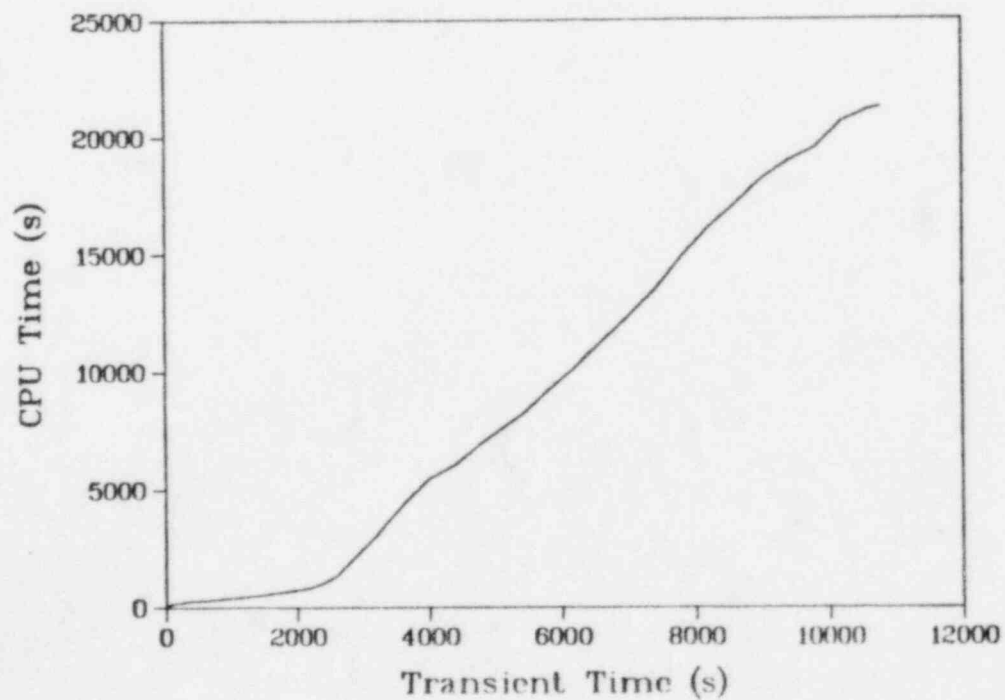


Fig. 219.  
CPU-time utilization for the LOFT L3-7 calculation.

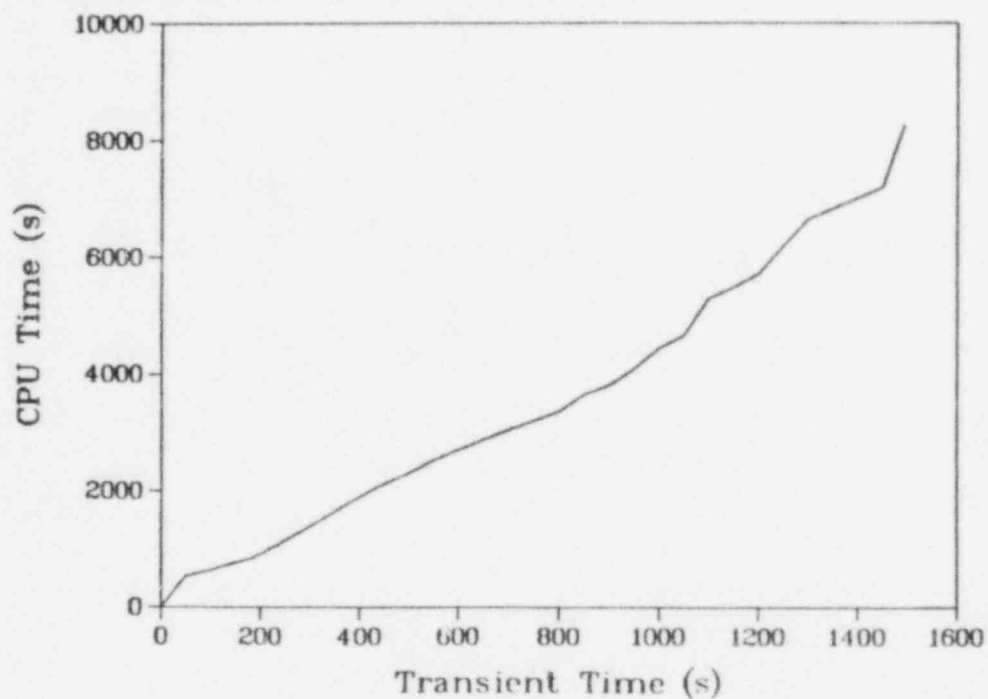


Fig. 220.  
CPU-time utilization for the Semiscale Test S-UT-2 calculation.

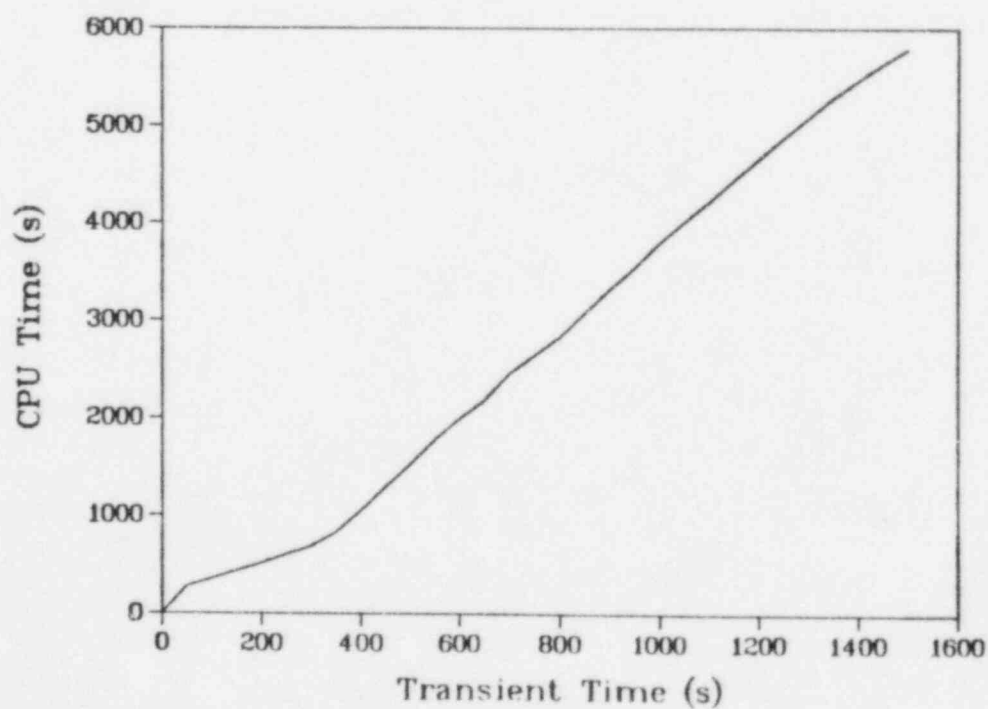


Fig. 221.  
CPU-time utilization for the Semiscale Test S-UT-6 calculation.

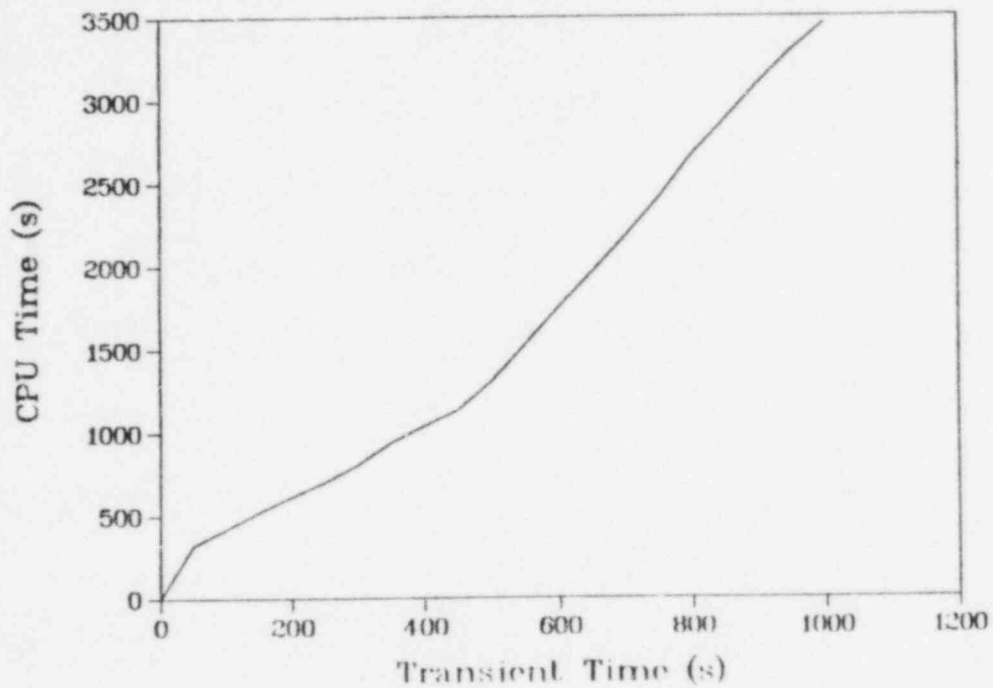


Fig. 222.  
CPU-time utilization for the Semiscale Test S-UT-7 calculation.

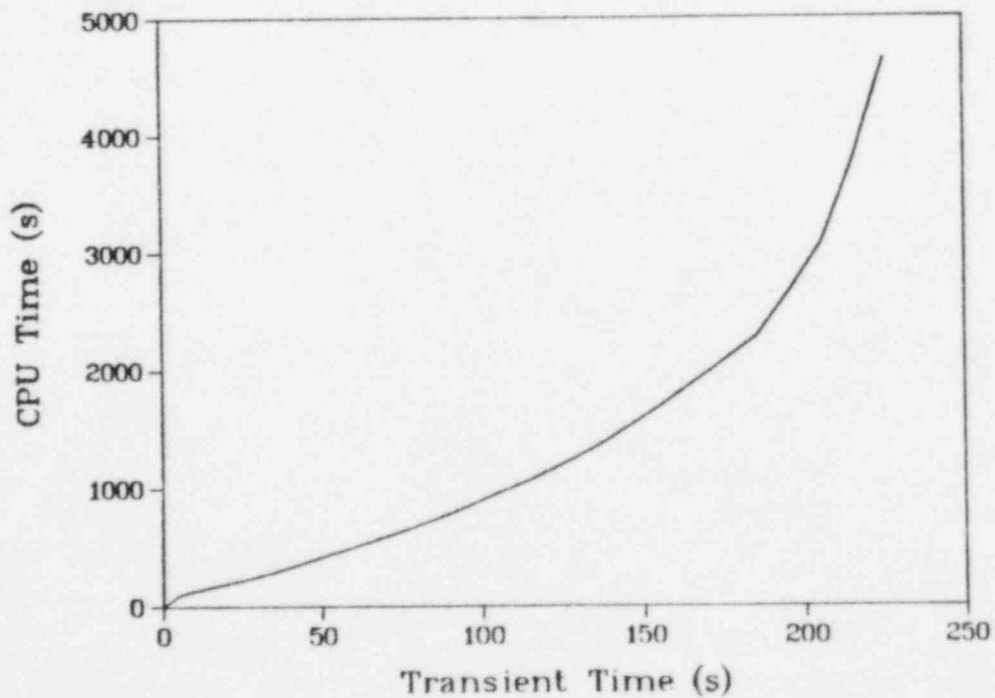


Fig. 223.  
CPU-time utilization for the LOFT LS-1 calculation.

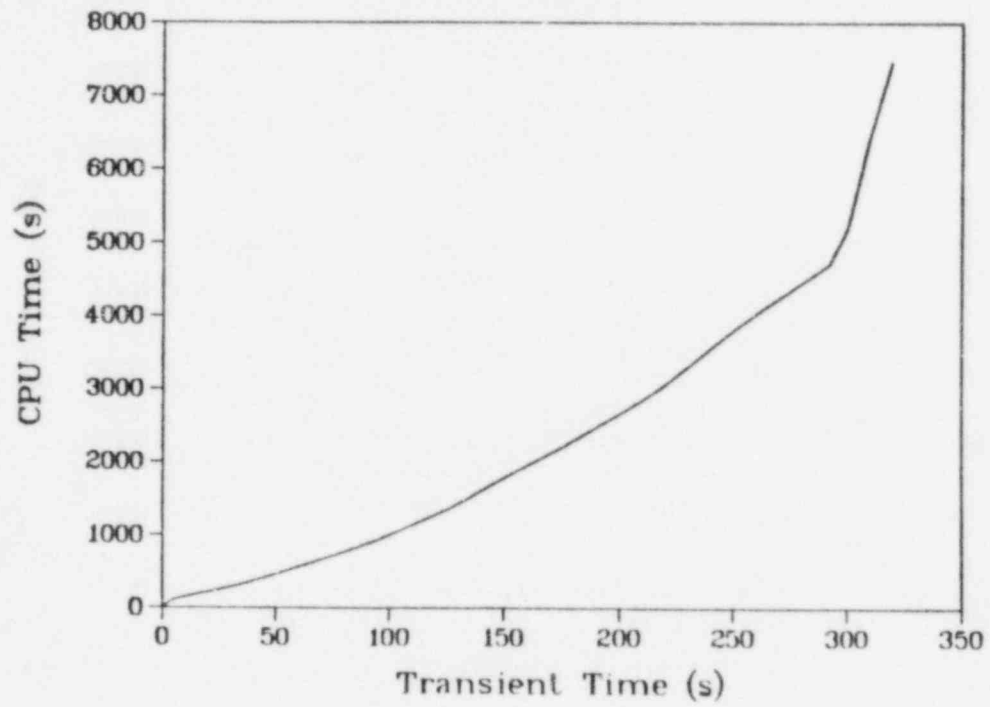


Fig. 224.  
CPU-time utilization for the LOFT L8-2 calculation.



## X. CONCLUSIONS

As the previous comparisons indicate, the TRAC-PF1 code calculates many phenomena very well. The major discrepancies in the comparisons can generally be traced to the critical-flow model and to the interphasic condensation model. The critical-flow model does not yield the correct dependence of critical flow on void fraction. The condensation model appears to underpredict the condensation rate under certain conditions.

The Semiscale natural-circulation comparisons show that the code calculates the magnitude of the natural-circulation flows as a function of void fraction reasonably well. The code also correctly makes the transition from natural-circulation cooling to reflux cooling. The comparisons indicate that the wall-condensation heat transfer in the released code is low. The reflux test with the noncondensable injection shows the calculated behavior of the noncondensable gas is calculated correctly. The natural-circulation test with the noncondensable injection indicates that the code does not predict the flow recovery after the period of stagnation; we currently do not know what phenomenon is driving the flow recovery.

The Semiscale small-break LOCA comparisons confirm the problems with the critical-flow model. However, when the multipliers to the critical-flow model are adjusted to offset the errors in the model, the comparisons throughout the primary system are reasonably good. The code calculates the core dryouts to occur early and the peak cladding temperature to be high. However, the core volume is very small, and small changes in the primary-system liquid inventory have significant impact on the core inventory.

The comparisons for the LOFT intermediate-break LOCA tests show that the core should be noded more finely in the axial direction to track better the core liquid level and its effect on core dryout. If the interface sharpener logic were incorporated in the one-dimensional CORE component, these types of tests could be successively run in a one-dimensional calculation. Similarly, if an interpolative scheme were used to distribute the fluid along the fuel rod, then the coarser VESSEL (and CORE) noding would be acceptable. The comparisons offer further confirmation of the inadequacy of the critical-flow model. An underprediction of condensation at high subcooling and low voids adversely affected the system pressure calculation, causing the calculated pressure to not drop as rapidly as the data when the cladding temperature exceeded the saturation temperature (subcooled nucleate boiling generated vapor, which failed to condense later). This problem does not occur with the one-dimensional CORE component because the subcooled nucleate-boiling heat-transfer mode does not exist in the one-dimensional components. Sensitivity calculations conducted as a part of the LS-1 and LS-2 analyses show the calculated results to be remarkably insensitive to the time-step size, and the mass errors are negligible.

The code calculated well the behavior of the two non-LOCA transients in LOFT. The results indicate the importance of modeling all structural mass and heat-transfer area, together with the leakage paths in the vessel, to the overall system response because of the impact on the energy balance. The heat- and mass-transfer mechanisms in the steam-generator secondary and in the pressurizer are also important factors in these tests.

The Crystal River analysis is significant in showing the application of the code to a real reactor transient. The code calculated the sequence of events very well and the calculated pressures, flows, and temperatures compare well with the data. The refill of the hot legs shows an adverse effect of condensation on filling individual cells. The code requires a combined wall- and interphasic-condensation model to smooth the condensation process as cells fill and the pressure increases.

## REFERENCES

1. "TRAC-PF1: An Advanced Best-Estimate Computer Program for Pressurized Water Reactor Analysis," Los Alamos National Laboratory report LA-9944-MS, NUREG/CR-3567 (February 1984).
2. B. E. Boyack, "TRAC-PF1 Developmental Assessment," Los Alamos National Laboratory report LA-9704-M, NUREG/CR-3280 (July 1983).
3. C. E. Watson, "TRAC News," Newsletter No. 6, Safety Analysis Group (Q-7), Los Alamos National Laboratory (January 1982).
4. C. E. Watson, "TRAC News," Newsletter No. 7, Safety Analysis Group (Q-7), Los Alamos National Laboratory (May 1982).
5. Thomas M. O'Connell, "Experiment Data Report for Semiscale MOD-2A Natural Circulation Tests S-NC-2B, S-NC-3, and S-NC-4B," EG&G Idaho, Inc. report NUREG/CR-2454, EGG-2141 (December 1981).
6. Thomas M. O'Connell, "Experiment Data Report for Semiscale MOD-2A Natural Circulation Tests S-NC-5 and S-NC-6," EG&G Idaho, Inc. report NUREG/CR-2501, EGG-2162 (January 1982).
7. Ronald A. Larson, "Experiment Data Report for Semiscale MOD-2A Natural Circulation Test S-NC-7C," EG&G Idaho, Inc. report NUREG/CR-2618, EGG-2179 (March 1982).
8. Guy G. Loomis and Kuniyasa Soda, "Results of the Semiscale MOD-2A Natural Circulation Experiments," EG&G Idaho, Inc. report NUREG/CR-2335, EGG-2200 (September 1982).
9. T. S. Andersen, "Correlation of Solubility Data for Hydrogen and Nitrogen in Water," Bettis Atomic Power Laboratory report WAPD-TM-633 (October 1967).
10. J. H. Mahaffy, D. R. Liles, and T. F. Bott, "TRAC Methods and Models," Proceedings of the American Nuclear Society Specialists Conference on Small Break Loss-of-Coolant Accident Analysis in LWRs, Monterey, California (August 25-27, 1981), Electric Power Research Institute report WS-81-201 (1981).
11. M. L. Patton, "Semiscale MOD-3 Test Program and System Description," NUREG/CR-0239, TREE-NUREG-1212 (July 1978).
12. Addendum I, Mod-2A Phase I Addendum to Mod-3 System Description, EG&G Idaho, Inc. (December 1980).
13. K. E. Sackett and L. B. Clegg, "Experiment Data Report for Semiscale MOD-2A Small Break Test Series (Tests S-UT-1 and S-UT-2)," EG&G Idaho, Inc. report NUREG/CR-2176 (July 1981).

14. P. North, "Experiment Operating Specification for Semiscale Mod-2A 10% Break Experiment (Tests S-UT-1 and S-UT-2)." EG&G Idaho, Inc., letter to R. E. Tiller, PN-120-80 (October 20, 1980).
15. G. G. Loomis, "Summary Report Semiscale Mod-2A Heat Loss Characterization Test Series," EG&G Idaho, Inc. report EGG-SEMI-5448 (May 1981).
16. D. J. Olson, "Transmittal of Semiscale Mod-3 Documents," EG&G Idaho, Inc., letter to R. E. Tiller, DJO-129-78 (October 5, 1978).
17. M. T. Leonard, "RELAP5 Standard Model Description for the Semiscale Mod-2A System," EG&G Idaho, Inc. report EGG-SEMI-5696 (December 1981).
18. J. E. Blakeley, R. A. Hansen, and D. J. Shimeck, "Quick Look Report for Semiscale Mod-2A Test S-UT-2," EG&G Idaho, Inc. report EGG-SEMI-5333 (January 1981).
19. B. E. Boyack, "Posttest Analysis of Semiscale Tests S-UT-6 and S-UT-7 Using TRAC-PF1," Los Alamos National Laboratory informal report LA-UR-82-1665 (September 1982).
20. R. A. Larson and L. B. Clegg, "Experiment Data Report for Semiscale Mod-2A Small Break Test Series (Tests S-UT-6 and S-UT-7)," EG&G Idaho, Inc. report NUREG/CR-2355 (November 1981).
21. J. M. Cozzuol and C. M. Kullberg, "Quick Look Report for Semiscale Mod-2A Test S-UT-6," EG&G Idaho, Inc. report EGG-SEMI-5446 (May 1981).
22. R. G. Hansen, D. J. Shimeck, and J. L. Steiner, "Quick Look Report for Semiscale Mod-2A Test S-UT-7," EG&G Idaho, Inc. report EGG-SEMI-5442 (May 1981).
23. R. G. Hansen, "Experiment Operating Specification for Semiscale Mod-2A 5% Break Experiments S-UT-6 and S-UT-7," EG&G Idaho, Inc. report EGG-SEMI-5421 (April 1981).
24. D. B. Jarrell and J. M. Divine, "Experiment Data Report for LOFT Intermediate Break Experiment L5-1 and Severe Core Transient Experiment L8-2," Idaho National Engineering Laboratory report NUREG/CR-2398, EGG-2136 (November 1981).
25. D. L. Reeder, "LOFT System and Test Description (5.5-ft Nuclear Core 1 LOCes)," Idaho National Engineering Laboratory report NUREG/CR-0247, TREE-1208 (July 1978).
26. B. E. Boyack, "TRAC-PF1 Developmental Assessment," Los Alamos National Laboratory report LA-9704-MS (July 1983).
27. D. P. Siska, "NSSS Transient Test at ANO-2," Electric Power Research Institute report NP-1708 (May 1981).

28. K. G. Condie, "RELAP5 Reference Calculation for LOFT Experiment L6-7/L9-2," Idaho National Engineering Laboratory report EGG-LOFT-6014 (January 1983).
29. Samuel L. Thompson and Lubomyra N. Kmetyk, "RELAP5 Assessment: LOFT Turbine Trip L6-7/L9-2," Sandia National Laboratories report SAND83-0832 (R4), NUREG/CR-3257 (July 1983).
30. S. C. Madden, "LOFT Experiment Operating Specification Nuclear Test L6-7/L9-2," Idaho National Engineering Laboratory report EGG-LOFT-5447 (June 1981).
31. Benjamin D. Stitt and Janice M. Divine, "Experiment Data Report for LOFT Anticipated Transient Experiment L6-7 and Anticipated Transient with Multiple Failures Experiment L9-2," Idaho National Engineering Laboratory report EGG-2121, NUREG/CR-2277 (September 1981).
32. John K. Meier, "A TRAC-PF1 Analysis of LOFT Steam-Generator Feedwater Transient Test L9-1," American Nuclear Society Meeting, "Anticipated and Abnormal Plant Transients in Light Water Reactors," Jackson, Wyoming, September 26-29, 1983, LA-UR-83-2780.
33. Doyle L. Baff and Janice M. Carpenter, "Experiment Data Report for LOFT Anticipated Transient Experiments L6-1, L6-2, and L6-3," Idaho National Engineering Laboratory report EGG-2067, NUREG/CR-1797 (December 1978).
34. G. J. E. Willcutt, Jr., "TRAC-PD2 Calculations of the Crystal River-3 Transient of February 26, 1980 Using Revised Assumptions," Los Alamos National Laboratory report LA-UR-83-1078 (April 1983).
35. "Crystal-River-FSAR," taken from "Crystal River Nuclear Generating Plant Unit 3. Preliminary Safety Analysis Report Amendment 11," Florida Power Corp., St. Petersburg (January 25, 1971).
36. "Analysis and Evaluation of Crystal River--Unit 3 Incident," Nuclear Safety Analysis Center report NSAC-3 (March 1980).
37. "Transient Assessment Report--Reactor Trip at Crystal River-3 Nuclear Station on February 26, 1980 (Preliminary)," Babcock & Wilcox report 07-08-02, Rev. 02 (March 9, 1980).
38. W. Brown, G. Caldwell, B. Chexal, and W. Layman, "Thermohydraulic Analysis of Crystal River Unit 3 Incident," Nuclear Safety Analysis Center report NSAC-15 (June 1981).

# DISTRIBUTION

Nuclear Regulatory Commission, R4, Laurel, Maryland	298
Technical Information Center, Oak Ridge, Tennessee	2
Los Alamos National Laboratory, Los Alamos, New Mexico	50
	<hr/>
	350



NRC FORM 335 (2-84) NRCM 1102, 3201, 3202		U.S. NUCLEAR REGULATORY COMMISSION		1. REPORT NUMBER (Assigned by NRC, and Vol. No., if any)  NUREG/CR-3646 LA-10548-MS	
SEE INSTRUCTIONS ON THE REVERSE					
2. TITLE AND SUBTITLE  TRAC-PF1 Independent Assessment			3. LEAVE BLANK		
5. AUTHOR(S) T. D. Knight, C. E. Booker, B. E. Boyack, J. K. Meier, James R. White (Consultant in Nuclear Reactor Safety Analysis, Idaho Falls, Idaho), Paul Coddington (Atomic			4. DATE REPORT COMPLETED MONTH YEAR September 1985		
7. PERFORMING ORGANIZATION NAME AND MAILING ADDRESS (Include Zip Code) Energy Establishment, Winfrith, Dorchester, Dorset, ENGLAND).  Los Alamos National Laboratory Los Alamos, NM 87545			6. DATE REPORT ISSUED MONTH YEAR October 1985		
10. SPONSORING ORGANIZATION NAME AND MAILING ADDRESS (Include Zip Code) Division of Accident Evaluation Office of Nuclear Regulatory Research US Nuclear Regulatory Commission Washington, DC 20555			8. PROJECT TASK WORK UNIT NUMBER  A7053		
12. SUPPLEMENTARY NOTES			9. FIN OR GRANT NUMBER  A7053		
13. ABSTRACT (200 words or less)  The Transient Reactor Analysis Code (TRAC) provides an advanced, best-estimate analysis capability for pressurized water reactors and for many thermal-hydraulic test facilities. The most recent publicly released version of TRAC is TRAC-PF1. This code version includes a full two-fluid modeling capability in both the three-dimensional vessel component and the one-dimensional components. We have improved the numerical methods in the one-dimensional components to provide a more stable solution and to permit the code to run faster. The Los Alamos report, "TRAC-PF1: An Advanced Best-Estimate Computer Program for Pressurized Water Reactor Analysis," LA-9944-MS (NUREG/CR-3567), provides a detailed description of the code.  This report documents the Los Alamos results of the second assessment phase, independent assessment for TRAC-PF1. We analyzed separate-effects tests in the Semiscale facility to investigate natural-circulation and reflux cooling. We analyzed integral tests from the Semiscale and the Loss-of-Fluid-Test facilities to explore the small- and intermediate-break loss-of-coolant accident (LOCA) capability and the non-LOCA capability. We also analyzed the loss-of-feedwater transient in the Crystal River plant. The results show reasonably good agreement with the data, but indicate that improvements are required for the critical-flow model and the interphasic-condensation model.			11a. TYPE OF REPORT Informal		
14. DOCUMENT ANALYSIS - a. KEYWORDS/DESCRIPTORS  b. IDENTIFIERS/OPEN-ENDED TERMS			11b. PERIOD COVERED (Inclusive dates)		
15. AVAILABILITY STATEMENT  Unlimited			16. SECURITY CLASSIFICATION (This page) Unclassified (This report) Unclassified		
17. NUMBER OF PAGES			18. PRICE		

Available from

Superintendent of Documents  
U.S. Government Printing Office  
Post Office Box 37082  
Washington, D. C. 20013-7982

and

National Technical Information Service  
Springfield, VA 22161

120555078877 1 1AN1R4  
US NRC  
ADM-DIV OF TIDC  
POLICY & PUB MGT BR-PDR NUREG  
W-501  
WASHINGTON DC 20555

Los Alamos